

The main aim of this thesis was to gain further insight in the developmental processes affecting leaf size. In our studies we used the model species *Arabidopsis thaliana*, because of the large variety of genetic resources and the background knowledge of leaf development and growth regulating genes available for this species. For the analysis we focused on the epidermis as it is thought to be the main tissue layer driving leaf growth. Moreover, divisions in this tissue are strictly anticlinal and therefore the evolution of the epidermal cell number is directly proportional to the cell division activity within this layer. To reach our goals, we decided to utilize recent advances in digital imaging technology and to develop new image analysis algorithms in order to boost the plant phenotyping throughput and to speed up and to increase the resolution of the functional analysis of genes that affect leaf growth.



Imaging as a tool to study leaf development in *Arabidopsis thaliana*

Imaging as a tool to study leaf development in *Arabidopsis thaliana*

Stijn Dhondt

Stijn Dhondt



FACULTY OF SCIENCES

Ghent University
Faculty of Sciences
Department of Plant Biotechnology and Bio-informatics

Imaging as a tool to study leaf development in *Arabidopsis thaliana*

Stijn Dhondt

thesis submitted as partial fulfillment of the requirements
for the degree of Doctor (Ph.D.) in Sciences: Biotechnology
Academic year 2011-2012

Promoters:

Prof. Dr. Dirk Inzé and Prof. Dr. ir. Gerrit T.S. Beemster

VIB - Plant Systems Biology
Systems Biology of Yield Group
Technologiepark 927, 9052 Ghent, Belgium



"Nature understands no jesting.

She is always true, always serious, always severe.

She is always right, and the errors are always those of man."

Johann von Goethe (1749 – 1832)

Cover Image:

Cellular content of the abaxial epidermis of an *Arabidopsis* leaf at 13 days after sowing. Color-coding of the pavement cells according to circularity allows visualization of the gradient along the longitudinal axis of the leaf established during the transition from primary to secondary morphogenesis. Guard cells are excluded from the analysis and are depicted in white. A fading image of the cellular content is superimposed on a dark field image of the corresponding leaf.

Dhondt, S. (2011-20121) "Imaging as a tool to study leaf development in *Arabidopsis thaliana*". PhD Thesis, Ghent University, Ghent, Belgium

The authors and promoters give the authorization to consult and copy parts of this work for personal use only. Every other use is subject to the copyright laws. Permission to reproduce any material contained in this work should be obtained from the author.

Stijn Dhondt was supported by a PhD fellowship grant from the Agency for Innovation through Science and Technology (IWT); a grant from the 'Bijzonder Onderzoeksfonds Methusalem project' (no. BOF08/01M00408) of Ghent University; and from the European Community (grant no. FP6 IP AGRON-OMICS, contract no. LSHG-CT-2006-037704).

JURY MEMBERS

Promoters:

Prof. Dr. Dirk Inzé

Department of Plant Biotechnology and Bio-informatics
Ghent University – WE09

Prof. Dr. Gerrit T.S. Beemster

Laboratory for Molecular Plant Physiology and Biotechnology
University of Antwerpen

Promotion commission:

Prof. Dr. Ann Depicker (chair)

Department of Plant Biotechnology and Bio-informatics
Ghent University – WE09

Prof. Dr. Tom Beeckman

Department of Plant Biotechnology and Bio-informatics
Ghent University – WE09

Prof. Dr. Veerle Cnudde

Department of Geology and Soil Science
Ghent University – WE13

Prof. Dr. Enrico Coen

Cell & Developmental Biology
John Innes Centre, United Kingdom

Prof. Dr. Lieven De Veylder

Department of Plant Biotechnology and Bio-informatics
Ghent University – WE09

Dr. Fabio Fiorani

Plant Sciences (IBG-2)
Forschungszentrum Jülich, Germany

Prof. Dr. Wilfried Philips

Department of Telecommunications and Information Processing
Ghent University – IR07

Prof. Dr. Kathy Steppe

Laboratory of Plant Ecology
Ghent University – BW09

Table of Contents

Summary

Research Objectives

List of Acronyms

Chapter 1	Imaging plant growth dynamics	1
Chapter 2	SHORT-ROOT and SCARECROW regulate leaf growth in Arabidopsis by stimulating S-phase progression of the cell cycle	41
Chapter 3	Model-based analysis of Arabidopsis leaf epidermal cells reveals distinct division and expansion patterns for pavement and guard cells	73
Chapter 4	Exit from proliferation during leaf development in Arabidopsis thaliana: a not so gradual process	99
Chapter 5	Quantitative analysis of venation patterns of Arabidopsis leaves by supervised image analysis	137
Chapter 6	Plant structure visualization by high-resolution X-ray computed tomography	161
Chapter 7	Towards an automated kinematic analysis of leaf growth	171
Chapter 8	Automated analysis of rosette growth parameters by time resolved imaging	191
Chapter 9	General conclusion and future perspectives	205
Acknowledgements		217
Curriculum Vitae		221

Summary

In contrast to humans and animals, the body plan of a plant is not completely defined within the embryonic stages. Organ formation continues throughout plant development and this iterative and modular process is continuously controlled by environmental cues such as light, gravity, temperature, humidity and chemicals. In most plant species, the above-ground plant body is dominated by leaves, the organs specialized in photosynthesis. This process converts carbon dioxide into organic components utilizing energy from sunlight; making leaves the energy production site and the growth engine of plants. In addition, in many cases the majority of a plant's biomass consists of leaves, also making them important organs for the production of food, feed and bio-energy.

The final leaf size is determined by the total number of cells and the average cell size that result from cell division and cell expansion, respectively. During leaf development of dicotyledonous species, a cell proliferation phase, characterized by actively dividing cells, is followed by a cell expansion phase, characterized by cell growth and differentiation. After expansion, cells mature and the final leaf size is reached. At the proliferation-to-expansion phase transition, cell division ceases along a longitudinal gradient from leaf tip to base. In this thesis, we set out to gain further insight in these developmental processes affecting leaf size, assisted by the use of imaging technology and automated image analysis. For these studies we used the model species *Arabidopsis thaliana*, focusing primarily on the epidermis of the developing leaves as divisions there are strictly anticlinal. Moreover this layer is thought to be the main tissue layer controlling leaf growth.

As a first step, we developed different image analysis tools to allow for a better and more efficient analysis of the leaf developmental process. In the first place we developed an online framework, designated Leaf Image Analysis Interface (LIMANI), in which venation patterns are automatically segmented and measured on dark-field images. Image segmentation may be manually corrected through use of an interactive interface, allowing supervision and rectification steps in the automated image analysis pipeline and ensuring high-fidelity analysis. We subsequently used this framework to study vascular differentiation during leaf development and to analyze the venation pattern in transgenic lines with contrasting cellular and leaf size traits. A major conclusion from this work was that, as vascular differentiation occurs relatively late in development, the influence of a fully functional and differentiated venation pattern on final leaf size is rather limited.

Furthermore, we describe a proof-of-concept to automate the kinematic analysis of leaf growth based on DIC pictures, by a sophisticated image processing chain and a data analysis pipeline. Next, we also developed imaging scripts to extract complete seedlings grown on soil and on Petri dishes and integrated those into three phenotyping platforms which monitor plant growth. Finally, we investigated the potential of emerging imaging

technologies, particularly X-ray computed tomography, for future applications in plant growth analysis.

The newly developed kinematic analysis tools allowed us to show that the transcription factors, SHORT-ROOT (SHR) and SCARECROW (SCR), next to their specific roles in cortex/endodermis differentiation and stem cell maintenance in the root, primarily function as general regulators of cell proliferation in leaves. The analysis of leaf growth revealed how these proteins affect the cellular growth dynamics and formed the basis to unravel the molecular mechanism controlling this. It turned out that they promote leaf growth mainly by the down-regulation of cell cycle inhibitors, known to restrain the activity of the transcription factor, E2Fa, stimulating S-phase progression.

Although the dynamics of cell division and cell expansion processes can be analyzed rigorously by the leaf growth kinematics, knowledge of cell cycle duration, cell expansion, and their interaction at the individual cell level is still poorly understood, not only because of technical obstacles to study these phenomena, but also because the processes are intimately intertwined, shown by the fact that a reduced cell proliferation is often compensated by an increase in cell size and vice versa. A mathematical model fitted to detailed cellular measurements retrieved by automated image analysis of microscopic drawings of the leaf epidermis, revealed that average cell cycle duration remains constant throughout leaf development. Surprisingly, no evidence for a maximum cell size threshold for cell division of pavement cells was found in this analysis. We could estimate the division and expansion parameters of pavement and guard cell populations within the growing leaf separately and the model predicted that neighboring cells of different sizes within the epidermis expand at distinctly different relative rates. We could finally verify this by direct observations using live imaging.

The mathematical model helped us to gain a better and more detailed insight into the processes that define leaf growth. But the transition from cell proliferation to cell expansion was a developmental time point that was still not characterized in detail. Differences in the timing of this transition strongly affects the number of cells formed and therefore potentially also serves as a control point determining mature leaf size. Several genes have been identified that alter leaf size by affecting the transition from primary to secondary morphogenesis. We characterized the progression of the transition on the morphological and molecular level using transcriptome analysis and imaging algorithms to visualize and quantify the size and shape of pavement cells along the proximal-distal axis of the leaf during transition. Both analyses showed that the transition from cell proliferation to expansion was established and abolished abruptly. Furthermore, the establishment of the cell cycle arrest front occurs simultaneously with the onset of photomorphogenesis. We provide evidence that retrograde signaling from chloroplasts can affect the onset of transition, revealing a previously unknown level of regulatory complexity during the transition from primary to secondary morphogenesis.

Samenvatting

In tegenstelling tot mensen en dieren, is het bouwplan van een plant niet volledig gedefinieerd in de embryonale stadia. Orgaanvorming gaat verder tijdens de ontwikkeling van de plant en dit herhalend en modulair proces wordt continu gecontroleerd door omgevingsfactoren zoals licht, zwaartekracht, temperatuur, vochtigheid en chemicaliën. In de meeste plantenspecies wordt het bovengrondse bouwplan gedomineerd door bladeren, de organen gespecialiseerd in fotosynthese. Dit proces zet koolstofdioxide om in organische componenten gebruikmakend van zonne-energie, wat bladeren de energieproductieplaats en groeimotor van planten maakt. Bovendien bestaat het merendeel van de plantenbiomassa veelal uit bladeren, wat van hen ook belangrijke organen maakt voor de productie van voedsel, voeder en bio-energie.

Finale bladgrootte wordt bepaald door het totaal aantal cellen en de gemiddelde celoppervlakte, die respectievelijk het resultaat zijn van celdeling en celexpansie. Tijdens de bladontwikkeling van dicotyle soorten, wordt een celproliferatiefase, gekarakteriseerd door actief delende cellen, gevolgd door een celexpansiefase, gekarakteriseerd door groei en differentiatie. Na expansie, verouderen de cellen en is de finale bladgrootte bereikt. Bij de transitie van proliferatie naar expansie, stopt celdeling volgens een longitudinale gradient van de bladtip naar de bladbasis. In deze thesis gingen we van start om verder inzicht te vergaren in deze ontwikkelingsprocessen die bladgrootte beïnvloeden. Hierbij maakten we gebruik van de modelplant *Arabidopsis thaliana*, waarbij we vooral focuseerden op de epidermis van ontwikkelende bladeren, aangezien delingen hier louter anticlinaal gebeuren. Daarenboven wordt de epidermis gezien als de belangrijkste weefsellaag in het sturen van groei.

Als een eerste stap, ontwikkelden we verschillende beeldanalyse toepassingen om een betere en meer efficiënte analyse van de bladontwikkelingsprocessen toe te laten. In de eerste plaats, ontwikkelden we een online framework, LIMANI genaamd, waarin venatiepatronen automatisch gesegmenteerd en opgemeten worden op basis van donkerveld beelden. De beeldsegmentatie kan manueel gecorrigeerd worden door gebruik van een interactieve interface, die supervisie- en correctiestappen in de geautomatiseerde beeldanalyse toelaat en een betrouwbare analyse garandeert. We gebruikten het framework om vasculaire differentiatie te bestuderen tijdens bladontwikkeling en om venatiepatronen in trangene lijnen met contrasterende cellulaire en bladgrootte-eigenschappen te analyseren. Een belangrijke conclusie van dit werk was dat de invloed van een volledig functioneel en gedifferentieerd venatiepatroon op finale bladgrootte eerder beperkt is, aangezien de vasculaire differentiatie redelijk laat gebeurt tijdens ontwikkeling.

Daarenboven beschrijven we een 'proof-of-concept' voor het automatiseren van de kinematische analyse van bladgroei gebaseerd op DIC foto's, via een gesofisticeerde beeldverwerkingsketting en een data-analysepipeline. Verder ontwikkelden we ook

beeldanalysescripts voor het extraheren van complete zaailingen gegroeid op aarde en in Petri-schalen en integreerden deze in drie phenotyperingsplatforms die plantengroei opvolgen. Tenslotte, onderzochten we het potentieel van opkomende imaging technologieën, meer specifiek van 'X-ray computed tomography', voor de toekomstige toepassing in planten groei analyse.

Aan de hand van de nieuw ontwikkelde kinematische analyse toepassingen toonden we aan dat de transcriptiefactoren, SHORT-ROOT (SHR) en SCARECROW (SCR), naast hun specifieke rol in de cortex/endodermis differentiatie en stamcelbehoud in de wortel, vooral functioneren als algemene regulatoren van celproliferatie in bladeren. De analyse van bladgroei onthulde hoe deze eiwitten de cellulaire groeidynamica beïnvloeden en vormde de basis voor het ontrafelen van het moleculair mechanisme dat dit controleert. Het bleek dat ze bladgroei vooral bevorderen door neerregulatie van celcyclusinhibitoren, gekend voor het beperken van de activiteit van de transcriptiefactor, E2Fa, waardoor S-phase progressie gestimuleerd wordt.

Alhoewel de dynamica van celdelings- en celexpansieprocessen grondig kan geanalyseerd worden door bladgroei kinematica, is de kennis van celcyclusduratie, celexpansie en hun interactie op individueel celniveau nog beperkt. Dit niet alleen omwille van technische hindernissen voor het bestuderen van deze fenomenen, maar ook omdat de processen praktisch verweven zijn, aangetoond doordat een reductie in celproliferatie vaak gecompenseerd wordt door een stijging in celgrootte, en omgekeerd. Een wiskundig model gefit aan gedetailleerde cellulaire metingen, verkregen door geautomatiseerde beeldanalyse van microscopische tekeningen van de bladepidermis, onthulde dat de gemiddelde celcyclusduratie constant blijft tijdens bladontwikkeling. Verassend genoeg werd er in deze analyse geen aanwijzing gevonden voor een maximale celoppervlaktelimit voor celdeling. We konden de delings- en expansieparameters van pavementcel- en sluitcelpopulaties in een groeiend blad afzonderlijk schatten en het model voorspelde dat naburige cellen van verschillende groottes expanderen met duidelijk verschillende groeisnelheden. Dit konden we uiteindelijk verifiëren door directe observaties via 'live imaging'.

Het wiskundig model hielp ons om een beter en meer gedetailleerd inzicht te krijgen in de processen die bladgroei bepalen. Maar de transitie van celproliferatie naar celexpansie was een ontwikkelingstijdpunt dat nog niet in detail gekarakteriseerd was. Verschillen in de timing van de transitie beïnvloedt sterk het aantal gevormde cellen, waardoor het mogelijk ook fungeert als een controle punt dat finale bladgrootte bepaald. Verschillende genen die de bladgrootte veranderen door het beïnvloeden van de transitie van primaire naar secundaire morfogenese zijn reeds geïdentificeerd. Wij karakteriseerden de progressie van de transitie op morfologisch en moleculair niveau door gebruik van transcriptoom analyse en beeldanalyse algoritmen, die de grootte en vorm van pavementcellen visualiseren en kwantificeren langs de proximale-distale as van het blad. Beide analyses toonden dat de transitie van celproliferatie naar celexpansie abrupt gevormd en ontbonden wordt. Bovendien gebeurt de vorming van het celcyclusarrestfront gelijktijdig met de aanvang van

fotomorfogenese. We vonden aanwijzingen dat retrograde signalisatie van chloroplasten de aanvang van de transitie kan beïnvloeden, waardoor een voorheen ongekend niveau van regulatorische complexiteit tijdens de transitie van primaire naar secundaire morfogenese wordt onthuld.

Research objectives

The main aim of this thesis was to gain further insight in the developmental processes affecting leaf size. In our studies we used the model species *Arabidopsis thaliana*, because of the large variety of genetic resources and the background knowledge of leaf development and growth regulating genes available for this species. For the analysis we focused on the epidermis as it is thought to be the main tissue layer driving leaf growth. Moreover, divisions in this tissue are strictly anticlinal and therefore the evolution of the epidermal cell number is directly proportional to the cell division activity within this layer. To reach our goals, we decided to utilize recent advances in digital imaging technology and to develop new image analysis algorithms in order to boost the plant phenotyping throughput and to speed up and to increase the resolution of the functional analysis of genes that affect leaf growth.

The thesis comprises of four large sections, an introduction (Chapter 1), a section (Chapter 5-8) where we utilize recent advances in digital imaging technology and develop new imaging algorithms, a section where we implement these to analyze leaf development (Chapter 2-4) and finally a general conclusion (Chapter 9).

The introduction (Chapter 1) introduces the reader to the field of plant growth imaging. For this we chose to focus on the imaging aspect of the research project, because the leaf developmental processes and the molecular components regulating them are described in the introduction of chapters at issue. We highlighted the imaging of cell division and expansion with increasing temporal resolution, using destructive and non-destructive methods, automated growth measurements of plant roots and shoots, with a focus on the extraction of spatial and temporal growth patterns. Furthermore, we explore the electromagnetic spectrum in order to reveal the physiological status of plants and we reviewed the state-of-the-art in 3-D plant imaging.

To allow a better and more efficient analysis of plant growth a major aim of this work is to develop new imaging tools. In chapter 5 we set out to develop an online framework for the automatic segmentation and measurement of venation patterns in *Arabidopsis* leaves starting from dark-field images. In Chapter 6 we investigate the possibility to use X-ray computed tomography to study overall plant morphology and cellular organization in three dimensions. The state-of-the-art and proof of concept of steps taken towards the automation of kinematic growth analysis in leaves, starting from DIC images, is covered in Chapter 7. Finally, Chapter 8 describes the development of imaging scripts for the extraction of complete seedlings, grown on soil or on Petri dishes, and their integration into three phenotyping platforms, which monitor plant growth.

In the experimental part the main aim is to gain deeper understanding of the leaf growth process. In Chapter 2 we use the newly developed automation of the kinematic analysis to examine the role of *SHORT-ROOT* and *SCARECROW* in regulating leaf growth, which gives an entry to unravel the molecular mechanisms downstream of these transcription

factors. Next to the functional analysis of growth regulating genes, we use the increased cellular resolution offered by this method to gain a better and more detailed insight into the processes that define leaf growth, cell division and expansion, and into their interaction at the individual cell level. A mathematical model to achieve this is presented in Chapter 3. The transition from cell proliferation to cell expansion is identified as an important developmental time point affecting final leaf size. The increased spatio-temporal resolution of the newly developed kinematic analysis tools is eventually used to characterize this transition at the morphological and molecular level, using imaging algorithms and transcriptome analyses, is described in Chapter 4.

Finally we conclude this thesis with a general discussion and future perspectives in Chapter 9.

List of Acronyms

2-D	Two-dimensional
3-D	Three-dimensional
Col	Columbia
CT	Computed tomography
DAS	Days after sowing
CYC	Cyclin
DIC	Differential interference contrast
DNA	Deoxyribonucleic acid
GRA	Grandifolia
GUI	Graphical user interface
HRXCT	High resolution X-ray computed tomography
HSV	Hue-value-saturation
IGIS	In vitro Growth Imaging System
IR	Infrared
KRP	Kip-related protein
LIMANI	Leaf IMage ANalysis Interface
MIRGIS	Multi camera In vivo Rosette Growth Imaging System
MRI	Magnetic resonance imaging
MS	Murashige and Skoog
NF	Norflurazon
NIR	Near-infrared
NMR	Nuclear magnetic resonance
OPT	Optical projection tomography
PET	Positron emission tomography
Q-RT-PCR	Quantitative reverse transcription polymerase chain reaction
RGB	Red-green-blue
RGR	Relative growth rate
RSA	Root structure architecture
SAM	Shoot apical meristem
SCR	SCARECROW
SE	Standard error
SHR	SHORT-ROOT
T-DNA	Transfer DNA
WIWAM	Weighing Imaging and Watering Machine
WT	Wild-type

1

Imaging plant growth dynamics

INTRODUCTION

Today there is a growing awareness that global agriculture is facing major challenges. There is a drastically increasing demand for food, feed and fuel and this will have to be realized in less favorable conditions due to global climate changes. The world population is increasing steadily at an exponential rate to a projected 9 Billion people by 2050. As a result more and more arable land is sacrificed for living purposes. Furthermore, annual yields of many crops have hit plateaus. Already now, worldwide yield increases can no longer meet the projected demand for the major cereal crops. The Food and Agriculture Organization of the United Nations postulate that cereal grain yields alone must increase by at least 70 % by 2050. Moreover, rice demand has already exceeded the supply during the last years (Furber et al., 2009). Shortage of food is raising the prices dramatically and many countries are struggling

with a food crisis. These statements indicate that food security is more than ever a global issue. On top of that, climate change is approaching and extreme weather conditions destroy harvests. Its impact on global temperatures and rainfall patterns are likely to lead to reduction in yields due to abiotic stress (Tester and Langridge, 2010). Furthermore, the rapid increasing standard of living in developing countries is driving the rising energy needs, while the natural resources are running out. This indicates that growing feedstock crops for biofuel production will become more important in the future. However, these cannot go in competition with food crops for arable land. Taken together to tackle these challenges, in the next decades agricultural crops must be developed that have a higher intrinsic yield, while they ensure yield stability under abiotic stresses.

Since conventional breeding programs are likely not to fulfill these needs in a short timeframe, new approaches coming from the field of plant biotechnology offer an additional approach to further increase crop productivity. Sequencing the genome of the model plant *Arabidopsis thaliana* is a landmark in plant genomics and started the “genomics era” in plant biology (Arabidopsis Genome Initiative, 2000). Subsequently many economically important crop varieties have been sequenced and annotated, including rice (Sequencing Project International Rice Genome, 2005) and maize (Schnable et al., 2009). Furthermore, plant genomics is entering a new era by the introduction of high-throughput sequencing technologies. Many more plant genomes are becoming available and re-sequencing will be adopted to assess allelic variation in multiple species. Researchers are currently obtaining terabytes of sequence data, from both genomic and transcriptional origin. Moreover, over the years, researchers have also acquired a large variety of genetic resources to perform functional genomics. Homozygous genome wide knockout lines (O’Malley and Ecker, 2010), a collection of gain-of-function transgenics by full length cDNA overexpression (Ichikawa et al., 2006), sets of recombinant inbred lines (Lister and Dean, 1993) and collections of different accessions (Nordborg et al., 2005) represent some of the available resources in the model plant *Arabidopsis thaliana*. Comparable initiatives are also set up in crop species, such as rice (Kuromori et al., 2009). Nevertheless, it is becoming apparent that the current plethora of sequence information and genetic resources has not yet been adequately exploited. A significant proportion of the genes in the *Arabidopsis* genome are still annotated with “unknown function” and many functional analyses report “no visible phenotype”. Genetic resources and sequence data are accumulating quickly, while linking this information to gene function is progressing at a much slower pace, indicating that plant phenotyping is the major bottleneck in the process of understanding the genomic code and implementing this knowledge to improve crop yield (Furbank and Tester, 2011). Phenotyping is widely recognized as the most laborious and technically challenging part of the process, making it costly and time consuming. However, this ‘phenotyping bottleneck’ can now be addressed by combining novel image capturing technologies, robotics, image analysis, and data integration; introducing the rapid emerging area of plant phenomics. The goal of plant phenomics is to accelerate the progress in understanding gene function and environmental

plant responses, closing the gap between genomics and functional biology (Furbank, 2009; Finkel, 2009).

High-throughput plant phenotyping usually involves image acquisition, automated image analysis, data extraction and storage in order to extract growth dynamics, morphological traits, or plant physiological parameters. Image acquisition comprises the process of obtaining the pictures of interest by capturing the desired range of the electromagnetic light spectrum, such as visible light, infrared or X-rays, by combination of digital sensors and filters. At this stage robotics can be applied to bring multiple samples to the imaging station or to move the camera over different positions (sensor to plant vs. plant to sensor) (Granier et al., 2006). Next, image analysis is employed to extract the desired features from the images, often by generating a binary image. The final imaging result is obtained by combination of a series of imaging procedures, which can include segmentation and the application of thresholds. Automated image analysis is usually the most crucial step towards high-throughput plant phenotyping. Next, mathematical treatment of the imaging data allows extracting the measurements, such as color information, shape features, and area values. This represents a major step in the data transformation, reducing the raw image data to a number of data points. A single image has the potential to yield a large number of measurements or phenotypic descriptions, adding further to the complexity of the subsequent data analysis, making high capacity computing and data storage essential (Berger et al., 2010). However, one should always carefully consider the biological relevance of the recorded measurements. Converting the image to a set of numerical values allows precise quantification of the phenotypes, whereas larger manual screens often only include qualitative information (Kuromori et al., 2009). Finally, the data is stored together with its metadata, preferably in a searchable database (Fabre et al., 2011), followed by statistical data analysis. These are the different steps to setup a high-throughput plant phenotyping system.

Spatial and temporal resolution are the main features affecting the imaging setups. What is the desired time interval between consecutive measurements and do you want to phenotype features at the cellular, organ or whole plant level? Time wise it is important to note that while cell expansion is continuous, cell division is a stochastic process and cell cycle duration can be up to several days (Reddy et al., 2004). Also whole organ growth can take weeks. This diverse set of requirements has led to a diverse set of approaches. Over the last decade, many software tools have been developed to extract phenotypic plant data. In this introduction we give an overview of the available applications that extract morphological and growth parameters from plant shoots and roots. Furthermore, we examine the possibilities to follow cellular growth dynamics and we scout the electromagnetic spectrum to reveal information on the plant's physiological status. Finally, we discuss recent advances in three-dimensional (3-D) plant visualization and reveal our future perspectives on plant growth imaging and high-throughput phenotyping.

IMAGING THE DIVISION AND EXPANSION OF CELLS WITH INCREASING TEMPORAL RESOLUTION

Why choosing cells as the focus for growth analysis

Organ growth has traditionally been viewed in two contrasting ways: The 'organismal theory' considers the individual organ as the basic unit of morphogenesis and growth regulation in a multi-cellular organism. Consequently, growth analysis of plants could be restricted to the organ level, and cells are merely there to compartmentalize the generated organismal space. Inversely, the 'cell theory' considers the cell as the basic regulatory unit of growth regulation that forms the building blocks of the plant and the observed growth at the organ level is a consequence of cell division and expansion activity at the cellular level. Observations in transgenic plants with altered expression of cell cycle genes could be classified as supporting one or the other theory (Kaplan, 1992; Tsukaya, 2002). However, during the last decades more and more observations were published that could not be adequately explained by either model. There is accumulating evidence that growth factors, such as KLUH/CYP78A5, can act non-cell-autonomously to coordinate organ size (Anastasiou et al., 2007; Eriksson et al., 2010; Kawade et al., 2010). Furthermore, different compensation modes, in which a decrease in cell number triggers an increase in mature cell size, suggest an interaction between cellular processes during organogenesis (Ferjani et al., 2007). These results evoke a more complicated growth model, called the neo cell theory, involving the interaction between cellular and higher scale mechanisms (Tsukaya, 2002; Beemster et al., 2003), which must feedback on the cellular level, controlling plant morphogenesis, because organ growth is in essence the result of two processes which integrate molecular processes and occur at the cellular level, being cell expansion and cell division (Green, 1976). This means that to understand the nature of growth differences, observations at the cellular level are key.

Moreover, during the last decade, transcriptome, proteome, and metabolome profiling techniques are more and more applied to unravel the basis of growth phenotypes caused by genetic differences or changing environmental conditions. However, these approaches often only focus on the molecular level and lack details on the growth process at cellular resolution. In order to fully understand growth regulatory mechanisms, profiling experiments should be combined with cellular growth analysis to be able to link regulatory processes at the molecular level to whole plant growth. This indicates that knowledge of the regulation of cell division and cell expansion at the cellular level are pivotal to obtain a mechanistic view on how molecular changes can lead to observed growth phenomena.

Destructive measurements of cell growth and division

Endpoint measurements of cell size and cell number can readily reveal whether a changed growth phenotype is caused by an effect on cell expansion and / or cell division. However, to unravel the dynamics of these processes a so called 'kinematic growth analysis' is needed. Kinematics describes the motion of bodies (cells) and systems (group of cells) without consideration of the forces that cause the motion. In biology, kinematic methods have been pioneered halfway last century (Goodwin and Stepka, 1945; Erickson and Sax, 1956a) and a rigorous mathematical framework was developed based on laws of fluid dynamics a few decades later (Silk and Erickson, 1979). This method has been adapted to specific characteristics of various plant organs (Erickson and Sax, 1956a; Silk and Erickson, 1979; Fiorani and Beemster, 2006). In the root, cell length distributions are combined with a velocity profile, both covering the different developmental zones in the root, in order to extract cell division and cell expansion rates. Kinematic measurements of the monocot leaf are a derivative of this approach. For the dicot leaf, the basis of a kinematic growth study is that recording cell number and cell size at several developmental stages together with following overall organ growth allows for the calculation of cell division rates and cell expansion rates over time. For a detailed description of the experimental approaches and calculations we refer the reader to a methods book chapter to which I contributed (Rymen et al., 2010). When working with non-transparent organs kinematic measurements often require the clearing of plant samples to visualize the cellular content. Plant cells can be quantified using microscopic pictures (Horiguchi et al., 2005) or by making microscopic drawings of the cell outlines using a drawing tube (Figure 1) (De Veylder et al., 2001). Also epidermal peels can be used to extract cellular information (Walker and Smith, 2002). Above methods make use of differential interference contrast (DIC) imaging to increase the visibility of the cell walls. Image analysis scripts have been developed to automatically distinguish between leaf epidermal cell types and to extract individual cell sizes starting from microscopic drawings (Chapter 7) (Andriankaja, Dhondt, De Bodt et al., 2011). Combination of these measurements with a mathematical modeling approach revealed distinct division and expansion patterns for pavement and guard cells (Chapter 3) (Kheibarshekan Asl, Dhondt et al., 2011). Next to DIC, also confocal imaging has been applied to extract cellular size and shape parameters on plant organs. Extensive clearing protocols combined with propidium iodine staining allow the visualization of cell outlines and the measurement of 3-D cell volumes in multiple plant tissues (Truernit et al., 2008; Wuyts et al., 2010).

Cell expansion rates at whole organ level are calculated as the change in cell size over time. The examination of cell division rates, on the other hand, is more complicated and often involves the visualization of cell divisions in order to define meristem size. This can be done by the observation of mitotic figures in tissues stained with nuclear stains such as propidium iodine, DAPI, and basic fuchsin. Furthermore, these stains can also be used to define the mitotic index, as the ratio between the number of cells in mitosis and the total number of

cells. In addition, it is possible to use mitotic cell cycle markers, such as pCYCB1;2::GUS with a cyclin destruction box (-DB), to visualize actively dividing cells, which can lead to the determination of the cyclin index, as the ratio between the number of GUS positive cells and the total number of cells (Donnelly et al., 1999). Nevertheless, such indexes cannot be equated to cell division rates (Erickson and Sax, 1956a). All techniques described above are destructive methods and require the harvesting of multiple samples to increase the statistical power of the measurements. Biological variation in growth between samples limits their application to time lapse assays with relatively low temporal resolution (usually a day).

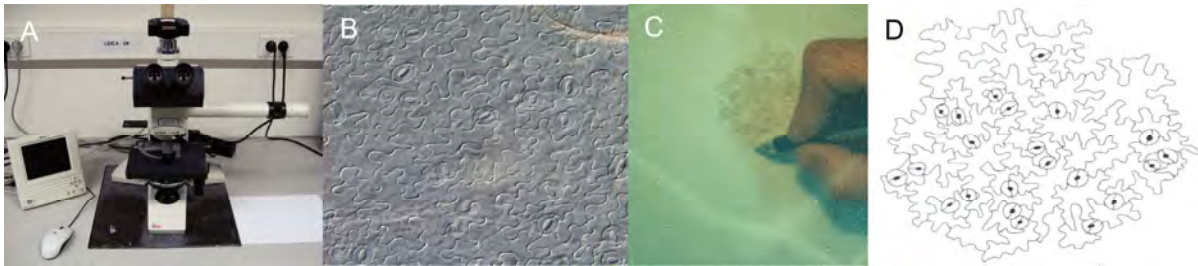


Figure 1: Manual microscopic drawing of *Arabidopsis* epidermal cells. (A) Microscopic setup containing DIC optics equipped with a drawing tube. (Note the piece of paper underneath the drawing tube.) (B) DIC image of the abaxial epidermis of an *Arabidopsis* leaf. (C) Opening the drawing tube visualizes the microscopic sample as a layer on top of the piece of paper, allowing for the manual tracing of the cell outlines. (D) Resulting epidermal drawing used to extract cellular leaf content.

Live imaging increases temporal resolution

The most important step to increase the resolution of studies on cell growth and division was to follow these processes over time by repeated measurements of the same living sample. This was first achieved using the primary maize root (Erickson and Sax, 1956b), but was also applied to unravel key events in stomatal development by making dental impressions with a 12h time interval of the epidermis of cotyledons (Geisler et al., 2000). With this technique, a thin layer of liquid plastic or varnish is peeled from the leaf surface after evaporation (Williams, 1973; Mathur and Koncz, 1997; Granier and Tardieu, 1998; Christensen, 2010), but also agarose has been used for imprints (Mathur and Koncz, 1997; Christensen, 2010). Imprints of epidermal tissue can be examined under a light microscope or scanning electron microscope. Sometimes, a cast is created before microscopic observation. This technology reached a summit in the recording of geometric changes and relative growth rates of epidermal cells on shoot and flower primordia of *Arabidopsis* by 3-D shape reconstruction (Kwiatkowska, 2004, 2006; Kwiatkowska and Routier-Kierzkowska, 2009). The technique is also often applied to visualize cell wall outlines as unique measurements for kinematic analyses, comparable to epidermal peels or microscopic drawings / pictures of cleared samples (Tisné et al., 2008).

The modern version of this approach is currently known as 'live imaging'. The temporal resolution of the analysis is further increased by using non-destructive imaging methods, such as confocal microscopy, creating a lot of opportunities to study cellular dynamics in a variety of species and organs. In this case, fluorescent stains or the expression of fluorescent proteins that localize to the nucleus or plasma membrane assist in the visualization of cell division and growth patterns (Reddy et al., 2004; Campilho et al., 2006; Harrison et al., 2009). Another advantage is that growth analysis can easily be correlated with protein localization and gene expression dynamics (Heisler et al., 2005). Tracking differential expression of the mitotic cyclin *CYCB1;1* using a promoter *CYCB1;1::CYCB1;1:GFP* fusion revealed temporal variation in mitotic activity in the shoot apical meristem (SAM) of *Arabidopsis*, where cell cycle duration ranges from 12h to 96h with a peak at 24h-30h (Reddy et al., 2004). In the same paper the authors also examine, cell division orientation and cell expansion patterns related to flower primordium development. Live imaging also showed that stem-cell homeostasis and growth dynamics can be uncoupled in the SAM (Reddy and Meyerowitz, 2005). For an overview on novel insights from live-imaging in shoot meristem development we refer to a recent review by Sijacic and Liu (2010). In root stem cells, numbers and orientations of cell divisions were analyzed by the establishment of a confocal tracking system, which provided direct evidence that stem cells have lower division rates than cells in the proximal meristem (Campilho et al., 2006). Furthermore in sepals, it was shown that the observed cell size diversity is due to the variability in decisions of individual cells about when to divide and when to stop dividing and enter the specialized endoreduplication cell cycle (Roeder et al., 2010). Observations in *Arabidopsis* leaves disclosed differential cell expansion within the epidermis, which may explain the jigsaw puzzle shape of pavement cells as a way to cope with internal tissue tension (Kheibarshekan Asl, Dhondt et al., 2011). Detailed analysis of the growth of pavement cells revealed alternating waves of lobe initiation and a phase of lateral isotropic expansion (Zhang et al., 2011). Together these results highlight that live imaging unveiled several key findings about growth and cell division in plants, generating insight in the underlying mechanisms controlling these processes and unraveling the links between them.

Selecting the weapons of choice

Although live imaging allows addressing a number of fundamental questions related to cellular growth dynamics, it is not always appropriate to choose these new advances in imaging technology over the more conventional methods. The difficult and complex nature of live imaging presents the researcher with a number of challenges. Since the plant should stay intact it is not always straightforward to access the tissue of interest. For example, it is not easy to fit a living plant under a microscope and to keep the plant alive and healthy during the time frame of live imaging in order to assure that the measurements are comparable to normal growth conditions (Chickarmane et al., 2010). This, compared to destructive

methods, which allow for the dissection of the organ of interest and ensure reliable measurements as new plants are sampled at each time point, making them more appropriate for longer time lapses that cover the complete developmental window of a specific organ, e.g. typically 20 days for a kinematic analysis of leaf growth (De Veylder et al., 2001). Another major hurdle in the analysis of live imaging time lapses is the image processing, which includes the visualization of the data, segmentation of the objects of interest and tracking of these objects over time. Visualization of real-time imaging data often requires specific software packages such as Amira (Visage, GmbH), Imaris (Bitplane, AG) and Volocity (PerkinElmer) which allow volume rendering. Image segmentation is the most crucial step in the quantification of cellular measurements as it results in the extraction of the objects of interest. It often involves filtering, noise reduction, contrast enhancement and thresholding of the input images. In a next step, images obtained at different time points should be aligned, allowing for growth measurements and cell tracking. Bringing image segmentation and registration to a good end demands a detailed knowledge of the biological sample, image acquisition and image processing procedures. The most elaborate approach published today focused on the quantitative analysis of *Arabidopsis* flower development at cellular resolution (Fernandez et al., 2010). It involves multiangle image acquisition, 3-D reconstruction, cell segmentation and automated cell lineage tracking. The latter also has been automated by local graph matching (Liu et al., 2010). A tool for the automatic detection of cell division in the *Arabidopsis* root using information on nuclear shape has also been developed (Marcuzzo, Guichard, et al., 2009). The same research group also developed software for automated root cell segmentation based on object classification and region merging (Marcuzzo, Quelhas, et al., 2009). On the other hand, one can choose to develop semi-automated cell segmentation protocols or to apply the labor-intensive approach of manual image segmentation (Barbier de Reuille et al., 2005; Roeder et al., 2010; Kheibarshekan Asl, Dhondt et al., 2011; Zhang et al., 2011). Both options ensure that the segmentation quality meets the expectations.

Taken together, the complexities described above should be taken into consideration for the decision whether a research question should be tackled by live imaging or destructive methods. This is the reason why larger screens for growth phenotypes are in general performed using destructive methods (Ferjani et al., 2007; Tisné et al., 2008). On the other hand, studying cell expansion of adjacent cells and the variation in cell cycle duration between cells requires live imaging and cannot be solved using destructive methods, indicating that the method of choice depends on biological question and the experimental setup. Nevertheless, the fact remains that findings based on destructive methods should be in line with live imaging results, and vice versa. A good example originates from our own work using a mathematical modeling approach of kinematic leaf growth data obtained by destructive measurements, which predicted differential cell expansion within the epidermis that could be confirmed by live imaging (Kheibarshekan Asl, Dhondt et al., 2011). For further details see Chapter 3.

AUTOMATED GROWTH MEASUREMENTS ON ORGAN SCALE

Imaging complete plant organs is the most widely spread application of automated plant phenotyping. While cellular imaging was primarily focusing on increasing the temporal resolution of growth analyses to unravel underlying mechanisms, imaging of plant organs also tried to increase the throughput of growth measurements. In a first instance this means the analysis of a larger amount of samples, but automation of plant phenotyping is also often accompanied with an increase in the number of output parameters. This is because image segmentation, which is the extraction of the organ(s) of interest from the background of the picture, is usually the most crucial and difficult step in the image processing. Once this step is succeeded, the extraction of different size, shape, and color features, such as area, perimeter, maximum width, circularity, color/intensity etc., is in general more straightforward. In this section we will review the available imaging tools for different plant organs. We will focus on 2-D image analysis as 3-D imaging will be handled in a separate section. Next to the whole organ growth we will also address image procedures that cover spatiotemporal growth measurements by particle tracking and flow-based approaches.

Roots, imaging the architecture of the hidden half

Although roots are generally growing in the soil, hidden from the human eye, researchers often prefer to grow them in a more accessible way, such as along the surface of paper or agar in containers, pouches or Petri dishes, or in hydroponic cultures, allowing a more straightforward characterization of growth phenotypes (Tuberosa et al., 2002; Bengough et al., 2004; Hund et al., 2009). Several studies revealed that these artificial growth environments do not always represent the development of root structures comparable to soil grown samples (Bengough et al., 2004; Hargreaves et al., 2008; Hummel et al., 2009). The observed differences are likely due to the exposure of roots to light; the distribution of nutrients, which is not comparable to soil samples; the changed mechanical interaction between the root and the medium; and differences in environmental temperature (Bengough et al., 2006; Nagel et al., 2009). Furthermore, the artificial growth conditions force the roots to grow in one plain, whereas the root architecture is a typical 3-D structure. Growing roots in clear gel media in transparent containers allows them to grow in three dimensions while they are still accessible for imaging (Fang et al., 2009; Iyer-Pascuzzi et al., 2010). The use of rhizotrons and new advances in 3-D imaging technology allow imaging roots in more natural conditions (described below), but in controlled laboratory conditions researches are often forced to resort to 2-D imaging techniques with clear access to the root system.

The labor-intensive nature and difficulty in non-invasively observing root system architecture (RSA) explains the limited knowledge of genes affecting RSA. The development of automated root phenotyping tools attempts to change this. Several laboratories published software packages to quantify the architecture of complete root systems, such as EZ-Rhizo, DART,

RootLM, GROWSCREEN_ROOT, and, RootTrace, (Qi et al., 2007; Mühlich et al., 2008; French et al., 2009; Armengaud et al., 2009; Hund et al., 2009; Le Bot et al., 2009). Furthermore, there are also several commercial software packages available for RSA quantification, such as IMAGEJ (Abramoff et al., 2004), OPTIMAS analysis software (Media Cybernetics, <http://www.mediacy.com>), WINRHIZO (Arsenault et al., 1995) and, Delta-T-Scan (www.delta-t.co.uk). Total root length / surface / volume, main root length, depth and maximum horizontal width of the RSA, number and length of lateral roots, branching densities and curvature are some of the root architecture traits that can be extracted using the imaging applications. Most of them focus on the analysis of plants with rather simple root systems, such as *Arabidopsis*, and are not suitable for the quantification of the complex root systems of monocots as maize and rice. The image processing is in general based on the segmentation of root systems from images acquired from flatbed scanners or digital cameras. These are non-invasive methods which allow imaging the RSA over time to examine dynamics in root traits. Besides, all applications have in common that they largely depend on image quality and resolution, in such a way that the sometimes narrow roots should contain enough pixels to allow for the operations during image analysis. Furthermore, roots are sometimes difficult to distinguish from the background due to their transparency and also root branching and the crossing of two roots is difficult to distinguish by image processing. This explains why many labs rely on manual root measurements. To overcome these problems, EZ-Rhizo, Root LM, and DART were developed as semi-automated computer programs, requiring different levels of user interaction to ensure a correct extraction of the root systems (Qi et al., 2007; Armengaud et al., 2009; Le Bot et al., 2009). DART and RootLM allow following root growth by the tracing of new newly formed segments with different colors (Qi et al., 2007; Le Bot et al., 2009). RootTrace can analyze sequences of images with little user input, opening the door to high-throughput screens of root growth (French et al., 2009). The latter application has been extended to count emerged lateral roots and to recover strongly curved and agravitropic roots (Naeem et al., 2011). Iyer-Pascuzzi et al. developed an imaging and analysis platform to analyze complex root systems of monocot plants in agar filled cylinders allowing for the 3-D outgrowth of roots (Iyer-Pascuzzi et al., 2010). Images are captured from 20 angles around the cylinder to get a complete view on the 3-D RSA and a large range of RSA features can be extracted. Finally, Devienne-Barret and co-workers designed a culture system, Ara-rhizotron, to study RSA of *Arabidopsis* plants grown in a soil layer between transparent plates (Devienne-Barret et al., 2006).

The list of commercial and non-commercial software packages shows that the imaging of root systems is a fast expanding research field. Applications become more accurate and require less user input. These advancements in technology indicate that automated high-throughput analysis of the architecture of complex root systems is on its way. New applications will allow for detailed screens of mapping populations to identify QTLs that affect RSA, which will boost the discovery of genes that could be utilized to improve the root architecture of crops.

Analyzing visible traits of plant shoots

Compared to the imaging of root architecture, image capturing and processing of shoots is more straightforward. As above ground organs they are more accessible to the camera and the production of chlorophyll ensures a higher contrast with the background, compared to roots which are often transparent. One complication often encountered is that, although the plant as a whole is assumed to be sessile through the anchoring in the ground by the root system, the shoot is moving throughout the day, mainly due to photomorphogenic effects and the circadian movement of leaves. As a consequence, this means that the location of individual leaves in consecutive pictures of a time series can change position and that projected leaf area measurements can yield significantly different results during the day. Furthermore, as the root, the shoot naturally develops as a 3-D object growing in space. However, this cannot be restricted to a 2-D plane as the root which can be grown on the surface of agar or paper. For plants that develop a rosette, like *Arabidopsis*, this is less of a problem during the imaging, but for plants with an erect 3-D architecture this has to be taken into account. Such plants should be oriented before imaging or should be imaged from different angles to get a good representation of the biomass. Besides, shoots are in general grown in day-night conditions whereas roots are often grown in continuous light to get a steady growth. These changing light conditions evoke a diurnal growth pattern, which is species specific. Concerning the imaging, the diurnal growth pattern has as a consequence that daily image capturing has to be performed at fixed time points and that imaging time should be minimized in high-throughput analyses to exclude significant size differences between replicate plants due to time. The movement of plants, the 3-D architecture, and the diurnal growth pattern are the major hurdles in shoot imaging, which should be taken into account when deciding on the timing and setup of shoot imaging platforms.

Leister and co-workers were the first to describe the use of non-invasive image analysis for plant growth phenotyping (Leister et al., 1999). Projected leaf area measurements of individual *Arabidopsis* seedlings were utilized to determine plant growth rates and were correlated with biomass. Although very promising, only few studies employed this methodology to identify QTLs and genes involved in plant growth (El-Lithy et al., 2004). Nevertheless, imaging of projected rosette area in visible light was incorporated in several growth analysis platforms (Granier et al., 2006; Walter et al., 2007; Skiryicz et al., 2011; Arvidsson et al., 2011). Two approaches were utilized for distinction between plant and background. The first approach applies a red, green and blue (RGB) channel weighting to create an 8-bit grayscale image which is especially bright for green-colored areas, followed by the application of a global threshold (Figure 2) (Skiryicz et al., 2011; Arvidsson et al., 2011). The second approach converts the RGB-value into the hue, saturation, and value (HSV) parameters which allow for a direct selection of a green color region in the HSV color space, usually presented as a color cone (Walter et al., 2007). Traits determined from extracted plants include projected rosette area; leaf number; surface coverage (ratio of leaf-covered

area and the convex hull of the plant); stockiness (ratio of leaf area to the square of rosette perimeter); where surface coverage relates to the compactness of the rosette and stockiness is good parameter to extract serrated plants (Jansen et al., 2009; Pérez-pérez et al., 2011). Extracting leaf number by counting the local maxima of a distance map usually yields an underestimation of the actual number of leaves as small leaves in the center of the rosette are overlapping existing leaves, preventing the formation of an extra local maximum. Furthermore, one should keep in mind that leaf overlap in the rosette can account for a 20% reduction in measured plant area (Leister et al., 1999). Actual rosette area at final growth stages is acquired by the sum of the area of the individual leaves, which are detached from the rosettes, placed side by side and imaged. Semi-automatic image segmentation scripts assist in the analysis of these leaf series (Figure 3) (Fabre et al., 2011). Plant area detection by the extraction of green pixels has also been applied to measure and estimate leaf area and biomass in crops and to identify early wilting symptoms in tomato (Takayama and Nishina, 2007; Golzarian et al., 2011).

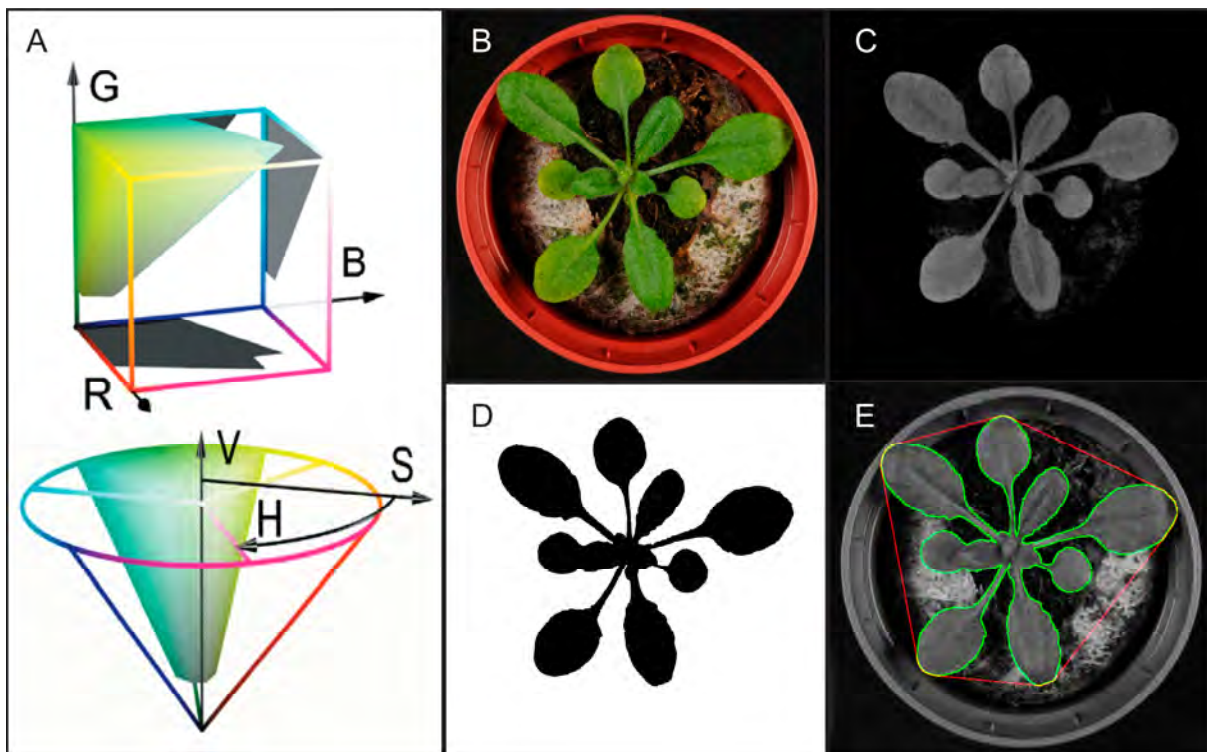


Figure 2: Extraction of plants from a background.

(A) Selection of green colors in the Red-Green-Blue (RGB) cube (above) and Hue-Saturation-Value (HSV) cone (below) (Walter et al., 2007). (B) Original picture of an Arabidopsis plant. (C) Green pixels are high-lighted by a channel weighting according to $G-(G-R+B)$. (D) Cleaned threshold image of C. A comparable image can be extracted by selecting for the following HSV values: H, 45–85; S, 110–255; V, 1–255 (Walter et al., 2007). (E) Visualization of the extracted rosette perimeter (green) and the computed convex hull (red) superimposed on the original image.

Besides for area measurements, image processing has been conducted for leaf shape analysis. General shape features are leaf length, width, roundness, asymmetry, and the perimeter to area ratio. The development of the image processing application “LeafAnalyser” allows for a rapid and large-scale analysis of leaf shape variation in several species by recording the position of evenly distributed landmarks along the leaf margin (Weight et al., 2008). Also “LAMINA” has been designed to automatically extract shape and size measurements from leaf images (Bylesjö et al., 2008). In addition, shape analysis has been useful in the automatic identification of plant species and the discrimination between weed and crops on field pictures for the development of site-specific weed management systems (Brown and Noble, 2005; Neto et al., 2006). In such studies, principal component analysis (PCA) is often used for the classification of samples based on measurements of several shape features and the application of sophisticated mathematical functions, such as elliptic fourier descriptors and the multiscale Minkowski fractal dimension, can be useful (Plotze et al., 2005; Neto et al., 2006). Next to geometric traits, also color classification can help in the identification of plant species or plant parts or in the quantification of the degree of leaf senescence (Humphries and Simonton, 1993; Rajendran et al., 2009). Finally, there are also a number of tools available to quantify venation patterns in leaves, in which the pattern extraction ranges from manual to fully-automated (Rolland-Lagan et al., 2009; Dhondt et al., 2011; Price et al., 2011). During the course of this PhD I developed one of these tools, which will be discussed in detail in Chapter 5.

Automated image analysis of individual plants is used for fundamental as well as applied research performed in growth chambers, greenhouses or in the field, and is also well introduced in the area of pre-breeding and horticulture. In the latter, objective and quantitative measurements of flower and leaf cover, color, uniformity and leaf canopy height by automated image processing are some of the traits recorded during quality assessment and grading of ornamental crops in glasshouses, not only at marketing but at all stages of production (Parsons et al., 2009). These examples show the broad and versatile application of computer vision in plant growth phenotyping.

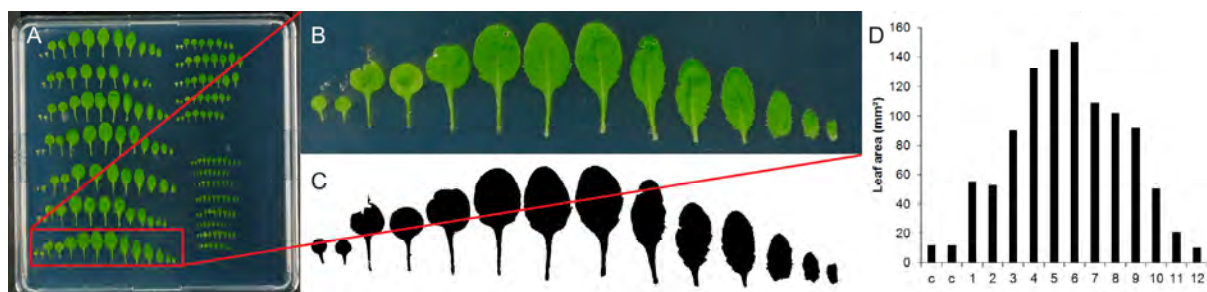


Figure 3: Arabidopsis leaf series analysis.

(A) Square plate with an agar layer on the bottom containing leaf series. (B) Selection of a single leaf series. (C) Segmentation of the individual leaves using imaging procedures comparable to Figure 2. (D) Bar chart of leaf areas measured in C. c= cotyledons. 1-12 indicate positions of true leaves.

Imaging spatial and temporal growth patterns in plant organs

Single time point measurements of plants organs can identify growth differences between genotypes or between different environmental stimuli. Nevertheless, linking the information coming from multiple time point measurements in a single plant drastically increases the resolution of the growth analysis and often reveals a more mechanistic insight into the growth phenotype. Identifying local differences in relative growth rates in growing root tips along the growth zone or within the lamina of a leaf are classic examples of a spatial analysis, whereas the observation of diel leaf growth patterns and root growth responses to environmental factors represent temporal analyses (Walter, Spies, et al., 2002; Walter et al., 2003; Walter and Schurr, 2005; Matsubara et al., 2005; Nagel et al., 2006; Wiese et al., 2007). Several image acquisition setups have been developed to accomplish spatial and temporal measurements, all including time resolved image capturing. Methods to analyze spatial and temporal growth patterns can be classified in three groups: morphometric, particle tracking and optical flow-based approaches (Walter et al., 2009).

Morphometric measurements are applied to reveal temporal growth patterns. They enable the calculation of growth rates of plant organs and include the recording of traits like root length, hypocotyl length, leaf area and projected shoot area over time. These measurements can be done manually but several computational tools include the possibility to analyze image sequences, taking away the tedious and labor-intensive nature of manual analysis. Such tools, including the imaging platforms described above, combine image segmentation procedures on the plant organ of interest with automated data extraction protocols. Software packages to analyze root growth, such as Roottrace and SmartRoot, allow for the analysis of sequences of images (French et al., 2009; Nagel et al., 2009; Lobet et al., 2011) and PlaRoM is an imaging platform with software application which can simultaneously investigate root extension profiles of up to 50 seedlings (Yazdanbakhsh and Fisahn, 2009). The same developers present a software tool to measure root growth kinetics of *Arabidopsis* by tracking root tip displacement (Yazdanbakhsh and Fisahn, 2010). Furthermore, a number of sophisticated tools have been developed to assess hypocotyl growth. HyDE (Hypocotyl Determining Engine) is a tool to automatically measure hypocotyl lengths of time-resolved image stacks of *Arabidopsis* seedlings, developed to study shade avoidance (Cole et al., 2011). After segmentation of the seedlings, the center line is calculated by identification of local maxima of a Euclidean distance transform (EDT). Hypocotyl length is measured from the base of the images to the shoot apical meristem (SAM), identified as the first local maximum in the EDT of the center line. HYPOTrace is a standalone program with graphical user interface to automatically quantify hypocotyl growth rate, apical hook opening and phototropic bending with high spatiotemporal resolution (Wang et al., 2009). Adaptive local principal component analysis is used to extract a set of midline points and weighing pixel intensity makes sure that the medial axis is not diverted at the point where the cotyledons are in close proximity. Next, a local regression algorithm helps to terminate the midline at the

hypocotyl apex. This tool shows that morphometric measurements can also be used to investigate changes in organ shape; another example is the investigation of the timing and place of gravitropic curvature along the root axis (Miller et al., 2007). Tataw and co-workers present a method for performing quantitative analysis of primordial growth in *Arabidopsis* (Tataw et al., 2010). Individual primordia are isolated from 3-D live imaging data by a contour based approach. Two vectors, representing the curvature observation along the contour and across slices, are created for each 3-D sliding window. Regions of growth are detected by analyzing eigenvalues of curvature covariance matrices. Next, a Dynamic Time Warping (DTW) Algorithm is applied to compute the rate of growth. These computational tools show that morphometric measurements can range from straightforward manual measurements to fully automated imaging procedures revealing temporal growth patterns of plant organs.

With the particle tracking approach, a discrete number of artificial landmarks is applied on the surface of the plant organ of interest. Commonly used landmarks are small ink droplets, graphite particles, and printer toner powder (Beemster and Baskin, 1998; Walter et al., 2008; Rymen et al., 2010). Also characteristic features on the plant organ, such as vein crossings, trichomes and distinctive cell walls can be used (Bengough et al., 2010). Particle tracking analysis reveals the movement of these landmarks relatively to each other. In an automated analysis, this requires the registration of the location of these landmarks and their recognition in successive images via pattern matching of the local neighborhood of these landmarks. This approach allows calculating local relative growth rates and their spatial distribution on the plant organ. Relative growth rate is in general calculated with algorithms that record pixel velocities (Schmundt et al., 1998). Kineroot, is a software application that tracks the displacement of patterns created by the graphite particles over space and time to study spatio-temporal patterns of growth and curvature in roots (Basu et al., 2007). Wang and co-workers presented a special approach of particle tracking. They designed an inkjet micropatterning system to print a grid composed of 0.19 mm² squares on small developing leaves to monitor leaf expansion in two dimensions. Tracking the displacements of the marks over time allowed identifying expansion hot spots in *Hedera helix* leaves (Wang et al., 2011). Nevertheless, calculation of longer time series of growth is difficult because the local neighborhood of each landmark changes with time (Walter et al., 2009).

The analysis of longer time series is, however, more convenient with the flow-based approach (Figure 4A). Here, the local surrounding of the landmarks needs to remain steady for only a short time frame (Figure 4B), compared to the particle tracking approach in which the same landmarks are followed throughout the time lapse. The calculations are based on a short time interval which is shifted through the dataset. The optical flow approach provides high temporal and spatial resolution and relies on the evaluation of the entire optical field (Walter et al., 2009). Any structure showing a suitable grey value contrast within its local spatio-temporal neighborhood results in an oriented streak in a virtual image stack (Figure

4C-D) (Walter, Spies, et al., 2002). Calculation of the inclination of these streaks by a structure tensor algorithm provides orientation and velocity data on the displacement of the landmarks over time (Figure 4E). Combination of moving visible landmarks renders a velocity field, which divergence allows for the extraction of local distributions in relative growth rates (Figure 4F) (Schmundt et al., 1998, 1998; Matsubara et al., 2005). Individual images are acquired with time intervals ranging from 20 seconds to 5 minutes, for roots and shoots respectively, to ensure continuous streak recording. In leaves, this approach revealed a basipetal growth rate in several species, including *Arabidopsis thaliana* and *Populus deltoides* (Walter et al., 2005; Wiese et al., 2007). A disadvantage is that the leaves have to be fixed in the focal plane of the camera, because of nyctinastic movements (curling of leaves) (Walter, Feil, et al., 2002), excluding the analysis of small and young leaves. This problem is absent in roots, and optical flow approaches revealed distributions of relative growth along the root axis of multiple species (Walter, Spies, et al., 2002; van der Weele et al., 2003; Nagel et al., 2006, 2009). RootFlowRT is a software algorithm that calculates the velocity field by combining the structure tensor and robust matching procedures (van der Weele et al., 2003). The structure tensor approach tries to find a line through a stack of images starting from a landmark in the first image, minimizing the changes in intensity (Jähne, 2005). The robust matching approach tries to match a landmark neighborhood between the first and last image (Black and Anandan, 1996). The combination of both procedures drastically increases the number of tracked landmarks, increasing the spatial resolution and statistical power of the analysis. The development and optimization of the flow-based analysis of leaf and root growth permits the mapping of relative growth rates at almost cellular resolution without measuring cells.

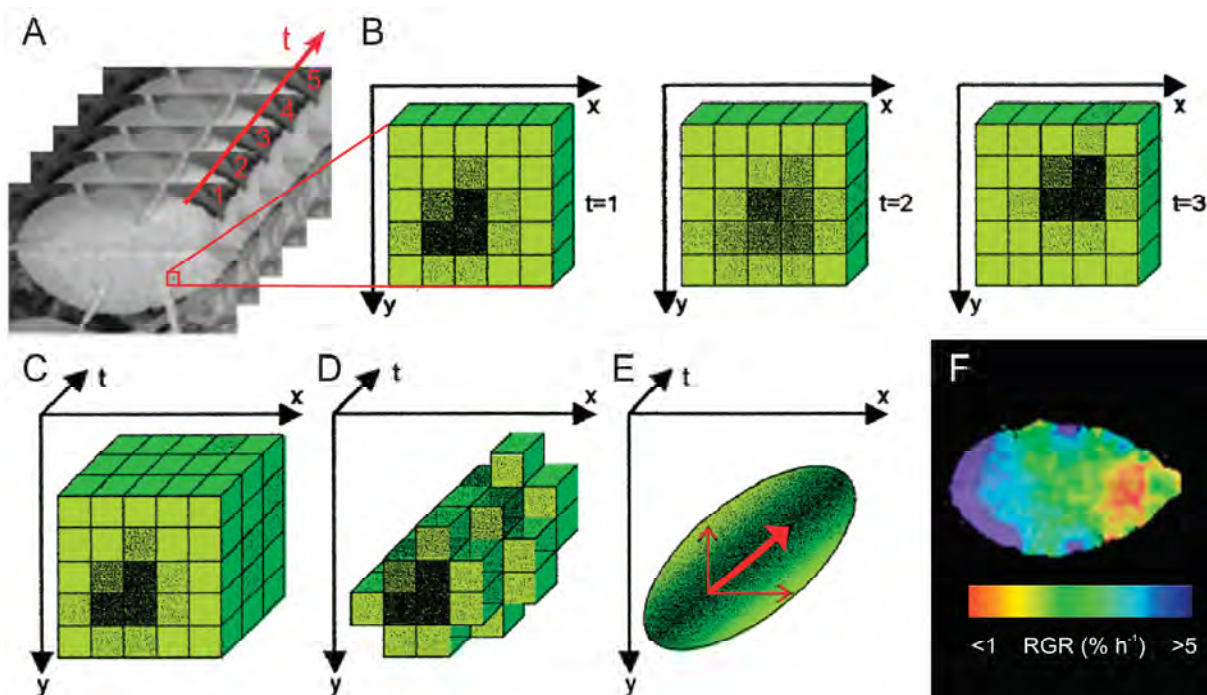


Figure 4: Analyzing spatio-temporal growth patterns using optical flow.

(A) Consecutive pictures of a leaf are captured with a short time interval. (B) Selection of a landmark from the pictures at $t=1$, $t=2$, and $t=3$, shows a moving grey value pattern. (C) Combination of the local surrounding of the selected landmark over time in a virtual image stack. (D) Extraction of a grey value structure from the virtual image stack results in an oriented grey value streak. (E) A structure tensor algorithm calculates the orientation and velocity of the displacement of the landmark based on the vector of constant brightness. (F) Representation of the local distribution of relative growth rates calculated from a velocity field rendered by combination of structure tensors of multiple landmarks (adjusted from (Walter, Spies, et al., 2002; Walter et al., 2009)).

Taken together, this section indicates that there are multiple computational tools available which can help to quantify morphological traits, such as size, shape, architecture, color, and growth pattern, of several plant organs. Nevertheless, it is clear that the majority of the software packages focuses on the analysis of roots, grown in ways that must facilitate the optical registration and increase the accessibility. Future developments should aim at analyzing plant organs in conditions as natural as possible.

MAKING THE INVISIBLE VISIBLE BY SURFING THE LIGHT SPECTRUM

Apart from the shoot and root traits visible to the human eye, which are discussed above, developments in imaging technology also support capturing plant information coming from distinct ranges within or completely outside the visible light spectrum. The combination of digital sensors, sensitive to a specific range of wavelengths, and filters, blocking part of the light before it reaches the sensor, can be used to assess both the biomass and the physiological status of a plant. When light strikes a leaf, part of the light spectrum is reflected. It is this reflected light that can be detected by sensors and that is used to extract information. The reason why the human eye observes a leaf as being green is due to the absorption of light by pigments, such as chlorophyll, which show a characteristic peak of reflection in the green region around 550 nm. Particular ranges in the electromagnetic spectrum can yield information on the water content, the nutrient status, and the stress response of plants well before any visible change is apparent (Peñuelas and Filella, 1998; Berger et al., 2010). These applications indicate the power of digital plant imaging at specific wavelengths to quantify the plant's physiological status. Moreover, it also allows anticipating to particular plant needs before color changes or wilting can be observed. Figure 5 gives an overview of the data that can be extracted from the different parts of the light spectrum.

In order to extract more information, two approaches are possible. A first approach focuses on the extraction of data from specific bands in the visible spectrum, whereas a second approach gets information from other regions in the electromagnetic spectrum, such as infrared (IR), near infrared (NIR), microwaves, and X-rays. Fluorescence imaging belongs to the first approach and can yield data on the photosynthetic performance and the chlorophyll

content of leaves. A fluorescent transient is generally measured in the 690 nm fluorescence band of dark-adapted leaves. Upon illumination, chlorophyll fluorescence has an induction kinetic with two phases: a rapid increase from the ground fluorescence (F_0) to a maximum fluorescence level (F_m), followed by a slower decline to a steady state fluorescence (F_s) with the onset of photosynthesis. The variable chlorophyll fluorescence ($F_v = F_m - F_0$) relates to the maximum capacity for photochemical quenching. The ratio F_v/F_m is used to indicate the maximum quantum efficiency of Photosystem II and is considered to be a sensitive indicator of plant photosynthetic performance (Lichtenthaler and Miehe, 1997; Peñuelas and Filella, 1998; Chaerle and Van Der Straeten, 2000). Chlorophyll content, on the other hand, is correlated to the red / far-red emission ratio. UV-laser induced fluorescence imaging, which allows capturing the fluorescence emission of the blue, green, red, and far-red spectral bands, introduced a number of new ratios which can reflect the stress status of the plant (Lichtenthaler and Miehe, 1997). Short-term stress events disturb the photosynthetic performance, whereas long-term stress events result in a decline in the chlorophyll content (Lichtenthaler and Miehe, 1997). Fluorescence imaging has been applied for the presymptomatic detection of virus and fungus infections and for revealing water stress, nutrient stress, senescence and nitrogen deficiency in plants (Lichtenthaler and Miehe, 1997; Chaerle and Van Der Straeten, 2000; Chaerle et al., 2007; Scholes and Rolfe, 2009). A notable change in photosynthetic efficiency is however only apparent under severe water stress conditions (Woo et al., 2008). The development of chlorophyll fluorescence imaging platforms allows for the detection of photosynthetic mutants or stress tolerant plants (Varotto et al., 2000; Jansen et al., 2009).

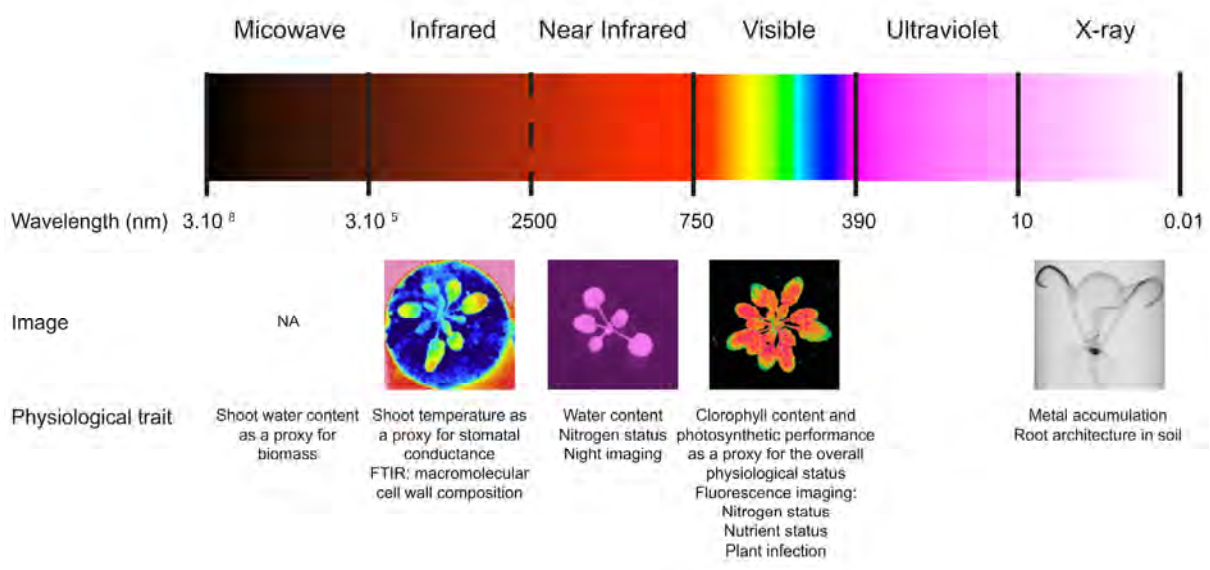


Figure 5: Overview of the applicability of different ranges in the electromagnetic spectrum for extraction of information on the physiological status of plants. Representative images are shown if available. NA = not available.

Compared to the visible spectrum, plants reflect much more light in the near infrared (NIR). More specifically, at the transition from the visible to the NIR wavelengths, there is a sharp increase in reflectance. The wavelength which coincides with the maximum change in reflectance, known as the red edge, correlates well with the chlorophyll content of the leaf (Filella and Penuelas, 1994). The high reflection of NIR light, which is mainly caused by scattering within the leaf mesophyll (Knipling, 1970), makes it the perfect application to visualize plants in the dark. NIR light emitting diodes and a digital camera without IR filter are the only requisites needed to image plants during the night in order to reveal diurnal growth patterns (Walter, Spies, et al., 2002; Walter et al., 2008). Further in the NIR spectrum, the reflection decreases by the absorption of NIR light by water present in the plant. This happens at specific water absorption bands near 1450 nm, 1930 nm and 2500 nm and can be applied to estimate the water content of the leaves as a direct readout of the plant water stress status (Knipling, 1970). Although, the current technology suffers from low sensitivity and the fact that no absolute measurements can be obtained, new developments and the incorporation of time lapse imaging sound promising (Seelig et al., 2008, 2009; Kobori and Tsuchikawa, 2009).

A more established technique to monitor the plant stress status is the use of thermal infrared imaging, or infrared thermography (IRT) to monitor leaf temperature. Plants control the transpiration stream that enables uptake of water and nutrients from the soil by regulating stomatal aperture. In case of biotic or abiotic stress, stomata close and stomatal conductance drops, resulting in decreased transpirational cooling. Hence, the leaf temperature increases upon stress perception. This phenomenon allows detecting plant stress responses by IR imaging before any visual change is apparent (Jones et al., 2002, 2009; Chaerle et al., 2007). The use of thermal cameras drastically increases the resolution and throughput, compared to temperature sensors. On the down side, measurements by thermal cameras are influenced by environmental conditions, such as air temperature, wind speed and the orientation of the leaves to the light source and the camera (Chaerle et al., 2009; Jones et al., 2009). Therefore, precise temperature measurements with thermal imaging are much more straightforward in optimized imaging setups under controlled environmental conditions (Grant et al., 2006; Sirault et al., 2009).

Further up in the electromagnetic spectrum, the use of microwaves is also introduced as a method for non-invasive plant phenotyping. The shoot water content of plants leads to a discrete shift in the centre frequency of a microwave cavity resonator and can be used as a proxy for plant biomass (Menzel et al., 2009). Finally, X-rays can reveal relative differences in the density and atomic number of materials. In plant biology, X-rays have primarily been applied to visualize in-soil grown root systems and to examine the accumulation of metals (Kim et al., 2006; Tappero et al., 2007; Tracy et al., 2010). In chapter 5, we present the use of high resolution X-ray computed tomography to visualize 3-D morphological traits and the cellular organization of plant structures (Dhondt et al., 2010).

Taken together, ranges in almost the entire electromagnetic spectrum have been screened for their applicability in the phenotyping and stress identification of plants. Future developments lie primarily in the integration of multispectral imaging, which refers to simultaneous imaging in different spectral regions (e.g. far infrared, near infrared, visual). In order to provide an early warning signal for a wide range of stress factors, a combination of the available techniques is the approach of the future (Chaerle et al., 2009). Furthermore, the application of hyperspectral imaging, which involves simultaneous measurements performed in narrow spectral bands, is also very promising. Hyperspectral imaging in the IR range is applied to examine the macromolecular chemical composition of leaf tissue by Fourier transform infrared (FTIR) microspectroscopy (Heraud et al., 2007). This technology allows for the classification and identification of *Arabidopsis* cell wall mutants (Mouille et al., 2003). In the visual – NIR range, hyperspectral reflectance imaging is a promising way to detect specific waveband signatures for a particular stress and a given plant species.

3-D IS WHERE TECHNOLOGY TAKES US

Plant shoot growth and the development of the root system are in essence processes that occur in three dimensions. Leaves originate from different sites of the SAM, branches grow in all directions, and the root system spreads out into the substrate. Nevertheless, the vast majority of the imaging tools available today extract information as 2-D images. As a result, valuable information of the plant architecture is lost in the analysis. Moreover, roots are often grown in a 2D plane, along the surface of agar in Petri dishes, in paper pouches or between transparent plates in rhizotrons (Devienne-Barret et al., 2006; Hund et al., 2009). This approach allows capturing the entire root system in a single image, but has its impact on the growth and development (Bengough et al., 2004; Hargreaves et al., 2008; Hummel et al., 2009). In the case of shoot growth analyses, images are usually captured by a top or a side-view image. This means that measurements of the projected area are underestimations of the actual area because of the overlap between leaves and the non-perpendicular orientation of leaves towards the camera. Pictures taken from multiple angles can partially account for this, but an accurate 3-D representation of the root and shoot should be the ultimate goal to perform high-fidelity measurements and to learn more about the 3-D morphology of the plant structures. On the down side, such a 3-D representation drastically complicates the data extraction. In the following, we present several techniques that can reveal information on the 3-D structure of plants, ranging from surface measurements to 3-D volume renderings (Figure 6).

Surface measurements are a first step in the extraction of spatial information from shoots. Stereoscopic approaches can be employed to calculate the morphology of surface structures from matching object patterns on images that are taken from multiple cameras or camera positions at slightly different angles (Scharf and Kusters, 2002). Stereoscopic imaging has been applied for the estimation of geometric attributes such as height and total leaf area of

single wheat seedlings (Andersen et al., 2005) and the examination of the diurnal growth cycle of isolated leaf discs (Figure 6A) (Biskup et al., 2009). Furthermore, several techniques aim to retrieve data on the distance between the plant structures and the camera position. A laser rangefinder, which is a device that uses a laser beam to determine the distance to an object, has been applied to scan the surfaces of young *Arabidopsis* plants to quantify the direction of the blade surface and epinasty of individual leaves (Figure 6B) (Kaminuma et al., 2004). A LIDAR (Light Detection And Ranging) system usually involves a laser range finder reflected by a rotating mirror. The laser scans the scene being digitized, in one or two dimensions, gathering distance measurements at specified angle intervals. The generated point cloud is used to reconstruct a 3-D model by triangulation. This technology is used to extract growth parameters at different scales, ranging from forest and canopy structure down to individual plants (Figure 6C) (Omasa et al., 2007; Hosoi et al., 2011). 3-D laser scanning is applied to 3-D reconstruction and dynamic modeling of root architecture of rice and soybean grown in a transparent cylinder (Fang et al., 2009). A time-of-flight (TOF) camera resolves distance based on the known speed of light, measuring the time-of-flight of a light signal between the camera and the subject. It is a relative recent device in which the entire scene is captured with each laser or light pulse, rather than being scanned point-by-point with a moving laser. This technology is the future for accurate and high-throughput 3-D phenotyping of plants. The systems described above allow creating depth maps of plant shoots, which facilitate the segmentation of individual leaves and optimize area measurements.

Besides these techniques, which extract morphological information based on surface measurements, there are a number of technologies available which can visualize plants by 3-D volume rendering, revealing the complete 3-D morphology instead of visualizing the plant surface facing the detector. Positron emission tomography (PET) and magnetic resonance imaging (MRI) are two non-destructive and non-invasive scanning technologies that have been applied in plant sciences to acquire 3-D structural information. PET scanning detects positron-emitting radio nuclides and can be used to measure the distribution of products labeled with unstable isotopes, such as ^{11}C -labeled photoassimilates (Figure 6D) (Jahnke et al., 2009). In plants, MRI is especially used to map and quantify water flows in xylem and phloem vessels by the nuclear magnetic resonance (NMR) of water protons, but can also be used to deliver structural information (Windt et al., 2009). In MRI images, the contrast depends on differences in water content. In 2006, optical projection tomography (OPT) was introduced as a method to capture 3-D data of primarily *ex vivo* plant specimens (Figure 6E) (Lee et al., 2006). In transmission OPT the signal depends on the amount of light absorbed by a cleared specimen. This optical technique also allows the visualization of gene expression patterns from whole-mount RNA *in situ* hybridization or GUS staining patterns. Comparable optical technology for bigger samples is used for 3-D root phenotyping (Clark et al., 2011) and small samples, such as the SAM, can also be examined by reconstruction of serial histological sections (Vanhaeren et al., 2010). High resolution X-ray computed tomography

(HRXCT) or microCT or is yet another non-destructive and minimally invasive scanning technique applied for the visualization of plant structures (Figure 6F). Here, the signal intensity depends on the attenuation of the X-rays as they pass through the sample which is correlated with the density and the atomic number of the imaged material. In Chapter 6 we present a more in depth description of the principles and application of this technology. There we also demonstrate the rapid extraction of 3-D morphological traits from *in vivo* Arabidopsis seedlings and the visualization of the cellular organization of *ex-vivo* plant tissue samples at submicron resolution (Dhondt et al., 2010). Furthermore, microCT, MRI, and PET all allow visualizing root architecture in soil, but microCT imaging is currently reaching the highest resolution (Tracy et al., 2010; Beer et al., 2010; Hillnhütter et al., 2011).

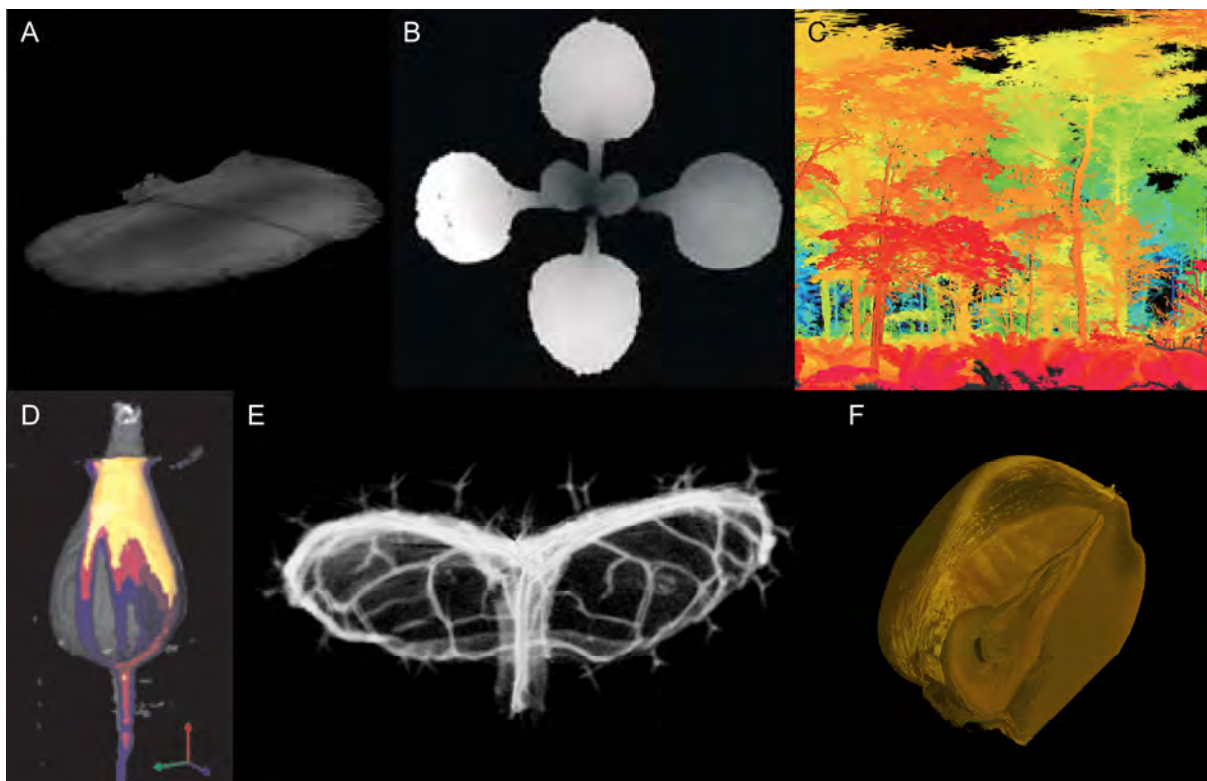


Figure 6: 3-D imaging methods. (A) Reconstruction of a leaf disc captured with stereoscopic imaging (Biskup et al., 2009). (B) A range image on an Arabidopsis seedling produced by a laser rangefinder. Pixel intensity indicates the depth of the object (Kaminuma et al., 2004). (C) False-colour image of a Japanese larch forest measured using a ground-based scanning lidar system. The color range shows the distance from the lidar (Omasa et al., 2007). (D) 3-D reconstruction of a radish bulb. ^{11}C -labeled photoassimilates captured with PET (color) are superposed on the morphological structure captured with MRI (grey) (Jahnke et al., 2009). (E) 3-D reconstruction of a cleared Arabidopsis leaf at 22 DAS scanned with OPT technology. Note the trichomes on the adaxial leaf surface. (F) 3-D reconstruction of a maize grain scanned with microCT technology, showing a cross section through the seed embryo.

Visualizations of 3-D volume renderings obtained by the techniques described above look very appealing, but the primary objective should be the extraction of additional morphological information. Recording volume and surface area of 3-D objects is relatively straightforward, but defining shoot and root branching patterns and leaf blade area or the characterization of shape variables is a challenge, requiring high-level image processing. One example is the segmentation of cells in an *Arabidopsis* hypocotyl (Dhondt et al., 2010). Recording 3-D coordinates by the manual placement of landmarks on the 3-D object can be used to extract shape information (van der Niet et al., 2010). Furthermore, detailed 3-D renderings are very suited to digitize morphological features of biological structures to be used as a template for dynamic modeling approaches (Cresswell et al., 2007; Green et al., 2010). Future imaging challenges lie also in the combination of imaging technologies including the superposition of 3-D measurements. A nice example is the combination of PET and MRI data to reveal transport routes and the translocation dynamics of recently fixed photoassimilates in sugar beet and radish (Jahnke et al., 2009).

CONCLUSIONS AND FUTURE PERSPECTIVES

In this introduction I reviewed the available image acquisition technologies and automated image analysis tools. Such tools can ensure a fast and precise phenotypic description of plant structures, limiting laborious, costly, and often repetitive manual intervention. Furthermore, in comparison to manual screening experiments, often more phenotypic measurements are recorded. High-precision measurements of multiple traits can lead to the discovery of subtle phenotypes, not prominent to the human eye. Functional analyses yielding the disappointing result of “no visible phenotype” are often attributed to functional redundancy, but can also be explained by inadequate detection methods. Future evolutions must further focus on the development of imaging applications useful for the scientific community, which are of greater value compared to in-house analyses. Of course, this requires the programming of a graphical user interface and usually asks for some flexibility in the input images. Furthermore, a non-expert user must be able to access and interpret the image-derived phenotypic data without prior knowledge of the image analysis procedures (Berger et al., 2010). Larger screens focus on throughput, whereas small scale scientific experiments ask for precision. This is why imaging tools for the scientific community should not be designed as a data generating black box. Moreover, one should realize that imaging algorithms often do not implement enough knowledge to cover all possible variability. A visual control of the analysis is a first requisite, but a semi-automated approach with an interface which allows for minor manual corrections to the automatic segmentation is desirable (Dhondt et al., 2011).

Shoots are often imaged to extract growth parameters, but advances in imaging technology make it affordable to image the physiological status of the plant. Infrared thermography, near-infrared imaging, and chlorophyll fluorescence reveal physiological changes and plant stress responses well before any visible change is apparent. Such image acquisition

technology is currently often incorporated in high-throughput plant phenotyping setups (Hartmann et al., 2011). Even a bigger range of imaging tools is available to study root growth parameters and root structure architecture and the application of microCT, PET, and MRI imaging show the astonishing possibility of visualizing 3-D root architecture in soil. 3-D representation of shoots is also feasible with this technology, but is more straightforward by distance measurements. Computer modeling can help to rebuild sophisticated structures such as trees (Livny et al., 2010). Future efforts should concentrate on extracting morphological phenotypic data from 3-D reconstructions. Furthermore, one should not underestimate how 3-D imaging is posing increasing demands on data processing and storage. Upcoming challenges lie also in the combination of different imaging technologies. A progressive example is using combined range and chlorophyll fluorescence imaging for testing the effects of herbicides on plants (Konishi et al., 2009). Moreover, one should realize that cellular observations are key to understand the nature of growth differences and that knowledge on cell division and cell expansion processes are crucial to obtain a mechanistic view on how molecular changes can lead to observed growth phenomena. Live imaging and automated cell tracking are recent technologies that provide further insight in the cellular mechanisms controlling growth.

Overall, it is apparent that the majority of the imaging tools are developed on the model species *Arabidopsis*. Nevertheless, the objective is to bring the imaging knowledge to the crop level, where it can be integrated to screen for high-yielding and stress resistant germplasm. Gene discovery must be scaled from the biological process, through the cellular dynamics, to the growth response on the organ and plant level, to its effect on canopy structure and field crops. Plant phenomics, with automated and high-throughput plant growth imaging as its major pillar, has the potential to make a large contribution to the demanding increase in crop productivity, by acceleration of the high-precision phenotyping process. Nevertheless, imaging should be considered as a tool, and a general effort is needed to correlate gene function, plant performance, and environmental response, in order to ensure food security in a world that is facing several major challenges.

REFERENCES

- Anastasiou, E., Kenz, S., Gerstung, M., MacLean, D., Timmer, J., Fleck, C., and Lenhard, M.** (2007) Control of plant organ size by *KLUH/CYP78A5*-dependent intercellular signaling. *Developmental Cell*, **13**, 843-856.
- Andersen, H.J., Reng, L., and Kirk, K.** (2005) Geometric plant properties by relaxed stereo vision using simulated annealing. *Computers and Electronics in Agriculture*, **49**, 219-232.
- Andriankaja, M., Dhondt, S., De Bodt, S., Vanhaeren, H., Coppens, F., De Milde, L., Mühlenbock, P., Skiryecz, A., Gonzalez, N., Beemster, G.T.S., and Inzé, D.** (2011) Exit

from proliferation during leaf development in *Arabidopsis thaliana*: a not so gradual process. *Dev Cell*, **22**, 64-78.

Arabidopsis Genome Initiative (2000) Analysis of the genome sequence of the flowering plant *Arabidopsis thaliana*. *Nature*, **408**, 796-815.

Armengaud, P., Zambaux, K., Hills, A., Sulpice, R., Pattison, R.J., Blatt, M.R., and Amtmann, A. (2009) EZ-Rhizo: integrated software for the fast and accurate measurement of root system architecture. *The Plant Journal*, **57**, 945-956.

Arvidsson, S., Pérez-Rodríguez, P., and Mueller-Roeber, B. (2011) A growth phenotyping pipeline for *Arabidopsis thaliana* integrating image analysis and rosette area modeling for robust quantification of genotype effects. *New Phytologist*, **191**, 895-907.

Barbier de Reuille, P., Bohn-Courseau, I., Godin, C., and Traas, J. (2005) A protocol to analyse cellular dynamics during plant development. *The Plant Journal*, **44**, 1045-1053.

Basu, P., Pal, A., Lynch, J.P., and Brown, K.M. (2007) A novel image-analysis technique for kinematic study of growth and curvature. *Plant Physiology*, **145**, 305 -316.

Beemster, G.T.S. and Baskin, T.I. (1998) Analysis of cell division and elongation underlying the developmental acceleration of root growth in *Arabidopsis thaliana*. *Plant Physiol*, **116**, 1515-1526.

Beemster, G.T.S., Fiorani, F., and Inzé, D. (2003) Cell cycle: the key to plant growth control? *Trends in Plant Science*, **8**, 154-158.

Beer, S., Streun, M., Hombach, T., Buehler, J., Jahnke, S., Khodaverdi, M., Larue, H., Minwuyelet, S., Parl, C., Roeb, G., Schurr, U., and Ziemons, K. (2010) Design and initial performance of PlanTIS: a high-resolution positron emission tomograph for plants. *Phys. Med. Biol.*, **55**, 635-646.

Bengough, A.G., Bransby, M.F., Hans, J., McKenna, S.J., Roberts, T.J., and Valentine, T.A. (2006) Root responses to soil physical conditions; growth dynamics from field to cell. *Journal of Experimental Botany*, **57**, 437 -447.

Bengough, A.G., Gordon, D.C., Al-Menaie, H., Ellis, R.P., Allan, D., Keith, R., Thomas, W.T.B., and Forster, B.P. (2004) Gel observation chamber for rapid screening of root traits in cereal seedlings. *Plant and Soil*, **262**, 63-70.

Bengough, A.G., Hans, J., Bransby, M.F., and Valentine, T.A. (2010) PIV as a method for quantifying root cell growth and particle displacement in confocal images. *Microscopy Research and Technique*, **73**, 27-36.

- Berger, B., Parent, B., and Tester, M.** (2010) High-throughput shoot imaging to study drought responses. *Journal of Experimental Botany*, **61**, 3519 -3528.
- Biskup, B., Scharr, H., Fischbach, A., Wiese-Klinkenberg, A., Schurr, U., and Walter, A.** (2009) Diel growth cycle of isolated leaf discs analyzed with a novel, high-throughput three-dimensional imaging method is identical to that of intact leaves. *Plant Physiology*, **149**, 1452 -1461.
- Black, M. and Anandan, P.** (1996) The robust estimation of multiple motions: parametric and piecewise-smooth flow fields. *Computer Vision and Image Understanding*, **63**, 75-104.
- Le Bot, J., Serra, V., Fabre, J., Draye, X., Adamowicz, S., and Pagès, L.** (2009) DART: a software to analyse root system architecture and development from captured images. *Plant Soil*, **326**, 261-273.
- Brown, R.B. and Noble, S.D.** (2005) Site-specific weed management: sensing requirements— what do we need to see? *Weed Science*, **53**, 252-258.
- Bylesjö, M., Segura, V., Soolanayakanahally, R.Y., Rae, A.M., Trygg, J., Gustafsson, P., Jansson, S., and Street, N.R.** (2008) LAMINA: a tool for rapid quantification of leaf size and shape parameters. *BMC Plant Biol*, **8**, 82-82.
- Campilho, A., Garcia, B., Toorn, H. v. d, Wijk, H. v, Campilho, A., and Scheres, B.** (2006) Time-lapse analysis of stem-cell divisions in the *Arabidopsis thaliana* root meristem. *The Plant Journal*, **48**, 619-627.
- Chaerle, L. and Van Der Straeten, D.** (2000) Imaging techniques and the early detection of plant stress. *Trends in Plant Science*, **5**, 495-501.
- Chaerle, L., Leinonen, I., Jones, H.G., and Van Der Straeten, D.** (2007) Monitoring and screening plant populations with combined thermal and chlorophyll fluorescence imaging. *Journal of Experimental Botany*, **58**, 773 -784.
- Chaerle, L., Lenk, S., Leinonen, I., Jones, H.G., Van Der Straeten, D., and Buschmann, C.** (2009) Multi-sensor plant imaging: Towards the development of a stress-catalogue. *Biotechnology Journal*, **4**, 1152-1167.
- Chickarmane, V., Roeder, A.H.K., Tarr, P.T., Cunha, A., Tobin, C., and Meyerowitz, E.M.** (2010) Computational morphodynamics: A modeling framework to understand plant growth. *Annu. Rev. Plant Biol.*, **61**, 65-87.
- Christensen, S.** (2010) Agarose imprints of plant cell surfaces for imaging. *Cold Spring Harb Protoc*, **2010**, pdb.prot4932.

- Clark, R.T., MacCurdy, R.B., Jung, J.K., Shaff, J.E., McCouch, S.R., Aneshansley, D.J., and Kochian, L.V.** (2011) Three-dimensional root phenotyping with a novel imaging and software platform. *Plant Physiol*, **156**, 455-465.
- Cole, B., Kay, S.A., and Chory, J.** (2011) Automated analysis of hypocotyl growth dynamics during shade avoidance in Arabidopsis. *The Plant Journal*, **65**, 991-1000.
- Cresswell, J.E., Henning, K., Pennel, C., Lahoubi, M., Patrick, M.A., Young, P.G., and Tabor, G.R.** (2007) Conifer ovulate cones accumulate pollen principally by simple impaction. *P Natl Acad Sci USA*, **104**, 18141-18144.
- Devienne-Barret, F., Richard-Molard, C., Chelle, M., Maury, O., and Ney, B.** (2006) Ara-Rhizotron: An effective culture system to study simultaneously root and shoot development of Arabidopsis. *Plant and Soil*, **280**, 253-266.
- Dhondt, S., Van Haerenborgh, D., Van Cauwenbergh, C., Merks, R.M.H., Philips, W., Beemster, G.T.S., and Inzé, D.** (2011) Quantitative analysis of venation patterns of Arabidopsis leaves by supervised image analysis. *The Plant Journal*, **in press**.
- Dhondt, S., Vanhaeren, H., Van Loo, D., Cnudde, V., and Inzé, D.** (2010) Plant structure visualization by high-resolution X-ray computed tomography. *Trends Plant Sci*, **15**, 419-422.
- Donnelly, P.M., Bonetta, D., Tsukaya, H., Dengler, R.E., and Dengler, N.G.** (1999) Cell cycling and cell enlargement in developing leaves of Arabidopsis. *Dev Biol*, **215**, 407-419.
- EI-Lithy, M.E., Clerckx, E.J.M., Ruys, G.J., Koornneef, M., and Vreugdenhil, D.** (2004) Quantitative trait locus analysis of growth-related traits in a new Arabidopsis recombinant inbred population. *Plant Physiol*, **135**, 444-458.
- Erickson, R.O. and Sax, K.B.** (1956a) Rates of cell division and cell elongation in the growth of the primary root of *Zea mays*. *Proceedings of the American Philosophical Society*, **100**, 499-514.
- Erickson, R.O. and Sax, K.B.** (1956b) Elemental growth rate of the primary root of *Zea mays*. *Proceedings of the American Philosophical Society*, **100**, 487-498.
- Eriksson, S., Stransfeld, L., Adamski, N.M., Breuninger, H., and Lenhard, M.** (2010) KLUH/CYP78A5-dependent growth signaling coordinates floral organ growth in Arabidopsis. *Current Biology*, **20**, 527-532.
- Fabre, J., Dauzat, M., Nègre, V., Wuyts, N., Tireau, A., Gennari, E., Neveu, P., Tisné, S., Massonnet, C., Hummel, I., and Granier, C.** (2011) PHENOPSIS DB: an Information System for *Arabidopsis thaliana* phenotypic data in an environmental context. *BMC Plant Biol*, **11**, 77.

- Fang, S., Yan, X., and Liao, H.** (2009) 3D reconstruction and dynamic modeling of root architecture in situ and its application to crop phosphorus research. *The Plant Journal*, **60**, 1096-1108.
- Ferjani, A., Horiguchi, G., Yano, S., and Tsukaya, H.** (2007) Analysis of leaf development in fugu mutants of Arabidopsis reveals three compensation modes that modulate cell expansion in determinate organs. *Plant Physiology*, **144**, 988 -999.
- Fernandez, R., Das, P., Mirabet, V., Moscardi, E., Traas, J., Verdeil, J.-L., Malandain, G., and Godin, C.** (2010) Imaging plant growth in 4D: robust tissue reconstruction and lineaging at cell resolution. *Nat Meth*, **7**, 547-553.
- Filella, I. and Penuelas, J.** (1994) The red edge position and shape as indicators of plant chlorophyll content, biomass and hydric status. *International Journal of Remote Sensing*, **15**, 1459-1470.
- Finkel, E.** (2009) With "phenomics," plant scientists hope to shift breeding into overdrive. *Science*, **325**, 380 -381.
- Fiorani, F. and Beemster, G.T.S.** (2006) Quantitative analyses of cell division in plants. *Plant Mol Biol*, **60**, 963-979.
- French, A., Ubeda-Tomás, S., Holman, T.J., Bennett, M.J., and Pridmore, T.** (2009) High-throughput quantification of root growth using a novel image-analysis tool. *Plant Physiology*, **150**, 1784 -1795.
- Furbank, R.T.** (2009) Foreword: Plant phenomics: from gene to form and function. *Functional Plant Biol.*, **36**, v-vi.
- Furbank, R.T., von Caemmerer, S., Sheehy, J., and Edwards, G.** (2009) C4 rice: a challenge for plant phenomics. *Funct. Plant Biol.*, **36**, 845-856.
- Furbank, R.T. and Tester, M.** (2011) Phenomics – technologies to relieve the phenotyping bottleneck. *Trends in Plant Science*, **16**, 635-644.
- Geisler, M., Nadeau, J., and Sack, F.D.** (2000) Oriented Asymmetric Divisions That Generate the Stomatal Spacing Pattern in Arabidopsis Are Disrupted by the too many mouths Mutation. *Plant Cell*, **12**, 2075-2086.
- Golzarian, M.R., Frick, R.A., Rajendran, K., Berger, B., Roy, S., Tester, M., and Lun, D.S.** (2011) Accurate inference of shoot biomass from high-throughput images of cereal plants. *Plant Methods*, **7**, 2.

Goodwin, R.H. and Stepka, W. (1945) Growth and differentiation in the root tip of *Phleum pratense*. *American Journal of Botany*, **32**, 36-46.

Granier, C., Aguirrezabal, L., Chenu, K., Cookson, S.J., Dauzat, M., Hamard, P., Thioux, J., Rolland, G., Bouchier-Combaud, S., Lebaudy, A., Muller, B., Simonneau, T., and Tardieu, F. (2006) PHENOPSIS, an automated platform for reproducible phenotyping of plant responses to soil water deficit in *Arabidopsis thaliana* permitted the identification of an accession with low sensitivity to soil water deficit. *New Phytologist*, **169**, 623-635.

Granier, C. and Tardieu, F. (1998) Spatial and temporal analyses of expansion and cell cycle in sunflower leaves. *Plant Physiology*, **116**, 991 -1001.

Grant, O.M., Chaves, M.M., and Jones, H.G. (2006) Optimizing thermal imaging as a technique for detecting stomatal closure induced by drought stress under greenhouse conditions. *Physiologia Plantarum*, **127**, 507-518.

Green, A.A., Kennaway, J.R., Hanna, A.I., Bangham, J.A., and Coen, E. (2010) Genetic control of organ shape and tissue polarity. *PLoS Biol*, **8**, e1000537.

Green, P.B. (1976) Growth and cell pattern formation on an axis: critique of concepts, terminology, and modes of study. *Botanical Gazette*, **137**, 187-202.

Hargreaves, C.E., Gregory, P.J., and Bengough, A.G. (2008) Measuring root traits in barley (*Hordeum vulgare* ssp. *vulgare* and ssp. *spontaneum*) seedlings using gel chambers, soil sacs and X-ray microtomography. *Plant Soil*, **316**, 285-297.

Harrison, C.J., Roeder, A.H.K., Meyerowitz, E.M., and Langdale, J.A. (2009) Local cues and asymmetric cell divisions underpin body plan transitions in the moss *Physcomitrella patens*. *Current Biology*, **19**, 461-471.

Hartmann, A., Czauderna, T., Hoffmann, R., Stein, N., and Schreiber, F. (2011) HTPPheno: An image analysis pipeline for high-throughput plant phenotyping. *BMC Bioinformatics*, **12**, 148.

Heisler, M.G., Ohno, C., Das, P., Sieber, P., Reddy, G.V., Long, J.A., and Meyerowitz, E.M. (2005) Patterns of auxin transport and gene expression during primordium development revealed by live imaging of the *Arabidopsis* inflorescence meristem. *Current Biology*, **15**, 1899-1911.

Heraud, P., Caine, S., Sanson, G., Gleadow, R., Wood, B.R., and McNaughton, D. (2007) Focal plane array infrared imaging: a new way to analyse leaf tissue. *New Phytologist*, **173**, 216-225.

Hillnhütter, C., Sikora, R.A., Oerke, E.-C., and van Dusschoten, D. (2011) Nuclear magnetic resonance: a tool for imaging belowground damage caused by *Heterodera schachtii* and *Rhizoctonia solani* on sugar beet. *Journal of Experimental Botany*, in press.

Horiguchi, G., Kim, G., and Tsukaya, H. (2005) The transcription factor AtGRF5 and the transcription coactivator AN3 regulate cell proliferation in leaf primordia of *Arabidopsis thaliana*. *The Plant Journal*, **43**, 68-78.

Hosoi, F., Nakabayashi, K., and Omasa, K. (2011) 3-D modeling of tomato canopies using a high-resolution portable scanning lidar for extracting structural information. *Sensors*, **11**, 2166-2174.

Hummel, G.M., Schurr, U., Baldwin, I.T., and Walter, A. (2009) Herbivore-induced jasmonic acid bursts in leaves of *Nicotiana attenuata* mediate short-term reductions in root growth. *Plant, Cell & Environment*, **32**, 134-143.

Humphries, S. and Simonton, W. (1993) Identification of plant parts using color and geometric image data. *Transactions of the ASABE*, **36**, 1493-1500.

Hund, A., Trachsel, S., and Stamp, P. (2009) Growth of axile and lateral roots of maize: I development of a phenotyping platform. *Plant Soil*, **325**, 335-349.

Ichikawa, T., Nakazawa, M., Kawashima, M., Iizumi, H., Kuroda, H., Kondou, Y., Tsubara, Y., Suzuki, K., Ishikawa, A., Seki, M., Fujita, M., Motohashi, R., Nagata, N., Takagi, T., Shinozaki, K., et al. (2006) The FOX hunting system: an alternative gain-of-function gene hunting technique. *The Plant Journal*, **48**, 974-985.

Iyer-Pascuzzi, A.S., Symonova, O., Mileyko, Y., Hao, Y., Belcher, H., Harer, J., Weitz, J.S., and Benfey, P.N. (2010) Imaging and analysis platform for automatic phenotyping and trait ranking of plant root systems. *Plant Physiology*, **152**, 1148 -1157.

Jähne, B. (2005) Digital image processing (Springer: Berlin).

Jahnke, S., Menzel, M.I., Van Dusschoten, D., Roeb, G.W., Bühler, J., Minwuyelet, S., Blümner, P., Temperton, V.M., Hombach, T., Streun, M., Beer, S., Khodaverdi, M., Ziemons, K., Coenen, H.H., and Schurr, U. (2009) Combined MRI–PET dissects dynamic changes in plant structures and functions. *The Plant Journal*, **59**, 634-644.

Jansen, M., Gilmer, F., Biskup, B., Nagel, K.A., Rascher, U., Fischbach, A., Briem, S., Dreissen, G., Tittmann, S., Braun, S., De Jaeger, I., Metzlauff, M., Schurr, U., Scharr, H., and Walter, A. (2009) Simultaneous phenotyping of leaf growth and chlorophyll fluorescence via GROWSCREEN FLUORO allows detection of stress tolerance in *Arabidopsis thaliana* and other rosette plants. *Funct. Plant Biol.*, **36**, 902-914.

- Jones, H.G., Serraj, R., Loveys, B.R., Xiong, L., Wheaton, A., and Price, A.H.** (2009) Thermal infrared imaging of crop canopies for the remote diagnosis and quantification of plant responses to water stress in the field. *Funct. Plant Biol.*, **36**, 978-989.
- Jones, H.G., Stoll, M., Santos, T., Sousa, C. de, Chaves, M.M., and Grant, O.M.** (2002) Use of infrared thermography for monitoring stomatal closure in the field: application to grapevine. *Journal of Experimental Botany*, **53**, 2249 -2260.
- Kaminuma, E., Heida, N., Tsumoto, Y., Yamamoto, N., Goto, N., Okamoto, N., Konagaya, A., Matsui, M., and Toyoda, T.** (2004) Automatic quantification of morphological traits via three-dimensional measurement of Arabidopsis. *The Plant Journal*, **38**, 358-365.
- Kaplan, D.R.** (1992) The relationship of cells to organisms in plants: problem and implications of an organismal perspective. *International Journal of Plant Sciences*, **153**, S28-S37.
- Kawade, K., Horiguchi, G., and Tsukaya, H.** (2010) Non-cell-autonomously coordinated organ size regulation in leaf development. *Development*, **137**, 4221-4227.
- Kheibarshekan Asi, L., Dhondt, S., Boudolf, V., Beemster, G.T.S., Beeckman, T., Inzé, D., Govaerts, W., and De Veylder, L.** (2011) Model-based analysis of Arabidopsis leaf epidermal cells reveals distinct division and expansion patterns for pavement and guard cells. *Plant Physiology*, **156**, 2172 -2183.
- Kim, S.A., Punshon, T., Lanzirrotti, A., Li, L., Alonso, J.M., Ecker, J.R., Kaplan, J., and Gueriot, M.L.** (2006) Localization of iron in Arabidopsis seed requires the vacuolar membrane transporter VIT1. *Science*, **314**, 1295-1298.
- Knipling, E.B.** (1970) Physical and physiological basis for the reflectance of visible and near-infrared radiation from vegetation. *Remote Sensing of Environment*, **1**, 155-159.
- Kobori, H. and Tsuchikawa, S.** (2009) Prediction of water content in *Ligustrum japonicum* leaf using near infrared chemometric imaging. *J. Near Infrared Spectrosc.*, **17**, 151.
- Konishi, A., Eguchi, A., Hosoi, F., and Omasa, K.** (2009) 3D monitoring spatio-temporal effects of herbicide on a whole plant using combined range and chlorophyll a fluorescence imaging. *Funct. Plant Biol.*, **36**, 874-879.
- Kuromori, T., Takahashi, S., Kondou, Y., Shinozaki, K., and Matsui, M.** (2009) Phenome analysis in plant species using loss-of-function and gain-of-function mutants. *Plant and Cell Physiology*, **50**, 1215 -1231.

- Kwiatkowska, D.** (2004) Surface growth at the reproductive shoot apex of *Arabidopsis thaliana* pin-formed 1 and wild type. *Journal of Experimental Botany*, **55**, 1021 -1032.
- Kwiatkowska, D.** (2006) Flower primordium formation at the Arabidopsis shoot apex: quantitative analysis of surface geometry and growth. *Journal of Experimental Botany*, **57**, 571 -580.
- Kwiatkowska, D. and Routier-Kierzkowska, A.-L.** (2009) Morphogenesis at the inflorescence shoot apex of *Anagallis arvensis*: surface geometry and growth in comparison with the vegetative shoot. *Journal of Experimental Botany*, **60**, 3407 -3418.
- Lee, K., Avondo, J., Morrison, H., Blot, L., Stark, M., Sharpe, J., Bangham, A., and Coen, E.** (2006) Visualizing Plant Development and Gene Expression in Three Dimensions Using Optical Projection Tomography. *Plant Cell*, **18**, 2145-2156.
- Leister, D., Varotto, C., Pesaresi, P., Niwergall, A., and Salamini, F.** (1999) Large-scale evaluation of plant growth in *Arabidopsis thaliana* by non-invasive image analysis. *Plant Physiology and Biochemistry*, **37**, 671-678.
- Lichtenthaler, H.K. and Miehe, J.A.** (1997) Fluorescence imaging as a diagnostic tool for plant stress. *Trends in Plant Science*, **2**, 316-320.
- Lister, C. and Dean, C.** (1993) Recombinant inbred lines for mapping RFLP and phenotypic markers in *Arabidopsis thaliana*. *The Plant Journal*, **4**, 745-750.
- Liu, M., Yadav, R.K., Roy-Chowdhury, A., and Reddy, G.V.** (2010) Automated tracking of stem cell lineages of *Arabidopsis* shoot apex using local graph matching. *The Plant Journal*, **62**, 135-147.
- Livny, Y., Yan, F., Olson, M., Chen, B., Zhang, H., and Sana, J.** (2010) Automatic reconstruction of tree skeletal structures from point clouds. In ACM SIGGRAPH Asia 2010 papers (ACM: Seoul, South Korea).
- Lobet, G., Pagès, L., and Draye, X.** (2011) A novel image-analysis toolbox enabling quantitative analysis of root system architecture. *Plant Physiology*, **157**, 29 -39.
- Marcuzzo, M., Guichard, T., Quelhas, P., Mendonça, A.M., and Campilho, A.** (2009) Cell division detection on the *Arabidopsis thaliana* root. In Pattern Recognition and Image Analysis, H. Araujo, A.M. Mendonça, A.J. Pinho, and M.I. Torres, eds (Springer Berlin Heidelberg: Berlin, Heidelberg), pp. 168-175.

- Marcuzzo, M., Quelhas, P., Campilho, A., Mendonça, A.M., and Campilho, A.** (2009) Automated Arabidopsis plant root cell segmentation based on SVM classification and region merging. *Computers in Biology and Medicine*, **39**, 785-793.
- Mathur, J. and Koncz, C.** (1997) Method for preparation of epidermal imprints using agarose. *BioTechniques*, **22**, 280-282.
- Matsubara, S., Hurry, V., Druart, N., Benedict, C., Janzik, I., Chavarría-Krauser, A., Walter, A., and Schurr, U.** (2005) Nocturnal changes in leaf growth of *Populus deltoides* are controlled by cytoplasmic growth. *Planta*, **223**, 1315-1328.
- Menzel, M.I., Tittmann, S., Bühler, J., Preis, S., Wolters, N., Jahnke, S., Walter, A., Chlubek, A., Leon, A., Hermes, N., Offenhäuser, A., Glimmer, F., Blümler, P., Schurr, U., and Krause, H.-J.** (2009) Non-invasive determination of plant biomass with microwave resonators. *Plant, Cell & Environment*, **32**, 368-379.
- Miller, N.D., Parks, B.M., and Spalding, E.P.** (2007) Computer-vision analysis of seedling responses to light and gravity. *The Plant Journal*, **52**, 374-381.
- Mouille, G., Robin, S., Lecomte, M., Pagant, S., and Höfte, H.** (2003) Classification and identification of Arabidopsis cell wall mutants using Fourier-Transform InfraRed (FT-IR) microspectroscopy. *The Plant Journal*, **35**, 393-404.
- Mühlich, M., Truhn, D., Nagel, K., Walter, A., Scharr, H., and Aach, T.** (2008) Measuring plant root growth. In Pattern Recognition, G. Rigoll, ed (Springer Berlin Heidelberg: Berlin, Heidelberg), pp. 497-506.
- Naeem, A., French, A.P., Wells, D.M., and Pridmore, T.P.** (2011) High-throughput feature counting and measurement of roots. *Bioinformatics*, **27**, 1337 -1338.
- Nagel, K.A., Kastenholz, B., Jahnke, S., van Dusschoten, D., Aach, T., Mühlich, M., Truhn, D., Scharr, H., Terjung, S., Walter, A., and Schurr, U.** (2009) Temperature responses of roots: impact on growth, root system architecture and implications for phenotyping. *Funct. Plant Biol.*, **36**, 947-959.
- Nagel, K.A., Schurr, U., and Walter, A.** (2006) Dynamics of root growth stimulation in *Nicotiana tabacum* in increasing light intensity. *Plant, Cell & Environment*, **29**, 1936-1945.
- Neto, J.C., Meyer, G.E., Jones, D.D., and Samal, A.K.** (2006) Plant species identification using Elliptic Fourier leaf shape analysis. *Computers and Electronics in Agriculture*, **50**, 121-134.

- van der Niet, T., Zollikofer, C.P.E., León, M.S.P. de, Johnson, S.D., and Linder, H.P.** (2010) Three-dimensional geometric morphometrics for studying floral shape variation. *Trends in Plant Science*, **15**, 423-426.
- Nordborg, M., Hu, T.T., Ishino, Y., Jhaveri, J., Toomajian, C., Zheng, H., Bakker, E., Calabrese, P., Gladstone, J., Goyal, R., Jakobsson, M., Kim, S., Morozov, Y., Padhukasahasram, B., Plagnol, V., et al.** (2005) The pattern of polymorphism in *Arabidopsis thaliana*. *PLoS Biol*, **3**, e196.
- O'Malley, R.C. and Ecker, J.R.** (2010) Linking genotype to phenotype using the Arabidopsis unimutant collection. *The Plant Journal*, **61**, 928-940.
- Omasa, K., Hosoi, F., and Konishi, A.** (2007) 3D lidar imaging for detecting and understanding plant responses and canopy structure. *Journal of Experimental Botany*, **58**, 881 -898.
- Parsons, N.R., Edmondson, R.N., and Song, Y.** (2009) Image analysis and statistical modelling for measurement and quality assessment of ornamental horticulture crops in glasshouses. *Biosystems Engineering*, **104**, 161-168.
- Peñuelas, J. and Filella, I.** (1998) Visible and near-infrared reflectance techniques for diagnosing plant physiological status. *Trends in Plant Science*, **3**, 151-156.
- Pérez-pérez, J.M., Rubio-díaz, S., Dhondt, S., Hernández-romero, D., Sánchez-soriano, J., Beemster, G.T.S., Ponce, M.R., and Micol, J.L.** (2011) Whole organ, venation and epidermal cell morphological variations are correlated in the leaves of Arabidopsis mutants. *Plant, Cell & Environment*, **34**, 2200-2211.
- Plotze, R. de O., Falvo, M., Pádua, J.G., Bernacci, L.C., Vieira, M.L.C., Oliveira, G.C.X., and Bruno, O.M.** (2005) Leaf shape analysis using the multiscale Minkowski fractal dimension, a new morphometric method: a study with *Passiflora* (Passifloraceae). *Can. J. Bot.*, **83**, 287-301.
- Price, C.A., Symonova, O., Mileyko, Y., Hilley, T., and Weitz, J.S.** (2011) Leaf extraction and analysis framework graphical user interface: segmenting and analyzing the structure of leaf veins and areoles. *Plant Physiol*, **155**, 236-245.
- Qi, X., Qi, J., and Wu, Y.** (2007) RootLM: a simple color image analysis program for length measurement of primary roots in Arabidopsis. *Plant Root*, **1**, 10-16.
- Rajendran, K., Tester, M., and Roy, S.J.** (2009) Quantifying the three main components of salinity tolerance in cereals. *Plant, Cell & Environment*, **32**, 237-249.

Reddy, G.V., Heisler, M.G., Ehrhardt, D.W., and Meyerowitz, E.M. (2004) Real-time lineage analysis reveals oriented cell divisions associated with morphogenesis at the shoot apex of *Arabidopsis thaliana*. *Development*, **131**, 4225 -4237.

Reddy, G.V. and Meyerowitz, E.M. (2005) Stem-cell homeostasis and growth dynamics can be uncoupled in the Arabidopsis shoot apex. *Science*, **310**, 663-667.

Roeder, A.H.K., Chickarmane, V., Cunha, A., Obara, B., Manjunath, B.S., and Meyerowitz, E.M. (2010) Variability in the control of cell division underlies sepal epidermal patterning in *Arabidopsis thaliana*. *PLoS Biol*, **8**, e1000367.

Rolland-Lagan, A., Amin, M., and Pakulska, M. (2009) Quantifying leaf venation patterns: two-dimensional maps. *Plant J*, **57**, 195-205.

Rymen, B., Coppens, F., Dhondt, S., Fiorani, F., and Beemster, G.T.S. (2010) Kinematic analysis of cell division and expansion. In *Plant Developmental Biology*, L. Hennig and C. Köhler, eds (Humana Press: Totowa, NJ), pp. 203-227.

Scharr, H. and Kusters, R. (2002) A linear model for simultaneous estimation of 3D motion and depth. In *Workshop on Motion and Video Computing, 2002. Proceedings (IEEE)*, pp. 220-225.

Schmundt, D., Stitt, M., Jähne, B., and Schurr, U. (1998) Quantitative analysis of the local rates of growth of dicot leaves at a high temporal and spatial resolution, using image sequence analysis. *The Plant Journal*, **16**, 505 -514.

Schnable, P.S., Ware, D., Fulton, R.S., Stein, J.C., Wei, F., Pasternak, S., Liang, C., Zhang, J., Fulton, L., Graves, T.A., Minx, P., Reily, A.D., Courtney, L., Kruchowski, S.S., Tomlinson, C., et al. (2009) The B73 Maize genome: complexity, diversity, and dynamics. *Science*, **326**, 1112 -1115.

Scholes, J.D. and Rolfe, S.A. (2009) Chlorophyll fluorescence imaging as tool for understanding the impact of fungal diseases on plant performance: a phenomics perspective. *Funct. Plant Biol.*, **36**, 880-892.

Seelig, H.-D., Hoehn, A., Stodieck, L.S., Klaus, D.M., Adams III, W.W., and Emery, W.J. (2008) The assessment of leaf water content using leaf reflectance ratios in the visible, near-, and short-wave-infrared. *International Journal of Remote Sensing*, **29**, 3701-3713.

Seelig, H.-D., Hoehn, A., Stodieck, L.S., Klaus, D.M., Adams, W.W., and Emery, W.J. (2009) Plant water parameters and the remote sensing R 1300/R 1450 leaf water index: controlled condition dynamics during the development of water deficit stress. *Irrigation Science*, **27**, 357-365.

- Sequencing Project International Rice Genome** (2005) The map-based sequence of the rice genome. *Nature*, **436**, 793-800.
- Sijacic, P. and Liu, Z.** (2010) Novel insights from live-imaging in shoot meristem development. *Journal of Integrative Plant Biology*, **52**, 393-399.
- Silk, W.K. and Erickson, R.O.** (1979) Kinematics of plant growth. *Journal of Theoretical Biology*, **76**, 481-501.
- Sirault, X.R.R., James, R.A., and Furbank, R.T.** (2009) A new screening method for osmotic component of salinity tolerance in cereals using infrared thermography. *Funct. Plant Biol.*, **36**, 970-977.
- Skirycz, A., Vandenbroucke, K., Clauw, P., Maleux, K., De Meyer, B., Dhondt, S., Pucci, A., Gonzalez, N., Hoeberichts, F., Tognetti, V.B., Galbiati, M., Tonelli, C., Van Breusegem, F., Vuylsteke, M., and Inzé, D.** (2011) Survival and growth of Arabidopsis plants given limited water are not equal. *Nat Biotech*, **29**, 212-214.
- Takayama, K. and Nishina, H.** (2007) Early detection of water stress in tomato plants based on projected plant area. *Environment Control in Biology*, **45**, 241-249.
- Tappero, R., Peltier, E., Gräfe, M., Heidel, K., Ginder-Vogel, M., Livi, K.J.T., Rivers, M.L., Marcus, M.A., Chaney, R.L., and Sparks, D.L.** (2007) Hyperaccumulator *Alyssum murale* relies on a different metal storage mechanism for cobalt than for nickel. *New Phytol*, **175**, 641-654.
- Tataw, O.M., Min Liu, Roy-Chowdhury, A., Yadav, R.K., and Reddy, G.V.** (2010) Pattern analysis of stem cell growth dynamics in the shoot apex of Arabidopsis. In 2010 17th IEEE International Conference on Image Processing (ICIP) (IEEE), pp. 3617-3620.
- Tester, M. and Langridge, P.** (2010) Breeding technologies to increase crop production in a changing world. *Science*, **327**, 818 -822.
- Tisné, S., Reymond, M., Vile, D., Fabre, J., Dauzat, M., Koornneef, M., and Granier, C.** (2008) Combined genetic and modeling approaches reveal that epidermal cell area and number in leaves are controlled by leaf and plant developmental processes in Arabidopsis. *Plant Physiology*, **148**, 1117 -1127.
- Tracy, S.R., Roberts, J.A., Black, C.R., McNeill, A., Davidson, R., and Mooney, S.J.** (2010) The X-factor: visualizing undisturbed root architecture in soils using X-ray computed tomography. *J. Exp. Bot.*, **61**, 311-313.
- Truernit, E., Bauby, H., Dubreucq, B., Grandjean, O., Runions, J., Barthélémy, J., and Palauqui, J.-C.** (2008) High-resolution whole-mount imaging of three-dimensional tissue

organization and gene expression enables the study of phloem development and structure in *Arabidopsis*. *The Plant Cell*, **20**, 1494 -1503.

Tsukaya, H. (2002) Interpretation of mutants in leaf morphology: Genetic evidence for a compensatory system in leaf morphogenesis that provides a new link between cell and organismal theories. In *A Survey of Cell Biology* (Academic Press), pp. 1-39.

Tuberosa, R., Sanguineti, M.C., Landi, P., Giuliani, M.M., Salvi, S., and Conti, S. (2002) Identification of QTLs for root characteristics in maize grown in hydroponics and analysis of their overlap with QTLs for grain yield in the field at two water regimes. *Plant Mol. Biol.*, **48**, 697-712.

Vanhaeren, H., Gonzalez, N., and Inzé, D. (2010) Hide and seek: uncloaking the vegetative shoot apex of *Arabidopsis thaliana*. *The Plant Journal*, **63**, 541-548.

Varotto, C., Pesaresi, P., Maiwald, D., Kurth, J., Salamini, F., and Leister, D. (2000) Identification of photosynthetic mutants of *Arabidopsis* by automatic screening for altered effective quantum yield of photosystem 2. *Photosynthetica*, **38**, 497-504.

De Veylder, L., Beeckman, T., Beemster, G.T.S., Krols, L., Terras, F., Landrieu, I., Van Der Schueren, E., Maes, S., Naudts, M., and Inzé, D. (2001) Functional analysis of cyclin-dependent kinase inhibitors of *Arabidopsis*. *The Plant Cell*, **13**, 1653 -1668.

Walker, K.L. and Smith, L.G. (2002) Investigation of the role of cell-cell interactions in division plane determination during maize leaf development through mosaic analysis of the tangled mutation. *Development*, **129**, 3219 -3226.

Walter, A., Christ, M.M., Barron-gafford, G.A., Grieve, K.A., Murthy, R., and Rascher, U. (2005) The effect of elevated CO₂ on diel leaf growth cycle, leaf carbohydrate content and canopy growth performance of *Populus deltoides*. *Global Change Biology*, **11**, 1207-1219.

Walter, A., Christ, M.M., Rascher, U., Schurr, U., and Osmond, B. (2008) Diel leaf growth cycles in *Clusia spp.* are related to changes between C₃ photosynthesis and crassulacean acid metabolism during development and during water stress. *Plant, Cell & Environment*, **31**, 484-491.

Walter, A., Feil, R., and Schurr, U. (2002) Restriction of nyctinastic movements and application of tensile forces to leaves affects diurnal patterns of expansion growth. *Functional Plant Biol.*, **29**, 1247-1258.

Walter, A., Feil, R., and Schurr, U. (2003) Expansion dynamics, metabolite composition and substance transfer of the primary root growth zone of *Zea mays L.* grown in different external nutrient availabilities. *Plant, Cell & Environment*, **26**, 1451-1466.

Walter, A., Scharr, H., Gilmer, F., Zierer, R., Nagel, K.A., Ernst, M., Wiese, A., Virnich, O., Christ, M.M., Uhlig, B., Jünger, S., and Schurr, U. (2007) Dynamics of seedling growth acclimation towards altered light conditions can be quantified via GROWSCREEN: a setup and procedure designed for rapid optical phenotyping of different plant species. *New Phytologist*, **174**, 447-455.

Walter, A. and Schurr, U. (2005) Dynamics of leaf and root growth: endogenous control versus environmental impact. *Ann. Bot.*, **95**, 891-900.

Walter, A., Silk, W.K., and Schurr, U. (2009) Environmental effects on spatial and temporal patterns of leaf and root growth. *Annual Review of Plant Biology*, **60**, 279-304.

Walter, A., Spies, H., Terjung, S., Küsters, R., Kirchgeßner, N., and Schurr, U. (2002) Spatio-temporal dynamics of expansion growth in roots: automatic quantification of diurnal course and temperature response by digital image sequence processing. *Journal of Experimental Botany*, **53**, 689 -698.

Wang, L., Beyer, S.T., Cronk, Q.C., and Walus, K. (2011) Delivering high-resolution landmarks using inkjet micropatterning for spatial monitoring of leaf expansion. *Plant Methods*, **7**, 1.

Wang, L., Uilecan, I.V., Assadi, A.H., Kozmik, C.A., and Spalding, E.P. (2009) HYPOTrace: image analysis software for measuring hypocotyl growth and shape demonstrated on *Arabidopsis* seedlings undergoing photomorphogenesis. *Plant Physiology*, **149**, 1632 -1637.

van der Weele, C.M., Jiang, H.S., Palaniappan, K.K., Ivanov, V.B., Palaniappan, K., and Baskin, T.I. (2003) A new algorithm for computational image analysis of deformable motion at high spatial and temporal resolution applied to root growth. Roughly uniform elongation in the meristem and also, after an abrupt acceleration, in the elongation zone. *Plant Physiology*, **132**, 1138 -1148.

Weight, C., Parnham, D., and Waites, R. (2008) LeafAnalyser: a computational method for rapid and large-scale analyses of leaf shape variation. *The Plant Journal*, **53**, 578-586.

Wiese, A., Christ, M.M., Virnich, O., Schurr, U., and Walter, A. (2007) Spatio-temporal leaf growth patterns of *Arabidopsis thaliana* and evidence for sugar control of the diel leaf growth cycle. *New Phytologist*, **174**, 752-761.

Williams, J.A. (1973) A considerably improved method for preparing plastic epidermal imprints. *Botanical Gazette*, **134**, 87-91.

Windt, C.W., Gerkema, E., and Van As, H. (2009) Most water in the tomato truss is imported through the xylem, not the phloem: a nuclear magnetic resonance flow imaging study. *Plant Physiol*, **151**, 830-842.

Woo, N.S., Badger, M.R., and Pogson, B.J. (2008) A rapid, non-invasive procedure for quantitative assessment of drought survival using chlorophyll fluorescence. *Plant Methods*, **4**, 27.

Wuyts, N., Palauqui, J.-C., Conejero, G., Verdeil, J.-L., Granier, C., and Massonnet, C. (2010) High-contrast three-dimensional imaging of the Arabidopsis leaf enables the analysis of cell dimensions in the epidermis and mesophyll. *Plant Methods*, **6**, 17-17.

Yazdanbakhsh, N. and Fisahn, J. (2009) High throughput phenotyping of root growth dynamics, lateral root formation, root architecture and root hair development enabled by PlaRoM. *Funct. Plant Biol.*, **36**, 938-946.

Yazdanbakhsh, N. and Fisahn, J. (2010) Analysis of *Arabidopsis thaliana* root growth kinetics with high temporal and spatial resolution. *Annals of Botany*, **105**, 783 -791.

Zhang, C., Halsey, L., and Szymanski, D. (2011) The development and geometry of shape change in *Arabidopsis thaliana* cotyledon pavement cells. *BMC Plant Biology*, **11**, 27.

2

SHORT-ROOT and SCARECROW regulate leaf growth in Arabidopsis by stimulating S-phase progression of the cell cycle

Stijn Dhondt, Frederik Coppens, Freya De Winter, Kamal Swarup, Roeland M.H. Merks, Dirk Inzé*, Malcolm J. Bennett and Gerrit T.S. Beemster

Department of Plant Systems Biology, Flanders Institute for Biotechnology, 9052 Ghent, Belgium (S.D, F.C., F.D.W., R.M.H.M., D.I., G.T.S.B.); Department of Plant Biotechnology and Genetics, Ghent University, 9052 Ghent, Belgium (S.D, F.C., F.D.W., R.M.H.M., D.I., G.T.S.B.); School of Biosciences and Centre for Plant Integrative Biology, University of Nottingham, Sutton Bonington LE12 5RD, United Kingdom (K.S., M.J.B.); Netherlands Consortium for Systems Biology, 1090 6B Amsterdam, The Netherlands (R.M.H.M.); CWI, 1090 6B Amsterdam, The Netherlands (R.M.H.M.); Department of Biology, University of Antwerp, 2020 Antwerp, Belgium (G.T.S.B.)

This chapter is adapted from: Plant Physiology, 154, 1183-1195.

Received May 5, 2010; accepted August 21, 2010; published August 25, 2010.

Supplemental data is available online:

www.plantphysiol.org/cgi/doi/10.1104/pp.110.158857/

* Corresponding author; e-mail: dirk.inze@psb.vib-ugent.be.

ABSTRACT

SHORT-ROOT (*SHR*) and SCARECROW (*SCR*) are required for stem cell maintenance in the *Arabidopsis* (*Arabidopsis thaliana*) root meristem, ensuring its indeterminate growth. Mutation of *SHR* and *SCR* genes results in disorganization of the quiescent center and loss of stem cell activity, resulting in the cessation of root growth. This paper reports on the role of *SHR* and *SCR* in the development of leaves, which, in contrast to the root, have a determinate growth pattern and lack a persistent stem cell niche. Our results demonstrate that inhibition of leaf growth in *shr* and *scr* mutants is not a secondary effect of the compromised root development but is caused by an effect on cell division in the leaves: a reduced cell division rate and early exit of the proliferation phase. Consistent with the observed cell division phenotype, the expression of *SHR* and *SCR* genes in leaves is closely associated with cell division activity in most cell types. The increased cell cycle duration is due to a prolonged S-phase duration, which is mediated by up-regulation of cell cycle inhibitors known to restrain the activity of the transcription factor, E2Fa. Therefore, we conclude that, in contrast to their specific roles in cortex/endodermis differentiation and stem cell maintenance in the root, *SHR* and *SCR* primarily function as general regulators of cell proliferation in leaves.

INTRODUCTION

Stem cells are undifferentiated, totipotent cells that are able to duplicate themselves and to form offspring that differentiates into multiple cell types. They are situated in a microenvironment, the stem cell niche, where extracellular signals maintain stem cell division at low rates and prevent differentiation (Ohlstein et al., 2004; Li and Xie, 2005). In plants, the best studied stem cell niches are within the root and shoot apical meristems. There, stem cells produce somatic daughter cells that go on dividing and expanding, thereby forming the postembryonic tissues and organs that make up the body of the plant. It is the balance between stem cell maintenance within the meristem and differentiation of cells that exit the niche that facilitates indeterminate root and shoot growth.

SHORT-ROOT (*SHR*) and SCARECROW (*SCR*) are members of the GRAS family of transcription factors (Pysh et al., 1999; Lee et al., 2008), required for stem cell maintenance in the root apical meristem. Mutation of *SHR* and *SCR* genes causes a disorganization of the quiescent center (QC) and loss of stem cell activity, resulting in the depletion of proliferating cells in the root meristem and, consequently, cessation of root growth. Essentially, loss of *SHR/SCR* function renders root growth determinate. Furthermore, *shr* and *scr* mutants lack longitudinal cell divisions that separate the cortex/endodermis initial daughter cells, resulting in only one ground tissue cell layer (Benfey et al., 1993; Scheres et al., 1995; Di Laurenzio et al., 1996; Helariutta et al., 2000; Sabatini et al., 2003; Heidstra et al., 2004). In the *shr* mutant, this cell layer displays only cortex characteristics, whereas the *scr* ground tissue layer shows a mixed cortex/endodermis identity. The *shr* phenotype indicates that *SHR* is necessary both for the asymmetric division that generates cortex and endodermis and for endodermis cell fate

specification (Benfey et al., 1993; Scheres et al., 1995; Di Laurenzio et al., 1996). Expression of *SCR* in the QC of *shr* mutants cannot rescue QC function and only partially rescues stem cell maintenance (Sabatini et al., 2003). The observations that *shr* is epistatic to *scr*, *SCR* expression is reduced in *shr* roots, and SHR binds to the *SCR* promoter indicate that SCR acts directly downstream of SHR (Helariutta et al., 2000; Levesque et al., 2006).

In shoots, loss of SHR or SCR function affects differentiation of the bundle sheath cell layer in leaves and the endodermis in hypocotyls and inflorescence stems, suggesting that the radial patterning of ground tissue in both root and shoot is regulated by the same molecular mechanism (Fukaki et al., 1998; Wysocka-Diller et al., 2000). Furthermore, several studies reported an overall shoot growth phenotype in the *shr* and *scr* mutants. The *shoot gravitropism1* mutant, later identified to be allelic to *scr*, has small leaves, and growth of the *shr* mutant is severely retarded, resulting in a stunted shoot phenotype (Benfey et al., 1993; Fukaki et al., 1996, 1998). Here, we show that retarded leaf growth in *shr* and *scr* mutants is not a secondary effect of the compromised root but is caused by the loss of SHR and SCR function in the leaf tissue. Besides their function in ground tissue specification, SHR and SCR also affect proliferative cell division, driving growth in leaves. This is surprising, as in the root the effect of *shr* and *scr* on organ growth appears to be primarily mediated through their effect on stem cell maintenance, not proliferation outside the stem cell niche. Here, we use the Arabidopsis (*Arabidopsis thaliana*) leaf as a system to specifically study the function of these genes in cell cycle regulation (separate from their role in stem cell specification) and how this relates to the shoot growth phenotype.

RESULTS

Rosette Growth Is Reduced in *shr* and *scr* Mutants

Besides their characteristically strong reduction in primary root growth (Benfey et al., 1993; Di Laurenzio et al., 1996), *shr* and *scr* mutants display a severely dwarfed shoot phenotype (Fig. 1A). Following the development of *shr* and *scr* plants in vitro shows that germination is not affected, the seedlings being essentially the same size as the wild type 100 h after sowing. Thereafter, however, the rate of growth of *shr* and *scr* plants is severely inhibited (Fig. 1B). At 18 d after sowing (DAS), the projected rosette area was reduced 6.1-fold in *shr* plants and 2.6-fold in *scr* plants. The observed reduced rosette size is due to fewer leaves being present and leaves at any position being smaller (Fig. 1C; Supplemental Fig. S1). The largest difference occurs under our experimental conditions in leaf 5 and 7 for *scr* and *shr*, with reductions of 73% and 95% in leaf area, respectively. Thus, besides a reduction in individual leaf growth, these results indicate that, in contrast to the complete termination in the root apical meristem (Benfey et al., 1993; Di Laurenzio et al., 1996; Helariutta et al., 2000; Sabatini et al., 2003), the activity of the shoot apical meristem is partially inhibited in *scr* and *shr* mutant lines.

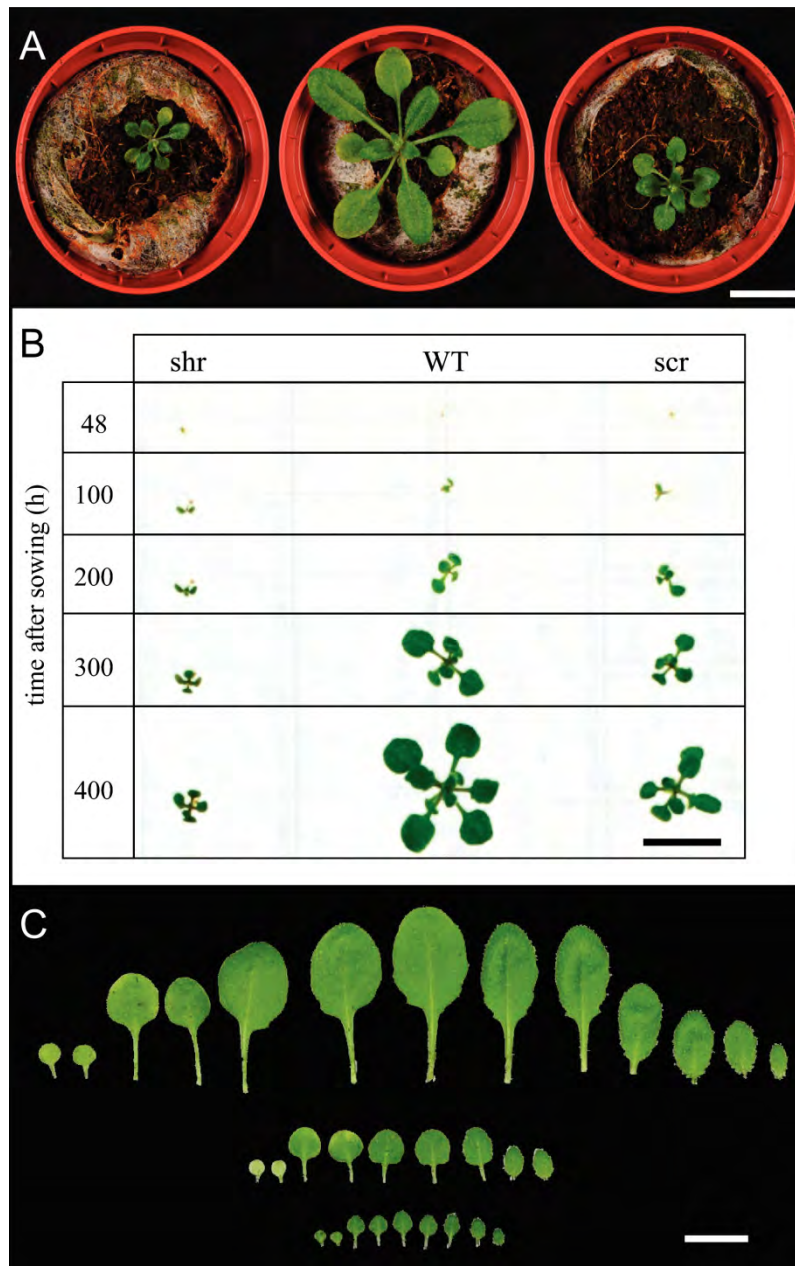


Figure 1. Rosette growth of *shr* and *scr* mutants. A, Rosettes of *shr-6* (left), wild-type (middle), and *scr-3* (right) plants at 20 DAS. Bar = 1 cm. B, Representative images for *shr-6*, *scr-3*, and wild-type (WT) plants 48, 100, 200, 300, and 400 h after sowing. Bar = 1 cm. C, Rosette leaves of soil-grown wild-type (top), *scr-3* (middle), and *shr-6* (bottom) plants harvested before bolting, from oldest (left) to youngest (right), including the two cotyledons. Bar = 1 cm.

The Shoot Phenotype Is Not a Consequence of the Aberrant Root Phenotype

A plausible explanation for the observed shoot phenotype of the *shr* and *scr* mutants is that it is an indirect effect of the compromised root development. Therefore, we set out to investigate whether the *shr* and *scr* mutant leaf phenotype can be attributed to a direct function of these genes during leaf development. First, *SHR* expression was analyzed in developing leaves using the *SHR:GUS* line (Helariutta et al., 2000). Staining of proliferating

leaves of 6- and 7-d-old plants for 5 h showed an expression signal throughout the leaf (Fig. 2, A and B). At later stages of leaf development, this global expression pattern changed: from day 10 onward, when cell proliferation is known to stop (Beemster et al., 2005), the pattern gradually became confined to the vascular network (Fig. 2, C–F). In mature leaves of 24-d-old plants, the expression was still high in the vascular bundle. More detailed analysis showed that the GUS signal was present in the entire vascular bundle and bundle sheath cells surrounding it (Fig. 2G). In leaves of 5-, 6-, and 7-d-old plants, incubation for only 2 h revealed that, although the expression occurred throughout the leaf, during the early stages the GUS signal was already higher in developing vascular traces than in the surrounding ground tissue (Fig. 2, H–J). Notably, the data show that the expression was specific for the vascular pattern well before differentiation of the vascular bundles can be observed at the cellular level (data not shown). Thus, analysis of *SHR:GUS* shows the expression of the *SHR* gene in proliferating cells, the vascular system, and the surrounding bundle sheath cells. This expression pattern closely resembles that of *SCR*, which is also expressed in most tissues in young proliferating leaves, whereas during expansion and maturation of the leaf the expression pattern becomes specific to the bundle sheath cells associated with the veins (Wysocka-Diller et al., 2000). Therefore, we conclude that the expression pattern of both genes coincides with general cell proliferation and vascular differentiation during leaf development.

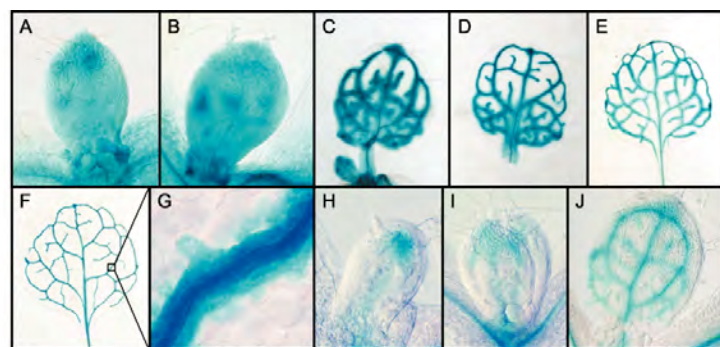


Figure 2. *SHR* expression during leaf development. A to F, *SHR:GUS* expression in leaves 1 and 2 of 6-d-old (A), 7-d-old (B), 10-d-old (C), 12-d-old (D), 16-d-old (E), and 24-d-old (F) plants after 5 h of incubation. (G), Expression in the vascular bundle and the bundle sheath cells surrounding it at 24 DAS. H to J, Incubation for 2 h at day 5 (H), day 6 (I), and day 7 (J).

To also obtain genetic evidence that the *SHR* expression in the leaf directly affects leaf development, we used the *shr-3* mutant, which contains the En-1 transposon in the coding sequence of the *SHR* gene (Helariutta et al., 2000). *shr-3* plants were grown on vertical plates and screened for reverted wild-type root phenotypes (indicative of En-1 transposon) at 20 DAS. Approximately 3% of the plants developed a root system that was much longer than normal *shr-3* roots, closely resembling a wild-type root system (Fig. 3). The plants with normal root systems could be divided into two groups, those with shoots comparable to shoots of wild-type plants and those with a *shr* rosette. This second class demonstrates that

having normal root development does not rescue the *shr* shoot phenotype. To investigate whether the reverted shoot and root phenotypes were due to reactivation of the *SHR* gene, we analyzed DNA from individual shoots and roots, with *shr* or wild-type phenotypes, respectively. To this end, we performed a quantitative (Q)-PCR using a set of primers that bridge the joint between the *SHR* coding sequence and the En-1 transposon and therefore only yield a PCR fragment when the transposon is present in the gene (*SHR* primers). Additionally, we used a second set of primers that flank the insertion site of the complete 8-kb-long En-1 transposon in the *SHR* gene, which only gives a PCR fragment in the absence of the transposon (i.e. after excision from its original locus [wild-type primers]). The ratio between the relative signals for these primer pairs was used to determine the genotype with respect to *shr-3*. As expected, in plants with a *shr* phenotype in both root and shoot, the expression ratio between the signal from *SHR* and wild-type primers was significantly higher than 1 in root and shoot samples, consistent with a *shr-3* genotype. In contrast, in plants showing a completely reverted phenotype, both shoot and root samples gave a signal ratio below 1, consistent with the absence of the En-1 transposon in the *SHR* gene. Finally, in plants with a dwarfed shoot but a root with a wild-type phenotype, the expression ratio in the shoot was higher than 1, corresponding to a *shr* genotype, whereas in the root it was below 1, indicating the restoration to the wild-type genotype (Fig. 3). The reduction of the expression ratio in the plants with only a reversion in the roots was smaller than in fully reverted plants. This can be explained by the presence of the transposon in a part of the root because the reversion events that give rise to root-only rescue probably occurred later in development than whole plant reversions. Nevertheless, these results suggest that translocation of the En-1 transposon in *shr-3* plants independently reverts the dwarfed shoot and short root phenotype to the wild type, indicating that *SHR* expression in the shoot is needed for normal rosette growth, irrespective of the genotype and the associated phenotype of the root.

To confirm physiologically that the *shr* and *scr* shoot phenotypes are due to their function in the leaf, rather than a consequence of their effect on root development, we compared their effect on leaf growth with that of plants in which the root growth was physically restricted to the same extent. For this, the roots of wild-type plants growing in vitro were cut at 2 cm below the hypocotyl every 3 d after germination, roughly the size that the roots of *shr* plants reach. At 24 DAS, leaves 1 and 2 of untreated controls and derooted plants were harvested and compared with *shr* and *scr* leaves. Removing the roots of wild-type plants did reduce the size of the first leaves by 33% compared with control plants. The leaf area in *scr* and *shr*, however, was reduced by 55% and 80%, respectively (Supplemental Fig. S2A). In plants from which the roots were cut, the reduced leaf area was related to a 17% reduction in cell size in the abaxial epidermis compared with control plants. In contrast, the cell size in the *shr* and *scr* mutants was not significantly different from the wild type (Supplemental Fig. S2B). In the absence of an effect on cell size, the decrease in leaf area in *scr* and *shr* was due to a reduced number of epidermal cells per leaf by 52% and 79%, respectively, whereas cutting

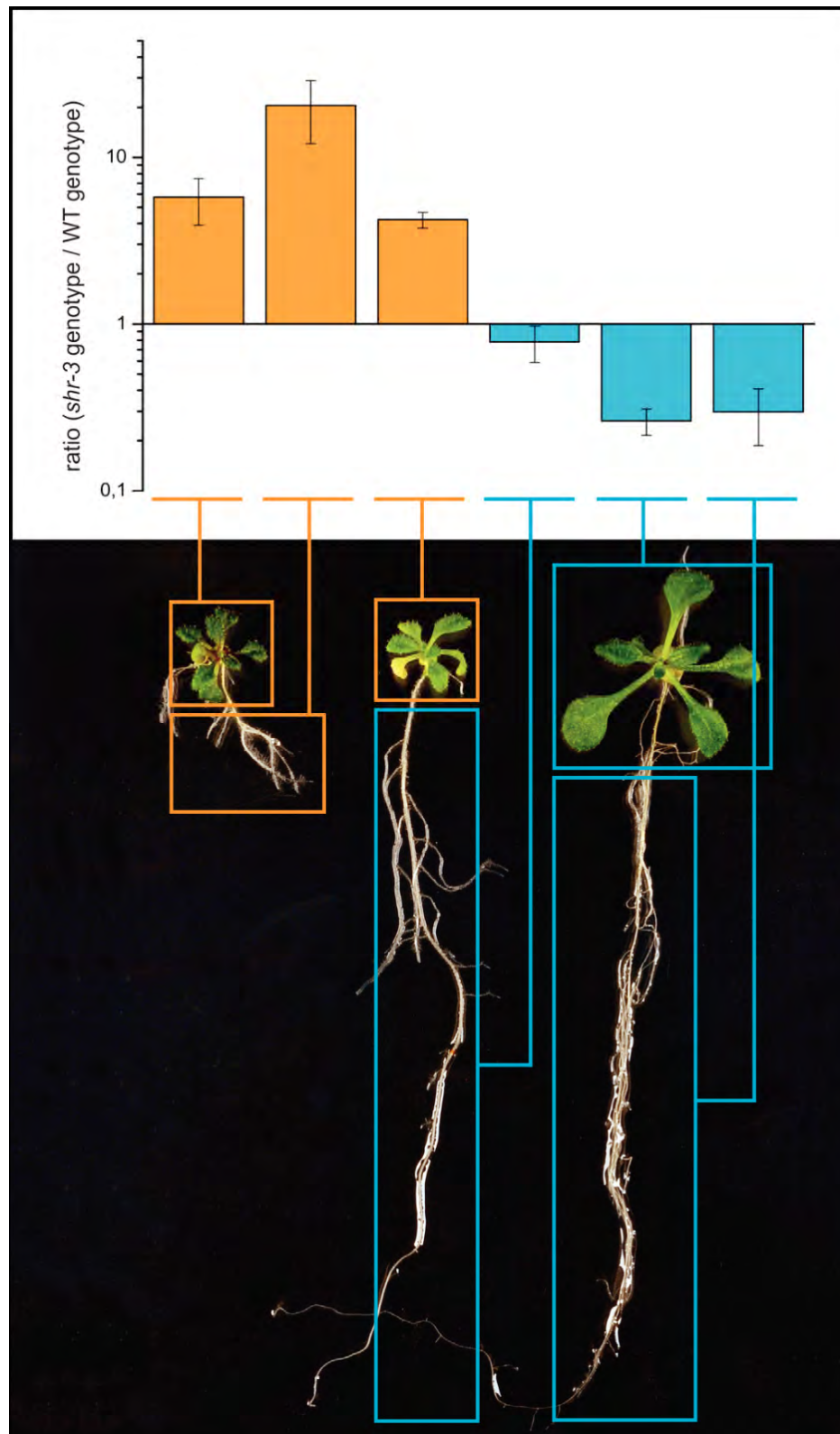


Figure 3. The effect of *SHR* mutation in the shoot is independent of its effect on root growth. Revertant transposon mutants show genetic independence of the root and shoot phenotypes in *shr-3* mutants. The genotype of reverted shoot and root phenotypes (left, normal *shr-3* plant; middle, reverted root, *shr-3* rosette; right, reverted root and shoot) was analyzed in individual roots and shoots. The ratio between DNA containing the *shr-3* genotype and the wild-type (WT) genotype was measured via Q-RT-PCR. Error bars represent SE ($n \geq 3$).

the roots reduced the number of cells by only 18% (Supplemental Fig. S2C). Thus, cutting the roots of wild-type plants decreases the final leaf area by reducing cell number and cell size in approximately equal amounts, whereas in *shr* and *scr* leaves, the reduction in leaf size is entirely due to a decrease in cell number. Moreover, despite the comparable reduction of the root system and the potential induction of additional wounding stress, the effect of cutting the roots on leaf growth was only small compared with the phenotypes in *shr* and *scr*. In the light of these observations, it is unlikely that the shoot phenotype in the mutants is due to an indirect effect of the compromised root growth. Together, the expression patterns of *SHR* and *SCR* and the genetic and physiological experiments provide evidence that the rosette phenotype observed in the *shr* and *scr* mutants is due to the loss of SHR/SCR function in the shoot itself.

Kinematic Analysis of Leaf Growth

The global expression of *SHR* and *SCR* in proliferating leaf tissues, together with the reduced cell number in mature *shr* and *scr* leaves, suggest a function of SHR and SCR in the regulation of proliferative cell divisions in the leaf. To investigate this possibility, a kinematic growth analysis of the first leaf pair was performed starting at 5 DAS, when the leaves are actively proliferating, until maturity, at 24 DAS.

Measurements of leaf blade area during leaf development showed that leaf area increased exponentially until day 11 in wild-type plants, after which expansion rates gradually decreased until the mature size was reached at approximately 18 DAS (Fig. 4A). Until day 8 or 9, there is very little difference in leaf area between the wild type and mutants, but at that time the growth rate of *scr* and especially *shr* declines more rapidly than in the wild type, resulting in a 2- and 5-fold reduction in mature leaf blade area. To understand whether the differences in leaf growth were related to cell division or cell expansion, we obtained cellular data of the abaxial leaf epidermis during development. The average epidermal cell size in *scr* and *shr* mutants was comparable to the wild type throughout leaf development (Fig. 4B), suggesting that differences in the number of cells per leaf are responsible for the smaller leaf size. Similar to the leaf blade area, the number of cells first increases exponentially, followed by a slower increase until the final number of cells per leaf is reached (Fig. 4C). Again, the rate of increase in *shr* and *scr* decreased earlier and more rapidly than in wild-type plants, resulting in a 4.6- and 1.8-fold reduction in cell number per leaf compared with wild-type plants at 24 DAS. This indicates that the duration of the proliferation phase, the period in which cell division occurs, is strongly reduced by *shr* mutation. Indeed, there is a rapid drop in the calculated rates of cell division that occurs between day 9 and 11 in the wild type and between day 8 and 10 in *shr*. In *scr*, the initial decline also starts already at day 8 but continues until day 13 (Fig. 4D). Cell division rates were also reduced in the mutants during the first 3 d of the kinematic analysis, when all leaves were still fully proliferative: average cell division rates were 0.046, 0.048, and 0.054 cells cell⁻¹ h⁻¹ for *scr*, *shr*, and wild-type

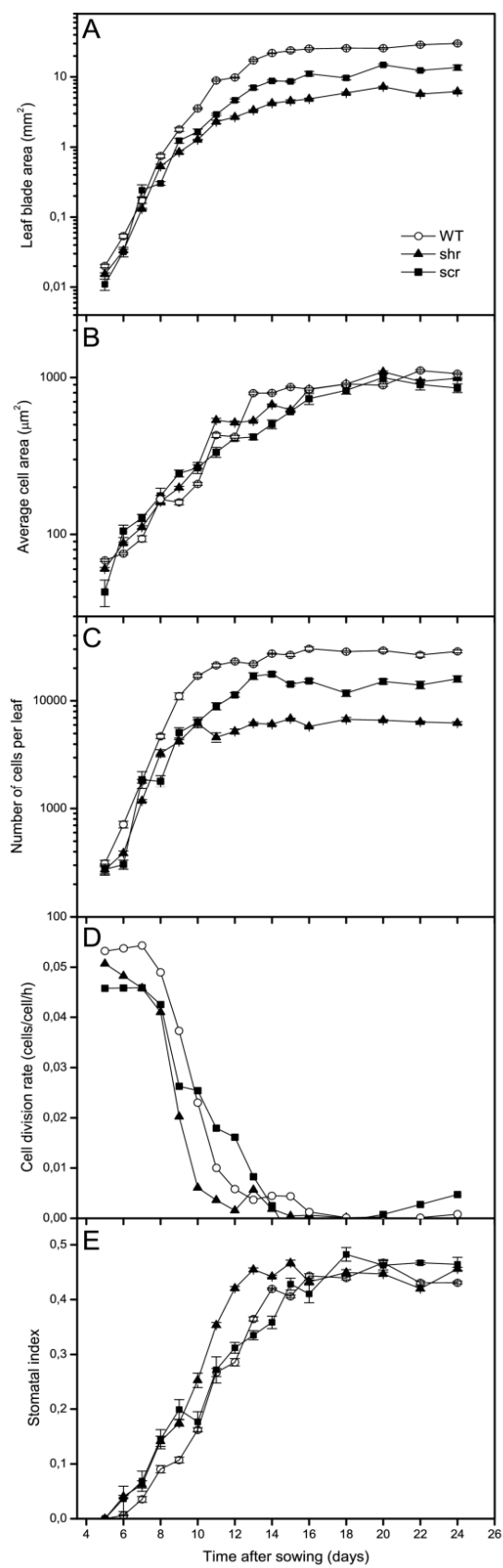


Figure 4. Kinematic analysis of leaf growth in *shr* and *scr* mutants. Characteristics of the abaxial epidermis of leaves 1 and 2 of *shr-6*, *scr-3*, and wild-type (WT) plants are shown. A, Leaf blade area. B, Average cell size. C, Number of cells per leaf. D, Cell division rate. E, Stomatal index. Error bars represent SE ($n = 5$).

leaves, corresponding to mean cell cycle durations of 21.8, 20.7, and 18.6 h, respectively, indicating that cell cycle duration increased in both mutants. Curiously, our results suggest that in the *scr* mutant cell division continues at a very slow rate for a few more days before stopping completely, which partly compensates the reduced cell division rate during proliferation. The appearance of guard cells marks the exit from proliferation. Consistent with an earlier exit from mitosis, the first guard cells are observed at day 6 in the mutants compared with day 7 in the wild type. In mature *shr* and *scr* leaves, however, the stomatal index, the fraction of guard cells in the total number of epidermal cells, is comparable to that of the wild type (Fig. 4E). Curiously, we found that the mature guard cell area is reduced, with 38% and 23% in *shr* and *scr* leaves, respectively, indicating that mutation of *SHR* and *SCR* somehow specifically affects the expansion of guard cells (Supplemental Fig. S3). Due to their relatively small size, this reduction in guard cell area has a negligible effect on the average cell size and whole leaf area. In conclusion, the results of the kinematic analysis indicate that both *shr* and *scr* reduce leaf growth primarily by inhibition of cell division rates and an earlier exit of cell proliferation for *shr*.

Progression of the Cell Division Gradient in *shr* and *scr* Mutants

To further investigate the effect of the *shr* mutation on cell division, we analyzed its effect on the spatiotemporal pattern of cell cycle activity during leaf development. In Arabidopsis leaves, cell division stops in a tip-to-base gradient, as can be shown by expression of the B-type cyclin *CYCB1;1* (Ferreira et al., 1994; Donnelly et al., 1999; Kang and Dengler, 2002). Therefore, we crossed the cell division marker *CYCB1;1:GUS* (Ferreira et al., 1994; Donnelly et al., 1999) into the *shr* and *scr* background. The expression of this cell cycle marker illustrated that retraction of the cell division gradient in *shr* occurs significantly earlier than in *scr* and wild-type leaves (Fig. 5). Furthermore, in wild-type and *scr* leaves, the GUS signal was elevated at the position of the hydathodes, which is much less pronounced in the *shr* mutant. After retraction of the cell division gradient, *CYCB1;1* expression in wild-type plants remained in the dispersed meristematic cells, where divisions occur in the stomatal lineage, and in cells near the vascular tissue (White, 2006). In *shr* plants, this expression was absent. The analyses of *CYCB1;1* expression patterns confirm the early exit of the cell proliferation phase in *shr* shown by kinematic analysis of leaf growth.

SHR and SCR Affect Endoreduplication

In leaves, exit from the cell proliferation phase coincides with the onset of endoreduplication (Beemster et al., 2005). Because mutants affecting cell division often show altered endoreduplication levels, we performed flow cytometry. Leaves 1 and 2 of *shr*, *scr*, and wild-type plants were harvested throughout leaf development. In mature leaves, at day 28, endoreduplication levels of *shr* and *scr* leaves were lower than those of wild-type leaves, as

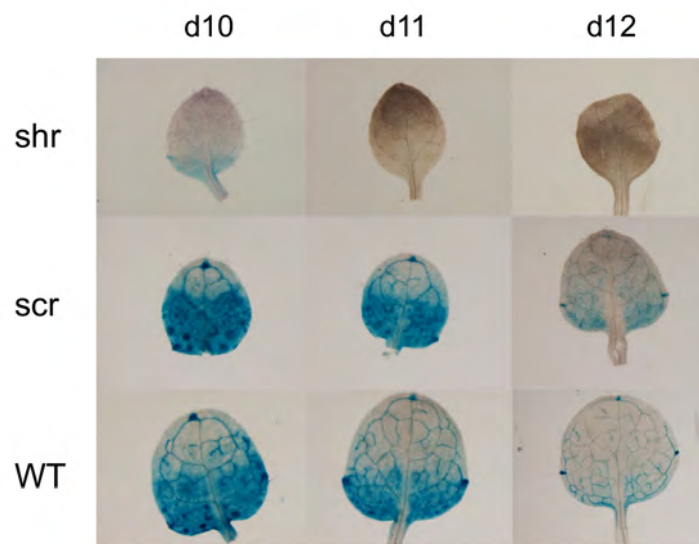


Figure 5. Spatiotemporal pattern of cell cycle activity during leaf development in *shr*, *scr*, and wild-type (WT) plants. *GUS* expression driven by the *CYCB1;1* promoter in *shr-6*, *scr-3*, and wild-type leaves from 10 to 12 DAS is shown. Note the early retraction of *CYCB1;1* expression in the *shr-6* background.

can be seen from the reduced fraction of 8C (*shr* and *scr*) and 16C (*scr*) in ploidy distributions (Fig. 6A). The corresponding endoreduplication index, which is the average number of endoreduplication cycles per nucleus, is 1.47, 1.31, and 0.97 for the wild type, *shr*, and *scr*, respectively. The transition from proliferation to endoreduplication around day 10 is evident from the strong increase in cells with 4C DNA content at that time (Fig. 6B). Consistent with the early exit of the proliferation phase, this transition occurred earlier in the *shr* mutant than that in *scr* and the wild type. After this stage, the decrease of the fraction of nuclei with a 4C DNA content was slower in *shr* than in the wild type, together with a later and slower accumulation of 8C and 16C cells. At late time points, when the leaf was mature, the amount of 8C and 16C nuclei in wild-type leaves reached a plateau, whereas in the *shr* mutant, the amount of 8C and 16C nuclei continued to increase. This result suggests that in the *shr* mutant endoreduplication starts off earlier than in the wild type but proceeds at a lower rate, so that the wild type reaches its final level before *shr* does. Thus, in addition to an effect on the mitotic cell cycle, *shr* and *scr* also perturb the endoreduplication cycle without affecting cell size.

Microarray Analysis

After finding that *SHR* and *SCR* affect cell division in the leaf, we set out to investigate the molecular basis of this inhibition. Therefore, a genome-wide expression analysis was performed using Affymetrix ATH1 microarrays. To this end, *shr*, *scr* and wild-type plants were grown in vitro on agar-solidified medium, and complete shoots were harvested at rosette developmental stage 1.04 (Boyes et al., 2001), which consists of roughly equal fractions of

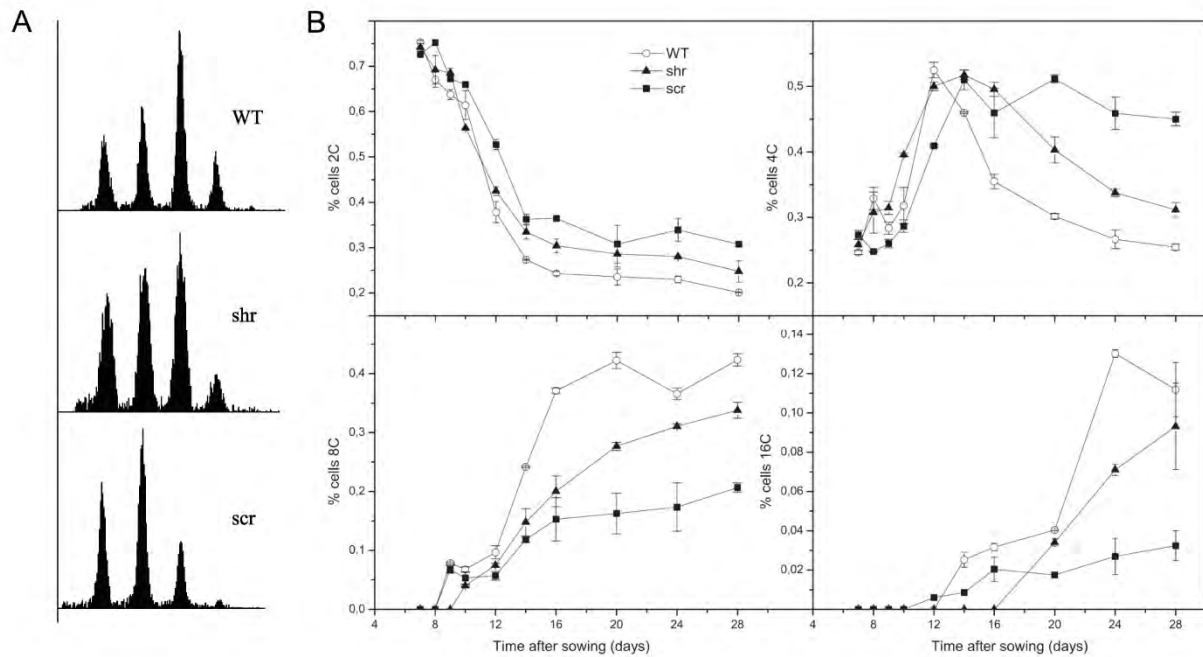


Figure 6. Endoreduplication in leaves of *shr*, *scr*, and wild-type (WT) plants. A, Ploidy distribution of *shr-6*, *scr-3*, and wild-type plants at 28 DAS. B, 2C, 4C, 8C, and 16C contents of *shr-6*, *scr-3*, and wild-type plants from 7 to 28 DAS. Error bars represent SE of two biological repeats.

proliferating, expanding, and mature tissue. From each genotype, RNA was extracted, labeled, and hybridized to the microarrays. Using a false discovery rate of 0.05 and a 2-fold expression level cutoff, 100 and 349 genes were differentially expressed in *scr* and *shr* shoots, respectively. There was a significant overlap between the genes that were affected in *scr* and *shr*: 88% of the genes differentially expressed in *scr* were also differentially regulated in *shr*, and all of them changed expression in the same direction, with a fold change that was on average 1.75 times higher in the *shr* mutant. Seven genes from the 10 most differentially expressed genes in *shr* were also present among the 10 most affected genes in *scr* (Supplemental Table S1). Furthermore, microarray data showed that SCR was differentially down-regulated in *shr* leaves, which could be confirmed by Q-reverse transcription (RT)-PCR (data not shown). These data, together with the comparable expression pattern in the leaf, are consistent with SCR acting downstream of SHR in the shoot, which is equivalent to the situation in the root (Helariutta et al., 2000; Levesque et al., 2006).

Genes differentially regulated in both *shr* and *scr* shoots with false discovery rate of 0.05 or less and a fold change greater than 1.5 were considered to be part of the regulatory SHR/SCR pathway in the shoot. This set of genes was used as a starting point for further analysis. To get a global overview of these differentially expressed genes, we first investigated which Gene Ontology categories were statistically overrepresented by means of a BiNGO analysis (Maere et al., 2005). Gene Ontology categories overrepresented among the genes down-regulated in

both *shr* and *scr* shoots were "response to auxin," "response to brassinosteroid," and "chromatin assembly." The latter showed that this was due to differential expression of histone *H2A* and *H2B* genes. Besides a down-regulation of auxin and brassinosteroid signaling, these data also suggest an effect on nucleosome assembly.

Among the genes up-regulated in both the *shr* and *scr* shoot transcriptomes was an overrepresentation of the flavonoid biosynthetic process, involved in protection against various biotic and abiotic stresses, the response to several stresses, and abscisic acid, suggesting a general stress response upon mutation of the *SHR* and *SCR* genes. Furthermore, the CCAAT-binding factor family was the only transcription factor family differentially regulated in the *shr* and *scr* shoot transcriptomes. This family, better known as the nuclear transcription factor Y (NF-Y) family, is, as in mammals, subdivided into A-, B-, and C-type subunits (Siefers et al., 2009). Strikingly, in *shr* and *scr*, the same seven out of 10 A-type subunits were up-regulated, compared with none of the B- and C-type subunits (Supplemental Table S2). This indicates a specific up-regulation of the A-type subunits of the CCAAT-binding factor complex, which function as transcriptional activators and cell cycle regulators by chromatin remodeling (van Ginkel et al., 1997; Elkon et al., 2003; Gurtner et al., 2008).

Differential expression of histone *H2A* and *H2B* genes and A-type *NF-Y* genes indicates a role for *SHR* and *SCR* in chromatin-related cell cycle regulation. Consistently, the cell cycle regulators *CYCD6;1*, *CDKB2;1*, *CDKB2;2*, *KRP5*, and *CYCD3;3* have been identified as targets of *SHR* (Levesque et al., 2006; Sozzani et al., 2010). Nevertheless, of the 61 core cell cycle genes (Vandepoele et al., 2002), only *CYCB1;1* in *shr* was differentially expressed in our transcriptome data. Using synchronized *Arabidopsis* cell cultures, Menges et al. (2003) identified a much larger set of 1,372 genes that are differentially expressed in one of the cell cycle phases. Comparing this set of cell cycle-regulated genes, we found a 2.5- and 2.6-fold overrepresentation of cell cycle-regulated genes in the *scr* and *shr* shoot transcriptomes, respectively. These data indicate that cell cycle regulation in whole shoot samples is affected upon mutation of the *SHR* and *SCR* genes.

Cell Cycle Regulation

Kinematic leaf growth and transcriptome analysis suggest that cell cycle regulation is downstream of the *SHR/SCR* pathway. Therefore, cell cycle progression in *scr* and *shr* mutants was analyzed in more detail. The relative duration of the different cell cycle phases was determined in both mutants using flow cytometry. To this end, leaves 1 and 2 were harvested at 7 DAS when they were fully proliferating and contained only 2C and 4C nuclei (Fig. 6B), allowing estimation of the relative amount of cells in G1-, S-, and G2-phase of the cell cycle (Fig. 7A). Data show that *shr* and *scr* have an enrichment of cells in S-phase, suggesting a relative increase of the S-phase duration in *shr* ($P = 0.036$) and *scr* ($P = 0.004$).

Since kinematic analysis showed a prolongation of the total cell cycle duration with 2 to 3 h in the mutants, this enrichment reflects a drastic impact on S-phase duration, which was estimated at 3.9 h in *shr* and 4.2 h in *scr* compared with only 2.9 h in the wild-type leaves. This suggests that S-phase takes significantly longer in the mutants than in the wild type, which is also consistent with the reduced endoreduplication rate.

To support the increased S-phase duration, suggested by flow cytometry, we tested the relative expression of the *Histone H4* and *CYCB1;1* genes, which are specifically expressed in S-phase and M-phase of the plant cell cycle, respectively (Menges et al., 2003). Q-RT-PCR analysis on mRNA from proliferating leaves of 7-d-old *shr*, *scr*, and wild-type plants (Fig. 7B) indicated that expression of *Histone H4* was 27% higher in *scr* and 24% higher in *shr* than in the wild type. Inversely, expression of *CYCB1;1* was reduced by 37% and 28% for *scr* and *shr*, respectively. The lower expression of *CYCB1;1* suggests that there is no arrest in M-phase in the *shr* and *scr* mutants because this would increase the fraction of cells in this phase and therefore increase the relative expression levels of M-phase marker genes. Inversely, the higher expression of the S-phase-specific *Histone H4* gene confirms that S-phase duration in *shr* and *scr* would be prolonged.

To investigate which cell cycle genes could be involved in the prolonged S-phase duration, the expression of a number of core cell cycle genes involved in the G1/S transition and S-phase progression, *CYCD1;1*, *CYCD3;1*, *CYCD4;2*, *CYCD5;1*, *CYCD6;1*, *DEL1*, *DEL2*, *DEL3*, *DPa*, *DPb*, *E2Fa*, *E2Fb*, *E2Fc*, *RBR*, and *WEE1*, was (in contrast to the above whole shoot-based microarray analysis) determined in proliferating leaves of 7-d-old *shr*, *scr*, and wild-type plants (Fig. 7C). Q-RT-PCR analysis revealed that in *scr* leaves the expression of *DEL1*, *E2Fc*, and *RBR*, all negative regulators of S-phase entry (del Pozo et al., 2002; Vlieghe et al., 2005; Wildwater et al., 2005), was significantly up-regulated. The same expression differences were observed for the *shr* leaves. Additionally, *CYCD4;2* and *CYCD6;1* (both negative regulators of RBR and, therefore, positive regulators of S-phase entry) were down-regulated. Expression of the transcription factor *E2Fa*, which controls the transcription of early S-phase genes involved in cell cycle regulation and DNA replication and is controlled by RBR (Ramirez-Parra et al., 2003), did not change significantly. These data suggest that in the leaf, SHR and SCR control the cell cycle in a similar way as in the root (Wildwater et al., 2005), by inhibiting RBR and thereby stimulating E2F-mediated S-phase gene expression.

DISCUSSION

Effects of Cell Cycle Inhibition on Leaf Growth

Leaf growth is the result of cell division and cell expansion. Kinematic analysis generates detailed data on the dynamics of these parameters during development (De Veylder et al., 2001a). *shr* and *scr* have a strong cell division defect, resulting in a severe reduction in final

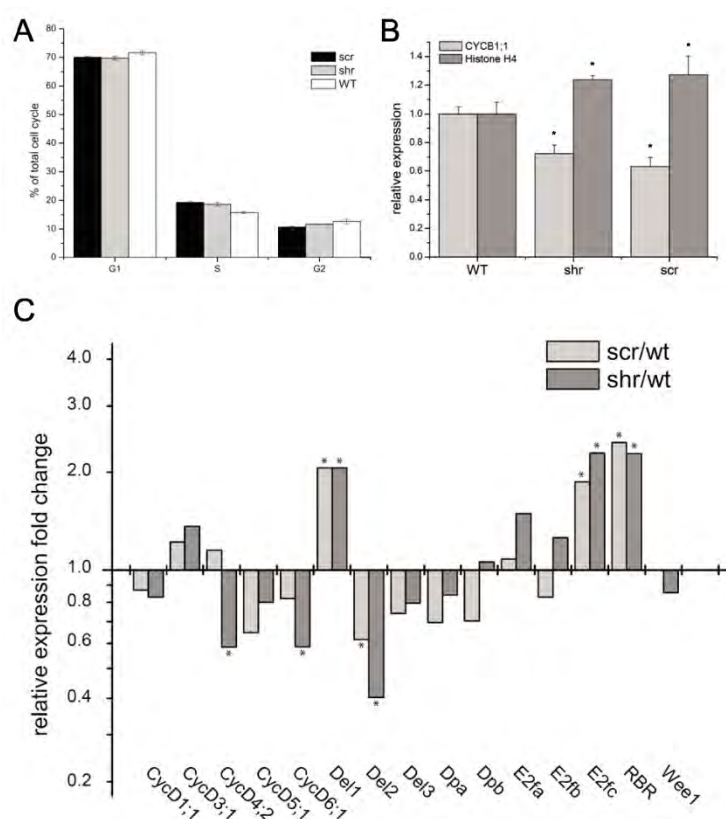


Figure 7. Cell cycle regulation in *shr* and *scr* mutants. A, Relative abundance of G1-, S-, and G2-phase cells in proliferating leaves 1 and 2 determined by flow cytometry at 7 DAS ($n \geq 3$). Note that cells in mitosis cannot be detected due to the absence of a nuclear membrane. B, Relative expression of the S-phase-specific gene, *Histone H4*, and the M-phase-specific gene, *CYCB1;1*, in *shr*, *scr*, and wild-type (WT) leaves ($P < 0.05$; $n = 2$). C, Relative expression of core cell cycle genes involved in the G1/S transition during the plant cell cycle in *shr* and *scr* compared with their expression in wild-type leaves. Asterisks indicate differentially expressed genes (fold change > 2 ; $P < 0.05$; $n = 2$).

leaf area. Two mechanisms underlie the reduced cell number in *shr* and *scr* leaves: reduction in cell division rate, and an early exit of the proliferation phase. Reduction in cell division rate (i.e. increased cell cycle duration) is also observed in overexpression lines of the core cell cycle genes *KRP2* and *CKS1*, in which this is accompanied by an increased proliferative cell size (De Veylder et al., 2001a, 2001b). A faster cell cycle progression, on the other hand, is reported for *E2Fb* overexpression, which was accompanied by a decreased cell size (Magyar et al., 2005; Sozzani et al., 2006). In *shr*, *scr*, and *hub1* (Fleury et al., 2007) mutants, however, which also affect cell cycle regulation, a decreased cell division rate did not result in a change in cell size. There is evidence that cell cycle progression depends on reaching a critical cell size, or cytoplasm-to-DNA ratio (Killander and Zetterberg, 1965; Carter and Jagdish, 1978; Donnan and John, 1983; Mitchison, 2003; Dolznig et al., 2004). These data suggest the existence of a cell growth coordination acting upstream of the cell cycle machinery. This mechanism would not be affected by mutations upstream of the cell cycle regulation, such as

shr, *scr*, and *hub1*, where a change in cell cycle duration did not affect cell growth, but would be disrupted by misexpression of the core cell cycle genes, such as *KRP2*, *CKS1*, and *E2Fb*.

In addition to the reduction in cell division rate, *shr* mutants also show an early exit of cell proliferation. Evidence that exit from proliferation is a mechanism underlying leaf size variation comes from a number of genotypes with increased leaf size, which is associated with an extension of the proliferation phase (Mizukami and Fischer, 2000; Bögre et al., 2008; Li et al., 2008; Horiguchi et al., 2009). Furthermore, study of leaf series in wild-type plants shows that leaf size reaches a pronounced maximum for leaves 4 to 6 of the rosette (Fig. 1D; Supplemental Fig. S1). In *shr* and *scr* mutants, consecutive leaves are very similar in size. Assuming that *shr* and *scr* also affect cell division and not cell expansion in higher order leaves suggests that the larger size difference in subsequent rosette leaves is due to even bigger changes in cell proliferation.

Despite the fact that the overall phenotype is less severe in the *scr* mutant than in *shr*, the effect on cell division rate, S-phase duration, and endoreduplication is at least as strong in the *scr* mutant as in *shr*. Inversely, the reduced expansion of guard cells and the early exit of the cell proliferation phase are more pronounced in *shr*. These observations suggest that the reduced rate of cell cycle progression in *shr* is mainly regulated through its effect on *SCR*, whereas the developmental transitions seem to be at least partly regulated through other *SHR* targets, making it possible to functionally discriminate *SCR*-dependent and -independent downstream pathways in leaf development.

Regulation of S-Phase Initiation and Progression in *shr* and *scr*

Our phenotypic analysis of *shr* and *scr* leaves confirms the drastic effect of these mutations on cell division reported previously for the QC and stem cell niche in roots. Local reduction of the expression of RBR, an inhibitor of the E2F/DP transcriptional complex, in the root meristem restores stem cell maintenance in *scr* and transiently in *shr* (Wildwater et al., 2005). Q-RT-PCR analysis on a number of core cell cycle genes (Vandepoele et al., 2002) involved in the G1/S transition revealed that DEL1, E2Fc, and RBR were up-regulated in *scr* and *shr* leaves. Compared with E2F, DEL proteins contain two DNA-binding domains and lack the transcription activation domain, which allow them to block the E2F/DP-binding sites as monomers and to repress the transcription of E2F target genes needed for S-phase progression (Kosugi and Ohashi, 2002; Mariconti et al., 2002; De Veylder et al., 2003). Notably, DEL1 has been demonstrated to regulate the expression of only a subset of E2F-dependent genes (Vlieghe et al., 2005). Also, E2Fc lacks the activation domain, allowing it to act as a repressor (Vandepoele et al., 2002), and binding of RBR to E2F represses the transcription of E2F target genes (Sekine et al., 1999; Durfee et al., 2000). Thus, all up-regulated cell cycle genes in both *shr* and *scr* inhibit S-phase entry. Additionally, *CYCD4;2* and *CYCD6;1* were down-regulated in *shr* leaves. The latter has recently been identified as a

direct target of SHR in the root (Sozzani et al., 2010). D-type cyclins in complex with cyclin-dependent kinases drive the inactivation of RBR proteins through hyperphosphorylation, releasing E2F target genes, and mark E2F ϵ for degradation (Sozzani et al., 2010). Curiously, CYCD4;2 and CYCD6;1 are the only Arabidopsis D-type cyclins that lack the RBR-binding motif (Vandepoele et al., 2002; Menges et al., 2007). Despite this, overexpression of CYCD4;2 has effects similar to those of other D-type cyclins (Kono et al., 2006), suggesting that somehow they are still positive regulators of E2F function. This suggests that in the *shr* and *scr* mutants, E2F action, needed for S-phase progression, is repressed at the protein level by a dual mechanism: up-regulation of inhibitors and simultaneous down-regulation of positive regulators, without affecting *E2Fa* expression. Furthermore, a 2.4- and 2.3-fold overrepresentation of E2F target genes (Vandepoele et al., 2005), for SHR and SCR, respectively, was observed in a recent microarray time-course experiment inducing SHR and SCR in the ground tissue of their respective mutant backgrounds (Sozzani et al., 2010). This mechanism is also consistent with the RBR data obtained in the root meristem (Wildwater et al., 2005). These results indicate that SHR and SCR could have comparable effects on the cell cycle regulation both in roots and leaves.

The E2F pathway controls the expression of genes required for both the G1/S transition and S-phase progression. E2F target genes are involved in cell cycle regulation, transcription, chromatin dynamics, defense responses, signaling, and DNA replication (Ramirez-Parra et al., 2003; Vandepoele et al., 2005). Also, many key regulators of DNA licensing and initiation of DNA replication, such as origin recognition complex subunits (Diaz-Trivino et al., 2005), members of the prereplication complexes, cell division control proteins (Castellano et al., 2001; Vandepoele et al., 2005) and minichromosome maintenance proteins (Stevens et al., 2002; Vandepoele et al., 2005; Shultz et al., 2009), genes involved in DNA replication and DNA synthesis, such as the DNA polymerase processivity factor PCNA (Chabouté et al., 2000; Egelkrout et al., 2002), ribonucleotide reductase subunits RNRs (Chabouté et al., 2000, 2002), replication factors, and DNA polymerases (Vandepoele et al., 2005), contain E2F-binding sites in their promoters. Inhibition of E2F action, therefore, will down-regulate the expression of these E2F target genes. Our results show that down-regulation of E2Fa activity in *shr* and *scr* did not lead to a block in G1-phase but rather to a slower S-phase progression, indicated by the relative duration of the G1-phase and the S-phase during proliferation, the up-regulation of S-phase-specific genes, and an effect on endoreduplication (which involves repeated cycles of S-phase in the absence of mitosis). This result suggests that the expression of E2F targets involved in DNA replication and DNA synthesis is rate limiting for S-phase progression in *scr* and *shr* mutants. The G1/S transition itself, driven by DNA licensing and initiation of DNA replication, either has a lower threshold for E2F activity or is controlled by additional regulators.

Stem Cell Maintenance and Cell Cycle Regulation Disentangled

Stem cell maintenance in the root meristem is needed to ensure indeterminate growth of plant organs. Mutation of *SHR*, *SCR*, and *PLETHORA (PLT)* genes results in a loss of the stem niche, followed by differentiation of the root meristem (Benfey et al., 1993; Scheres et al., 1995; Aida et al., 2004). Both *SHR* and *SCR* are required for QC identity, as *SCR* expression in the QC alone cannot rescue root growth in the *shr* background (Sabatini et al., 2003). Also, the *PLT* genes act in parallel with the *SHR/SCR* pathway in root stem cell specification (Aida et al., 2004). In addition, a number of core cell cycle genes have been shown to affect stem cell fate in roots. Overexpression of *CYCD3;1*, *KRP2*, *RBR*, and *E2Fa/DPa* results in differentiation or accumulation of stem cells, in agreement with their roles in the plant E2F pathway (Wildwater et al., 2005). *RBR* regulation occurs downstream of *SCR*, which provides a mechanistic link between the *SHR/SCR* pathway and cell cycle regulation in stem cell maintenance (Wildwater et al., 2005). Our data strongly suggest that *SCR* expression in the ground tissue contributes to overall meristem activity but cannot support indeterminate growth and maintenance of the stem cell niche. Interestingly, in the *scr* mutant background, restitution of *SCR* expression in the ground tissue, excluding the QC, contributes to overall meristem activity but not to stem cell maintenance (Sabatini et al., 2003). These data are in line with our observations indicating a role for *SHR* and *SCR* in proliferative cell division. However, to date, this has not been studied in detail in the root, presumably because the consumption of the meristem due to the loss of the stem cell niche has a more pronounced effect in this organ. In contrast to the leaf, the expression of *SCR* and *SHR* in the root tip does not appear in all cells but is restricted to the stem cell niche, endodermis, and, in the case of *SHR*, the stele (Di Laurenzio et al., 1996; Helariutta et al., 2000; Wysocka-Diller et al., 2000). The question raised whether this more general cell cycle regulatory function is specific for the leaf (and possibly other aerial structures) and whether other genes perform this function in proliferating root cells or cell cycle regulation in the root is independent of this regulatory mechanism.

RBR complexes also interact with chromatin-remodeling factors, which have recently been identified as key players in the maintenance of stem cell identity in mammals (Hennig et al., 2003; Narita et al., 2003; Lee et al., 2006; Jullien et al., 2008). Our transcriptome analysis of *scr* and *shr* shoots revealed the differential expression of histones and NF-Ya factors, which function as transcriptional activators and cell cycle regulators by chromatin remodeling (van Ginkel et al., 1997; Elkon et al., 2003; Gurtner et al., 2008). In human, it was shown that NF-Ya factors regulate G1/S gene expression, related to the loss of dividing potential during replicative senescence, and self-renewal of stem cells (Matuoka and Chen, 2000; Zhu et al., 2005). These data are consistent with the molecular phenotypes observed in the leaves of *shr* and *scr* mutants and suggest that the *SHR/SCR* pathway affects chromatin remodeling in plants and that this function is not restricted to stem cells.

Our data suggest the inhibition of E2F action as the primary target of core cell cycle regulation in *shr* and *scr* mutants. E2F action is crucial for both cell cycle progression and stem cell maintenance. Overexpression of *E2Fa* together with its dimerization partner, *DPa*, not only induces enhanced division and endoreduplication in leaves but also the accumulation of stem cells in roots (De Veylder et al., 2002; Kosugi and Ohashi, 2003). Moreover, transient overexpression of *E2Fa* and *DPa* can even induce nondividing mesophyll cells to reenter S-phase (Rossignol et al., 2002). Comparably, increasing E2F activity in leaves by inducible inactivation of RBR leads to epidermal cell hyperplasia during the late proliferation phase and allows differentiated pavement cells to reenter cell division later during development (Desvoyes et al., 2006). These data emphasize the role of E2F activity on both cell proliferation rate and the transition between stem cell, proliferative, and nonproliferative states. Consistent with a role upstream of E2F, our data demonstrate that SHR and SCR not only function in differentiation and stem cell maintenance in the root meristem but also play a role in the control of proliferative cell division in developing leaves.

CONCLUSION

The *shr* and *scr* mutants have been instrumental in unraveling the mechanism of stem cell maintenance in the root meristem (Benfey et al., 1993; Scheres et al., 1995; Di Laurenzio et al., 1996; Helariutta et al., 2000; Sabatini et al., 2003). In both *shr* and *scr*, cell fate changes result in the differentiation of the stem cell niche, causing an arrest of formative divisions and ultimately root growth. This indicates that in the root the function of SHR and SCR in differentiation is instrumental for growth. In leaves, *shr* and *scr* mutants affect differentiation of the bundle sheath (Wysocka-Diller et al., 2000) and the expansion of guard cells. These differentiation effects, however, contribute little to the overall leaf growth phenotype. Indeed, our kinematic data show that the reduced leaf growth in *shr* and *scr* mutants is primarily determined by an effect on cell proliferation. Furthermore, we show that this is a direct consequence of the lack of SHR and SCR function in the shoot rather than an indirect consequence of compromised root growth. These phenotypes cannot readily be understood, given the absence of a stem cell niche in the developing leaf (Tsukaya, 2002), indicating that SHR and SCR play a direct role in the control of proliferative cell division in developing leaves. Furthermore, these data indicate a much more pronounced function for SHR and SCR in the regulation of cell division than has been identified in root studies. Our transcriptome, endoreduplication, flow cytometric, and expression analyses reveal that SHR and SCR primarily drive S-phase progression, presumably by a stimulation of E2F action. However, future research is needed to unravel the molecular details of cell cycle regulation by the SHR/SCR pathway, taking into account the possible difference between proliferating cells in the root and leaf.

MATERIALS AND METHODS

Plant Materials and Growth Conditions

In this study, we used *Arabidopsis* (*Arabidopsis thaliana*) to study the mutants *shr-6* (SALK_002744), *shr-3* (Helariutta et al., 2000), and *scr-3*, (Fukaki et al., 1996) and the promoter fusions *CYCB1;1:GUS* (Ferreira et al., 1994) and *SHR:GUS* (Helariutta et al., 2000). These lines were all in the Columbia (Col-0) background. Seeds for in vitro analysis were sterilized in 3% bleach for 15 min and sown on medium containing 0.5x Murashige and Skoog medium (Duchefa) solidified with 0.9 g L⁻¹ plant tissue culture agar (Lab M) on round plates (1013; Becton-Dickinson). For the root experiments, we used 1.0 g L⁻¹ agar and square plates (Greiner Bio-One). After a stratification period of 2 d, the plates were placed horizontally (leaf growth) or inclined vertically (root growth) in a growth chamber under long-day conditions (16 h of light, 8 h of darkness) at 22°C with a light intensity of 80 to 100 mE m⁻² s⁻¹ supplied by cool-white fluorescent tubes (Spectralux Plus 36W/840; Radium).

Growth Analysis

Rosette growth was analyzed by taking photographs (Canon EOS 400D camera with an EFS 18-55 mm Canon ZOOM lens) of plants growing on petri dishes. Plants were followed for 18 DAS. Kinematic analysis of leaf growth was done as described previously (De Veylder et al., 2001a). Total leaf blade area of leaves 1 and 2 of five plants from 5 to 24 DAS was measured from dark-field binocular (days 8–24) or differential interference contrast light microscopy (days 5–7) images. Microscopic drawings containing about 100 cells, located 25% and 75% from the distance between the tip and the base of the leaf blade, of the abaxial epidermis of each leaf were made with a drawing tube attached to the microscope equipped with differential interference contrast optics.

Histochemical GUS Assays

Complete seedlings or tissue cuttings were stained on multiwell plates (3046; Becton-Dickinson). GUS assays were performed as described by Beeckman and Engler (1994). After staining, samples were mounted in lactic acid and observed and photographed with a stereomicroscope (MZ16; Leica) or with a differential interference contrast microscope (DMLB; Leica).

Flow Cytometry

For flow cytometry, leaves were lacerated with a razor blade and suspended in 1.5 mL of buffer (Galbraith et al., 1991). The supernatants was filtered over a 30- μ m mesh, and 1 μ L of 4',6-diamidino-2-phenylindole from a stock of 1 mg mL⁻¹ was added. The nuclei were analyzed with the CyFlow flow cytometer using FloMax software (Partec). On average, 10,000

nuclei were counted per sample. For cell cycle analysis on proliferative leaves, nuclei were detected on a linear scale and analyzed using MultiCYCLE AV software (Phoenix Flow Systems; Kallioniemi et al., 1994). A debris fitting, a single cell cycle analysis, and a histogram reliability and confidence estimation were performed for each histogram. The model used for debris fitting and peak analysis was sliced background. For the relative cell cycle phase calculations, only samples with a good S-phase confidence were used.

Q-RT-PCR

RNA was extracted using the RNeasy kit (Qiagen) according to the supplier's instructions. Poly(dT) cDNA was prepared from 1 mg of total RNA with SuperScript III reverse transcriptase (Invitrogen) and quantified on a LightCYCler 480 (Roche) with the qPCR LightCYCler 480 SYBR Green I Master (Roche). PCR was performed on 384-well reaction plates, which were heated for 10 min to 95°C, followed by 45 cycles of denaturation for 10 s at 95°C and annealing and extension for 15 s at 60°C and 72°C, respectively. Target quantifications were performed with specific primer pairs designed with the Beacon Designer 4.0 (Premier Biosoft International). All PCRs were done in three technical repeats, and at least two biological repeats were used for each sample. Expression levels were first normalized to CDKA, CBP20, and CKA2 expression levels, which did not show clear systematic changes in the cycle threshold value, and then to the respective expression levels in the wild type (Col-0). The primers used are listed in Supplemental Table S3.

Microarray Analysis and Data Processing

shr-2, *scr-3*, and Col-0 shoots were grown in vitro and harvested at stage 1.04 (Boyes et al., 2001). Each genotype was sampled in three biological replicates each containing approximately 20 rosettes from different petri dishes. RNA was extracted with the RNeasy kit (Qiagen). Arabidopsis ATH1 GeneChips (Affymetrix) were hybridized at the VIB Microarray Facility (www.microarrays.be) according to the manufacturer's instructions. Expression levels were based on an improved custom-made Chip Description File (Casneuf et al., 2007). The multiarray analysis algorithm implemented in the BioConductor Affy package (www.bioconductor.org; Gautier et al., 2004) was used for background correction, normalization, and summary expression value computation. For statistical analysis and hierarchical clustering of the normalized expression files, we used the Multiexperiment Viewer of The Institute for Genomic Research (www.tm4.org/mev.html). Because one of the *shr* arrays (*shr-3*) clustered separately from the others, this array was removed from further analysis. The remaining eight arrays were subjected to an ANOVA analysis using the false discovery rate method (Benjamini and Hochberg, 1995). The corrected *P* value threshold was set to 0.05.

The microarray data are available in the public repository Gene Expression Omnibus (<http://www.ncbi.nlm.nih.gov/geo/>) under accession number GSE21629. Sequence data from this article can be found in the Arabidopsis Genome Initiative or GenBank/EMBL databases under the following accession numbers: SHR (AT4G37650) and SCR (AT3G54220). Sequence data for all other genes described in this article can be found in the relevant databases using the accession numbers given in Supplemental Table S3.

Supplemental Data

The following materials are available in the online version of this article.
(www.plantphysiol.org/cgi/doi/10.1104/pp.110.158857/)

Supplemental Figure S1. Leaf series of *shr* and *scr* mutants.

Supplemental Figure S2. The effect of cutting the root system in wild-type plants on leaf growth is smaller compared with mutation of *SHR* and *SCR* genes.

Supplemental Figure S3. Guard cell areas in *shr* and *scr* mutants.

Supplemental Table S1. Top ten most differentially expressed genes in *shr* and *scr* shoot transcriptomes.

Supplemental Table S2. Expression of A-, B-, and C-type subunits of the NF-Y family.

Supplemental Table S3. Primer sequences used for Q-RT-PCR.

ACKNOWLEDGEMENTS

We thank Yrjo Helariutta and Lieven De Veylder for fruitful discussions. This work was supported by a doctoral fellowship from the Agency for Innovation by Science and Technology to S.D.; by a doctoral fellowship of the Research Foundation-Flanders to F.C.; by grants from the Belgian Network BARN (Growth and Development of Higher Plants grant no. IUAPVI/33), funded by the Interuniversity Attraction Poles Programme, initiated by the Belgian State, Science Policy Office; by a Marie Curie Intra-European Fellowship (no. MEIF-CT-2005-025084 to R.M.H.M.); by the Netherlands Genomics Initiative/Netherlands Organisation for Scientific Research; by a grant from the Bijzonder Onderzoeksfonds Methusalem project (no. BOF08/01M00408) of Ghent University; and by the European Community (grant no. FP6 IP AGRON-OMICS, contract no. LSHG-CT-2006-037704).

CONTRIBUTIONS

Stijn Dhondt performed the rosette growth measurements, conducted the experiments to show SHR functionality in the leaf, analyzed the micro-array data, examined the progression of the cell division gradient, performed the flow cytometry experiments, and gathered the information related to the cell cycle regulation. Frederik Coppens, Freya De Winter, and Stijn Dhondt performed the kinematic leaf growth analysis and Kamal Swarup selected *shr* mutants homozygous for the T-DNA insertion and crossed this mutant with the *CYCB1;1:GUS* marker line.

REFERENCES

- Aida M, Beis D, Heidstra R, Willemsen V, Blilou I, Galinha C, Nussaume L, Noh YS, Amasino R and Scheres B** (2004) The PLETHORA genes mediate patterning of the Arabidopsis root stem cell niche. *Cell* **119**: 109–120
- Beeckman T and Engler G** (1994) An easy technique for the clearing of histochemically stained plant tissue. *Plant Mol Biol Rep* **12**: 37–42
- Beemster GTS, De Veylder L, Vercruyse S, West G, Rombaut D, Van Hummelen P, Galichet A, Gruissem W, Inzé D and Vuylsteke M** (2005) Genome-wide analysis of gene expression profiles associated with cell cycle transitions in growing organs of Arabidopsis. *Plant Physiol* **138**: 734–743
- Benfey PN, Linstead PJ, Roberts K, Schiefelbein JW, Hauser MT and Aeschbacher RA** (1993) Root development in Arabidopsis: four mutants with dramatically altered root morphogenesis. *Development* **119**: 57–70
- Benjamini Y and Hochberg Y** (1995) Controlling the false discovery rate: a practical and powerful approach to multiple testing. *J R Stat Soc B* **57**: 289–300
- Bögre L, Magyar Z and López-Juez E** (2008) New clues to organ size control in plants. *Genome Biol* **9**: 226
- Boyes DC, Zayed AM, Ascenzi R, McCaskill AJ, Hoffman NE, Davis KR and Görlach J** (2001) Growth stage-based phenotypic analysis of *Arabidopsis*: a model for high throughput functional genomics in plants. *Plant Cell* **13**: 1499–1510
- Carter BL and Jagadish MN** (1978) Control of cell division in the yeast *Saccharomyces cerevisiae* cultured at different growth rates. *Exp Cell Res* **112**: 373–383

Casneuf T, Van de Peer Y and Huber W (2007) *In situ* analysis of cross-hybridisation on microarrays and the inference of expression correlation. *BMC Bioinformatics* **8**: 461

Castellano MM, del Pozo JC, Ramirez-Parra E, Brown S and Gutierrez C (2001) Expression and stability of *Arabidopsis* CDC6 are associated with endoreplication. *Plant Cell* **13**: 2671–2686

Chabouté ME, Clément B and Philipps G (2002) S phase and meristem-specific expression of the tobacco RNR1b gene is mediated by an E2F element located in the 5' leader sequence. *J Biol Chem* **277**: 17845–17851

Chabouté ME, Clément B, Sekine M, Philipps G and Chaubet-Gigot N (2000) Cell cycle regulation of the tobacco ribonucleotide reductase small subunit gene is mediated by E2F-like elements. *Plant Cell* **12**: 1987–2000

del Pozo JC, Boniotti MB and Gutierrez C (2002) *Arabidopsis* E2Fc functions in cell division and is degraded by the ubiquitin-SCF(AtSKP2) pathway in response to light. *Plant Cell* **14**: 3057–3071

Desvoyes B, Ramirez-Parra E, Xie Q, Chua NH and Gutierrez C (2006) Cell type-specific role of the retinoblastoma/E2F pathway during *Arabidopsis* leaf development. *Plant Physiol* **140**: 67–80

De Veylder L, Beeckman T, Beemster GTS, de Almeida Engler J, Ormenese S, Maes S, Naudts M, Van Der Schueren E, Jacquard A, Engler G, et al (2002) Control of proliferation, endoreduplication and differentiation by the *Arabidopsis* E2Fa-DPa transcription factor. *EMBO J* **21**: 1360–1368

De Veylder L, Beeckman T, Beemster GTS, Krols L, Terras F, Landrieu I, van der Schueren E, Maes S, Naudts M and Inzé D (2001a) Functional analysis of cyclin-dependent kinase inhibitors of *Arabidopsis*. *Plant Cell* **13**: 1653–1668

De Veylder L, Beemster GTS, Beeckman T and Inzé D (2001b) CKS1At overexpression in *Arabidopsis thaliana* inhibits growth by reducing meristem size and inhibiting cell-cycle progression. *Plant J* **25**: 617–626

De Veylder L, Joubès J and Inzé D (2003) Plant cell cycle transitions. *Curr Opin Plant Biol* **6**: 536–543

Diaz-Trivino S, del Mar Castellano M, de la Paz Sanchez M, Ramirez-Parra E, Desvoyes B and Gutierrez C (2005) The genes encoding *Arabidopsis* ORC subunits are E2F

targets and the two *ORC1* genes are differently expressed in proliferating and endoreplicating cells. *Nucleic Acids Res* **33**: 5404–5414

Di Laurenzio L, Wysocka-Diller J, Malamy JE, Pysh L, Helariutta Y, Freshour G, Hahn MG, Feldmann KA and Benfey PN (1996) The *SCARECROW* gene regulates an asymmetric cell division that is essential for generating the radial organization of the Arabidopsis root. *Cell* **86**: 423–433

Dolznic H, Grebien F, Sauer T, Beug H and Müllner EW (2004) Evidence for a size-sensing mechanism in animal cells. *Nat Cell Biol* **6**: 899–905

Donnan L and John PC (1983) Cell cycle control by timer and sizer in *Chlamydomonas*. *Nature* **304**: 630–633

Donnelly PM, Bonetta D, Tsukaya H, Dengler RE and Dengler NG (1999) Cell cycling and cell enlargement in developing leaves of Arabidopsis. *Dev Biol* **215**: 407–419

Durfee T, Feiler HS and Grissem W (2000) Retinoblastoma-related proteins in plants: homologues or orthologues of their metazoan counterparts? *Plant Mol Biol* **43**: 635–642

Egelkrot EM, Mariconti L, Settlage SB, Cella R, Robertson D and Hanley-Bowdoin L (2002) Two E2F elements regulate the proliferating cell nuclear antigen promoter differently during leaf development. *Plant Cell* **14**: 3225–3236

Elkon R, Linhart C, Sharan R, Shamir R and Shiloh Y (2003) Genome-wide *in silico* identification of transcriptional regulators controlling the cell cycle in human cells. *Genome Res* **13**: 773–780

Ferreira PC, Hemerly AS, de Almeida Engler J, Van Montagu M, Engler G and Inzé D (1994) Developmental expression of the *Arabidopsis* cyclin gene *cyc1At*. *Plant Cell* **6**: 1763–1774

Fleury D, Himanen K, Cnops G, Nelissen H, Boccardi TM, Maere S, Beemster GTS, Neyt P, Anami S, Robles P, et al (2007) The *Arabidopsis thaliana* homolog of yeast BRE1 has a function in cell cycle regulation during early leaf and root growth. *Plant Cell* **19**: 417–432

Fukaki H, Fujisawa H and Tasaka M (1996) SGR1, SGR2, SGR3: novel genetic loci involved in shoot gravitropism in *Arabidopsis thaliana*. *Plant Physiol* **110**: 945–955

- Fukaki H, Wysocka-Diller J, Kato T, Fujisawa H, Benfey PN and Tasaka M** (1998) Genetic evidence that the endodermis is essential for shoot gravitropism in *Arabidopsis thaliana*. *Plant J* **14**: 425–430
- Galbraith DW, Harkins KR and Knapp S** (1991) Systemic endopolyploidy in *Arabidopsis thaliana*. *Plant Physiol* **96**: 985–989
- Gautier L, Cope L, Bolstad BM and Irizarry RA** (2004) affy: analysis of Affymetrix GeneChip data at the probe level. *Bioinformatics* **20**: 307–315
- Gurtner A, Fuschi P, Magi F, Colussi C, Gaetano C, Dobbelstein M, Sacchi A and Piaggio G** (2008) NF-Y dependent epigenetic modifications discriminate between proliferating and postmitotic tissue. *PLoS ONE* **3**: e2047
- Heidstra R, Welch D and Scheres B** (2004) Mosaic analyses using marked activation and deletion clones dissect *Arabidopsis* SCARECROW action in asymmetric cell division. *Genes Dev* **18**: 1964–1969
- Helariutta Y, Fukaki H, Wysocka-Diller J, Nakajima K, Jung J, Sena G, Hauser MT and Benfey PN** (2000) The *SHORT-ROOT* gene controls radial patterning of the *Arabidopsis* root through radial signaling. *Cell* **101**: 555–567
- Hennig L, Taranto P, Walser M, Schönrock N and Grissem W** (2003) *Arabidopsis* MSI1 is required for epigenetic maintenance of reproductive development. *Development* **130**: 2555–2565
- Horiguchi G, Gonzalez N, Beemster GTS, Inzé D and Tsukaya H** (2009) Impact of segmental chromosomal duplications on leaf size in the *grandifolia-D* mutants of *Arabidopsis thaliana*. *Plant J* **60**: 122–133
- Jullien PE, Mosquna A, Ingouff M, Sakata T, Ohad N and Berger F** (2008) Retinoblastoma and its binding partner MSI1 control imprinting in *Arabidopsis*. *PLoS Biol* **6**: e194
- Kallioniemi OP, Visakorpi T, Holli K, Isola JJ and Rabinovitch PS** (1994) Automated peak detection and cell cycle analysis of flow cytometric DNA histograms. *Cytometry* **16**: 250–255
- Kang J and Dengler N** (2002) Cell cycling frequency and expression of the homeobox gene *ATHB-8* during leaf vein development in *Arabidopsis*. *Planta* **216**: 212–219

Killander D and Zetterberg A (1965) A quantitative cytochemical investigation of the relationship between cell mass and initiation of DNA synthesis in mouse fibroblasts *in vitro*. *Exp Cell Res* **40**: 12–20

Kono A, Ohno R, Umeda-Hara C, Uchimiya H and Umeda M (2006) A distinct type of cyclin D, CYCD4;2, involved in the activation of cell division in Arabidopsis. *Plant Cell Rep* **25**: 540–545

Kosugi S and Ohashi Y (2002) Interaction of the Arabidopsis E2F and DP proteins confers their concomitant nuclear translocation and transactivation. *Plant Physiol* **128**: 833–843

Kosugi S and Ohashi Y (2003) Constitutive E2F expression in tobacco plants exhibits altered cell cycle control and morphological change in a cell type-specific manner. *Plant Physiol* **132**: 2012–2022

Lee MH, Kim B, Song SK, Heo JO, Yu NI, Lee SA, Kim M, Kim DG, Sohn SO, Lim CE, et al (2008) Large-scale analysis of the GRAS gene family in *Arabidopsis thaliana*. *Plant Mol Biol* **67**: 659–670

Lee TI, Jenner RG, Boyer LA, Guenther MG, Levine SS, Kumar RM, Chevalier B, Johnstone SE, Cole MF, Isono K, et al (2006) Control of developmental regulators by Polycomb in human embryonic stem cells. *Cell* **125**: 301–313

Levesque MP, Vernoux T, Busch W, Cui H, Wang JY, Blilou I, Hassan H, Nakajima K, Matsumoto N, Lohmann JU, et al (2006) Whole-genome analysis of the SHORT-ROOT developmental pathway in Arabidopsis. *PLoS Biol* **4**: e143

Li L and Xie T (2005) Stem cell niche: structure and function. *Annu Rev Cell Dev Biol* **21**: 605–631

Li Y, Zheng L, Corke F, Smith C and Bevan MW (2008) Control of final seed and organ size by the DA1 gene family in *Arabidopsis thaliana*. *Genes Dev* **22**: 1331–1336

Maere S, Heymans K and Kuiper M (2005) BiNGO: a Cytoscape plugin to assess overrepresentation of gene ontology categories in biological networks. *Bioinformatics* **21**: 3448–3449

Magyar Z, De Veylder L, Atanassova A, Bakó L, Inzé D and Bögre L (2005) The role of the *Arabidopsis* E2FB transcription factor in regulating auxin-dependent cell division. *Plant Cell* **17**: 2527–2541

- Mariconti L, Pellegrini B, Cantoni R, Stevens R, Bergounioux C, Cella R and Albani D** (2002) The E2F family of transcription factors from *Arabidopsis thaliana*: novel and conserved components of the retinoblastoma/E2F pathway in plants. *J Biol Chem* **277**: 9911–9919
- Matuoka K and Chen KY** (2000) Possible role of subunit A of nuclear factor Y (NF-YA) in normal human diploid fibroblasts during senescence. *Biogerontology* **1**: 261–271
- Menges M, Hennig L, Gruissem W and Murray JAH** (2003) Genome-wide gene expression in an Arabidopsis cell suspension. *Plant Mol Biol* **53**: 423–442
- Menges M, Pavesi G, Morandini P, Bögre L and Murray JAH** (2007) Genomic organization and evolutionary conservation of plant D-type cyclins. *Plant Physiol* **145**: 1558–1576
- Mitchison JM** (2003) Growth during the cell cycle. *Int Rev Cytol* **226**: 165–258
- Mizukami Y and Fischer RL** (2000) Plant organ size control: AINTEGUMENTA regulates growth and cell numbers during organogenesis. *Proc Natl Acad Sci USA* **97**: 942–947
- Narita M, Nunez S, Heard E, Narita M, Lin AW, Hearn SA, Spector DL, Hannon GJ and Lowe SW** (2003) Rb-mediated heterochromatin formation and silencing of E2F target genes during cellular senescence. *Cell* **113**: 703–716
- Ohlstein B, Kai T, Decotto E and Spradling A** (2004) The stem cell niche: theme and variations. *Curr Opin Cell Biol* **16**: 693–699
- Pysh LD, Wysocka-Diller JW, Camilleri C, Bouchez D and Benfey PN** (1999) The GRAS gene family in Arabidopsis: sequence characterization and basic expression analysis of the *SCARECROW-LIKE* genes. *Plant J* **18**: 111–119
- Ramirez-Parra E, Fründt C and Gutierrez C** (2003) A genome-wide identification of E2F-regulated genes in Arabidopsis. *Plant J* **33**: 801–811
- Rosignol P, Stevens R, Perennes C, Jasinski S, Cella R, Tremousaygue D and Bergounioux C** (2002) AtE2F-a and AtDP-a, members of the E2F family of transcription factors, induce Arabidopsis leaf cells to re-enter S phase. *Mol Genet Genomics* **266**: 995–1003
- Sabatini S, Heidstra R, Wildwater M and Scheres B** (2003) SCARECROW is involved in positioning the stem cell niche in the Arabidopsis root meristem. *Genes Dev* **17**: 354–358

Scheres B, Di Laurenzio L, Willemsen V, Hauser MT, Janmaat K, Weisbeek P and Benfey PN (1995) Mutations affecting the radial organisation of the Arabidopsis root display specific defects throughout the embryonic axis. *Development* **121**: 53–62

Sekine M, Ito M, Uemukai K, Maeda Y, Nakagami H and Shinmyo A (1999) Isolation and characterization of the E2F-like gene in plants. *FEBS Lett* **460**: 117–122

Shultz RW, Lee TJ, Allen GC, Thompson WF and Hanley-Bowdoin L (2009) Dynamic localization of the DNA replication proteins MCM5 and MCM7 in plants. *Plant Physiol* **150**: 658–669

Siefers N, Dang KK, Kumimoto RW, Bynum WE, IV, Tayrose G and Holt BF, III (2009) Tissue-specific expression patterns of Arabidopsis NF-Y transcription factors suggest potential for extensive combinatorial complexity. *Plant Physiol* **149**: 625–641

Sozzani R, Cui H, Moreno-Risueno MA, Busch W, Van Norman JM, Vernoux T, Brady SM, Dewitte W, Murray JAH and Benfey PN (2010) Spatiotemporal regulation of cell-cycle genes by SHORTROOT links patterning and growth. *Nature* **466**: 128–132

Sozzani R, Maggio C, Varotto S, Canova S, Bergounioux C, Albani D and Cella R (2006) Interplay between Arabidopsis activating factors E2Fb and E2Fa in cell cycle progression and development. *Plant Physiol* **140**: 1355–1366

Stevens R, Mariconti L, Rossignol P, Perennes C, Cella R and Bergounioux C (2002) Two E2F sites in the Arabidopsis MCM3 promoter have different roles in cell cycle activation and meristematic expression. *J Biol Chem* **277**: 32978–32984

Tsukaya H (2002) Leaf development. *In* CR Somerville and EM Meyerowitz, eds, *The Arabidopsis Book*. American Society of Plant Biologists. Rockville, MD, doi/<http://www.aspb.org/publications/arabidopsis/>

Vandepoele K, Raes J, De Veylder L, Rouzé P, Rombauts S and Inzé D (2002) Genome-wide analysis of core cell cycle genes in *Arabidopsis*. *Plant Cell* **14**: 903–916

Vandepoele K, Vlieghe K, Florquin K, Hennig L, Beemster GTS, Gruissem W, Van de Peer Y, Inzé D and De Veylder L (2005) Genome-wide identification of potential plant E2F target genes. *Plant Physiol* **139**: 316–328

van Ginkel PR, Hsiao KM, Schjerven H and Farnham PJ (1997) E2F-mediated growth regulation requires transcription factor cooperation. *J Biol Chem* **272**: 18367–18374

Vlieghe K, Boudolf V, Beemster GTS, Maes S, Magyar Z, Atanassova A, de Almeida Engler J, De Groot R, Inzé D and De Veylder L (2005) The DP-E2F-like gene DEL1 controls the endocycle in *Arabidopsis thaliana*. *Curr Biol* **15**: 59–63

White DWR (2006) PEAPOD regulates lamina size and curvature in Arabidopsis. *Proc Natl Acad Sci USA* **103**: 13238–13243

Wildwater M, Campilho A, Perez-Perez JM, Heidstra R, Blilou I, Korthout H, Chatterjee J, Mariconti L, Grissem W and Scheres B (2005) The RETINOBLASTOMA-RELATED gene regulates stem cell maintenance in Arabidopsis roots. *Cell* **123**: 1337–1349

Wysocka-Diller JW, Helariutta Y, Fukaki H, Malamy JE and Benfey PN (2000) Molecular analysis of SCARECROW function reveals a radial patterning mechanism common to root and shoot. *Development* **127**: 595–603

Zhu J, Zhang Y, Joe GJ, Pompetti R and Emerson SG (2005) NF-Ya activates multiple hematopoietic stem cell (HSC) regulatory genes and promotes HSC self-renewal. *Proc Natl Acad Sci USA* **102**: 11728–11733

3

Model-based analysis of Arabidopsis leaf epidermal cells reveals distinct division and expansion patterns for pavement and guard cells

Leila Kheibarshekan Asl[#], Stijn Dhondt[#], Véronique Boudolf, Gerrit T.S. Beemster, Tom Beeckman, Dirk Inzé, Willy Govaerts, and Lieven De Veylder^{*}

Department of Applied Mathematics and Computer Science, Ghent University, 9000 Ghent, Belgium (L.K.A., W.G.); Department of Plant Systems Biology, VIB, 9052 Ghent, Belgium (L.K.A., S.D., V.B., G.T.S.B., T.B., D.I., L.D.V.); Department of Plant Biotechnology and Bioinformatics, Ghent University, 9052 Ghent, Belgium (S.D., V.B., G.T.S.B., T.B., D.I., L.D.V.); Department of Biology, University of Antwerp, 2020 Antwerp, Belgium (G.T.S.B.)

This chapter is adapted from: Plant Physiology, 156, 2172 -2183.

Received June 1, 2011; Accepted June 21, 2011; Published June 21, 2011.

Supplemental data is available online:

<http://www.plantphysiol.org/cgi/doi/10.1104/pp.111.181180/>

[#] These authors contributed equally to the article.

^{*} Corresponding author; e-mail: lieven.deveylder@psb.vib-ugent.be.

ABSTRACT

To efficiently capture sunlight for photosynthesis, leaves typically develop into a flat and thin structure. This development is driven by cell division and expansion, but the individual contribution of these processes is currently unknown, mainly because of the experimental difficulties to disentangle them in a developing organ, due to their tight interconnection. To circumvent this problem, we built a mathematic model that describes the possible division patterns and expansion rates for individual epidermal cells. This model was used to fit experimental data on cell numbers and sizes obtained over time intervals of 1 d throughout the development of the first leaf pair of *Arabidopsis thaliana*. The parameters were obtained by a derivative-free optimization method that minimizes the differences between the predicted and experimentally observed cell size distributions. The model allowed us to calculate probabilities for a cell to divide into guard or pavement cells, the maximum size at which it can divide, and its average cell division and expansion rates at each point during the leaf developmental process. Surprisingly, average cell cycle duration remained constant throughout leaf development, whereas no evidence for a maximum cell size threshold for cell division of pavement cells was found. Furthermore, the model predicted that neighboring cells of different sizes within the epidermis expand at distinctly different relative rates, which could be verified by direct observations. We conclude that cell division seems to occur independently from the status of cell expansion, whereas the cell cycle might act as a timer rather than as a size-regulated machinery.

INTRODUCTION

In most plant species, the above-ground plant body is dominated by leaves, the organs specialized in photosynthesis. This process converts carbon dioxide into organic components utilizing energy from sunlight, making leaves the energy production site and the growth engine of plants. To maximize its light-capturing capacity, a leaf is typically flat and thin. This characteristic shape is established during the leaf developmental process. Leaves arise on the flanks of the shoot apical meristem (SAM) at auxin accumulation sites (Benková et al., 2003). At these positions, a number of cells start to bulge out from the meristem and eventually will form the basis of the leaf primordium when cell division proceeds (Reinhardt et al., 2000; Pien et al., 2001). Dorsiventrality is specified early during primordium development and defines the adaxial and abaxial sides of the leaf (Bowman, 2000). Divisions at the margin of the primordium drive leaf blade inception. Further expansion of the leaf blade is controlled by a strong preference for anticlinal divisions, leading primarily to lateral outgrowth of the different tissue layers, of which the epidermis is the main layer driving leaf growth (Donnelly et al., 1999; Savaldi-Goldstein et al., 2007).

During leaf development of dicotyledonous species, a cell proliferation phase, characterized by actively dividing cells, is followed by a cell expansion phase, characterized by cell growth

and differentiation. After expansion, cells mature and the final leaf size is reached (Beemster et al., 2005). At the proliferation-to-expansion phase transition, cell division ceases along a longitudinal gradient from leaf tip to base (Donnelly et al., 1999). In the epidermis, the onset of differentiation coincides with the formation of stomata (De Veylder et al., 2001). A stomatal complex consists of two guard cells that control the aperture of the stomatal pore. Starting from a precursor meristemoid cell, a series of subsequent asymmetric divisions produce a number of guard mother and daughter cells. Subsequently, the guard mother cells divide symmetrically into two guard cells, ending the stomatal lineage. The daughter cells undergo cell fate specifications identical to those of the majority of the cells produced during the proliferation phase, resulting in puzzle-shaped pavement cells (Larkin et al., 1997; Geisler et al., 2000).

The final leaf size is determined by the total number of cells and the average cell size that result from cell division and cell expansion, respectively. Although the dynamics of these processes can be analyzed rigorously by the leaf growth kinematics (Fiorani and Beemster, 2006), knowledge of cell cycle duration, cell expansion, and their interaction at the individual cell level is still poorly understood, not only because of technical obstacles to study these phenomena, but also because a reduced cell proliferation is often compensated by an increase in cell size and vice versa (Tsukaya, 2002). Here, the individual cell sizes of pavement and guard cells were measured separately throughout leaf development. By fitting a mathematical model to these data, we could estimate the division and expansion parameters of pavement and guard cell populations within the growing leaf separately, allowing us to gain a better and more detailed insight into the processes that define leaf growth. Imaging of epidermal cells gave a good correlation between predicted and experimental cell growth data, supporting the model.

RESULTS

Following Leaf Growth during Development

Recent developments in microscopic and imaging technologies suggest that cell tracking is the most suitable manner to disentangle cell division and expansion in plants, allowing cells to be followed for 3 to 4 d and applied successfully to the root, the SAM, and sepals (Reddy et al., 2004; Campilho et al., 2006; Fernandez et al., 2010; Roeder et al., 2010). However, to cover the entire leaf development, a much longer time frame is needed. Furthermore, with these techniques only local observations can be made, which are not always easily correlated to global growth characteristics. Therefore, a general kinematic analysis of leaf growth in *Arabidopsis* (*Arabidopsis thaliana*) was used as a starting point (De Veylder et al., 2001). In this approach, the first developing leaf pair (leaves 1 and 2) was harvested on a daily basis 5 to 25 d after sowing (DAS). Leaves 1 and 2 were selected because they are nearly

indistinguishable and probably the best synchronized among replicate plants. Microscopic drawings of abaxial epidermal cells were made at 25% and 75% of the distance from the base to the tip of the leaf, giving an estimate of the average cell area. To approximate the total cell number per leaf, these average cell areas were combined with the measured total leaf area. When analyzed on a daily basis, average cell division and relative expansion rates can be calculated. Plotting of the leaf size evolution on a logarithmic scale revealed a linear increase until day 11, indicating exponential growth (Fig. 1A). From day 12 onward, relative leaf expansion rates decreased and the mature leaf size was reached approximately at 20 DAS. A similar evolution could be observed for the total cell number (Fig. 1B), with cell division rates being high until day 10 (Fig. 1C). Cell sizes remained relatively constant until day 10 (approximately $100 \mu\text{m}^2$), whereas from day 10 onward, the average cell size increased approximately 10-fold by day 20, as the result of cell expansion in the absence of cell division (Fig. 1D). Coinciding with the decrease in cell division rate, the stomatal index (fraction of guard cells among all cells) increased linearly (Fig. 1E). The relative leaf expansion rates were the highest during the high division rate period (Fig. 1F). When pavement and stomatal cells are considered separately, the total number of pavement cells increased gradually from day 5 to 14, while the number of guard cells continued to increase until day 17 (Supplemental Fig. S1), indicating that divisions giving rise to guard cells continued approximately 3 d longer than those forming pavement cells.

Cell Size Distributions

Although the kinematic data give an indication of the general growth processes during leaf development, leaves are considered as homogenous cell populations, which is a simplification because the epidermis consists of multiple cell types, each with distinct size characteristics at different time points during development. Furthermore, pavement cells and guard cells are interdependent, because pavement cells are formed together with stomata (Geisler et al., 2000). Additionally, the size of pavement cells ranges from 50 up to $20,000 \mu\text{m}^2$, illustrating the heterogeneity of the population. A better insight into the cell area distribution was gained by extension of the image analysis algorithm used for the kinematic analysis to allow size measurements of individual guard and pavement cells. To ascertain that the obtained data were representative for the complete leaf, we compared the data obtained from extrapolation of the measurements of cell sizes at two reference positions (25% and 75% between base and tip of the leaf blade) with those of microscopic drawings of five complete leaves at the transition from cell proliferation to cell expansion (namely in 9-d-old leaves). At this time point, the largest differences across the leaf would be expected because of the cell cycle arrest front that propagates along the leaf axis (Donnelly et al., 1999). Comparison of the data extracted from the complete leaves with those from the leaf reference sections revealed no significant differences for the average cell number and cell area. Furthermore, plotting of

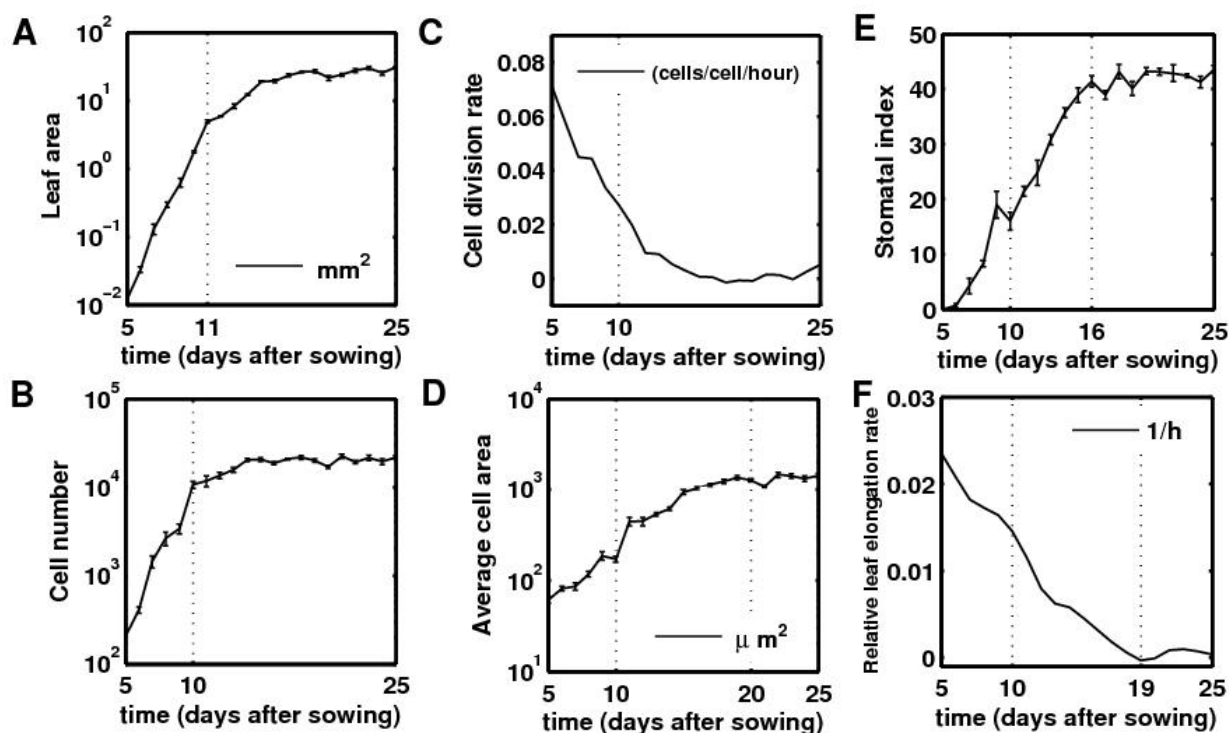


Figure 1. Kinematic growth data for the first true leaf pair of *Arabidopsis* seedlings. A, Leaf area. B, Total cell number. C, Cell division rate. D, Mean cell area. E, Stomatal index. F, Relative leaf elongation rate.

the cell size distributions also yielded a good overlay between the data resulting from the complete leaf and the leaf sections (Supplemental Fig. S2), demonstrating that the data sampling at the two reference positions is a valid approach to estimate cellular parameters for the complete leaf.

According to the cell area measurements as described above, 97% of the pavement cells of 5-d-old leaves were smaller than $100 \mu\text{m}^2$, whereas at day 8, only 62% of the cells had a size below this threshold, indicating that pavement cell sizes increase already during the cell proliferation phase. Early in the expansion phase, at 10 DAS, the maximum cell size detected was approximately $1,600 \mu\text{m}^2$ and 95% of the pavement cells were smaller than $500 \mu\text{m}^2$. From day 11 onward, the pavement cell area distribution broadened and the pavement cell population was distributed over a large range of cell sizes (Fig. 2A). Guard cell sizes ranged from 25 to $150 \mu\text{m}^2$, with a mean area of approximately $75 \mu\text{m}^2$. During leaf development, cell sizes increased continuously, reaching a maximum size of approximately $300 \mu\text{m}^2$ and an average area of $150 \mu\text{m}^2$ at 25 DAS (Fig. 2B).

To obtain quantitative information about the changes in cell size distributions during leaf development, we used the frequency distribution of the cell areas of pavement and guard cells for the whole leaf on day i (for details, see Supplemental Text S1). This absolute representation of the data revealed that from day 5 to 12, most pavement cells were very small (less than $300 \mu\text{m}^2$) and that the number of these small cells increased significantly

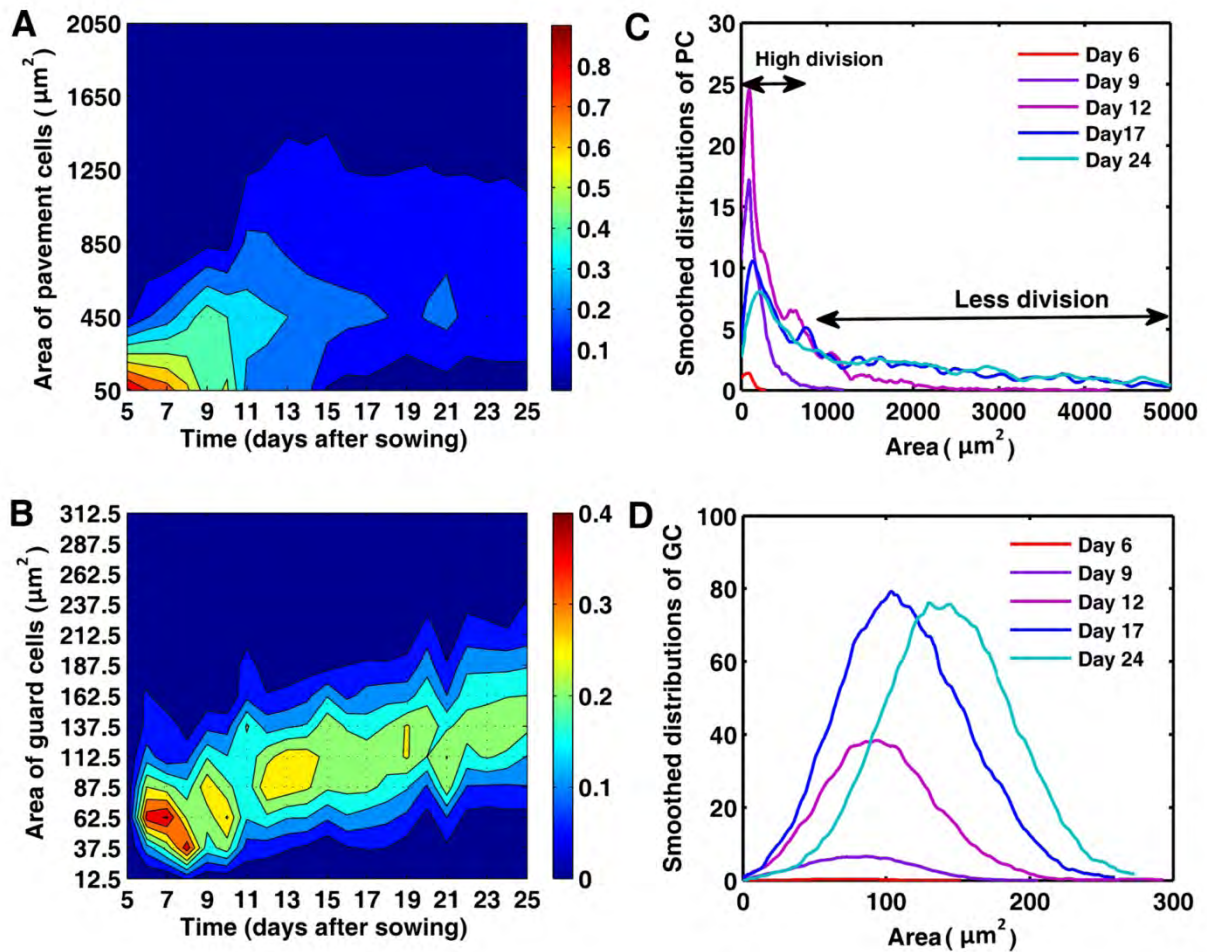


Figure 2. Cell size distributions during leaf development. A and B, Size distribution of pavement (A) and guard (B) cells in the abaxial epidermis of leaves 1 and 2. Color ranges indicate the fraction of the total number of cells present within a specific size bin. The vertical axis shows bins of cell areas (bin size is $400 \mu\text{m}^2$ and $25 \mu\text{m}^2$ for pavement and guard cells, respectively). Labels on the vertical axis mark the beginning of each bin. Red and blue correspond to high and low percentage of cells, respectively. The colors in the ranges between two consecutive bins are obtained by interpolation. C and D, Distribution of the number of pavement (C) and guard (D) cells per leaf during its development.

from day 6 to day 9 (Fig. 2C), corresponding to the high cell division rate during these days. From day 9 until day 12, the peak of the distribution curves was less pronounced and was accompanied by a high proportion of large cells, of which the number increased until day 17, after which the distribution of pavement cells remained relatively stable. The guard cell distribution was different. The graph had a symmetrical bell shape with a peak at the mean, revealing a roughly normal size distribution of guard cell sizes (Fig. 2D). Prior to day 9, the number of guard cells was low, but afterward increased significantly until day 17, indicating that most divisions of guard mother cells, leading to the formation of stomata, occurred relatively late during the epidermal development. After day 17, the complete guard cell size distribution continued to shift to the right, implying that cells had ceased dividing and continued to expand.

Mathematical Model for Leaf Development

To study in more detail the crucial parameters for cell division and cell expansion during leaf development, we built a general mathematical model that takes only the pavement and guard cells into account, because in our experimental system it is impossible to distinguish pavement from stomatal precursor cells. The model is based on the overall kinematics of leaf growth (Fig. 1), on the changes in size distribution of pavement and guard cells between successive days in function of cell expansion (Fig. 2), and on the changes in cell identity with each division event. Therefore, all possible transitions were considered that a cell can undergo from one day to the next: A precursor cell might either expand and divide into two pavement cells or two guard cells, or expand in the absence of division, whereas guard cells do not divide, but can expand. The model included a maximum guard cell size (GC_{\max}). As the final division in the stomatal lineage is symmetric, pavement cells larger than twice this size ($2GC_{\max}$), cannot divide into two guard cells. Additionally, a hypothetical threshold was introduced above which pavement cells can no longer divide (PC_{\max}). Apart from these, specific parameters used in the model were the average cell cycle duration time (T_c), average relative cell growth rates for pavement (g_{PC}) and guard cells (g_{GC}), and the probabilities p_1 and p_2 for a precursor cell to divide into pavement or guard cells, respectively. p_3 (equal to $1 - p_1 - p_2$) represented the probability for a pavement cell not to divide during a 24-h period. These probabilities represent different developmental pathways at the population level, rather than the status of an individual cell. This means that in principle cells that did not divide at day i , and in this way contribute to p_3 at that day, can still divide at day $i + 1$. This restriction to the population level is intrinsic to kinematic growth analysis, which does not track individual cells. PC_{\max} , T_c , g_{PC} , g_{GC} , p_1 , and p_2 are allowed to vary from day to day, whereas GC_{\max} , as a maximum size, remains constant throughout development.

Subsequently, we identified the different developmental categories for pavement cells at any given day (Fig. 3A). The first category contains cells with an area below $2GC_{\max}$ that can either divide into pavement or guard cells or stop dividing, contributing to fractions p_1 and p_2 . The second category contains cells with an area between $2GC_{\max}$ and PC_{\max} that can no longer become guard cells, because the resulting cells would exceed the maximum threshold size for guard cells. Therefore, a fraction p_1 of the cells in this category divided into pavement cells and the remainder ($1 - p_1$) expanded without division. The third category contains cells with an area above PC_{\max} that can no longer divide.

A precursor cell with an area a^* at day i could develop into a cell with area a at day $i + 1$ through several scenarios, called flows. These flows were defined by the state of cells at day i and $i + 1$ and the number of divisions required for the corresponding transition. Due to the 1-d time steps in the experimental data, in particular whether T_c is <24 h or ≥ 24 h, strongly affects the possible number of divisions during this time interval. The average cell cycle duration in a fully proliferating tissue, represented by days 5 to 8 in our analysis, was

calculated to be 25.6 ± 5.4 h (Supplemental Table S1). In a previous study, the average cell cycle duration for a fully proliferating tissue was found to be 20.7 h (De Veylder et al., 2001). Thus, to simplify the model, we restricted the parameter space by assuming that (on average) $T_c \geq 18$ h, implying that each pavement cell can undergo at most two divisions in 1 d.

Based on these assumptions, eight possible flows (F_1 – F_8) for pavement cells and one flow (F_9) related to guard cells were defined (Fig. 3B). Flow F_1 involves pavement cells that do not divide in 1 d, but only expanded. For dividing cells, possibilities differ based on whether the cell cycle duration time is shorter or longer than 24 h. For flows F_2 , F_3 , and F_6 , T_c was ≤ 24 h and pavement cells divide within 1 d either once (F_2) or twice (F_3) into pavement cells or guard cells (F_6). In flow F_3 , for the sake of simplicity, both newborn pavement cells are assumed to be dividing into pavement cells. Because $T_c > 18$ h, not many cells take part in this flow and therefore the number of missed events must be small. When $T_c > 24$ h, pavement cells can divide at most once in 1 d. In flow F_4 , pavement cells divide once, while in flow F_5 , they were dividing, but do not complete their division cycle within the 1-d time step. Flow F_7 is related to the pavement cells that divide into guard cells and flow F_8 to those that are in the process of dividing into guard cells, but do not complete the division in the 1-d time step. Finally, flow F_9 represents guard cells that expanded only.

For these flows, we constructed functions for the transitions between the size distributions of pavement and guard cells from a given day i , to the next. Although all flows differed, they have a common basic structure. To describe these functions mathematically, we introduced $G_k^i(a^*)$ as the distribution of cells (pavement or guard cells) with area a^* at day i that are transformed by the k -th flow and $F_k^{i+1}(a)$ as the distribution of cells (pavement or guard cells) with area a at day $i + 1$ into which they are transformed. We also introduced $f_{2,k}$ as a function defined by $f_{2,k}(a) = a^*$, meaning that a cell with area a at day $i + 1$ originates from a cell with area a^* that follows the k -th flow at day i . Therefore, for a small distance ε , the radius around a is:

$$f_{2,k}(a - \varepsilon) = a^* - \varepsilon_1 \quad (1)$$

$$f_{2,k}(a + \varepsilon) = a^* + \varepsilon_2 \quad (2)$$

where ε_1 and ε_2 are both approximately equal to $\frac{df_{2,k}(a)}{da} \varepsilon$. If $N_k(\varepsilon)$ is the number of cells at day $i + 1$ in $[a - \varepsilon, a + \varepsilon]$ that originates from the k -th flow, then this corresponds to $\frac{N_k(\varepsilon)}{n_k}$ cells in $[a^* - \varepsilon_1, a^* + \varepsilon_1]$ at day i , where n_k is the number of cells at day $i + 1$ that originate

from one cell at day i through the k -th flow. Hence, the distribution of cells with area a at day $i + 1$ is given by:

$$F_k^{i+1}(a) = \lim_{\varepsilon \rightarrow 0} \frac{N_k(\varepsilon)}{2\varepsilon} = \lim_{\varepsilon \rightarrow 0} \frac{n_k}{\varepsilon_1 + \varepsilon_2} n_k \lim_{\varepsilon \rightarrow 0} \frac{\varepsilon_1 + \varepsilon_2}{2\varepsilon} \quad (3)$$

$$= G_k^i(a^*) n_k \lim_{\varepsilon \rightarrow 0} \frac{\varepsilon_1 + \varepsilon_2}{2\varepsilon} \quad (4)$$

$$= G_k^i(f_{2,k}(a)) f_{1,k}(a) \quad (5)$$

where $f_{1,k}(a) = n_k \frac{df_{2,k}(a)}{da}$. The mathematical description of each flow and explicit form of each $f_{1,k}$ and $f_{2,k}$ is given in the model file (see Supplemental Text S1). Using the functions F_1, F_2, \dots, F_9 , we predicted the distribution of cells with area a at day $i + 1$ as follows

$$D_{PC}^{i+1}(a) = \sum_{k=1}^5 F_k^{i+1}(a) + F_8^{i+1}(a) \quad (6)$$

$$D_{GC}^{i+1}(a) = \sum_{k=6}^7 F_k^{i+1}(a) + F_9^{i+1}(a) \quad (7)$$

Where $D_{PC}^{i+1}(a)$ and $D_{GC}^{i+1}(a)$ are the predicted distributions of pavement and guard cells, at day $i + 1$, respectively. The right-hand sides of Equations 6 and 7 are obtained by using Equation 5 and the experimental distributions of pavement and guard cells at day i .

Parameter Estimation

The predicted distributions (Eqs. 6 and 7) were used to optimize the value of the parameters on which the functions F_1, F_2, \dots, F_9 depend, by optimizing the fit to the experimental data. To assess the optimization problem, two phases in the development of the leaf are considered: one that represents days 5 to 17, when cells divide regularly, implying that both cell division and expansion might happen simultaneously for some cells, and one from days 18 to 25, when the final cell numbers are reached and all cells stop dividing (Supplemental Fig. S1). Absence of cell division in the second stage of development reduces the number of parameters because both probabilities p_1 and p_2 are 0. Moreover, because of the lack of cell division, the maximum threshold for cell division of pavement cells (PC_{\max}) is irrelevant and can be eliminated. Therefore, g_{PC} , g_{GC} , and GC_{\max} are the remaining parameters to be estimated within the second phase of development.

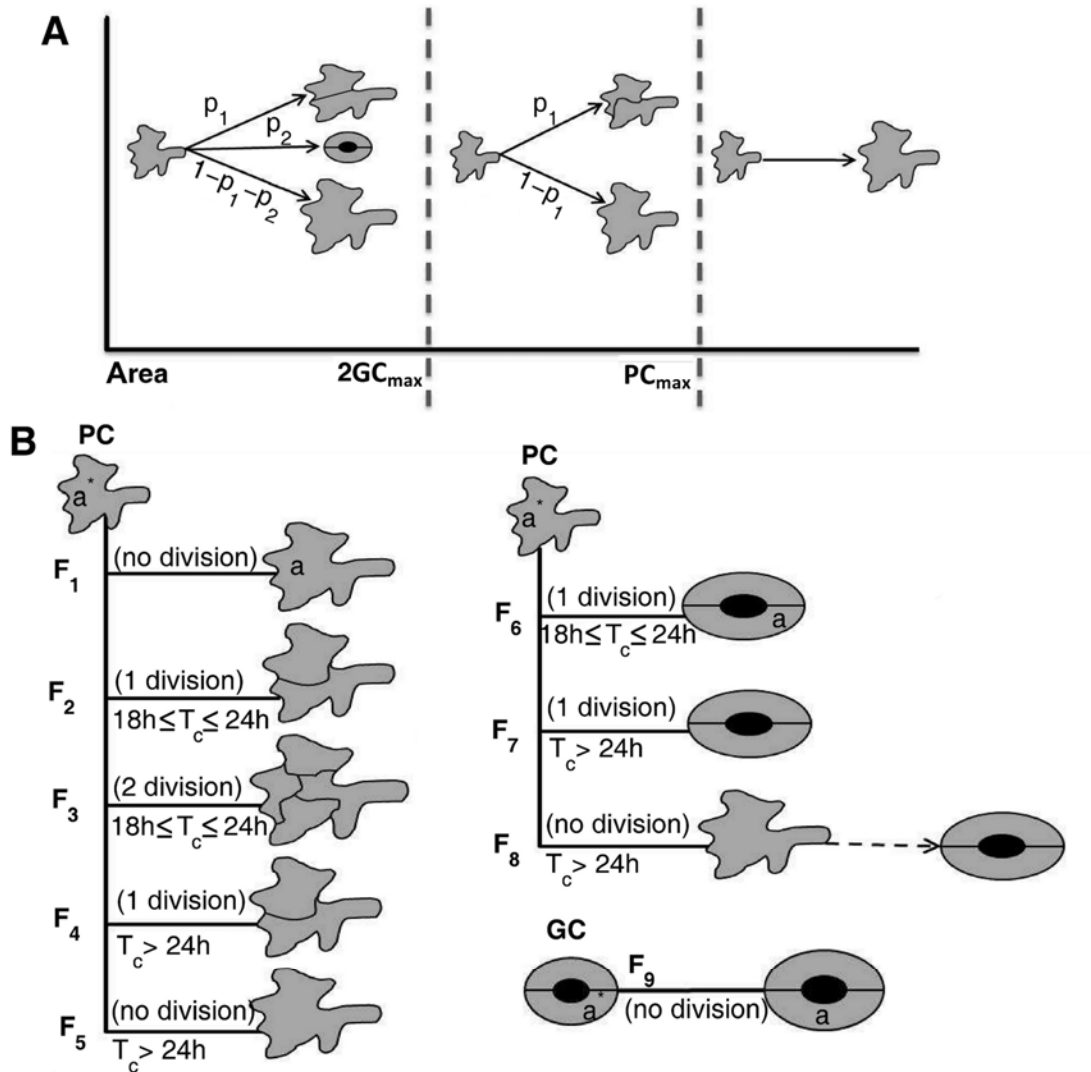


Figure 3. Different scenarios of division and expansion of pavement and guard cells over a 1-d interval. A, Size categories of pavement cells. B, Global scheme of the possible flows for pavement and guard cells. The flows are defined based on the fates of the cells and the duration of the cell cycle. PC and GC, Pavement and guard cells, respectively.

In the first phase of development, some a priori restrictions to the model are imposed to reduce the range in which parameters needed to be optimized. First, because no cell can divide into guard cell and pavement cell simultaneously, it is considered that $p_1 + p_2 \leq 1$. Second, we assume that at the early stages of leaf development all cells divide ($p_1 + p_2 = 1$ at days 5, 6, and 7), which is supported by the uniform expression of cell cycle marker genes in young leaves (de Almeida Engler et al., 2009). Accordingly, the number of cells during early leaf development approximately doubled every 24 h (Supplemental Table S1). Lastly, based on the size increase of guard cells over time (Fig. 2B), the maximum threshold for precursor cells to divide into guard cells ($2GC_{max}$) is based on GC_{max} computed in the second phase, which is then applied to the first phase. With the model and the experimental distributions of the pavement and guard cells on a given day, we predicted the distributions

for the next day. Although a best fit for the distribution of the guard cells at the earliest time points was difficult to find because of the low number of guard cells at the early stage of leaf development, experimental and computed data fitted well from 9 DAS onward (Supplemental Figs. S3 and S4).

Constancy of Average Cell Cycle Duration

Cell division rates quantify the rate at which cells progress through the cell cycle. In the kinematic growth analyses, the cell division rate decreased progressively (Fig. 1C). However, because division rates are calculated based on the total number of leaf cells, the observed decrease might be due to a reduction in the fraction of cells proliferating, an increase in the average cell cycle length, or a combination of both. To understand how the average division rate is controlled, it is essential to quantify the fraction of cells dividing into pavement (p_1) and guard (p_2) cells. As computed by the model, p_1 decreased gradually during leaf development, while p_2 increased, indicating a shift from basal proliferation to cell division in the stomatal lineage (Fig. 4A). The probability p_2 had the largest values between days 10 to 14, meaning that most stomata were produced during these days. After day 14, both probabilities dropped and decreased to 0, representing the exit of cell division during leaf development as indicated by an increase in probability p_3 , in which more than 80% of the cells did not divide after day 16.

Because the model allows us to split the total number of cells in a proliferative and an expanding population at the different stages of leaf development, a slowdown in the cell division rate can be discriminated from a reduction in the proliferative fraction. Average cell cycle duration (T_c) can be derived from the cell division rate and was determined for each day during leaf development. As discussed above, the impact of T_c in the model ended after day 18, when cell division stopped completely. Immediately prior to that, between days 16 and 18, the optimization results fluctuated a lot (Supplemental Fig. S5), implying that the proliferative fraction was too small to obtain reliable results. For earlier time points, however, a stable output value was obtained. Remarkably, when different days are compared, the obtained T_c value is nearly constant (Fig. 4B), indicating that the reduced cell division rate over the complete leaf during development by kinematic analysis was seemingly not caused by an increase in average cell cycle duration, but solely by a decrease in the proliferative fraction within the leaf.

Nonexistence of Size Threshold for Division

One of the parameters included in the model was the maximum guard cell size GC_{max} , which was designated a maximum threshold because guard mother cells, identified as pavement cells in our analysis, must have an area smaller than $2GC_{max}$ as a necessary condition for division into guard cells. As discussed above, the threshold for guard cells was calculated

easily in the second stage of development (from days 18–25), when no cells divided. When we assumed the threshold to be constant, the parameter optimization procedure provided a value equal to $354 \mu\text{m}^2$, which was only a little above that of the maximum guard cell size of $300 \mu\text{m}^2$ found in the experimental data (Fig. 2), illustrating the accuracy of the optimization methods. The value of GC_{max} indicated that cells with an area larger than approximately $700 \mu\text{m}^2$ are unable to divide into guard cells.

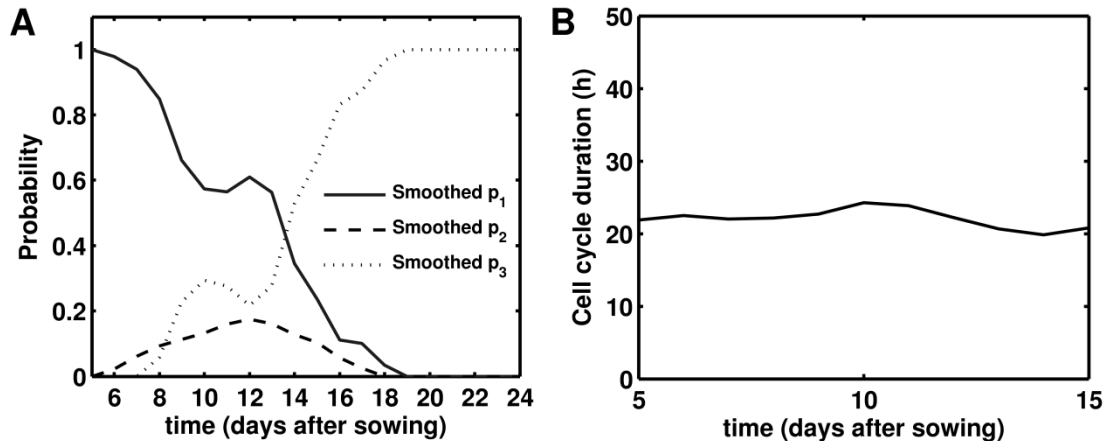


Figure 4. Predicted cell division parameters during leaf development. A, Probabilities for alternative divisions; p1: pavement cells, p2: guard cells, p3: no division. B, Average cell cycle duration.

In contrast to the robust value obtained for GC_{max} in nearly all simulations, the optimized parameter value for the threshold above which no divisions into pavement cells occur (PC_{max}) yielded erratic values. In cases with an optimal solution, the experimental cell size distribution (used to build the model) and the computed cell size distribution profiles strongly deviated (Fig. 5, A and B), implying that the found optimum was a spurious one. To strengthen this observation, simulations were done with fixed values for $\text{PC}_{\text{max}} = 300, 500, 1,000, \text{ and } 10,000 \mu\text{m}^2$ at day 11 to 12, when the leaf consists of both dividing and expanding cells. Consistently with the behavior of the model with fitted PC_{max} , small fixed values of PC_{max} resulted in a sharp deviation from the experimental data (Fig. 5C). As the PC_{max} value increased, the discrepancy between experimental and computed data gradually disappeared, which might be explained by the fact that most cells were smaller than the threshold and, thus that the PC_{max} value became less relevant. These observations demonstrate that the imposition of a threshold value for cell division in pavement cells is not compatible with the assumptions underlying the model. The nonexistence of a threshold for pavement cell division indicates that the size of a cell does not exclude it from dividing into a set of pavement cells, i.e. size alone does not prevent division. In accordance with this model prediction, pairs of relatively large pavement cells separated by a straight cell wall, indicative of a recent cell division event, could be observed in the epidermis of 14-d-old leaves (Supplemental Fig. S6).

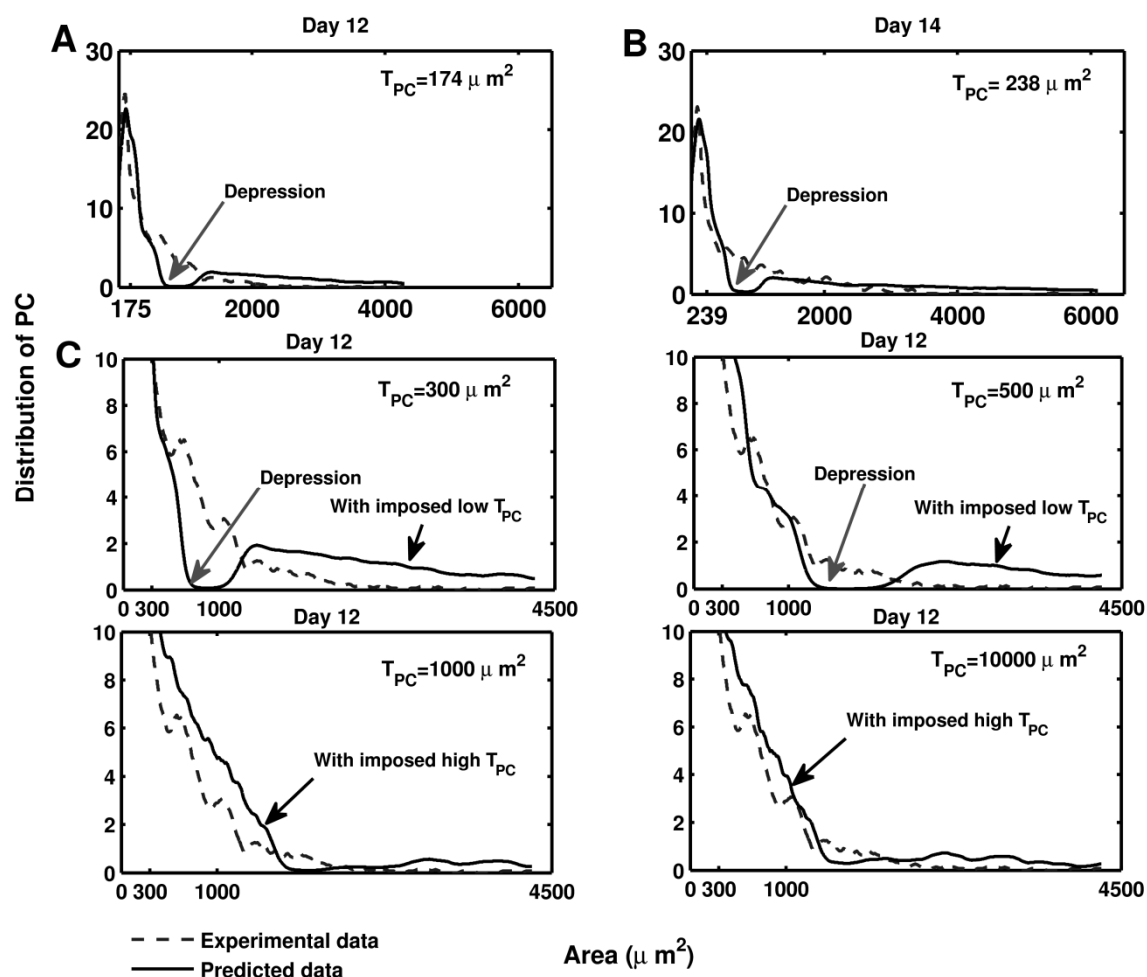


Figure 5. Observed and predicted pavement cell size distribution with optimized and imposed PC_{max} values. A and B, Comparison between the experimental and predicted pavement cell size distribution with optimized PC_{max} for day 12 (A) and day 14 (B). C, Comparison for different imposed values of PC_{max} at day 12. PC , Pavement cells.

Growth Rates of Epidermal Cells

The difference in maximum cell sizes found for pavement and guard cells suggests that the two cell types might expand at different rates. Therefore, the model allows for different relative growth rates (RGRs) for pavement and guard cells. Cell division and cell expansion are considered independently and RGRs do not only apply to expanding, but also proliferation cells.

The model results indicated that pavement cells had a high and increasing RGR from day 5 to day 13, with a profound increase between day 10 and 13 (Fig. 6A). From day 13 onward, the RGR declined steeply, suggesting that pavement cells grew faster in the young proliferating than in the older expanding leaves. Eventually, growth stopped completely after day 18. These observations are consistent with the experimental data because the average cell area

of pavement cells increased from $86 \mu\text{m}^2$ in the young leaf to nearly $1,500 \mu\text{m}^2$ between days 7 and 16, but did not change significantly after that (Fig. 1D). Similarly, guard cells displayed higher RGRs in the young than in the old leaves. Initially, the RGR of pavement cells was higher than that of guard cells, but from day 18 onward, stomata grew faster than pavement cells (Fig. 6A).

After day 18, pavement cells did not divide; hence, the RGR of small pavement cells ($<300 \mu\text{m}^2$) could be calculated by measuring the shift in the distribution peak in the experimental size distribution graphs (Fig. 2C). The average RGR of small cells determined this way was $0.009/\text{h}$, whereas the average RGR from day 18 until day 25 for all pavement cells calculated by the model was $0.0009/\text{h}$ (Fig. 6A). These results suggest that during the last days of leaf development, small pavement cells grow 10-fold faster than the average population. To confirm the surprising finding that adjacent cells of different size grow at different rates, we performed confocal imaging to directly measure RGRs for individual pavement and guard cells over a 36-h time interval. Cell-tracking experiments on leaves at 17 DAS confirmed that pavement cells smaller than $300 \mu\text{m}^2$ grew faster than large ones (P value = $3.65\text{e-}5$, Student's t test; Fig. 6, C and D). The average RGRs of small pavement cells decreased steeply from approximately 0.015 to 0.005 in the size range between 30 and $300 \mu\text{m}^2$. In larger cells, a relatively constant RGR was measured. Small guard cells ($<100 \mu\text{m}^2$) also grew faster than large ones (P value = 0.0017 , Student's t test; Fig. 6, C and E). In contrast to pavement cells, guard cells did not display a biphasic growth pattern, but a steady decrease in RGR with their cell size. Strikingly, at the transition of day 17 to 18 the average RGR of pavement cells measured by live imaging ($0.0065/\text{h}$) was nearly identical to the value obtained by the model ($0.0061/\text{h}$), independently confirming the model predictions (Fig. 6A).

DISCUSSION

Leaf development of *Arabidopsis* is driven by two processes, cell division and cell expansion (Green and Bauer, 1977). As both processes are intimately intertwined, their individual contribution to leaf growth is not easily studied experimentally. Here, we developed a mathematical model based on the fates of the two epidermal cell types found in the abaxial epidermis of the first leaf pair of *Arabidopsis* to fit experimentally derived data obtained over the course of its development from a young dividing leaf primordium into an adult organ. This model allowed us to disentangle cell division and cell expansion parameters for the individual cell types.

Differential Cell Expansion within the Leaf Epidermis

Individual cell size measurements yielded cell area distributions during leaf development. When the RGRs of guard cells and pavement cells were compared, the growth of these two cell types followed distinctly different dynamics. The guard cells initially grow more slowly but

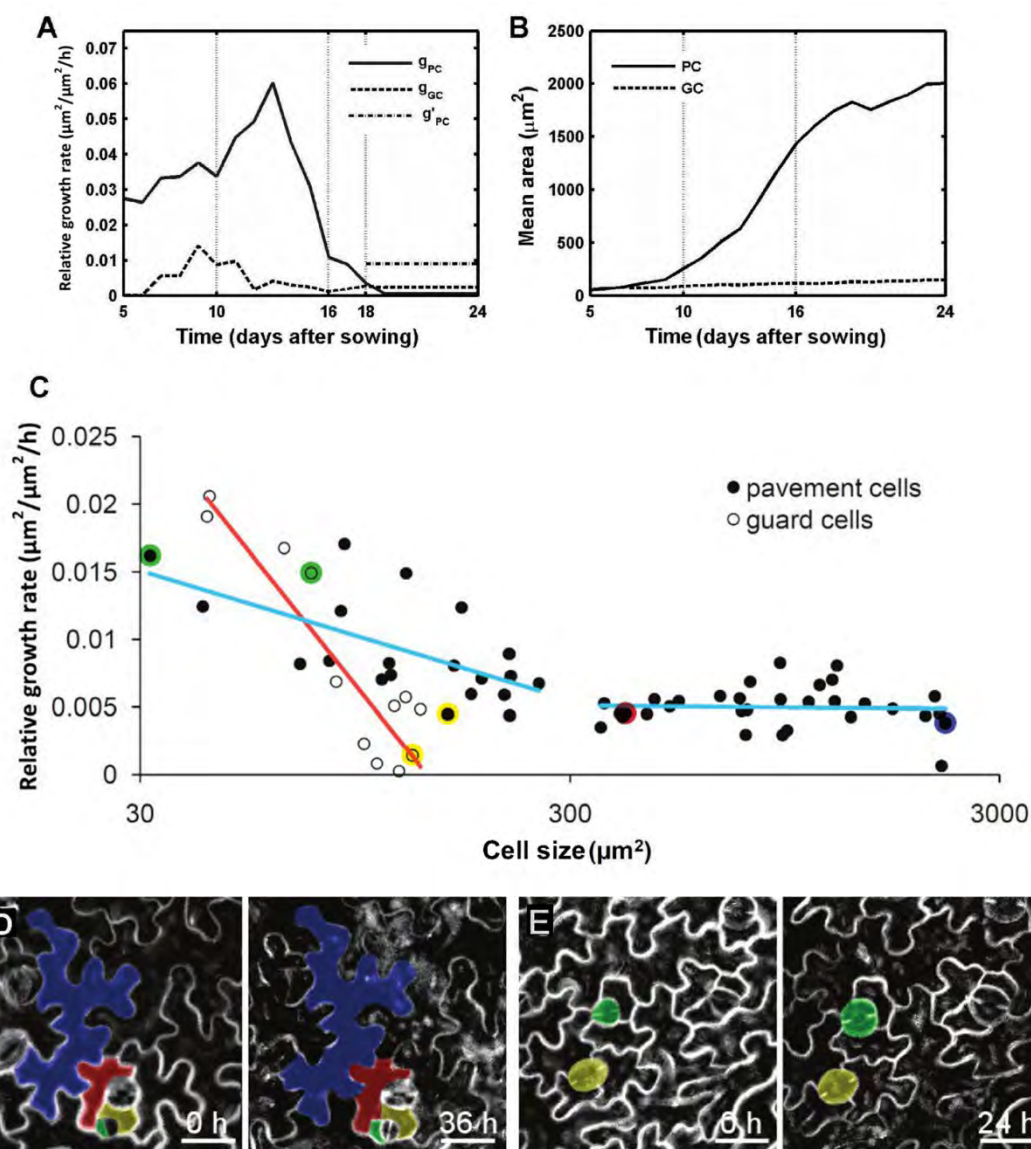


Figure 6. Differential cell growth rates during leaf development. A, Average RGRs of pavement (g_{PC}) and guard cells (g_{GC}). g'_{PC} is the experimentally observed average RGR of small pavement cells from days 18 to 25. B, Experimental mean area of pavement and guard cells. C to E, Live imaging of epidermal cell growth in leaves. C, RGRs of pavement and guard cells on the abaxial epidermis of leaves 1 and 2 of 17-d-old plants over a period of 36 h. Red and blue lines indicate a logistic regression for guard and pavement cells, respectively. Colored dots represent data of individual pavement and guard cells depicted in sections D and E. D, Time-lapse observations of epidermal cell development over a 36-h interval. E, Time-lapse observation of guard cells over a 24-h interval. Scale bars = 25 μm .

steadily, whereas the large pavement cells initially grow faster, but stop around day 16. Differences in RGRs between adjacent cells are surprising and have, to our knowledge, not been investigated in leaves. In the root, this problem has been studied by measuring cell sizes of different cell types (Beemster and Baskin, 1998). Root growth is linear and symplastic, meaning that neighboring cells grow uniformly, without altering the positions of adjacent walls. As a consequence, at a given distance from the tip, all cells have by definition

the same relative elongation rate (Green, 1976). This constraint implies that differences in mature cell sizes reflect differences in cell proliferation (Beemster and Baskin, 1998). In comparison, leaf growth is much more complex. As a leaf is a flat, exponentially growing structure with small and large cells dispersed over the epidermal surface, several parameters have to be taken into account in the equations. Time-lapse cell-tracking experiments on 17-d-old leaves indicate that small pavement and guard cells grow faster than large cells. Furthermore, modeling results indicated that relative cell growth rate of pavement cells is tightly regulated during development, peaking during the early leaf expansion phase, followed by a rapid reduction and no growth occurring at maturity. In other words, cells exiting the proliferative status grow faster than those being in full expansion phase. A high increase in the RGR was seen between days 10 and 14. Interestingly, this time frame coincides with the strongest increase in cellular DNA content through endoreduplication (Supplemental Fig. S7). During the endoreduplication cycle, cells do not divide but continue to increase their DNA content. A positive correlation is often seen between cell size and the level of endoreduplication (Sugimoto-Shirasu and Roberts, 2003). The observed correlation between the increase in relative cell growth rate and elevation in DNA content supports the generally assumed hypothesis that endoreduplication drives cell growth.

Taken together, the model reveals substantial differences in RGRs within the epidermal layer. Because guard cells, and small and large pavement cells are dispersed throughout the leaf, due to the patterning in the stomatal lineage, adjacent guard and pavement cells of various sizes might expand at different relative rates within the developing epidermis. Differential expansion of tissue layers in cylindrical organs, such as stems and roots, results in tissue tension, often redirecting growth, as in the case of shoot phototropism and root gravitropic curvature (Liscum and Stowe-Evans, 2000; Swarup et al., 2005). Leaf epinasty is also the consequence of differential growth of the abaxial and adaxial sides (Keller and Van Volkenburgh, 1997). Within one single tissue layer of a flat tissue structure, such as the abaxial leaf epidermis, tension is more difficult to translate into motion to release pressure. Disturbance of symplastic growth in the root by inducing differences in relative cell expansion rates between tissue layers causes cells to rupture and distort root growth (Ubeda-Tomás et al., 2009). However in the leaf, no cell ruptures are detected within the epidermis. Possibly, the lobes of epidermal pavement cells offer a way to dissipate the tissue tension. Remarkably, the characteristic jigsaw puzzle shape of pavement cells is established at the proliferation-to-expansion transition. Thus, the appearance of the puzzle shape fits with the moment at which differential relative cell expansion rates in adjacent cells would first appear. Furthermore, the emergence of lobes leading to the puzzle shape is preceded by the reorganization of cortical microtubules (Panteris and Galatis, 2005; Kotzer and Wasteneys, 2006) and application of external mechanical stresses to a tissue results in realignment of microtubules parallel to the maximal stress directions (Hamant et al., 2008). Based on these observations, it could be speculated that the occurrence of tissue tension within the epidermis

layer, caused by differential cell expansion, might realign cortical microtubules and trigger the puzzle-shape formation. More experimentation will be required to validate this intriguing hypothesis.

Interestingly, at maturity, the guard cells in *Arabidopsis* leaves are elevated above the surrounding pavement cells, presumably to increase their evaporative capacity. Faster relative growth of the guard cells and surrounding smaller pavement cells compared to the larger pavement cells that make up the bulk of the tissue area could explain the development of this elevation.

Control of Cell Cycle Duration

In the root, divisions in the meristematic zone ensure a constant cell production and indeterminate growth. While cells mature, they are displaced from the root tip and enter the elongation zone (Beemster et al., 2003). Thus, in the root, the developmental stages are separated in space. Furthermore, in the root meristem, practically all cells divide actively, implying that the cell division rate calculated for the meristem is a good overall average. In contrast, in leaves, the developmental stages are separated in time. Moreover, at the proliferation-to-expansion phase transition, the cell cycle arrest front that follows a longitudinal gradient, is accompanied by the differentiation of the first stomata (Donnelly et al., 1999; De Veylder et al., 2001), whereas cells at earlier stages in the stomatal lineage, dispersed through the leaf, keep proliferating for multiple days (Bergmann and Sack, 2007). Because of these constraints, the average cell division rate calculated on the basis of an increase in total cell number can only be measured experimentally during the early developmental stages, when all cells participate in division. Our mathematical model yielded probabilities for a cell to divide into two pavement cells, into two guard cells, or to exit the mitotic cycle, allowing the calculation of the proliferative fraction and the corresponding average cell cycle duration throughout the complete leaf development. Surprisingly, although the cell cycle length can vary significantly between adjacent cells within the SAM and sepals (Reddy et al., 2004; Roeder et al., 2010), the average cell cycle duration over the complete leaf epidermis remained constant during development. This observation is analogous to the situation in roots, where average cell cycle duration is considered to be constant between cell types and between different positions in the meristem (Ivanov et al., 2002). Moreover, the average cell cycle duration of approximately 20 h found for the leaf is comparable to that for the root (Beemster and Baskin, 1998). These data indicate that the constancy of cell cycle duration is widespread and that the basal cell division rate is strongly conserved at a cellular level (Baskin, 2000).

Interaction between Cell Division and Cell Growth

For decades, cell biologists have been interested in the process that links cell size and cell division (Neufeld and Edgar, 1998), but the interaction is currently unclear. Some reports have argued that epidermal pavement cells of *Arabidopsis* leaves divide only rarely at a cell size larger than $400 \mu\text{m}^2$ (Donnelly et al., 1999; Geisler et al., 2000), suggesting a possible size threshold preventing cell division. By contrast, a study on the root meristem hinted at the lack of a maximum cell size threshold for cell division, because cells divide at very different sizes (Ivanov et al., 2002; Beemster et al., 2003). Similarly, our mathematical model suggests no threshold for cell division, because such a threshold would result in a deviation from the observed cell size distributions. Furthermore, cell size distributions show that the average pavement cell size increases during the proliferation phase. Thus, in the leaf epidermis, cells of different sizes divide, providing additional evidence for the nonexistence of a fixed threshold size for division. Moreover, the increase in cell size during proliferation points toward a disequilibrium between cell growth and cell division. The constant average cell cycle duration implies that this increase in cell size is due to relative cell expansion rates exceeding cell division rates, uncoupling cell size from cell division. In conclusion, in wild-type plants, cell division seems to be relatively independent of the status of cell expansion, whereas the cell cycle might act more as a timer than as a size-regulated machinery. Interestingly, studies of mutants and transgenic lines have revealed that cell division and cell expansion are somehow coordinated by multiple mechanisms, so that inhibition of one will be compensated by increased activity of the other and vice versa (Ferjani et al., 2007). The new model-based analysis of cell size distributions of mutants displaying this compensation phenomenon could be a manner to pinpoint the underlying mechanisms.

MATERIALS AND METHODS

Plant Material and Growth Conditions

Wild-type *Arabidopsis* (*Arabidopsis thaliana*) Heyhn. plants of the Columbia-0 accession were used for kinematic analysis of leaf growth. The plasma membrane marker 35S::GFP-PIP2a was used for live imaging of epidermal cell growth (Cutler et al., 2000). Seeds for in vitro analysis were sterilized in 3% bleach for 15 min and sown on medium containing 0.5× Murashige and Skoog medium (Duchefa) solidified with 9 g/L plant tissue culture agar (Lab M) on round plates (1013; Becton-Dickinson). After a stratification period of 2 d, the plates were placed in a growth chamber under long-day conditions (16 h of light, 8 h of darkness) at 22°C with a light intensity of 80 to 100 $\text{mE m}^{-2} \text{s}^{-1}$ supplied by cool-white fluorescent tubes (Spectralux Plus 36W/840; Radium).

Kinematic Growth and Image Analysis

Leaf growth kinematics were analyzed as described (De Veylder et al., 2001). The leaf blade area of leaves 1 and 2 of five plants at 5 to 24 DAS was measured from dark-field binocular (days 8–24) or differential interference contrast light microscopy images (days 5–7). Microscopic drawings containing approximately 100 cells, located 25% and 75% from the tip and the base of the leaf blade on the abaxial side of each leaf were made with a drawing tube attached to the microscope equipped with differential interference contrast optics. The microscopic drawings were scanned for digitization. An in-house developed image analysis algorithm was subsequently used to automatically extract detailed measurements from the microscopic drawings, such as total area of the drawing, total number of cells, and number of stomata. Kinematic growth characteristics were calculated and plotted from these measurements. Extension of the image analysis algorithms allowed discrimination between pavement and guard cells and individual cell area measurements for these two cell types separately. Guard cells were extracted as cells $<500 \mu\text{m}^2$ neighboring the stomatal pores. The remaining cells were designated as pavement cells. These cell measurements were pooled by day and allowed the construction of cell area distributions. Therefore, cell areas of pavement and guard cells were classified into bins of $100 \mu\text{m}^2$ and $25 \mu\text{m}^2$, respectively. Relative and absolute frequency distributions were plotted with MATLAB. The image analysis algorithms were written in C++ scripts and used the SDC morphology toolbox for C++ (www.mmorph.com/cppmorph/).

Live Imaging of Epidermal Cell Growth in the Leaf

At 16 DAS, three complete plants harboring the plasma membrane marker 35S::GFP-PIP2a (Cutler et al., 2000) were transferred under sterile conditions from in vitro plates to a round microscopic chamber (Warner instruments) with liquid $0.5\times$ Murashige and Skoog growth medium (Duchefa). One leaf of the first leaf pair of each plant was flattened on the bottom of the chamber by overlaying it with a block of solidified agar. The abaxial epidermis was imaged with a confocal microscope with the software package LSM510 (Zeiss) from 17 to 18 DAS. Z stacks were recorded at five different positions with 12-h intervals over a total period of 36 h. Epidermal cells in the Z stacks were projected onto a single reconstructed view with the extended depth of field plug in (Forster et al., 2004) for ImageJ (<http://rsbweb.nih.gov/ij/>). Cell lineages were manually tracked and measured at each time point with ImageJ. The RGRs for each cell were calculated as the average RGR of this cell over the different time intervals. Growth rates of 53 pavement cells and 13 guard cells were tracked over time.

Flow Cytometry Analysis

Plant material was chopped in 200 μL of Cystain UV Precise P Nuclei extraction buffer (Partec), supplemented with 800 μL of staining buffer. The mix was filtered through a 50- μm green filter and read through the Cyflow MB flow cytometer (Partec). The nuclei were analyzed with the FloMax software. The endoreduplication index was calculated from the percentages of each ploidy class with the formula: endoreduplication index = $(0 \times \%2C) + (1 \times \%4C) + (2 \times \%8C) + (3 \times \%16C) + (4 \times \%32C)$.

SUPPLEMENTAL DATA

The following materials are available in the online version of this article.

(<http://www.plantphysiol.org/cgi/doi/10.1104/pp.111.181180/>)

Supplemental Figure S1. Experimental and smoothed total number of pavement and guard cells during leaf development.

Supplemental Figure S2. Validation of data extraction of two reference points for the whole-leaf cellular data analysis.

Supplemental Figure S3. Comparison between experimental and model-predicted cell size distributions of pavement cells.

Supplemental Figure S4. Comparison between experimental and model-predicted cell size distributions of guard cells.

Supplemental Figure S5. Result of 100 optimizations for the cell cycle duration.

Supplemental Figure S6. Putative recently divided pavement cells.

Supplemental Figure S7. Endoreduplication kinetics during leaf development.

Supplemental Table S1. Initial estimation of the average cell cycle duration T_c .

Supplemental Text S1. Mathematical description model.

ACKNOWLEDGMENTS

We thank Martine De Cock for help in preparing the manuscript. This work was supported by the Research Foundation-Flanders (grant no. G.0065.07) and the Interuniversity Attraction Poles Programme (grant no. IUAP VI/33), initiated by the Belgian State, Science Policy Office, the Agency for Innovation by Science and Technology in Flanders (predoctoral fellowship to S.D.), and the Research Foundation-Flanders (postdoctoral fellowship to V.B.).

CONTRIBUTIONS

Stijn Dhondt developed the image analysis scripts, performed the kinematic analysis, and extracted the cell size distributions. Subsequent data analysis was performed by Leila Kheibarshekan Asl and Stijn Dhondt. Leila Kheibarshekan Asl built the mathematical model and performed related calculations. Véronique Boudolf conducted the flow cytometry experiments and screened for putative recently divided pavement cells with a jig-saw puzzle shape. Stijn Dhondt performed the live imaging experiments.

REFERENCES

Baskin TI (2000) On the constancy of cell division rate in the root meristem. *Plant Mol Biol* 43: 545–554

Beemster GTS, Baskin TI (1998) Analysis of cell division and elongation underlying the developmental acceleration of root growth in *Arabidopsis thaliana*. *Plant Physiol* 116: 1515–1526

Beemster GTS, De Veylder L, Vercruyssen S, West G, Rombaut D, Van Hummelen P, Galichet A, Gruissem W, Inzé D, Vuylsteke M (2005) Genome-wide analysis of gene expression profiles associated with cell cycle transitions in growing organs of *Arabidopsis*. *Plant Physiol* 138: 734–743

Beemster GTS, Fiorani F, Inzé D (2003) Cell cycle: the key to plant growth control? *Trends Plant Sci* 8: 154–158

Benková E, Michniewicz M, Sauer M, Teichmann T, Seifertová D, Jürgens G, Friml J (2003) Local, efflux-dependent auxin gradients as a common module for plant organ formation. *Cell* 115: 591–602

Bergmann DC, Sack FD (2007) Stomatal development. *Annu Rev Plant Biol* 58: 163–181

Bowman JL (2000) Axial patterning in leaves and other lateral organs. *Curr Opin Genet Dev* 10: 399–404

Campilho A, Garcia B, Toorn HV, Wijk HV, Campilho A, Scheres B (2006) Time-lapse analysis of stem-cell divisions in the *Arabidopsis thaliana* root meristem. *Plant J* 48: 619–627

Cutler SR, Ehrhardt DW, Griffiths JS, Somerville CR (2000) Random GFP::cDNA fusions enable visualization of subcellular structures in cells of *Arabidopsis* at a high frequency. *Proc Natl Acad Sci USA* 97: 3718–3723

de Almeida Engler J, De Veylder L, De Groodt R, Rombauts S, Boudolf V, De Meyer B, Hemerly A, Ferreira P, Beeckman T, Karimi M, et al. (2009) Systematic analysis of cell-cycle gene expression during Arabidopsis development. *Plant J* 59: 645–660

De Veylder L, Beeckman T, Beemster GTS, Krols L, Terras F, Landrieu I, Van Der Schueren E, Maes S, Naudts M, Inzé D (2001) Functional analysis of cyclin-dependent kinase inhibitors of Arabidopsis. *Plant Cell* 13: 1653–1668

Donnelly PM, Bonetta D, Tsukaya H, Dengler RE, Dengler NG (1999) Cell cycling and cell enlargement in developing leaves of Arabidopsis. *Dev Biol* 215: 407–419

Ferjani A, Horiguchi G, Yano S, Tsukaya H (2007) Analysis of leaf development in fugu mutants of Arabidopsis reveals three compensation modes that modulate cell expansion in determinate organs. *Plant Physiol* 144: 988–999

Fernandez R, Das P, Mirabet V, Moscardi E, Traas J, Verdeil J-L, Malandain G, Godin C (2010) Imaging plant growth in 4D: robust tissue reconstruction and lineaging at cell resolution. *Nat Methods* 7: 547–553

Fiorani F, Beemster GTS (2006) Quantitative analyses of cell division in plants. *Plant Mol Biol* 60: 963–979

Forster B, Van De Ville D, Berent J, Sage D, Unser M (2004) Complex wavelets for extended depth-of-field: a new method for the fusion of multichannel microscopy images. *Microsc Res Tech* 65: 33–42

Geisler M, Nadeau J, Sack FD (2000) Oriented asymmetric divisions that generate the stomatal spacing pattern in Arabidopsis are disrupted by the too many mouths mutation. *Plant Cell* 12: 2075–2086

Green PB (1976) Growth and cell pattern formation on an axis: critique of concepts, terminology, and modes of study. *Bot Gaz* 137: 187–202

Green PB, Bauer K (1977) Analysing the changing cell cycle. *J Theor Biol* 68: 299–315

Hamant O, Heisler MG, Jönsson H, Krupinski P, Uyttewaal M, Bokov P, Corson F, Sahlín P, Boudaoud A, Meyerowitz EM, et al. (2008) Developmental patterning by mechanical signals in Arabidopsis. *Science* 322: 1650–1655

Ivanov VB, Dobrochaev AE, Baskin TI (2002) What the distribution of cell lengths in the root meristem does and does not reveal about cell division. *J Plant Growth Regul* 21: 60–67

Keller CP, Van Volkenburgh E (1997) Auxin-induced epinasty of tobacco leaf tissues. *Plant Physiol* 113: 603–610

Kotzer AM, Wasteneys GO (2006) Mechanisms behind the puzzle: microtubule-microfilament cross-talk in pavement cell formation. *Can J Bot* 84: 594–603

Larkin JC, Marks MD, Nadeau J, Sack F (1997) Epidermal cell fate and patterning in leaves. *Plant Cell* 9: 1109–1120

Liscum E, Stowe-Evans EL (2000) Phototropism: a “simple” physiological response modulated by multiple interacting photosensory-response pathways. *Photochem Photobiol* 72: 273–282

Neufeld TP, Edgar BA (1998) Connections between growth and the cell cycle. *Curr Opin Cell Biol* 10: 784–790

Panteris E, Galatis B (2005) The morphogenesis of lobed plant cells in the mesophyll and epidermis: organization and distinct roles of cortical microtubules and actin filaments. *New Phytol* 167: 721–732

Pien S, Wyrzykowska J, McQueen-Mason S, Smart C, Fleming A (2001) Local expression of expansin induces the entire process of leaf development and modifies leaf shape. *Proc Natl Acad Sci USA* 98: 11812–11817

Reddy GV, Heisler MG, Ehrhardt DW, Meyerowitz EM (2004) Real-time lineage analysis reveals oriented cell divisions associated with morphogenesis at the shoot apex of *Arabidopsis thaliana*. *Development* 131: 4225–4237

Reinhardt D, Mandel T, Kuhlemeier C (2000) Auxin regulates the initiation and radial position of plant lateral organs. *Plant Cell* 12: 507–518

Roeder AHK, Chickarmane V, Cunha A, Obara B, Manjunath BS, Meyerowitz EM (2010) Variability in the control of cell division underlies sepal epidermal patterning in *Arabidopsis thaliana*. *PLoS Biol* 8: e1000367

Savaldi-Goldstein S, Peto C, Chory J (2007) The epidermis both drives and restricts plant shoot growth. *Nature* 446: 199–202

Sugimoto-Shirasu K, Roberts K (2003) “Big it up”: endoreduplication and cell-size control in plants. *Curr Opin Plant Biol* 6: 544–553

Swarup R, Kramer EM, Perry P, Knox K, Leyser HMO, Haseloff J, Beemster GTS, Bhalerao R, Bennett MJ (2005) Root gravitropism requires lateral root cap and epidermal cells for transport and response to a mobile auxin signal. *Nat Cell Biol* 7: 1057–1065

Tsukaya H (2002) Interpretation of mutants in leaf morphology: genetic evidence for a compensatory system in leaf morphogenesis that provides a new link between cell and organismal theories. *Int Rev Cytol* 217: 1–39

Ubeda-Tomás S, Federici F, Casimiro I, Beemster GTS, Bhalerao R, Swarup R, Doerner P, Haseloff J, Bennett MJ (2009) Gibberellin signaling in the endodermis controls *Arabidopsis* root meristem size. *Curr Biol* 19: 1194–1199

4

Exit from proliferation during leaf development in *Arabidopsis thaliana*: a not so gradual process

Megan Andriankaja,^{1,2,#} Stijn Dhondt,^{1,2,#} Stefanie De Bodt,^{1,2,#} Hannes Vanhaeren,^{1,2} Frederik Coppens,^{1,2} Liesbeth De Milde,^{1,2} Per Mühlenbock,^{1,2} Aleksandra Skirycz,^{1,2} Nathalie Gonzalez,^{1,2} Gerrit T.S. Beemster^{1,2,3} and Dirk Inzé^{1,2,*}

¹Department of Plant Systems Biology, VIB, 9052 Gent, Belgium

²Department of Plant Biotechnology and Genetics, Ghent University, 9052 Gent, Belgium

³Department of Biology, University of Antwerp, 2020 Antwerp, Belgium

This chapter is adapted from: Developmental Cell (in press); Accepted November 23, 2011.

These authors contributed equally to the article

* Corresponding author; e-mail: dirk.inze@psb.vib-ugent.be

SUMMARY

Early leaf growth is sustained by cell proliferation and subsequent cell expansion that initiates at the leaf tip and proceeds in a basipetal direction. Using detailed kinematic and gene expression studies to map these stages during early development of the third leaf of *Arabidopsis thaliana*, we showed that the cell cycle arrest front did not progress gradually down the leaf, but rather was established and abolished abruptly. Interestingly, leaf greening and stomatal patterning followed a similar basipetal pattern, but proliferative pavement cell and formative meristemoid divisions were uncoordinated in respect to onset and persistence. Genes differentially expressed during the transition from cell proliferation to expansion were enriched in genes involved in cell cycle, photosynthesis, and chloroplast retrograde signaling. Proliferating primordia treated with norflurazon, a chemical inhibitor of retrograde signaling, showed inhibited onset of cell expansion. Hence, differentiation of the photosynthetic machinery is important for regulating the exit from proliferation.

INTRODUCTION

The plant leaf, by providing the basis for energy capture, is at the core of plant growth and ultimately an important part of human economic activities. Leaf development is extremely plastic and leaf size depends on genetic predisposition, leaf position, and environmental conditions. Many specific aspects of leaf development have been studied in the model plant *Arabidopsis thaliana*, including leaf initiation (Barbier de Reuille et al., 2006), abaxial/adaxial differentiation (Braybrook and Kuhlemeier, 2010), vascular development (Scarpella et al., 2010), stomatal development (Peterson et al., 2010), cell cycle regulation (Donnelly et al., 1999; Beemster et al., 2005; Boudolf et al., 2009), and trichome formation (Pesch and Hülkamp, 2009). Extensive collections of mutants in leaf shape and size have been generated (Berná et al., 1999; Horiguchi et al., 2006), but the regulatory networks that control growth and final organ size are still poorly understood (Byrne, 2005; Gonzalez et al., 2009). The development of a growing dicotyledonous leaf has been divided into three main stages: primordium initiation, primary morphogenesis, and secondary morphogenesis (Donnelly et al., 1999). Leaf primordia initiate off the flanks of the shoot apical meristem at regions of high auxin and low cytokinin accumulation (Traas and Monéger, 2010). During primary morphogenesis, leaf growth is sustained by successive cell divisions and specific structures, such as trichomes, vasculature, and stomata, begin to form. Lastly, during secondary morphogenesis, the cells cease proliferating and begin to expand, mainly by cell wall loosening that continues to fuel further leaf growth (Cosgrove, 2005). Thus, the overall change in cell size in a growing organ over time depends on the balance between cell growth and division rates (Green, 1976). As dividing cells also grow, we use the terms "proliferation" to refer to this joint activity (Beemster and Baskin, 1998) and "expansion" to cell growth without cell division.

The transition from cell proliferation to expansion is a complex process with many factors interacting to create a network of growth control at both the transcript and protein levels (Gonzalez et al. 2009). Over time, the transition was shown to proceed in a gradient down the leaf, with cell proliferation first ceasing in the tip and then progressively down the longitudinal axis (Donnelly et al., 1999; Kazama et al. 2010). Differences in the timing of this transition will affect the number of cells formed and therefore potentially also leaf size. To date, numerous leaf size mutants have been described (Lee et al., 2006; Gonzalez et al., 2009; Horiguchi et al., 2009; Pérez-Pérez et al., 2009). Some genes have been found also that alter leaf size by affecting the transition from primary to secondary morphogenesis, such as *SHORT-ROOT*, *DA1*, and *AINTEGUMENTA* (Mizukami and Fischer, 2000; Li et al., 2008; Horiguchi et al., 2009; Dhondt et al., 2010) and *KLUH/CYP78A5* and *GRF5* have been proposed to play a role in the arrest front progression (Gonzalez et al., 2010; Kazama et al., 2010). Curiously, inhibition of cell proliferation is often compensated by an induction in cell expansion, so that the effects on the whole organ size are often strongly diminished (De Veylder et al., 2001; Tsukaya, 2002; 2003; Beemster et al., 2003).

Transcriptome analysis of leaves at proliferation and expansion stages has allowed for the identification of many genes specific for proliferation and expansion (Beemster et al., 2005), while other transcriptome studies have identified marker genes that can be used as predictors of the differentiation status of leaves (Efroni et al., 2008). Although these studies have contributed to the broad understanding of leaf and rosette development, many questions remain regarding which transcriptional events occur precisely during the crucial transition from primary to secondary morphogenesis. These transcriptional events are of prime interest because they could potentially regulate the final cell number and, thus, the overall leaf size.

Here, we characterized the progression of the third leaf of *Arabidopsis* through the transition from primary to secondary morphogenesis by using our image analysis algorithms to visualize and quantify the size and shape of the cells and transcriptome analysis to show that the transition from cell proliferation to expansion occurs abruptly and simultaneously with the onset of photomorphogenesis. We provide evidence that retrograde signaling from chloroplasts can affect the onset of transition from proliferation to expansion, revealing a previously unknown level of regulatory complexity during the transition from primary to secondary morphogenesis.

RESULTS

Image analysis as a tool to quantify positional changes in cell morphology

In theory, the timing of the transition between primary and secondary morphogenesis determines the number of cells and, thus, to some extent, the final leaf size. This transition occurs when a significant increase in cell size is observed (Donnelly et al., 1999; Tsukaya,

2002; Beemster et al., 2003, 2005) and when the cell morphology changes from circular for proliferating cells to the typical jigsaw puzzle-shape for expanding and mature pavement cells. To map these morphological changes, third leaves of *in-vitro* grown *Arabidopsis* seedlings were harvested daily from day 8 to 14 after stratification, which spans the transition from primary to secondary leaf morphogenesis. At these time points, the length of the leaves increased throughout the time series from 0.29 ± 0.01 mm (SEM) to 1.92 ± 0.12 mm (SEM) (data not shown). Representative leaves from each time point were used to microscopically draw the cells of the abaxial epidermis along the complete proximal-distal axis. As individual drawings contained up to 7000 cells, we developed specific image-analysis algorithms to quantify and visualize the morphological and positional information of each cell (Figure 1). For this data extraction, guard cells and extremely large pavement cells lining the leaf margins and overlaying the midvein (Figure S1) were excluded from the drawings, because their size and shape were not representative for the developmental stage of the leaf. Pavement cell shape was measured with a circularity score ranging from 1 to 0, with 1 indicating a perfect circle. As the value approached 0, cells were progressively more lobed, indicative of expanding cells. Cell area, cell circularity, and the position of the center of mass of the pavement cells relative to the leaf tip were recorded. Cell shape and size gradients along the leaf lengths were visualized by coloring cells according to parameter values (Figures 1E and 1F). These in-house developed image-analysis algorithms allowed us to clearly visualize (Figures 1E and 1F) and quantify the changes in cell morphology along the length of transitioning leaves.

Pavement cell size and shape: indicators of the developmental stage during early leaf development

At early time points (days 8 and 9), the cells maintained a high circularity and a low and relatively constant average cell area (approximately $100 \mu\text{m}^2$ across the entire leaf length), a consequence of balanced cell division and cell growth rates and indicative of cell proliferation. At the start of day 10, cells in the leaf tip became larger and less circular, indicative of cell expansion (Figure 2), whereas at days 13 and 14, the cells at the leaf base also showed increased cell areas and reduced circularity scores, implying that the cells started to expand at all positions along the leaf length (Figure 2). Thus, at days 8 and 9, the third leaf consisted entirely of proliferating cells, whereas from day 10, the cells in the leaf tip started to expand and those at the base continued to proliferate. This gradient of cell proliferation and expansion persisted through days 11 and 12. At days 13 and 14, the majority of cells at the leaf base also began to expand. Interestingly, the trends of both changes in cellular shape and area were similar across the leaf length (Figures 2A and 2B). Between days 9 and 10, when the transition to cell expansion began at the tip, the cells differed significantly in both shape and area. As the pavement cell area increased in expanding cells, so too did the lobing

of the cell (Figure S2). Thus, image analysis revealed that size and shape of pavement cells are correlated indicators of the developmental stage of the leaf.

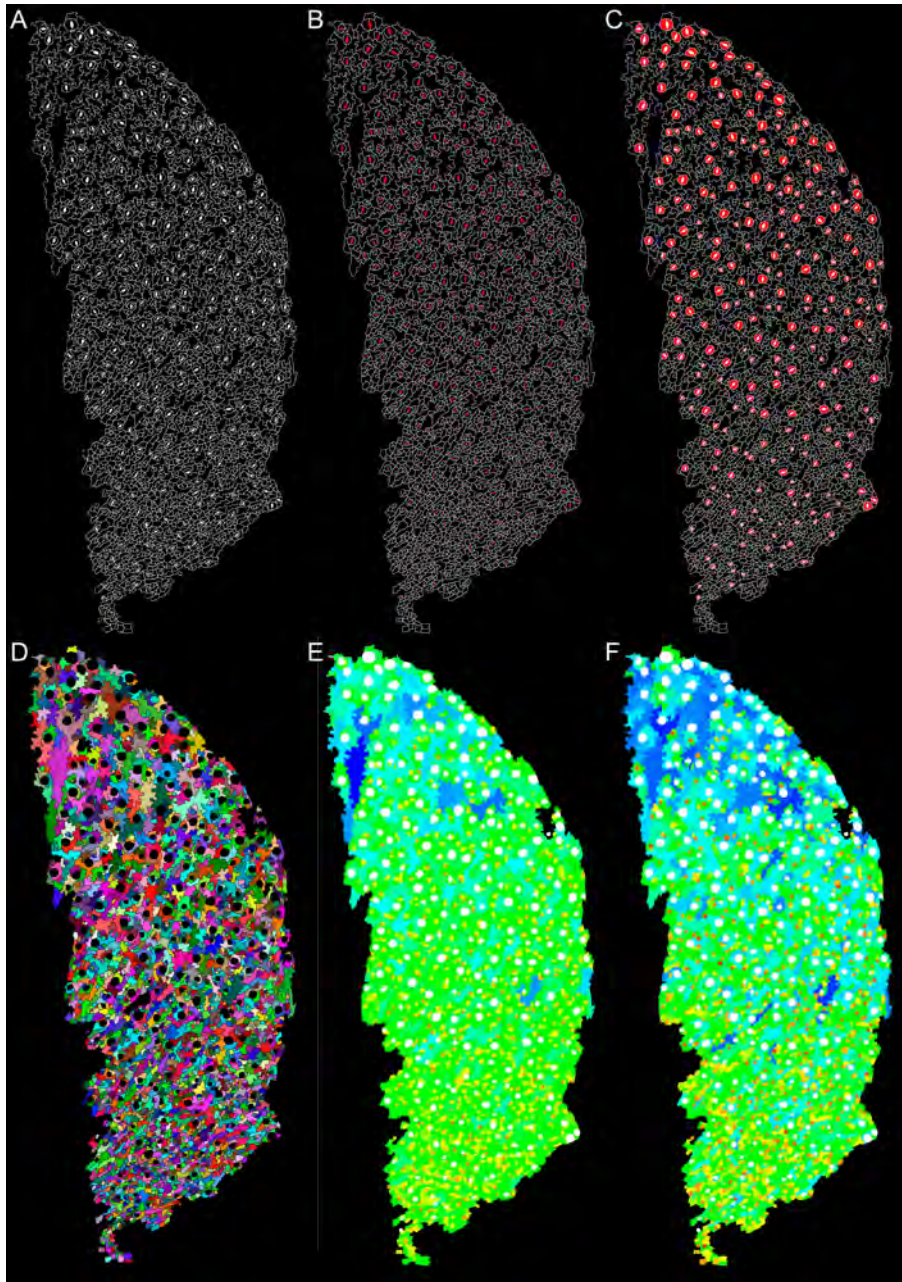


Figure 1. Image analysis of a microscopic drawing of the abaxial epidermis of the third leaf 12 days after stratification

(A) Original microscopic drawing.

(B and C) Guard cells were identified as cells with an area smaller than $500 \mu\text{m}^2$ adjacent to the stomatal pores.

(D) Pavement cells randomly colored for visualization of individual cells.

(E) Pavement cells color-coded according to cell size. The color gradient (red-yellow-green-cyan-blue) represents an exponential scale, ranging from the minimum to the maximum cell size measured in the image.

(F) Pavement cells color-coded according to circularity. The color gradient represents a linear scale ranging from the minimum to the maximum cell circularity measured in the image. See also Figure S1 for a representative pre-processed leaf drawing.

The cell proliferation gradient of pavement cells is established rapidly and then abruptly disappears

To characterize how the cell cycle arrest front migrates along the leaf, we used cell area and circularity as parameters to delimit the proliferation and expansion zones in the leaf. As leaf 3 at days 8 and 9 consisted completely of proliferating cells, it was possible to use these two time points to establish size and shape thresholds to define proliferating cells. With a confidence interval of 99%, the criteria for proliferation were a circularity score greater than 0.3894 and a cell area smaller than $261.38 \mu\text{m}^2$ (Figure 3A). These thresholds were applied

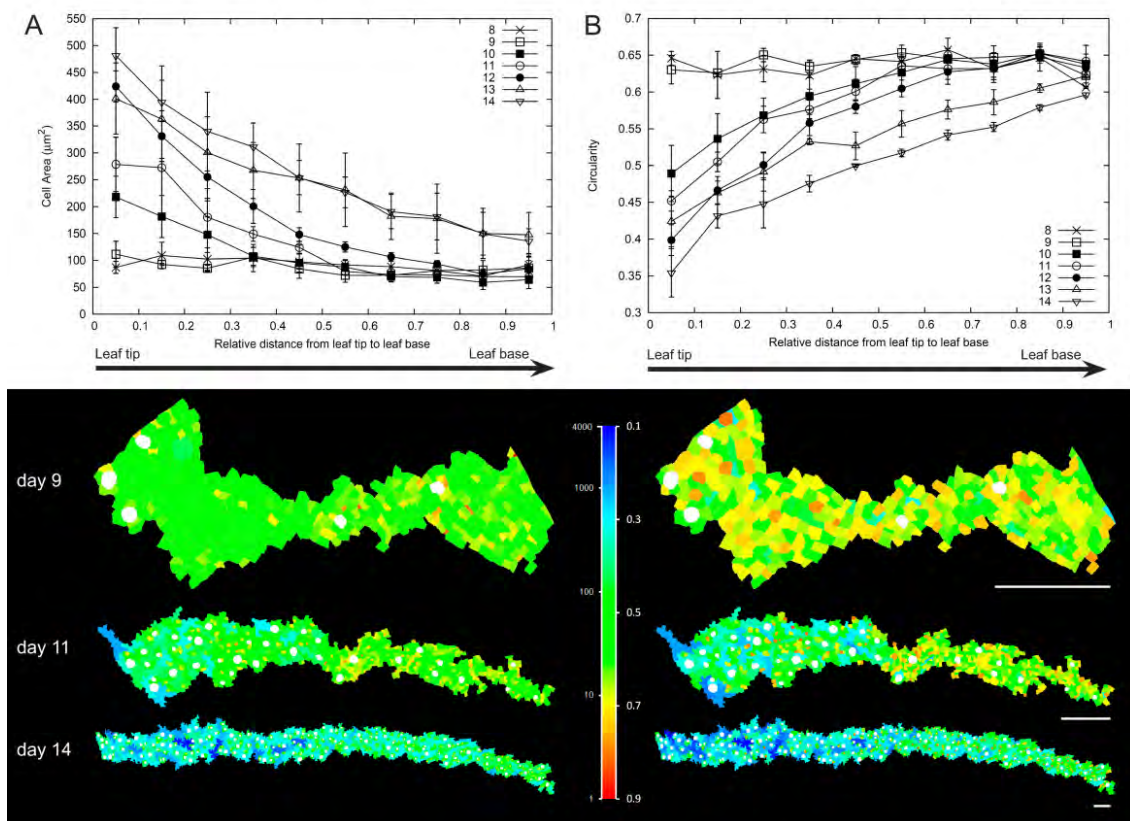


Figure 2. Spatial distributions of cell size and shape along the length of the leaf

The progressive change in cell area and cell shape along the length of the leaf was quantified by calculating the average size and shape of cells within 10-percentile distance bins ranging from the base to the tip of the leaf.

(A) Average cell area in function of the position along the leaf.

(B) Average cell circularity along the leaf. To accommodate for the increasing length of the leaf, position was expressed as the relative distance from the tip to the base and averages were calculated for all cells located in 10% intervals. For both cell area and cell shape, representative images are shown for day 9 (proliferative), day 11 (in transition), and day 14 (expanding) with the tip and base of each leaf aligned with one another to show the relative changes in cell size and shape across leaves at different time points. The color gradient (red-yellow-green-cyan-blue) represents an exponential and linear scale for cell size and circularity, respectively, ranging from the minimum to the maximum measurement in the total time series. Scale bar = 0.1 mm. Error bars are SEM. See also Figure S2 for correlations between cell sizes and shapes.

to the later time points to determine which cells fit the shape and size criteria for proliferation (Figure S3). Subsequently, we performed image analysis to visualize these cells and to extract positional information (Figure 3B). The proliferation zone was defined as the region of the leaf where at least 90% of the cells in a bin met the proliferation criteria defined above (Figure 3B). At days 8 and 9, proliferating cells occurred at every position along the leaf, whereas, at days 13 and 14, nowhere could leaves qualify as proliferative anymore. From these analyses, we observed that the proliferation zone of the leaf comprised 63%, 53%, and 38% of the proximal-distal leaf axis at days 10, 11, and 12, respectively (Figure 3B). These findings were confirmed by profiling a *CYCB1;1*-D-box:GUS-GFP translational fusion (Figure S4A). The B-type cyclin gene *CYCB1;1* was expressed uniformly throughout all cell layers, further supporting the use of the epidermis as a marker for tracking cell proliferation in the leaf (Figure S4B). Thus, between days 9 and 10, the proliferation zone was rapidly delimited; from days 10 to 12, it gradually decreased across the proximal-distal axis throughout transition; and between days 12 and 13, it was rapidly consumed because no zones had more than 90% proliferative cells anymore.

Characterization of the proliferation and expansion zones throughout early leaf development

While the relative length spanned by the proliferation zone in the leaf base decreased throughout development, both the proliferation and expansion zones increased in absolute size as the leaf developed. For the proliferation zone, this growth was achieved primarily through an increase in cell number, because the average cell area remained constant throughout the developmental time series (Figure 3C). For the expansion zone, the cell area increased by 24% between days 10 and 12, whereas its size tripled during the same period (Figure 3C), indicating that the increase in expansion zone size was also primarily due to an increased number of cells shifting from the proliferation to expansion state. Interestingly, the proportion of cells maintained within each zone was highly constant during transition. At all three transition time points (days 10, 11, and 12), approximately 80% of all the cells in the leaf were found in the proliferation zone and approximately 1000 new cells were recruited each day into the expansion zone to keep a proportion of 20% of the total cells (Figure 3C). Thus, even though the fraction of the leaf made up by the proliferation zone gradually decreased, the absolute size of this zone continued to increase until day 12, after which it abruptly disappeared. The only constant throughout the transition period was the proportion of cells within the two zones.

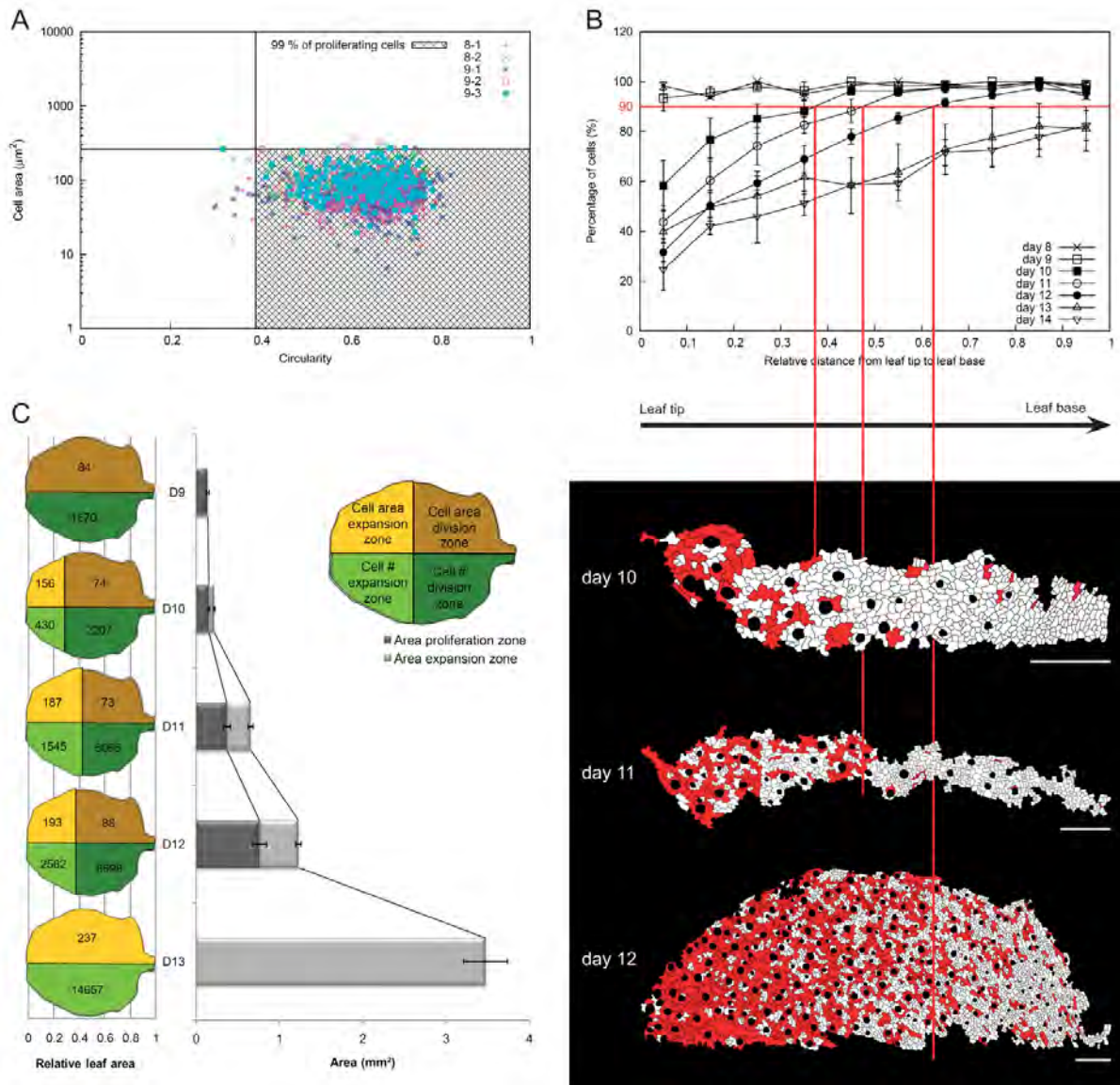


Figure 3. Definition and characterization of the proliferation and expansion zones

(A) Distribution of cell area and shape measurements of samples at days 8 and 9. Shaded box indicates 99% of the data points used to define the criteria for annotating the proliferation status of the cells for the subsequent time points.

(B) Percentage of cells in each time point that exceeded the proliferation thresholds set in (A) across the relative length of the leaf. Representative images are shown for the three time points during the transition (day 10, 11, and 12). Red-colored cells were defined as expanding according to the cell proliferation criterion established. Red lines mark the boundary region between the expanding and proliferation zones of the leaf.

(C) Relative and absolute areas of the proliferation and expansion zones for time points during the transition. The length of the proliferation arrest front from the leaf base is not to scale. Scale bar = 0.1 mm. Error bars are SEM. See also Figures S3 and S4.

Stomatal patterning and pavement cell transition follow different developmental gradients

Stomatal development during the transition from proliferation to expansion was analyzed in function of position along the leaf by image analysis. To this end, the stomatal index (SI), i.e. the fraction of guard cells in the total population of epidermal cells in a certain region, was calculated throughout the time course on the same images used for the pavement cell measurements. On days 8 and 9, the SI at the tip of leaf 3 was approximately 0.14, indicating that even before any pavement cells had begun to expand, stomatal guard cells had already differentiated in the same area (Figure 4A). At day 10, the SI ranged between 0.1 and 0.25 throughout the entire length of the leaf, excluding only the proximal 15% (Figure 4A), indicating that stomatal differentiation had already occurred even in the highly proliferative zone in the leaf base. Over the subsequent time points, the SI continued to increase throughout the length of the leaf and, at day 14, meristemoids, the stomatal precursor cells, were still present in the tips and bases of the leaves, implying a continued stomatal formation even after the last time point in the analysis (Figure 4B). Moreover, the SI continued to rise even through day 21, once all pavement cells were completely expanded (Skiryecz et al., 2010). Nevertheless, at day 14, the leaf tip already showed final values for the SI. These data indicate that stomatal differentiation also follows a temporal and spatial gradient in leaves, but that this gradient is independent from the one driving the transition from pavement cell proliferation to expansion.

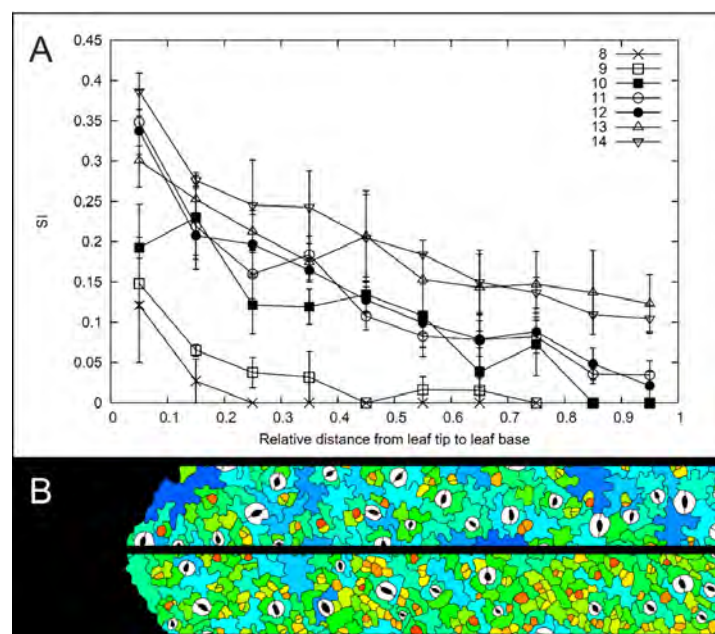


Figure 4. Stomatal development along the length of the leaf

(A) Stomatal index (SI) along the relative length of the leaf.

(B) Image from the distal region (top) and basal region (bottom) of an expanding leaf at day 13. Meristemoids are cells with the highest circularity and are colored red, whereas guard cells are white. Error bars are SEM.

Transcriptome analysis during transition

To identify the molecular events associated with early leaf development, gene expression profiles from whole leaves at six developmental time points (day 8 to day 13) were analyzed with AGRONOMICS1 tiling arrays (Rehrauer et al., 2010). This genome-wide array probes both the sense and antisense strands, with over 29,920 gene models represented by at least three probes. Over 9585 genes were differentially regulated between at least two time points, 1761 of which were not present on the Affymetrix ATH1 microarrays (see Experimental Procedures) (Figure S5A). To characterize the gene expression patterns, differentially expressed genes were clustered with a cluster affinity search technique (CAST) (Ben-Dor et al., 1999). A total of 35 clusters were found, with 80% of the genes present in the six main clusters (Figure S6). In general, these six clusters showed gradual expression changes (Figure 5): in the 4767 genes of clusters 1, 3, and 4, the expression gradually decreased, whereas in the 2916 genes of clusters 2, 5, and 6, it gradually increased. Functional enrichment, as determined by PageMan (Usadel et al., 2006), revealed that up-regulated genes in clusters 2, 5, and 6, were enriched in genes involved in photosynthesis, cell wall synthesis, secondary metabolism and transport, whereas the down-regulated genes in clusters 1, 3, and 4, were enriched for genes involved in general transcription, chromatin remodeling, DNA synthesis, cell cycle, and translation (Figure 5). Of the total number of differentially expressed genes, 18.9% were present only on the tiling array. A similar percentage of tiling array-specific genes were observed within each of these six main clusters. However, the genes that were not clustered, or were in clusters with less than 20 genes, had a much higher proportion, 69% of genes, present only on the tiling array. This observation indicated that the differentially expressed genes present only on the tiling array had distinct expression patterns (Figure S5B). Moreover, as seen previously (Redman et al., 2004; Laubinger et al., 2008; Rehrauer et al., 2010), the expression of many of these genes was low (Figure S5C).

The sharp transition from cell proliferation to expansion at days 10 and 13 is supported by the transcriptome

The morphometric data revealed that cell expansion began abruptly in the tip of leaf 3 at day 10 and in the leaf base at day 13 (Figure 2). To identify more precisely which molecular events coincided with these changes, each pair of consecutive days were compared directly (see Experimental Procedures; Figure 6A; Figure S7). The majority of transcriptional changes occurred between days 9 and 10, with 2208 transcripts differentially expressed, of which most were present in clusters 1 and 2. Remarkably, a second wave of transcriptional regulation was observed between days 12 and 13 with 463 transcripts differentially expressed (Figure 6A). Between these abrupt transitional shifts, few transcriptional changes were observed. No more than a total of 210 genes were differentially regulated between days

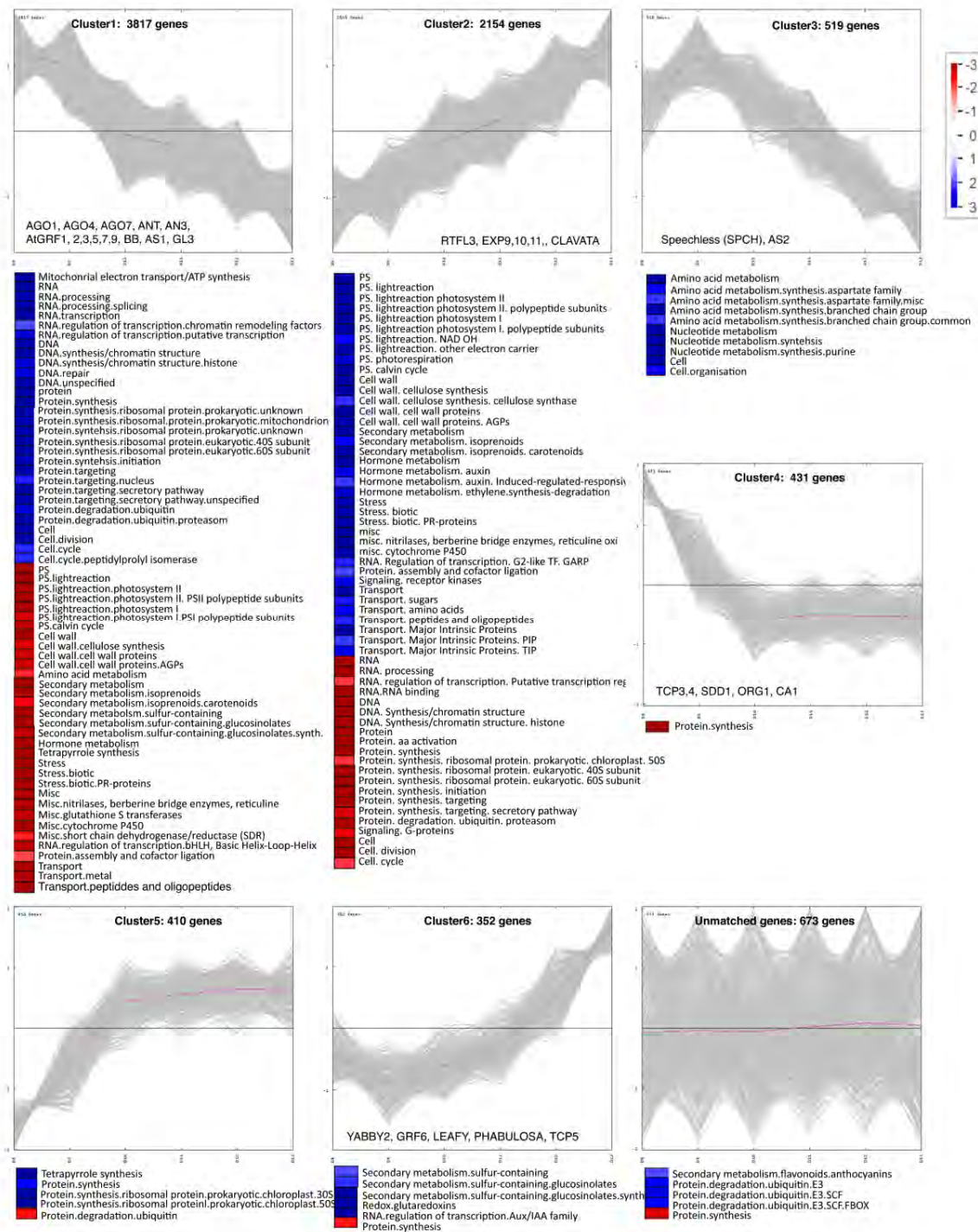


Figure 5. Six most populous clusters and unclustered genes from CAST clustering and PageMan enrichments of functional categories differentially expressed within each cluster

For clustering, a threshold parameter of 0.759 and a minimum of 20 genes per cluster were used (red, underrepresented; blue, overrepresented). Selected genes previously shown to be involved in leaf development are identified in the cluster they belong. See also Figures S5 and S6 for more details on the transcriptional analysis.

10 and 12. Genes activated during both transcriptional shifts of differentiation were involved in controlling cell wall formation, primarily the arabinogalactin proteins, fasciclin-like arabinogalactans, expansins, and cellulose synthases, while the down-regulated genes

functioned mostly in cell cycle and cell division (Figures S5B-S5E). Although the same processes were affected at both transitions, the specific genes differed. Genes involved in cell division were enriched at both transitions, but the D-type cyclin gene *CYCD3;2* was the only core cell cycle gene (Vandepoele et al., 2002) that was repressed during the two transitions and, interestingly, the cell cycle-inhibitory gene *SIAMESE-RELATED1 (SMR1)* was the only cell cycle gene activated over the time course. *SMR1* is highly similar to *SIAMESE (SIM)*, which has been shown previously to promote endoreduplication (Churchman et al., 2006). This molecular evidence supported the observed morphological transition from cell proliferation to expansion that happens rapidly between days 9 and 10 (onset of cell expansion) and days 12 and 13 (end of cell proliferation) (Figures S5B-S5E), although the precise mechanism probably differs.

Chloroplast differentiation: an important regulator of the simultaneous onset of cell expansion and photosynthesis

From the image analysis, we observed that stomata were already visible in the leaf by day 9 (Figure 4) and, correspondingly, between days 8 and 9, carbonic anhydrase transcripts and proteins responsible for shuttling carbon dioxide and regulating stomatal opening and closure were up-regulated (Figure S7) (Hu et al., 2010). Thus, this suggests that leaf 3 could start functioning as a photosynthetically active tissue just before the onset of cell expansion. Functional enrichment analysis revealed that indeed, besides cell proliferation and expansion, many processes were affected between days 9 and 10, including photosynthesis (photosystems I and II, photorespiration, and Calvin cycle) and transport (sugar and water) (Figures 7A and 7B; Figure S7), conspicuously coinciding with the greening of the leaf tip at day 10 that followed a similar basiplastic developmental pattern (Figure 7C). Most interestingly, transcripts in tetrapyrrole synthesis, the biochemical precursors of chlorophylls and hemes, were significantly enriched in cluster 5, which showed increasing expression between days 8 and 9, when the leaf is still fully proliferating (Figure 5). Curiously, the tetrapyrrole pathway was not affected in the branch leading to heme formation; instead, most up-regulated genes were upstream of Mg-protoporphyrinogen IX formation, an intermediate in chlorophyll biosynthesis that has been implicated in retrograde signaling (Voigt et al. 2010). These results suggest that chloroplastic retrograde signaling might precede the transition to cell expansion and differentiation of the photosynthetic machinery.

To investigate whether retrograde signaling plays a crucial role in the transition from cell proliferation to expansion, we manipulated this signaling pathway by means of norflurazon (NF), a chemical inhibitor of chloroplast differentiation that had been used to detect nuclear genes that might be targeted by retrograde signaling (Koussevitzky et al., 2007). The differentially expressed genes between days 9 and 10 were significantly enriched with genes also found to be differentially expressed in publicly available microarray data sets of plants treated with NF (Strand et al., 2003). In the up- and down-regulated genes between

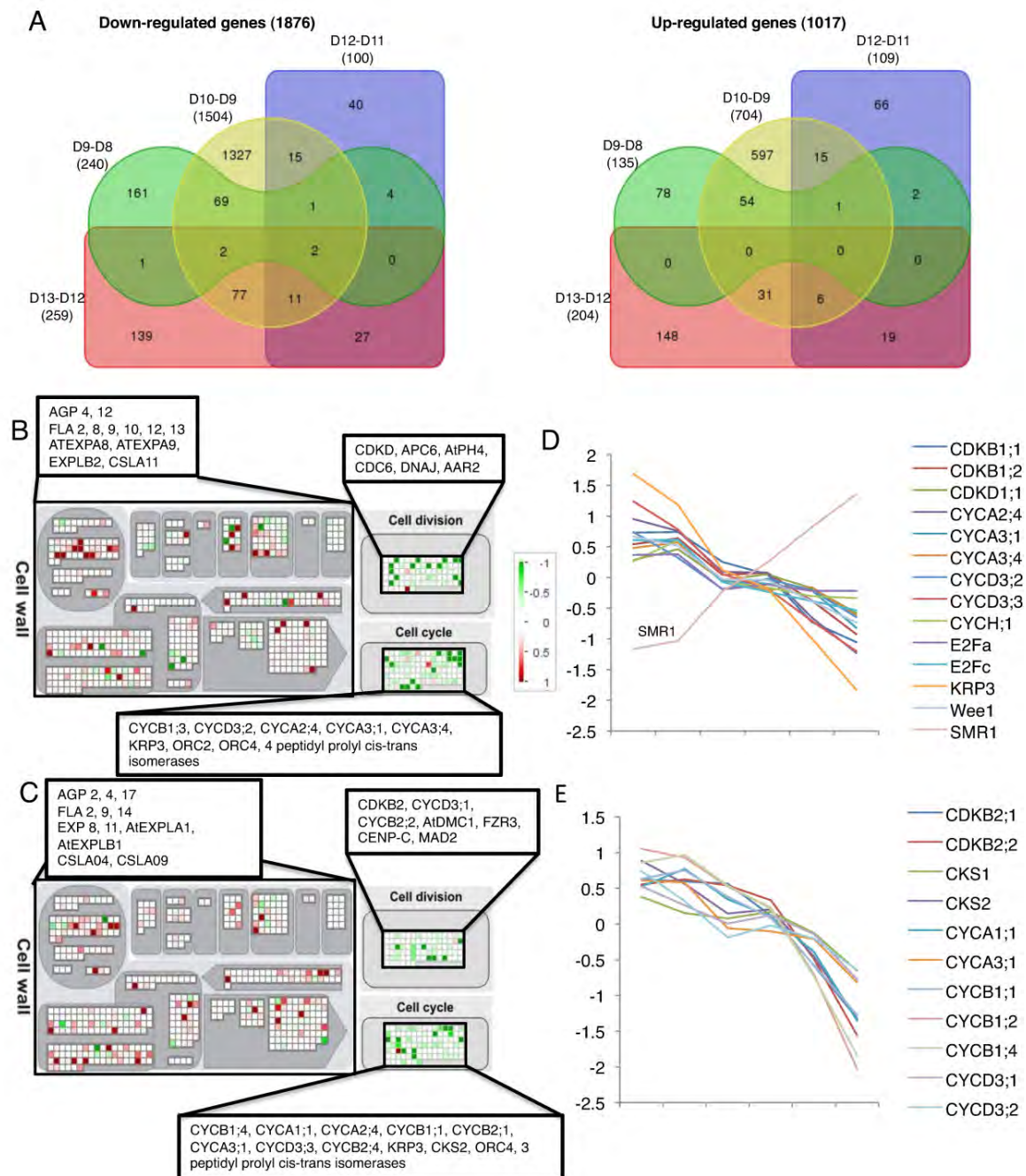


Figure 6. Differentially expressed genes between sequential time points

(A) Venn diagram (<http://bioinformatics.psb.ugent.be/webtools/Venn/>) of total numbers of differentially regulated genes specifically between sequential pairwise comparisons.

(B and C) Selected significantly differentially expressed genes specifically between days 9 and 10 and days 12 and 13, respectively, with FC >0.5 or <-0.5 and P -value <0.05.

(D and E) Expression profiles of core cell cycle regulators that were significantly differentially expressed (P -value <0.05) between days 9 and 10 and between days 12 and 13, respectively. See also Figure S7.

days 9 and 10, a 4-fold (P -value 9.57×10^{-114}) and 2-fold (P -value 1.30×10^{-10}) enrichment was found with genes that were down-regulated and up-regulated in the publicly available NF data sets, respectively, with most genes showing opposing expression patterns

during early leaf development and NF treatment (Figure 7D). To test the specific effects of NF and, thus, chloroplast retrograde signaling on transitioning leaves, plants were analyzed at the transcriptomic and cellular levels after transfer to NF at day 8. Leaf 3 did not develop chloroplasts and, consequently, was blocked in local chloroplast retrograde signaling (Figure 8A). Transcriptional profiling of leaf 3 from these plants revealed that cell wall and water transport proteins were down-regulated at day 9, after 1 day of NF treatment (Figure 8B). Simultaneously, markers of chloroplast oxidative stress, such as CSD2, were up-regulated, indicating that the NF actively affected the sampled tissues and, more specifically, those genes involved in cell expansion and chloroplastic oxidative stress responses. At day 10, photosynthesis was inhibited because transcripts involved in photosystem I and II were down-regulated (data not shown) and, in contrast to wild-type leaves, those treated with NF did not accumulate starch (Figure 8A, inset). Cellular analysis revealed that, at day 10, cells of leaves grown on NF were smaller throughout the leaf, even in the proliferation zone, but to a much greater extent in the leaf tip than at the leaf base (data not shown). Similarly, the

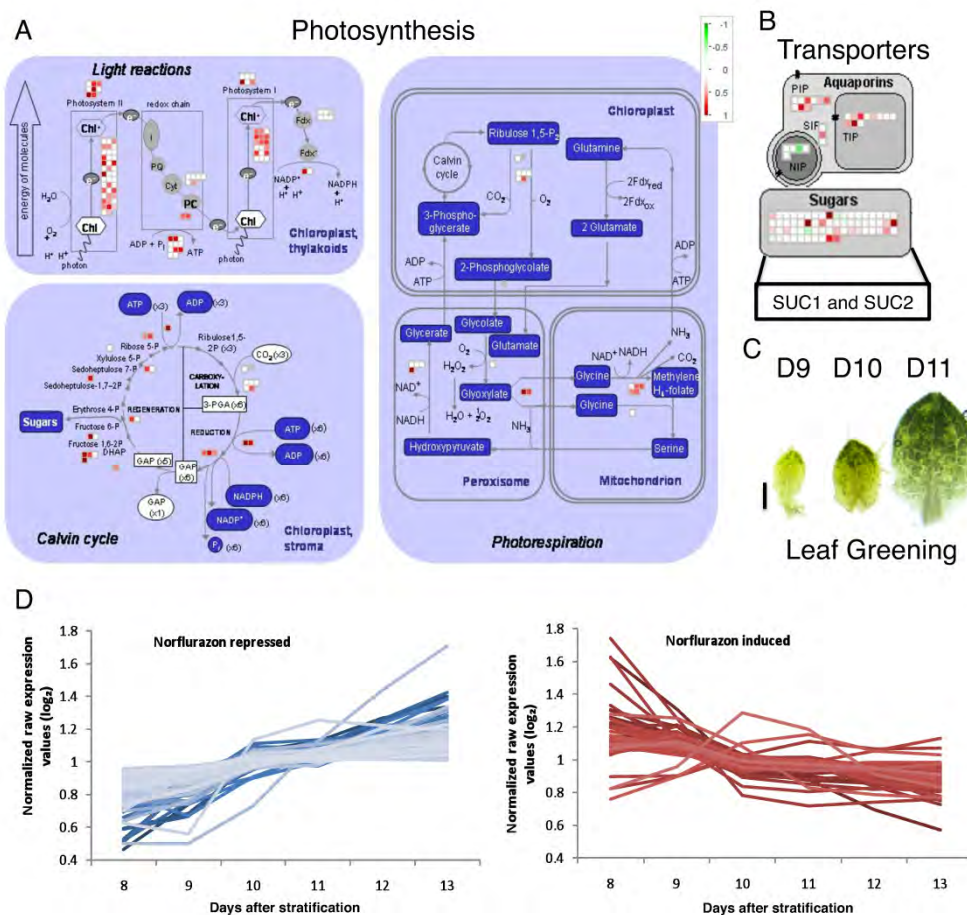


Figure 7. Transcriptional and morphological events during onset of photomorphogenesis

(A and B) Selected significantly differentially expressed genes specifically between days 9 and 10 with FC >0.5 or <-0.5 involved in photosynthesis and transport, respectively.

(C) Leaf greening shown for days 9, 10, and 11. Scale bar = 0.25 mm.

(D) Expression profiles for genes differentially expressed in publicly available NF data sets and between days 9 and 10. X-axis is days after stratification.

position of the cell cycle arrest front in NF-treated samples was closer to the leaf tip (Figure 8C) and leaves grown on NF had a higher cell production rate (Figure 8D) between days 9 and 10 than those grown on Murashige and Skoog (MS) medium, suggesting that the delayed transition is not due to a general inhibition of the developmental processes. These results were confirmed by the CYCB1;1-D-box:GUS-GFP line in which the proliferation zone extended farther along the proximal distal axis in NF-treated than in MS-grown leaves (Figure 8A, inset). To determine whether NF stimulated cell proliferation or inhibited the onset of cell expansion, we transferred plants to NF on day 7 instead of day 8 and harvested leaves 24 h and 48 h after transfer. Cellular analysis of these leaves revealed that cell division was unaffected because the cell production was the same in NF-treated and MS-grown leaves, thus indicating that NF did not directly affect cell proliferation, but rather inhibited the onset of cell expansion (Figure 8D). Taken together, these data suggest that retrograde signaling from the chloroplasts is a key factor driving the transition from cell proliferation to cell expansion.

DISCUSSION

The aim of this study was to profile the growth of the leaf at the cellular level by means of image-analysis algorithms and to identify the overall transcriptional responses in young developing leaves to identify how the regulatory networks driving overall leaf development processes are coordinated. The transcriptome profiling allowed us to discern events in the epidermis, such as stomatal formation, and photomorphogenesis in the mesophyll, whereas the epidermal profiling provided the phenotypic characterization of leaf growth at the cellular level. The epidermis was found to be a good marker of cell division status for both the epidermis and mesophyll at these early stages of development. These findings were supported by previous studies that revealed that epidermal cell size correlated well with the mitotic index (Donnelly et al. 1999) and could regulate the overall growth of the leaf (Savaldi-Goldstein et al., 2007; Marcotrigiano, 2010).

Transition to cell expansion is abrupt

Our current understanding of the transition to secondary morphogenesis is that post-mitotic cellular expansion begins in the leaf tip, followed by a cellular differentiation front that moves gradually down the leaf in a basipetal direction (Donnelly et al., 1999; Efroni et al., 2010). From our detailed analyses, it became evident that the transition from primary to secondary morphogenesis was not as gradual as previously thought, despite the gradual expression patterns in the many transcriptional regulators during these time points. No predominant “waves” of transcriptional activity were linked to the differentiation status of the leaf (Efroni et al., 2008), probably because leaf development was followed with high resolution during a short time. Previously, genes of which the expression peaks served as age-specific markers

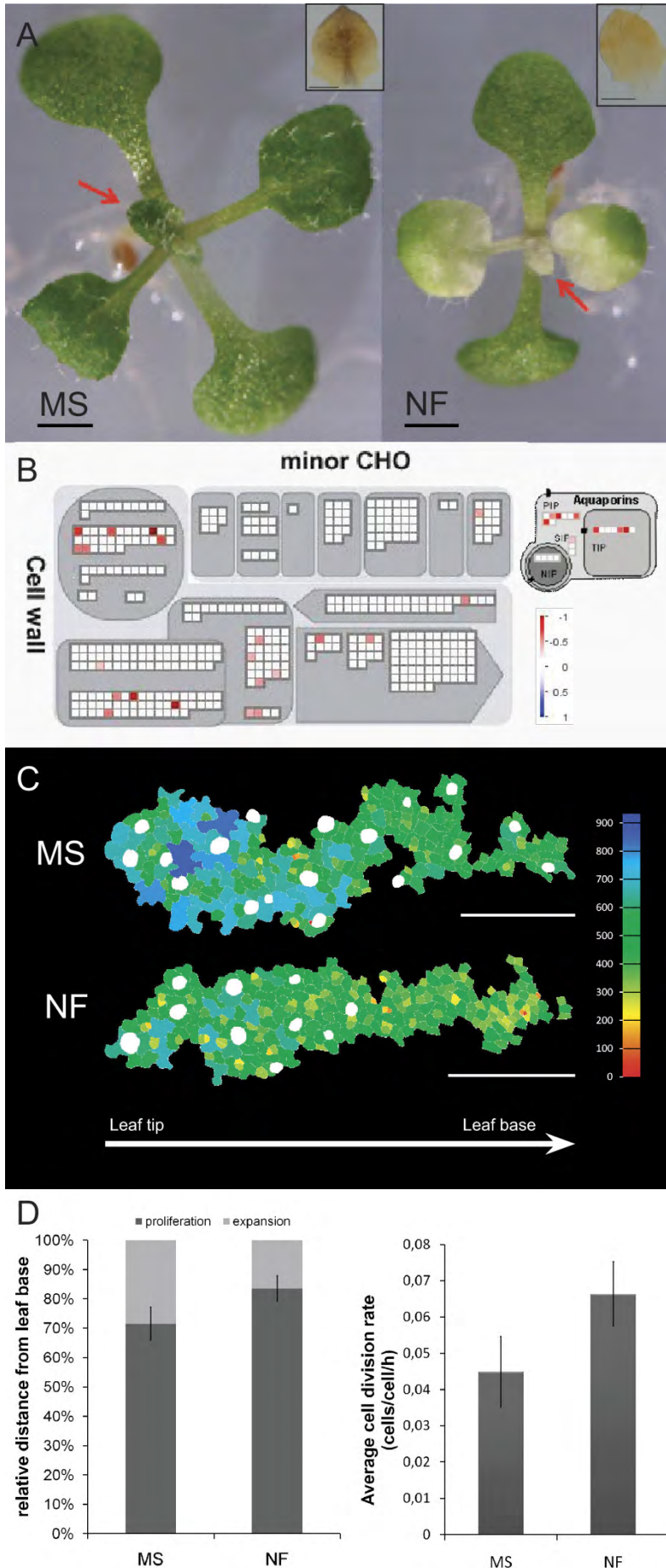


Figure 8. Effects of NF treatment on the cell cycle arrest front

(A) Image of plants at day 11 transferred to NF at day 8. Leaf 3 is indicated by red arrows (note the lack of greening). Scale bar = 1 mm. Inset is pCYCB1;1::D-box:GUS images and starch staining of leaf 3 at day 10. Scale bar = 0.25 mm.

(B) Mapman representations of enriched genes differentially expressed at day 9 in the third leaves from plants transferred to NF on day 8.

(C) Representative images showing the arrest front position at day 10 for leaf 3 of plants grown on NF and control media (MS). Cells are color-coded based on cell size. Scale bar = 0.1 mm.

(D) Graphical representations of the relative position of the arrest front from the tip of the leaf and average cell division rate between days 8 and 9 and days 9 and 10 in MS and NF-treated samples. Error bars are SEM.

(Efroni et al., 2008) were significantly enriched in the differentially expressed genes of our data set, confirming their developmental importance (data not shown). Taken on a whole-leaf basis, the onset of secondary morphogenesis appeared to progress gradually down the leaf length, but enhanced temporal and spatial resolution revealed two crucial shifts in the transition to secondary morphogenesis in leaf 3.

Possible mechanisms for coordinating arrest front progression

Although establishment and shutdown of the developmental gradient did not occur gradually, the progression of the arrest front during transition did. Throughout transition, the proliferation zone increased in absolute size, but decreased in the relative length spanned from the leaf base. The relative amount of cells maintained within the proliferation and expansion zones was almost constant across all three time points with $80\% \pm 4\%$ (SEM) of all cells contained in the proliferation zone. The progression of the cell cycle arrest front had been hypothesized to be driven by diffusion of a mobile growth factor, inducing cell proliferation and entering the leaf via the petiole (Kazama et al., 2010). One possible candidate, *KLUH* (*KLU*), was identified as regulating such a mobile growth factor and was shown to work in a non-cell-autonomous manner (Anastasiou et al., 2007; Eriksson et al., 2010). However, taking our results into account, it seems more likely that the progression of the cell cycle arrest front results from a balance between multiple antagonistic processes that act within the expansion and proliferation zones of the transitioning leaf. Such a mechanism might be a consequence of the antagonistic activities of the class I and II *TCP* genes in the control of the expression of cyclin and ribosomal protein genes during cell proliferation (Li et al., 2005), but it is unclear whether they are the main players in the regulation of this gradient.

Coordinated onset of cell expansion and photosynthesis

As mentioned above, the largest number of transcriptional changes was seen between days 9 and 10 and functional enrichment analysis revealed overrepresentation of genes involved in cell cycle and cell proliferation as well as photosynthesis, carbon sequestration, and sugar and water transporters. Thus, we hypothesized that this time point is critical not only for the establishment of secondary morphogenesis within the leaf, but also for the onset of photosynthesis. Previously, transcripts of the small subunit of ribulose-1,5-bisphosphate-carboxylase had already been detected in less than 100- μm -long leaf primordia of *Amaranthus hypochondriacus* (Ramsperger et al., 1996), but the specific timing of onset of photosynthesis in *Arabidopsis* is still unknown. Imaging revealed that intense greening of the tip of leaf 3 occurred at day 10, overlapping with the region that simultaneously underwent cellular expansion. This observation provides further support that the leaf becomes

photosynthetically active at the same time as it shifts from primary to secondary morphogenesis.

Role of chloroplastic retrograde signaling in regulating onset of cell expansion

Interestingly, a group of genes responsible for tetrapyrrole biosynthesis in chloroplasts were already significantly up-regulated prior to most other photosynthetically active enzymes and genes involved in cell expansion, indicating that chloroplast differentiation might initiate before the abrupt transition to cell expansion and photosynthesis. Inhibition of organellar DNA replication is known to repress nuclear DNA replication (Blamire et al., 1974; Rose et al., 1975). To date, the roles of chloroplast retrograde signals coordinating such events are still unclear, although tetrapyrroles, plastid gene expression, reactive oxygen species, and abscisic acid, all are proposed to be involved (Galvez-Valdivieso and Mullineaux, 2010; Voigt et al., 2010). In our data set, only genes that were differentially expressed between days 9 and 10 were strongly enriched with NF-regulated genes (Koussevitzky et al., 2007), providing evidence that retrograde signaling takes place during the abrupt induction of cell expansion and photomorphogenesis. Thus, because chloroplast development preceded that of general photosynthetic maturity and cell expansion and because retrograde signaling from the chloroplast to the nucleus had been shown to affect nuclear replication and CDKA activity (Kobayashi et al., 2009), chloroplast differentiation was postulated to be a key regulator during early leaf development coordinating and triggering the exit of cell proliferation and subsequent cellular differentiation in the context of both photosynthetic maturity and cell expansion.

In NF-treated leaves, the normal onset of cellular expansion in the leaf tip was strongly inhibited. Two possible situations might explain this phenomenon. First, by blocking retrograde signaling, cell proliferation was stimulated, thus prolonging the persistence of the cell proliferation zone. This possibility is improbable because retrograde signaling from chloroplasts probably takes place in the leaf tip where the majority of the chloroplasts are differentiated instead of in the leaf base where they are still undifferentiated. Second, by blocking chloroplast retrograde signaling, the onset of cell expansion was inhibited and, coincidentally, cells in the proliferation zone continued to divide until they received a signal to begin expanding. As the size of cells in NF-treated leaves was much more reduced in the tip than those at the base, this possibility seems the most plausible and was corroborated by the fact that cell production in NF-treated leaves did not differ from that of MS-grown leaves harvested prior to the onset of transition to cell expansion. Hence, when chloroplast retrograde signaling was blocked, the cell cycle arrest front was inhibited, primarily due to direct inhibition of cell expansion rather than to prolongation of proliferation. These findings strongly support the idea that proper onset of cell expansion in the leaf tip requires a retrograde signal from the chloroplasts.

Role of meristemoids in leaf growth

Each meristemoid has been shown to divide asymmetrically anywhere from 1 to 3 times before giving rise to guard mother cells that will divide symmetrically to form two stomatal guard cells (Peterson et al., 2010). Thus, for every stoma formed, one to three pavement cells arise from its meristemoid precursor. Therefore, the period of meristemoid proliferation is also crucial for determining the final size and shape of the leaf, as corroborated by the development of a dome-shaped enlarged leaf in plants that do not express the genes *PEAPOD1* (*PPD1*) and *PPD2*, which control the arrest of proliferation in meristemoids (White, 2006). In the leaf epidermis, 30% of the cells are guard cells and the remaining 70% are pavement cells, of which 48% are estimated to have arisen from asymmetric divisions of the stomatal lineage (Geisler et al., 2000; Bergmann and Sack, 2007). Thus, meristemoids dictate not only cell patterning, but also regulate the formation of the majority of the pavement cells within the leaf epidermis.

The proliferation program of meristemoids in the epidermis of leaf 3 seemed, intriguingly, independent of the proliferation program of their surrounding pavement cells. Even before any pavement cells had begun expanding, already differentiated stomata were present in the tip of the abaxial leaf epidermis. Moreover, the proliferation of meristemoids also persisted much longer than that of the pavement cells. Already during early leaf development, the SI increased gradually over the proximal-distal axis of the leaf to reach a value in the leaf tip at day 13 that was comparable to the overall SI in the mature leaf (Skiryicz et al., 2010). Hence, meristemoid patterning and shutdown of meristemoid proliferation also followed a basipetal gradient, confirming the existence of a previously proposed second cell-cycle arrest front that progressed from tip to base and determined arrest of meristemoid division (White, 2006). However, timing and progression of this secondary arrest front differs substantially from that of the first front that arrests proliferative pavement cell divisions.

In the future, characterization of meristemoid activity with meristemoid marker genes would provide an interesting perspective on how the meristemoid arrest front progresses and, more precisely, how meristemoid divisions contribute to the overall cell number and patterning in the leaf epidermis. Currently, no suitable marker lines can be used in young leaves because most lines have been profiled in highly expanded leaf tissues instead of in fully proliferating tissues and those that have been profiled in leaf primordia do not show meristemoid specificity (Shpak et al. 2005).

In conclusion, we can begin to unravel the role that early leaf development plays in determining the major aspects of leaf morphology, including size, shape, and productivity. From our data, transition from cell proliferation to expansion in pavement cells is clearly not as gradual as commonly assumed and this has strong implications for the regulation of the final leaf size. In fact, the timing of this transition was not only abrupt, but also concurrent with photomorphogenesis. The coregulation of these two transitions may be crucial in

understanding how leaves control their cellular differentiation status. Interestingly, by blocking chloroplast-derived retrograde signals, the onset of cell expansion and photomorphogenesis could be inhibited in the leaf tip. In other words, it is crucial for leaves to tightly coordinate the developmental timing of both emergence of cellular expansion and photomorphogenesis, at least in part, by means of a signal from the chloroplasts.

EXPERIMENTAL PROCEDURES

Plant material and growth conditions

Seeds of *Arabidopsis thaliana* (L.) Heyhn. ecotype Columbia-0 (Col-0) and CYCB1;1-D-box:GUS-GFP (Eloy et al., 2011) were grown on half-strength MS medium (Murashige and Skoog, 1962) and stratified at 4°C for 2 days on plates that were placed in growth rooms kept at 22°C and 16-h day/8-h night cycles. Seedlings were harvested at 8, 9, 10, 11, 12, 13, and 14 days after sowing in triplicate. Some of the plants were used for image analysis and others for transcriptome analysis. Tissues for tiling array and image analysis were always harvested at the same time of day, 3 h after the lights were on. Plants for the NF experiments were grown on permeable nylon meshes on half-strength MS media until day 8, at which time they were transferred to media supplemented with 5 µM NF. Plants were harvested at days 9 and 10 for transcriptomic and cellular analyses.

GUS staining

CYCB1;1-D-box:GUS plants were infiltrated with heptane for 5 min, left to dry for 5 min, and then were immersed in GUS staining solution as described (Beeckman and Engler, 1994). Plants were vacuum infiltrated for 15 min, subsequently incubated at 37°C for 24 h, and cleared with 100% ethanol at room temperature for approximately 4 h. Samples were mounted in lactic acid and imaged under bright-field illumination on a binocular microscope.

Microscopy for epidermal cell size measurements

Seedlings were cleared in 70% ethanol and the third leaf was removed from the plant and mounted in lactic acid on a microscope slide. The total leaf blade area was measured for 10 representative leaves from each time point under a dark-field binocular microscope. Abaxial epidermal cells along the complete proximal-distal axis of the leaves were drawn with a microscope equipped with differential interference contrast optics (DM LB with 40x and 63x objectives; Leica) and a drawing tube. The entire abaxial epidermis was drawn for samples of representative leaves at days 12 and 13. To image the greening of the leaf, leaf 3 was harvested directly from seedlings at days 9, 10, and 11 with precision microdissection scissors and a binocular microscope. The dissected leaves were mounted in water and imaged directly under a binocular microscope with bright-field illumination.

Image analysis

The microscopic drawings of the abaxial epidermis were scanned for digitalization. Atypically large cells at the leaf margin and overlaying the midvein were removed with Photoshop (Adobe Systems). Automated preprocessing of the images included: closing small drawing gaps, erasing small extrusions (drawing overshoots), and equally thinning of all the lines. Extraction of stomatal pores allowed the positioning of the stomata within the leaf and the identification of guard cells (cells $<500 \mu\text{m}^2$ neighboring the stomatal pores). The remaining non-guard cells were identified as pavement cells and were used for morphological analysis. For each pavement cell, we determined the center of mass, the cell size, and circularity [$4\pi \cdot (\text{area}/\text{perimeter}^2)$]. All data were calibrated according to the microscopic enlargement used to produce the drawings. The cells were color-coded according to their size and circularity, along an exponential and linear scale, respectively. The color gradient (red-yellow-green-cyan-blue) ranged from the minimum to the maximum size/circularity measured within the image or within the complete set of figures. The image analysis algorithms were written in C++ scripting, making use of the SDC Morphology Toolbox for C++ (www.mmorph.com/cppmorph/) and the ImageJ macro language (<http://rsbweb.nih.gov/ij/>). All data were analyzed by scripts written in Perl programming language (<http://www.perl.org/>) and graphs were plotted with Gnuplot (<http://www.gnuplot.info/>). Image and data analysis scripts are available upon request.

Material for transcriptomic analysis

Seedlings for transcriptomic analysis were placed in RNAlater (Ambion) and stored at 4°C until leaf 3 could be dissected from the plant. Plants stayed in RNAlater no longer than 5 days and dissected on a cooling plate under a stereomicroscope with precision microdissection scissors. The excised leaves were deposited in a new tube, frozen, and ground with a 3-mm metal ball (Retsch MM301). A minimum and maximum of 64 (day 13) and 256 (day 8) leaves per replicate were harvested.

RNA extraction

RNA was extracted from the samples, each replicate independently, with the RNeasy mini kit (Qiagen) and on-column DNase digestion by means of the Qiacube (Qiagen) robot.

AGRONOMICS1 tiling array hybridizations and data analysis

RNA samples were prepared at the Eidgenössische Technische Hochschule (ETH, Zürich, Switzerland) with the microarray target preparation method 3 and hybridized as described (Rehrauer et al., 2010). Expression data were processed with Robust Multichip Average (RMA; background correction, normalization, and summarization) as implemented in BioConductor (Irizarry et al., 2003; Gentleman et al., 2004). Dynamic probe selection was performed, only keeping probes that changed in expression over the six time points (Rehrauer et al., 2010). The BioConductor package Limma was used to identify differentially

expressed genes (Smyth, 2004). Genes that were differentially expressed between at least two time points were identified with a moderated F-test and a corrected P -value of 0.05. Pairwise comparisons between time points were tested with moderated t statistics and eBayes method as implemented in Limma. P values were corrected for multiple testing (for each contrast separately with topTable; Hochberg and Benjamini, 1990). The differentially expressed genes were CAST clustered with TMEV, a threshold parameter of 0.759, and a limit of minimum 20 genes per cluster. Transcription factors were identified by their annotation in the Gene Ontology (GO) and the Arabidopsis Gene Regulatory Information Server (AGRIS) databases (Davuluri et al., 2003; Harris et al., 2004). Differentially expressed genes were compared to gene expression data from publicly available microarrays downloaded from the Gene Expression Omnibus (GEO) (Edgar et al., 2002). Significant overlaps between these data sets were identified by means of Fisher's exact tests, followed by Bonferroni P value correction. Functional enrichments were calculated with PageMan (Usadel et al., 2006) and visualized with MapMan (Thimm et al., 2004).

ACKNOWLEDGEMENTS

We thank all colleagues of the Systems Biology of Yield research group for fruitful discussions and Martine De Cock for help in preparing the manuscript. This work was supported by grants from the Belgian Network BARN (Growth and Development of Higher Plants IUAP VI/33), funded by the Interuniversity Attraction Poles Program, initiated by the Belgian State, Science Policy Office, the 'Bijzonder Onderzoeksfonds Methusalem Project' (BOF08/01M00408) of the Ghent University, the European Community Grant FP6 IP AGRON-OMICS (contract LSHG-CT-2006-037704). S.D. is indebted to the Agency for Innovation through Science and Technology for a predoctoral fellowship. S.D.B. is a Postdoctoral Fellow and F.C. was a Research Fellow of the Research Foundation-Flanders. P.M. is the recipient of a Marie Curie Intra-European Fellowships for Career Development (PIEF-GA-2009-235827).

CONTRIBUTIONS

Megan Andriankaja produced the necessary plant material. Together with Liesbeth De Milde, she performed the microscopic drawings. These drawings were prepared for image analysis by Megan Andriankaja and Stijn Dhondt. Stijn Dhondt developed the image and data analysis scripts and performed the cellular analyses. Transcriptome analysis was conducted by Megan Andriankaja and Stefanie De Bodt. Megan Andriankaja did the GUS stainings and Hannes Vanhaeren performed the histological sectioning.

REFERENCES

- Anastasiou, E., Kenz, S., Gerstung, M., MacLean, D., Timmer, J., Fleck, C., and Lenhard, M.** (2007). Control of plant organ size by *KLUH/CYP78A5*-dependent intercellular signaling. *Dev. Cell* *13*, 843-856.
- Barbier de Reuille, P., Bohn-Courseau, I., Ljung, K., Morin, H., Carraro, N., Godin, C., and Traas, J.** (2006). Computer simulations reveal properties of the cell-cell signaling network at the shoot apex in *Arabidopsis*. *Proc. Natl. Acad. Sci. USA* *103*, 1627-1632.
- Beeckman, T., and Engler, G.** (1994). An easy technique for the clearing of histochemically stained plant tissue. *Plant. Mol. Biol. Rep.* *12*, 37-42.
- Beemster, G.T.S., and Baskin, T.I.** (1998). Analysis of cell division and elongation underlying the developmental acceleration of root growth in *Arabidopsis thaliana*. *Plant Physiol.* *116*, 1515-1526.
- Beemster, G.T.S., De Veylder, L., Vercruyse, S., West, G., Rombaut, D., Van Hummelen, P., Galichet, A., Gruissem, W., Inzé, D., and Vuylsteke, M.** (2005). Genome-wide analysis of gene expression profiles associated with cell cycle transitions in growing organs of *Arabidopsis*. *Plant Physiol.* *138*, 734-743.
- Beemster, G.T.S., Fiorani, F., and Inzé, D.** (2003). Cell cycle: the key to plant growth control? *Trends Plant Sci.* *8*, 154-158.
- Ben-Dor, A., Shamir, R., and Yakhini, Z.** (1999). Clustering gene expression patterns. *J. Comput. Biol.* *6*, 281-297.
- Bergmann, D.C., and Sack, F.D.** (2007). Stomatal development. *Annu. Rev. Plant Biol.* *58*, 163-181.
- Berná, G., Robles, P., and Micol, J.L.** (1999). A mutational analysis of leaf morphogenesis in *Arabidopsis thaliana*. *Genetics* *152*, 729-742.
- Blamire, J., Flechtner, V.R., and Sager, R.** (1974). Regulation of nuclear DNA replication by the chloroplast in *Chlamydomonas*. *Proc. Natl. Acad. Sci. USA* *71*, 2867-2871.
- Boudolf, V., Lammens, T., Boruc, J., Van Leene, J., Van Den Daele, H., Maes, S., Van Isterdael, G., Russinova, E., Kondorosi, E., Witters, E., De Jaeger, G., Inzé, D., and**

De Veylder, L. (2009) CDKB1;1 forms a functional complex with CYCA2;3 to suppress endocycle onset. *Plant Physiol.* *150*, 1482-1493

Braybrook, S.A., and Kuhlemeier, C. (2010). How a plant builds leaves. *Plant Cell* *22*, 1006-1018.

Byrne, M.E. (2005). Networks in leaf development. *Curr. Opin. Plant Biol.* *8*, 59-66.

Churchman, M.L., Brown, M.L., Kato, N., Kirik, V., Hülskamp, M., Inzé, D., De Veylder, L., Walker, J.D., Zheng, Z., Oppenheimer, D.G., Gwin, T., Churchman, J., and Larkin, J.C. (2006). SIAMESE, a plant-specific cell cycle regulator, controls endoreplication onset in *Arabidopsis thaliana*. *Plant Cell.* *18*, 3145-3157.

Cosgrove, D.J. (2005). Growth of the plant cell wall. *Nat. Rev. Mol. Cell Biol.* *6*, 850-861.

Davuluri, R.V., Sun, H., Palaniswamy, S.K., Matthews, N., Molina, C., Kurtz, M., and Grotewold E. (2003). AGRIS: Arabidopsis Gene Regulatory Information Server, an information resource of Arabidopsis *cis*-regulatory elements and transcription factors. *BMC Bioinformatics* *4*, 25.1-25.11.

De Veylder, L., Beeckman, T., Beemster, G.T.S., Krols, L., Terras, F., Landrieu, I., Van Der Schueren, E., Maes, S., Naudts, M., and Inzé, D. (2001). Functional analysis of cyclin-dependent kinase inhibitors of Arabidopsis. *Plant Cell* *13*, 1653-1667.

Dhondt, S., Coppens, F., De Winter, F., Swarup, K., Merks, R.M.H., Inzé, D., Bennett, M.J., and Beemster, G.T.S. (2010). SHORT-ROOT and SCARECROW regulate leaf growth in Arabidopsis by stimulating S-phase progression of the cell cycle. *Plant Physiol.* *154*, 1183-1195.

Donnelly, P.M., Bonetta, D., Tsukaya, H., Dengler, R.E., and Dengler, N.G. (1999). Cell cycling and cell enlargement in developing leaves of *Arabidopsis*. *Dev. Biol.* *215*, 407-419.

Edgar, R., Domrachev, M., and Lash, A.E. (2002). Gene Expression Omnibus: NCBI gene expression and hybridization array data repository. *Nucleic Acids Res.* *30*, 207-210.

Efroni, I., Blum, E., Goldshmidt, A., and Eshed, Y. (2008). A protracted and dynamic maturation schedule underlies *Arabidopsis* leaf development. *Plant Cell* *20*, 2293-2306.

Efroni, I., Eshed, Y., and Lifschitz, E. (2010). Morphogenesis of simple and compound leaves: a critical review. *Plant Cell* *22*, 1019-1032.

Eloy, N., Lima, M.F., Van Damme, D., Vanhaeren, H., Gonzalez, N., De Milde, L., Hemerly, A., Beemster, G.T.S., Inzé, D., and Ferreira, P.C.G. (2011). The APC/C subunit 10 plays an essential role in cell proliferation during leaf development. *Plant J.* *68*, 351-363.

Eriksson, S., Stransfeld, L., Adamski, N.M., Breuninger, H., and Lenhard, M. (2010). *KLUH/CYP78A5*-dependent growth signaling coordinates floral organ growth in *Arabidopsis*. *Curr. Biol.* *20*, 527-532.

Galvez-Valdivieso, G., and Mullineaux, P.M. (2010). The role of reactive oxygen species in signalling from chloroplasts to the nucleus. *Physiol. Plant.* *138*, 430-439.

Geisler, M., Nadeau, J., and Sack, F.D. (2000). Oriented asymmetric divisions that generate the stomatal spacing pattern in *Arabidopsis* are disrupted by the *too many mouths* mutation. *Plant Cell* *12*, 2075–2086.

Gentleman, R.C., Carey, V.J., Bates, D.M., Bolstad, B., Dettling, M., Dudoit, S., Ellis, B., Gautier, L., Ge, Y., and Gentry, J et al. (2004). Bioconductor: open software development for computational biology and bioinformatics. *Genome Biol.* *5*, R80.1-R80.16.

Gonzalez, N., Beemster, G.T.S., and Inzé, D. (2009). David and Goliath: what can the tiny weed *Arabidopsis* teach us to improve biomass production in crops? *Curr. Opin. Plant Biol.* *12*, 157-164.

Gonzalez, N., De Bodt, S., Sulpice, R., Jikumaru, Y., Chae, E., Dhondt, S., Van Daele, T., De Milde, L., Weigel, D., Kamiya, Y., Stitt, M., Beemster, G.T.S., and Inzé, D. (2010). Increased leaf size: different means to an end. *Plant Physiol.* *153*, 1261-1279.

Green, P.B. (1976). Growth and cell pattern formation on an axis: critique of concepts, terminology, and modes of study. *Bot. Gaz.* *137*, 187-202.

Harris, M.A., Clark, J., Ireland A., Lomax, J., Ashburner, M., Foulger, R., Eilbeck, K., Lewis, S., Marshall, B., and Mungall, C. et al. (2004). The Gene Ontology (GO) database and informatics resource. *Nucleic Acids Res.* *32*, D258-D261.

Hochberg, Y., and Benjamini, Y. (1990). More powerful procedures for multiple significance testing. *Stat. Med.* *9*, 811-818.

Horiguchi, G., Gonzalez, N., Beemster, G.T.S., Inzé, D., and Tsukaya, H. (2009). Impact of segmental chromosomal duplications on leaf size in the *grandifolia-D* mutants of *Arabidopsis thaliana*. *Plant J.* *60*, 122-133.

- Horiguchi, G., Fujikura, U., Ferjani, A., Ishikawa, N., and Tsukaya, H.** (2006) Large-scale histological analysis of leaf mutants using two simple leaf observation methods: identification of novel genetic pathways governing the size and shape of leaves. *Plant J.* *48*, 638-644.
- Hu, H., Boisson-Dernier, A., Israelsson-Nordström, M., Böhmer, M., Xue, S., Ries, A., Godoski, J., Kuhn, J.M., and Schroeder, J.I.** (2010). Carbonic anhydrases are upstream regulators of CO₂-controlled stomatal movements in guard cells. *Nat. Cell Biol.* *12*, 87-93.
- Irizarry, R.A., Bolstad, B.M., Collin, F., Cope, L.M., Hobbs, B., and Speed, T.P. (2003b). Summaries of Affymetrix GeneChip probe level data. *Nucleic Acids Res.* *31*, e15.
- Kazama, T., Ichihashi, Y., Murata, S., and Tsukaya, H.** (2010). The mechanism of cell cycle arrest front progression explained by a *KLUH/CYP78A5*-dependent mobile growth factor in developing leaves of *Arabidopsis thaliana*. *Plant Cell Physiol.* *51*, 1046-1054.
- Kobayashi, Y., Kanesaki, Y., Tanaka, A., Kuroiwa, H., Kuroiwa, T., and Tanaka, K.** (2009). Tetrapyrrole signal as a cell-cycle coordinator from organelle to nuclear DNA replication in plant cells. *Proc. Natl. Acad. Sci. USA* *106*, 803-807.
- Koussevitzky, S., Nott, A., Mockler, T.C., Hong, F., Sachetto-Martins, G., Surpin, M., Lim, J., Mittler, R., and Chory, J.** (2007). Signals from chloroplasts converge to regulate nuclear gene expression. *Science* *316*, 715–719.
- Laubinger, S., Zeller, G., Henz, S.R., Sachsenberg, T., Widmer, C.K., Naouar, N., Vuylsteke, M., Schölkopf, B., Rättsch, G., and Weigel, D.** (2008). At-TAX: a whole genome tiling array resource for developmental expression analysis and transcript identification in *Arabidopsis thaliana*. *Genome Biol.* *9*, R112.1-R112.16.
- Lee, Y.K., Kim, G. T., Kim, I. J., Park, J., Kwak, S. S., Choi, G., and Chung, W. I.** (2006). *LONGIFOLIA1* and *LONGIFOLIA2*, two homologous genes, regulate longitudinal cell elongation in *Arabidopsis*. *Development.* *133*, 4305-4314.
- Li, C., Potuschak, T., Colón-Carmona, A., Gutiérrez, R.A., and Doerner, P.** (2005). *Arabidopsis* TCP20 links regulation of growth and cell division control pathways. *Proc. Natl. Acad. Sci. USA* *102*, 12978-12983.
- Li, Y., Zheng, L., Corke, F., Smith, C., and Bevan, M.W.** (2008). Control of final seed and organ size by the *DA1* gene family in *Arabidopsis thaliana*. *Genes Dev.* *15*, 1331-1336.

Marcotrigiano, M. (2010). A role for leaf epidermis in the control of leaf size and the rate and extent of mesophyll cell division. *Am. J. Bot.* *97*, 224-233.

Mizukami, Y., and Fischer, R.L. (2000). Plant organ size control: AINTEGUMENTA regulates growth and cell numbers during organogenesis. *Proc Natl Acad Sci U S A.* *18*, 942-7.

Murashige, T., and Skoog, F. (1962). A revised medium for rapid growth and bio assays with tobacco tissue cultures. *Physiol. Plant.* *15*, 473-497.

Pérez-Pérez, J.M., Candela, H., Robles, P., Quesada, V., Ponce, M.R., and Micol, J.L. (2009). Lessons from a search for leaf mutants in *Arabidopsis thaliana*. *Int. J. Dev. Biol.* *53*, 1623-1634.

Pesch, M., and Hülskamp, M. (2009). One, two, three ... models for trichome patterning in *Arabidopsis*? *Curr. Opin. Plant Biol.* *12*, 587-592.

Peterson, K.M., Rychel, A.L., and Torii, K.U. (2010). Out of the mouths of plants: the molecular basis of the evolution and diversity of stomatal development. *Plant Cell* *22*, 296-306.

Ramsperger, V.C., Summers, R.G., and Berry, J.O. (1996). Photosynthetic gene expression in meristems and during initial leaf development in a C₄ dicotyledonous plant. *Plant Physiol.* *111*, 999-1010.

Redman, J.C., Haas, B.J., Tanimoto, G., and Town, C.D. (2004). Development and evaluation of an *Arabidopsis* whole genome Affymetrix probe array. *Plant J.* *38*, 545-561.

Rehrauer, H., Aquino, C., Gruissem, W., Henz, S., Hilson, P., Laubinger, S., Naouar, N., Patrignani, A., Rombauts, S., and Shu, H. et al. (2010). AGRONOMICS1: a new resource for *Arabidopsis* transcriptome profiling. *Plant Physiol.* *152*, 487-499.

Rose, R.J., Cran, D.G., and Possingham, J.V. (1975). Changes in DNA synthesis during cell growth and chloroplast replication in greening spinach leaf disks. *J. Cell Sci.* *17*, 27-41.

Savaldi-Goldstein, S., Peto, C., and Chory, J. (2007). The epidermis both drives and restricts plant shoot growth. *Nature.* *446*, 199-202.

Scarpella, E., Barkoulas, M., and Tsiantis, M. (2010). Control of leaf and vein development by auxin. *Cold Spring Harb. Perspect. Biol.* *2*, a001511.

Shpak, E., McAbee, J., Pillitteri, L., and Torii, K. (2005). Stomatal patterning and differentiation by synergistic interactions of receptor kinases. *Science*. *309*, 290-293.

Skirycz, A., De Bodt, S., Obata, T., De Clercq, I., Claeys, H., De Rycke, R., Andriankaja, M., Van Aken, O., Van Breusegem, F., Fernie, A.R., and Inzé, D. (2010). Developmental stage specificity and the role of mitochondrial metabolism in the response of *Arabidopsis* leaves to prolonged mild osmotic stress. *Plant Physiol.* *152*, 226-244.

Smyth, G.K. (2004). Linear models and empirical Bayes methods for assessing differential expression in microarray experiments. *Stat. Appl. Genet. Mol. Biol.* *3*, Article 3.

Strand, Å., Asami, T., Alonso, J., Ecker, J.R., and Chory, J. (2003). Chloroplast to nucleus communication triggered by accumulation of Mg-protoporphyrinIX. *Nature* *427*, 79-83.

Thimm, O., Bläsing, O., Gibon, Y., Nagel, A., Meyer, S., Krüger, P., Selbig, J., Müller, L.A., Rhee, S.Y., and Stitt, M. (2004). MAPMAN: a user-driven tool to display genomics data sets onto diagrams of metabolic pathways and other biological processes. *Plant J.* *37*, 914-939.

Traas, J., and Monéger, F. (2010). Systems biology of organ initiation at the shoot apex. *Plant Physiol.* *152*, 420-427.

Tsukaya, H. (2002). Interpretation of mutants in leaf morphology: genetic evidence for a compensatory system in leaf morphogenesis that provides a new link between cell and organismal theories. *Int. Rev. Cytol.* *217*, 1-39.

Tsukaya, H. (2003). Organ shape and size: a lesson from studies of leaf morphogenesis. *Curr Opin Plant Biol.* *6*, 57-62.

Usadel, B., Nagel, A., Steinhauser, D., Gibon, Y., Bläsing, O.E., Redestig, H., Sreenivasulu, N., Krall, L., Hannah, M.A., Poree, F., Fernie, A.R., and Stitt, M. (2006). PageMan: an interactive ontology tool to generate, display, and annotate overview graphs for profiling experiments. *BMC Bioinformatics* *7*, 535.1-535.8.

Vandepoele, K., Raes, J., De Veylder, L., Rouzé, P., Rombauts, S., and Inzé, D. (2002). Genome-wide analysis of core cell cycle genes in *Arabidopsis*. *Plant Cell* *14*, 903-916.

Voigt, C., Oster, U., Börnke, F., Jahns, P., Dietz, K.-J., Leister, D., and Kleine, T. (2010). In-depth analysis of the distinctive effects of norflurazon implies that tetrapyrrole

biosynthesis, organellar gene expression and ABA cooperate in the GUN-type of plastid signaling. *Physiol. Plant.* *138*, 503-519.

White, D.W.R. (2006). *PEAPOD* regulates lamina size and curvature in *Arabidopsis*. *Proc. Natl. Acad. Sci. USA* *103*, 13238-13243.

SUPPLEMENTAL INFORMATION

Supplemental information includes seven figures. Microarray data was deposited in NCBI's Gene Expression Omnibus and the GEO series accession number is GSE33936.

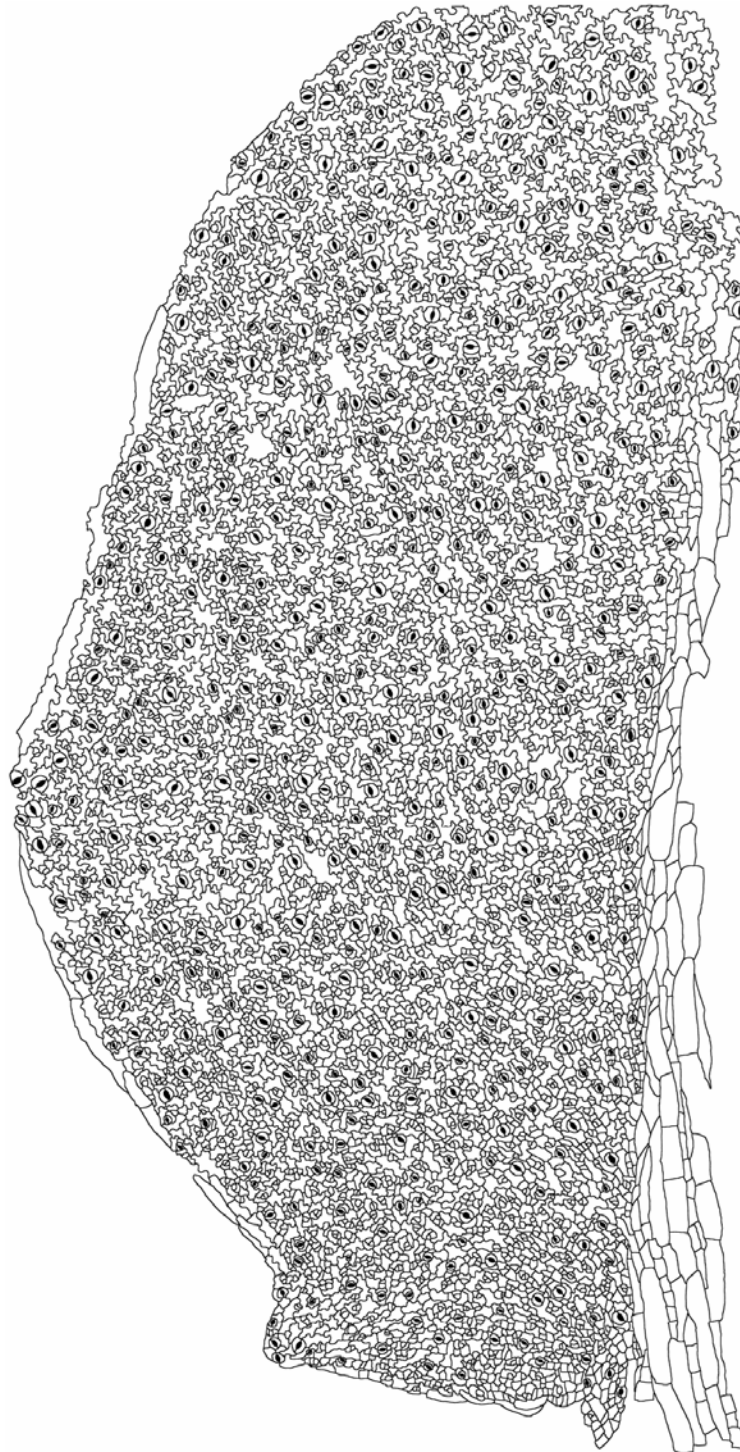


Figure S1, related to Figure 1. Drawing of leaf at day 13 showing the placement of large cells along the leaf margin and overlaying the midvein.

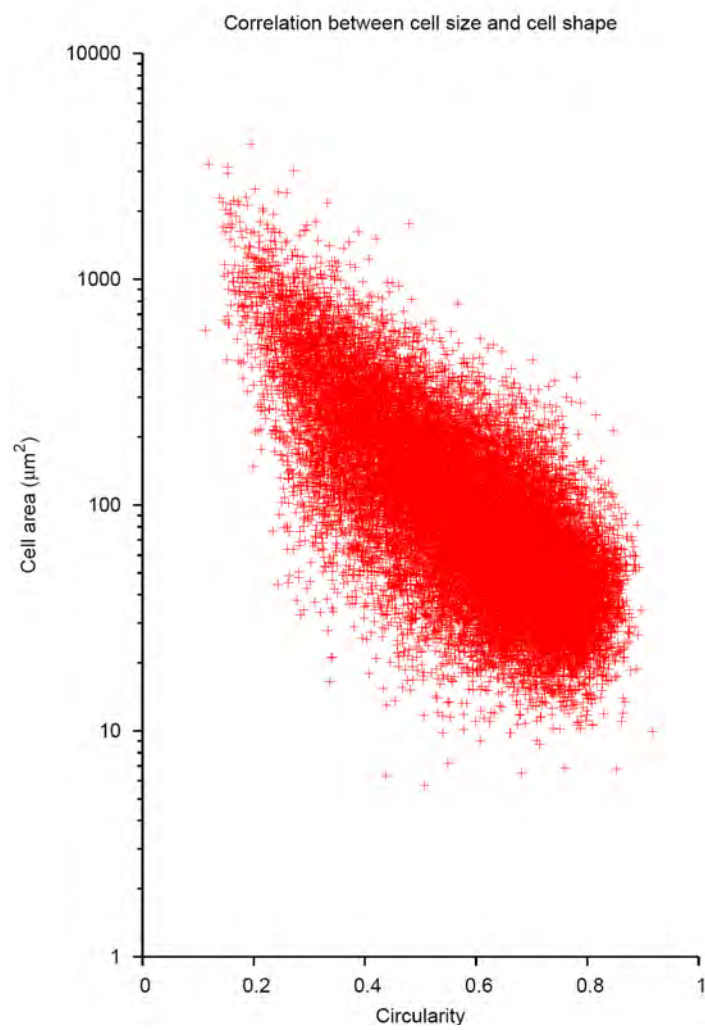


Figure S2, related to Figure 2. Correlation between cell size and cell shape for cells from all images throughout the time series. $R^2 = 0.65$

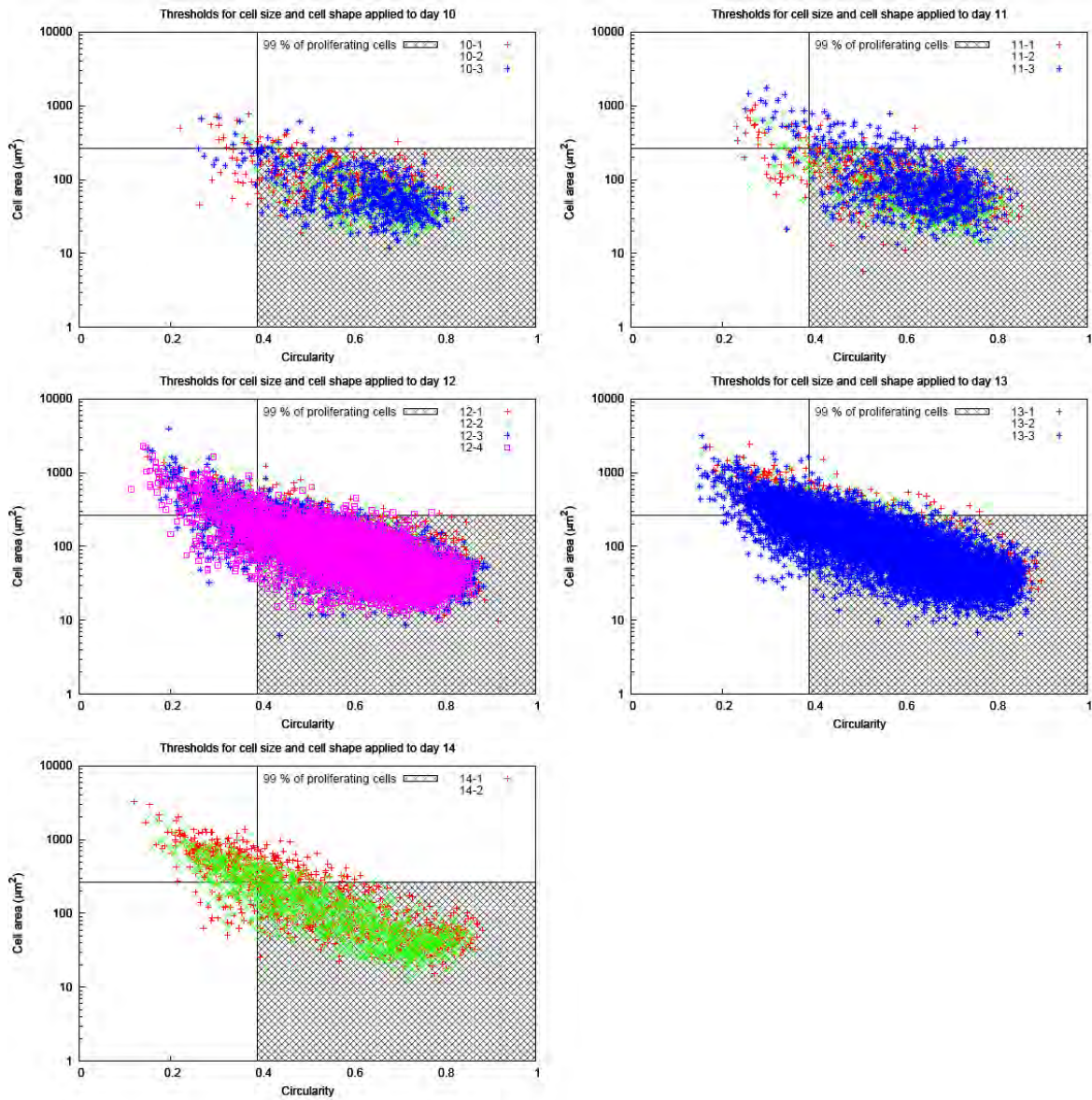


Figure S3, related to Figure 3. Proliferation thresholds applied to leaves from day 10 - 14. Different colors in one plot refer to the individual replicate leaves.

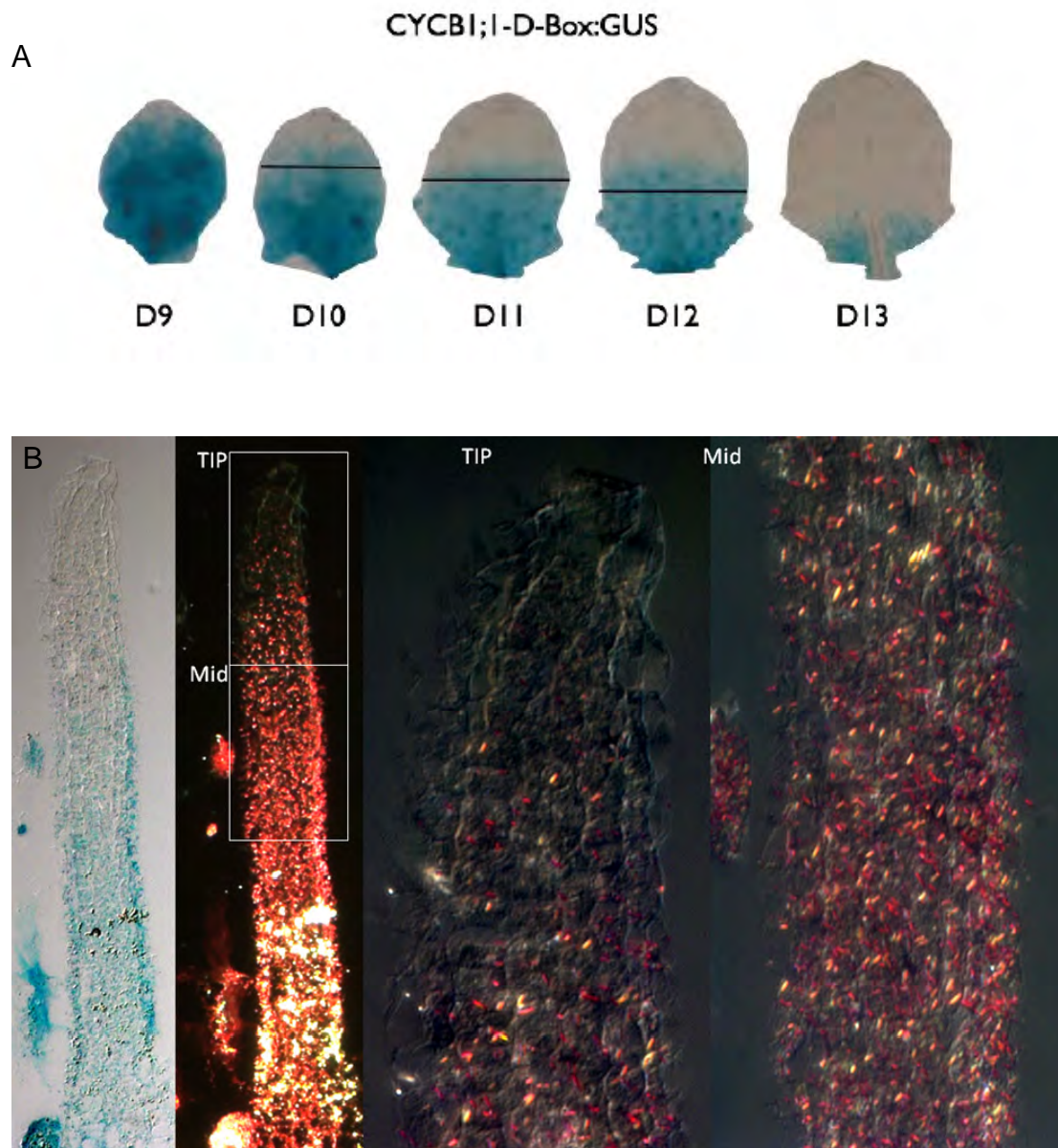
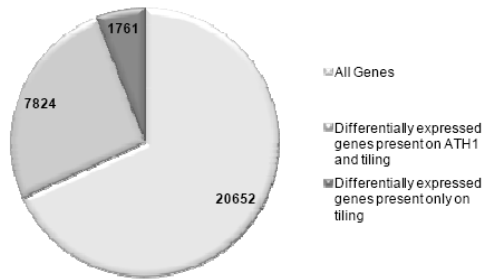
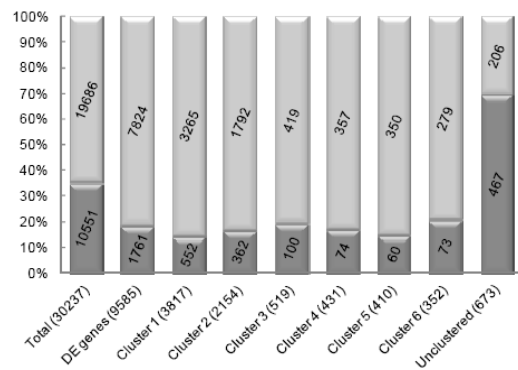


Figure S4, related to Figure 3. Expression pattern of CYCB1;1-D-box:GUS translational fusion protein (A) during the transition time points and (B) at day 10 in longitudinal sections of leaf primordia. CYCB1;1 expression can be seen in all cell layers. Black line in (A) indicates the arrest front position as predicted by the cellular data.

A



B



C

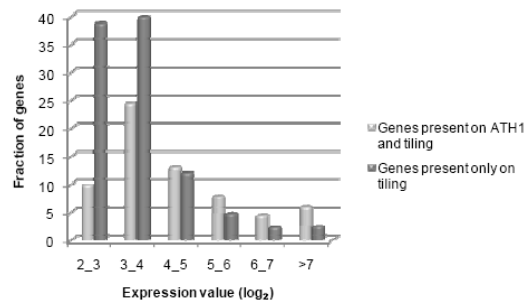


Figure S5, related to Figure 5. Transcriptional changes in leaf 3 between days 8 and 13. (A) Total annotated genes that are differentially expressed and present only on tiling arrays. (B) CAST cluster analysis on all differentially expressed (DE) genes showing the percentage of genes present on both ATH1 and tiling arrays and genes present only on tiling arrays within each cluster. (C) Expression values of genes on tiling arrays only and of those on both the ATH1 and tiling arrays.

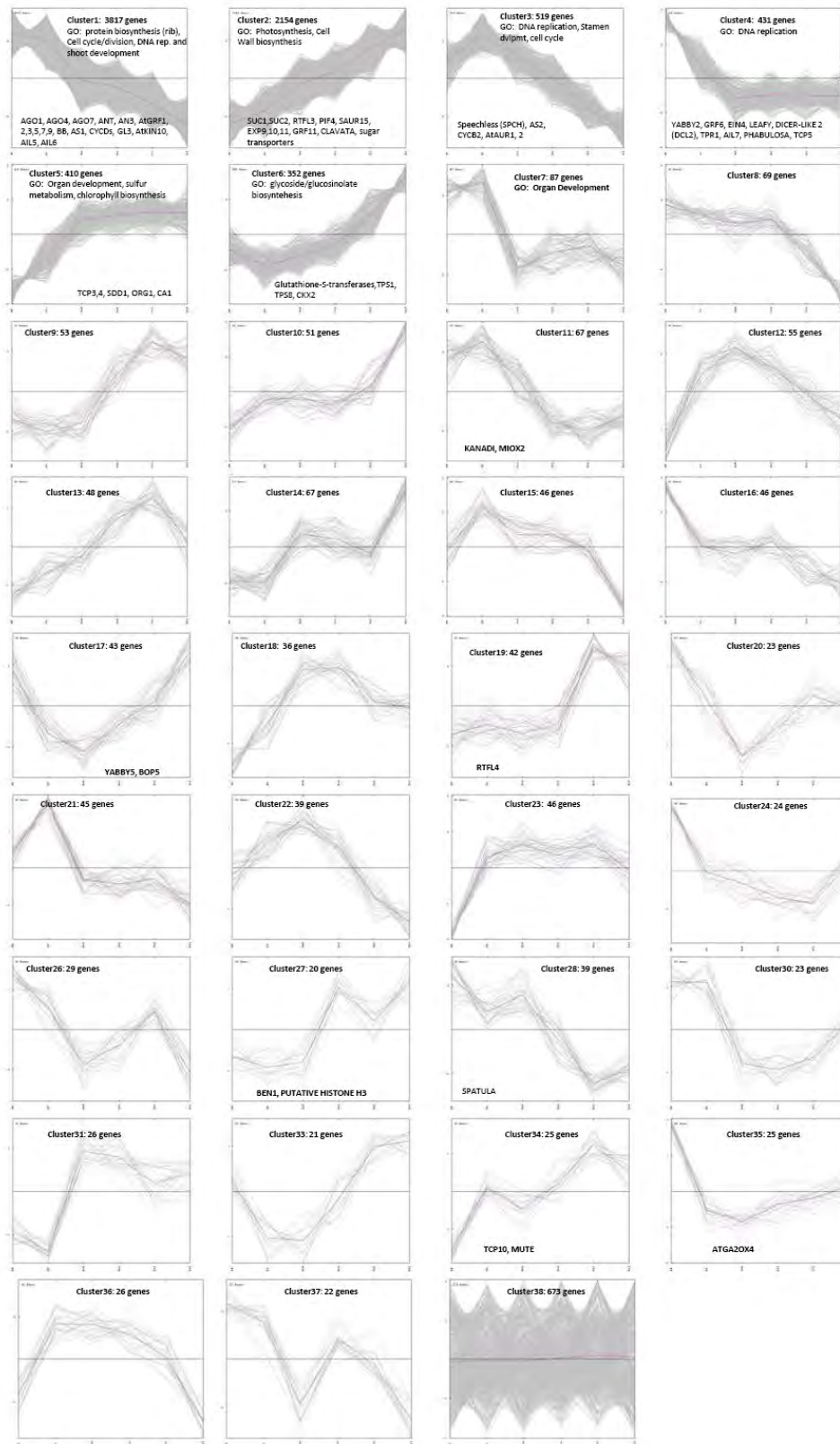


Figure S6, related to Figure 5. All clusters from the CAST clustering of genes differentially expressed between any two time-points. Clustered using a threshold parameter of 0.759 and requiring a minimum of 20 genes per cluster. GO enrichments and select genes shown to be involved in leaf development are indicated overlaying the cluster they are contained within.

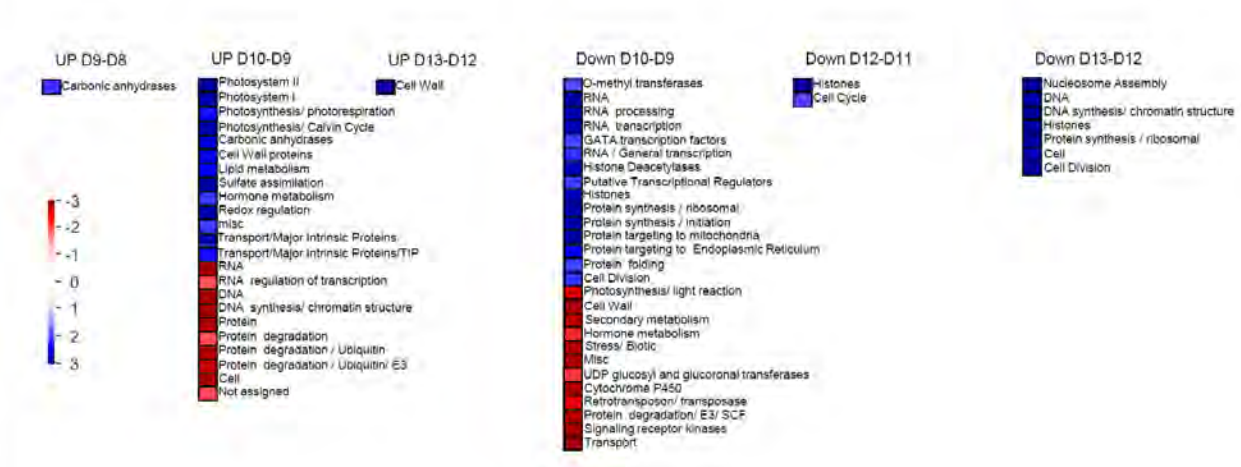


Figure S7, related to Figure 6. PageMan enrichments of differentially expressed genes specifically between sequential pairwise comparisons. Up, up-regulated genes; Down, down-regulated genes; red, underrepresented; blue, overrepresented.

5

Quantitative analysis of venation patterns of Arabidopsis leaves by supervised image analysis

Stijn Dhondt^{1,2}, Dirk Van Haerenborgh^{1,2,3}, Caroline Van Cauwenbergh^{1,2}, Roeland M. H. Merks^{1,2,4,5}, Wilfried Philips³, Gerrit T. S. Beemster^{1,2,6,†}, Dirk Inzé^{1,2,*,†}

¹ Department of Plant Systems Biology, VIB, 9052 Gent, Belgium

² Department of Plant Biotechnology and Bioinformatics, Ghent University, 9052 Gent, Belgium

³ Department of Telecommunications and Information Processing/Image Processing and Interpretation, Interdisciplinary Institute for Broadband Technology, Ghent University, 9000 Gent, Belgium

⁴ Centrum Wiskunde & Informatica, 1098 XG Amsterdam, The Netherlands

⁵ Netherlands Consortium for Systems Biology/Netherlands Institute for Systems Biology, 1098 XG Amsterdam, The Netherlands

⁶ Department of Biology, University of Antwerp, 2020 Antwerpen, Belgium

This chapter is adapted from: The Plant Journal, (in press) doi: 10.1111/j.1365-313X.2011.04803.x

Received June 29, 2011; accepted September, 2011; published online November 8, 2011.

Supplemental data is available online: <http://onlinelibrary.wiley.com/doi/10.1111/j.1365-313X.2011.04803.x/supinfo/>

* For correspondence: Dirk Inzé, e-mail: dirk.inze@psb.vib-ugent.be.

† These authors contributed equally to this work.

SUMMARY

The study of transgenic *Arabidopsis* lines with altered vascular patterns has revealed key players in the venation process, but details of the vascularization process are still unclear, partly because most lines have only been assessed qualitatively. Therefore, quantitative analyses are required to identify subtle perturbations in the pattern and to test dynamic modeling hypotheses using biological measurements. We developed an online framework, designated Leaf Image Analysis Interface (LIMANI), in which venation patterns are automatically segmented and measured on dark-field images. Image segmentation may be manually corrected through use of an interactive interface, allowing supervision and rectification steps in the automated image analysis pipeline and ensuring high-fidelity analysis. This online approach is advantageous for the user in terms of installation, software updates, computer load and data storage. The framework was used to study vascular differentiation during leaf development and to analyze the venation pattern in transgenic lines with contrasting cellular and leaf size traits. The results show the evolution of vascular traits during leaf development, suggest a self-organizing mechanism for leaf venation patterning, and reveal a tight balance between the number of end-points and branching points within the leaf vascular network that does not depend on the leaf developmental stage and cellular content, but on the leaf position on the rosette. These findings indicate that development of LIMANI improves understanding of the interaction between vascular patterning and leaf growth.

INTRODUCTION

The vascular system of plants consists of a continuous network of vascular bundles (Esau, 1965). This network plays a crucial role in the mechanical support and transport of fluids within, from and towards leaves. The xylem is the main conduit for minerals and water, whereas the phloem ensures the transfer of dissolved photoassimilates. Both tissues comprise a number of specialized cell types, but all vascular cells differentiate from a single meristematic tissue, the procambium. Procambial cells are the first visible indication of specification during the vascular patterning process (Busse and Evert, 1999), and the phytohormone auxin has been identified as the initial signal triggering their formation. Gradually restricted auxin transport routes, visualized by the expression domains of the PIN-FORMED1 (PIN1) auxin efflux carrier, define sites of procambium formation (Scarpella *et al.*, 2006; Wenzel *et al.*, 2007). During leaf development in *Arabidopsis*, this process produces a reticulate pattern that becomes more complex as the leaf develops (Candela *et al.*, 1999; Scarpella *et al.*, 2006; Wenzel *et al.*, 2007). Secondary veins are joined in a series of prominent arches, leading to classification of *Arabidopsis* venation as brochidodromous (Hickey, 1988). Although many mutants with altered leaf venation patterns have been identified (Scarpella and Meijer, 2004; Sieburth and Deyholos, 2006), most have only been assessed qualitatively. The fact that vascular phenotypes have been identified visually

suggests that perturbation of the vascular network in these mutants is relatively strong. Previous studies have demonstrated the usefulness of quantification of vascular traits, such as vein thickness, vein density, distributions of branching angles and vein lengths, and the number of branching points, free-ending veins and loops (Hill, 1980; Candela *et al.*, 1999; Bohn *et al.*, 2002; Steynen and Schultz, 2003; Kang and Dengler, 2004; Alonso-Peral *et al.*, 2006; Brodribb *et al.*, 2007; Boyce *et al.*, 2009; Rolland-Lagan *et al.*, 2009; Brodribb and Feild, 2010; Price *et al.*, 2011). As manual analysis of these traits is very laborious and time-consuming, most analyses focused on a part of the leaf. Recently, two enhanced methods have been described that allow quantification of the linear dimensions of vein patterns in entire leaves: a tool that allows manual vein pattern tracing (Rolland-Lagan *et al.*, 2009) and a framework for manual vein extraction with built-in image analysis and drawing functions (Price *et al.*, 2011). Both methods rely completely on user input, do not allow analysis of a batch of pictures, and are relatively time-consuming. Here, we introduce an online framework, Leaf Image Analysis Interface (LIMANI), for analysis of vascular networks in leaves, which automatically segments and measures venation patterns in a batch of cleared leaf images. The framework also includes a user-friendly interactive interface, enabling manual segmentation corrections for high-precision analysis. Using this framework, we investigated vascular differentiation throughout leaf development, and examined the role of cellular traits and leaf growth traits on vascular patterning in transgenic *Arabidopsis* lines.

RESULTS AND DISCUSSION

Online analysis of vascular patterns using the interactive interface LIMANI

Here we describe LIMANI, an online image analysis framework which includes the possibility of manual image segmentation corrections. The online approach allows complete freedom for the developer and has a number of advantages for the user: the tool does not require installation, avoiding problems of operating system compatibility and software dependency, as encountered with image analysis libraries, and the user always has access to the most recent software version and can run the analysis on a remote server, preventing local overload of the user's machine and avoiding data loss by a back-up system. Furthermore, the framework was built in a modular fashion, making it relatively straightforward to plug different image processing and analysis algorithms into the same interface. Imaging tools often consist of two major parts: segmentation of an image for extraction of the content of interest, followed by measurement and calculation of specific traits. Thus, numerous applications within and beyond plant research may be integrated into LIMANI.

The LIMANI framework incorporates an image analysis algorithm for quantification of vascular patterns in *Arabidopsis* leaves. In this application, vascular networks are extracted from dark-field images of whole-mount, cleared leaves, and the extracted networks are quantified. Furthermore, the image analysis algorithm is implemented into an interactive user interface

(Figure 1). To start, the user adds a new task or group by uploading images to the server and setting a number of image analysis parameters. Next, the user is directed to the task overview page, showing the status and parameter settings of all the user tasks in the database. Here, the user can compare and summarize the results of selected tasks or groups. Grouping biological replicates enables a quick comparison between genotypes by calculating mean values and SE for each genotype. Every task is also linked to its task detail page, which visually represents the extracted venation pattern and the values of the vascular parameters calculated from the extracted pattern. Furthermore, the user can re-start the segmentation algorithm with different initial parameter settings or review the extraction by making manual adjustments to the segmentation in a user-friendly manner. This latter possibility functions as a supervision and rectification step in the automated image analysis pipeline, making the analysis tool less of a 'black box' and ensuring that the output quality is in line with the user's expectations.

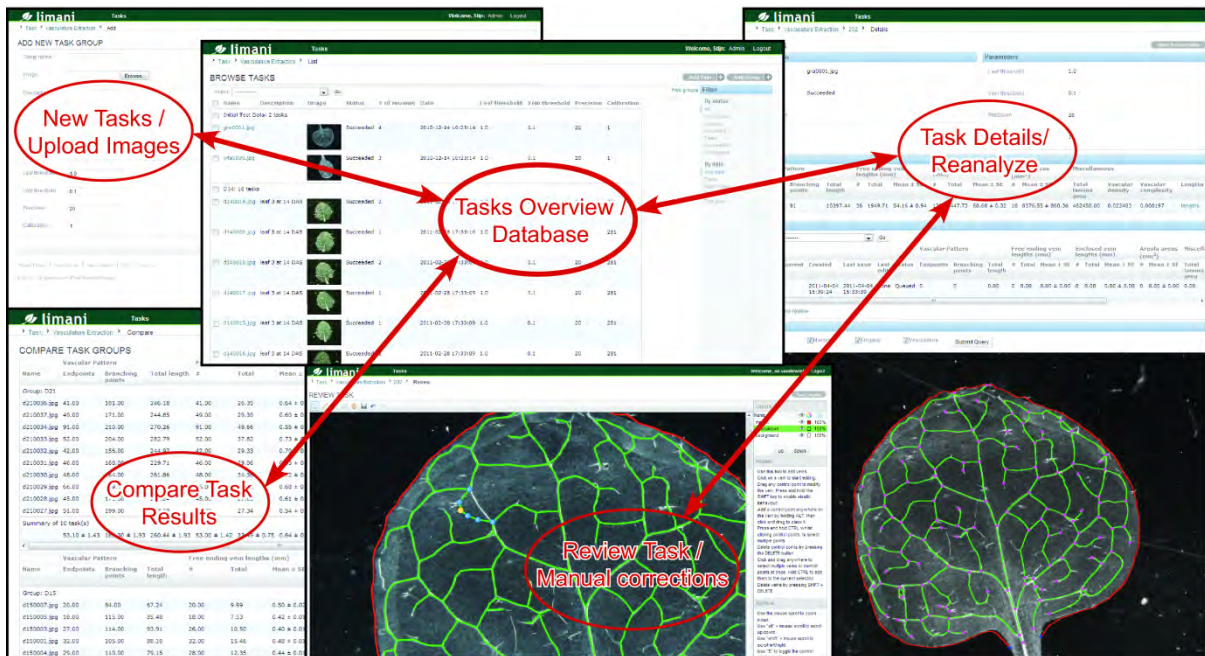


Figure 1. The LIMANI interface.

Screenshots represent the various web pages, which functions describe a schematic overview of the architecture of the framework.

The review page contains an interactive canvas that allows editing and drawing of lines in the web interface, linking user-defined changes to the segmentation of the vascular network. The implemented drawing tools provide the opportunity to zoom in or out, scroll, change colors, select, move or remove complete vascular segments or parts thereof, draw free-ending segments and connect existing segments using a freehand or segmented line-drawing tool, and save corrections. 'Undo' and 're-do' functionalities are also implemented. In the review page, the segmentation consists of multiple layers that can be hidden or visualized. Combined with the input image displayed in the background, the extracted and actual

networks can be compared quickly. After approval of the adjusted segmentation, the vascular network is updated and sent to the server for quantification.

In essence, we have created an online interface to run image analysis algorithms for quantification of vascular networks in leaves, allowing us to control and rectify the automatically extracted patterns by incorporation of an interactive drawing application. This approach provides a fast, user-friendly and reliable method to analyze vascular networks in *Arabidopsis* leaves.

Extraction of vascular networks

The first and most important step is extraction of the vascular network. A gray-scale mathematical morphology image analysis algorithm (Dougherty and Lotufo, 2003) executes a sequence of functions on an input image (see below). The input image of choice is a dark-field picture of a single leaf cleared first in ethanol and then in lactic acid and mounted in lactic acid (Figure 2a). Dark-field microscopy creates a high contrast between the vascular strands and the background, primarily by light scattering on differentiated xylem vessels, and preferably an intermediate brightness within the leaf tissue. Starch accumulation in the leaf can complicate visualization of the vascular pattern, but clearing with chloral hydrate solution usually resolves this issue.

In the first image analysis step, the leaf is extracted from the background by recursive opening and closing of the input image using an increasing structuring element that results in an enhanced contrast between leaf and background while preserving the global shape of the structure (Figure 2b). The leaf is then extracted by thresholding the image, in which the threshold is a user-defined fraction of the mean intensity of the entire image. When the segmentation yields more than one object, due to the presence of an air bubble for instance, the largest object is assumed to be the leaf. Possible holes in the resulting leaf mask are filled automatically. The intersection between this leaf mask and the original image results in removal of the background (Figure 2c). The leaf margin is obtained by subtraction of the leaf mask erosion from its dilation (Figure 2d).

The next step is extraction of the vascular pattern from the leaf. To remove the local background within the leaf, recursive opening and closing with an increasing structuring element is again applied (Figure 2e). In this case, the number of iterations is fewer than those for leaf segmentation to preserve local differences in background intensities. Subtraction of the resulting image from the leaf image results in a gray-scale extraction of the vascular pattern (Figure 2f). Gray-scale dilation, to highlight the venation, is followed by thresholding using an adjustable percentage of the maximum intensity of the image (Figures 2g and S1a). Small structures disconnected from the vascular network are removed in a few steps, depending on their size and proximity to the network (Figures 2h and S1b) and the resulting binary image is thinned, after which small spurs are removed by end-point detection and recursive pruning of small segments (Figures 2i and S1c). At this point, the number of disconnected components is determined, and the vascular network is assumed to

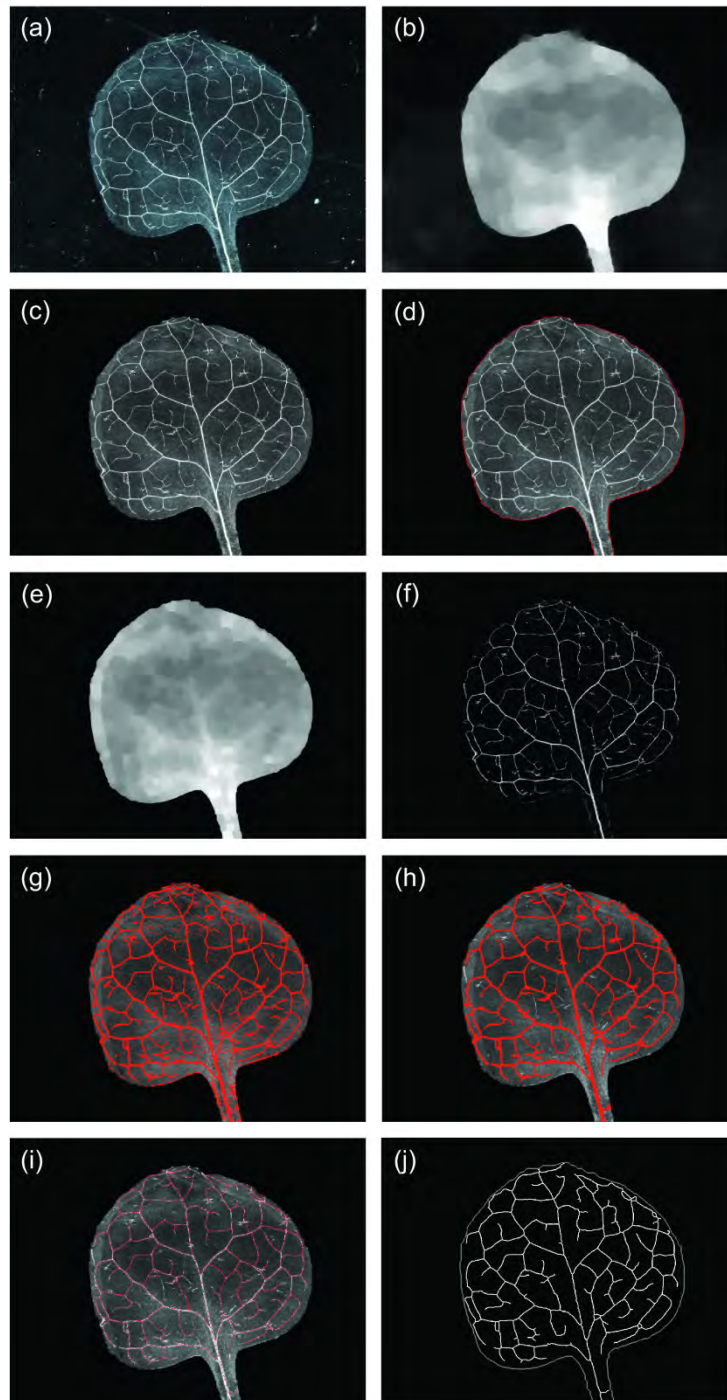


Figure 2. Automated extraction of the vascular network of an Arabidopsis leaf.

(a) Dark-field picture of a cleared leaf used as the input image for the analysis. (b) Contrast between the leaf and background enhanced by recursive opening and closing using an increasing structuring element. (c) Extraction of the leaf from the background by thresholding the image in (b) using the mean intensity of the complete image. (d) Detection of the leaf margin by subtraction of the eroded leaf mask from the dilated one. (e) Application of recursive opening and closing using an increasing structuring element to remove the local background within the leaf. (f) Subtraction of the image in (e) from the leaf image in (c) results in a gray-scale extraction of the vascular pattern. (g) Dilation of the pattern, followed by thresholding using an adjustable percentage of the maximum intensity of the image. (h) Removal of small structures disconnected from the vascular network. (i) Thinning of the resulting image, after which small spurs are removed. (j) Segmentation completion by combination of the extracted leaf margin and the vascular pattern.

be the largest component. This step removes disconnected structures from the network, such as trichomes, that are often also illuminated by dark-field imaging. As a consequence, the algorithm is only suited for extraction of interconnected vascular networks. Hence, mutants such as *fkd2/sfc/van3*, *trn1*, *trn2*, *cvp1* and *cvp2*, which generate a vascular pattern consisting of vascular islands (Carland *et al.*, 1999; Deyholos *et al.*, 2000; Steynen and Schultz, 2003; Cnops *et al.*, 2006), cannot be analyzed by the algorithm. The picture segmentation is completed by combining the extracted leaf margin and venation pattern by addition of the two images (Figure 2j).

These steps represent the workflow by which the leaf margin and vascular network are segmented from a dark-field leaf image. Subsequently, the resulting pattern is quantified (see below), and, as mentioned before, is made available in the interactive drawing application for visual control, rectification and approval of the network, ensuring segmentation of the vascular pattern with the desired quality.

Quantification of vascular traits

Once the vascular network and leaf margins have been extracted, the next step is to quantify the vascular parameters. The actual measurements are implemented in a second algorithm for which the input is the vascular pattern and leaf margin obtained using the first algorithm (Figure 3a). The algorithm is partly derived from an approach developed previously for analysis of *in vitro* vascular networks in human endothelial cell cultures (Mezentzev *et al.*, 2005; Merks *et al.*, 2006). First, the leaf lamina is defined and separated from the petiole in a standardized manner to avoid the possibility that petiole length affects leaf size and vascular measurements. The leaf lamina is separated by recursive dilation of the binary leaf margin image, closing the petiole (Figure 3b). Recursive thinning of this object results in a closed object, excluding most of the petiole (Figure 3c). The area enclosed by both this object and the leaf margin defines the leaf lamina. The vascular network to be analyzed is reduced to the part inside the leaf lamina by taking the intersection of both (Figure 3d). Because the segmentation algorithm extracts the vascular pattern as a four-connected skeletonized line, branching points and end-points in the network can be identified as pixels with three or four neighbors and those with only one neighbor, respectively (Figure 3e). Points positioned on vascular strands have two neighbors. Branching points that are in close proximity to each other (fewer than seven pixels) are considered as a single branching point because this is how it would be defined by visual recording. Subtraction of branching points from the vascular pattern divides the network into disconnected lines, hereafter called vascular elements. The network is then represented as a graph structure, defining which branching points and end-points are connected to which vascular elements, and the topology of each vascular element is defined by its coordinates. The above transformations allow a more mathematical and faster processing of the data. To measure vein lengths, the detected vascular elements are sub-divided into line sections of user-defined length. The length of a vein is calculated as the sum of the Euclidean distances between the end-points of the line

sections. The total length of the vascular system in the leaf is the sum of the lengths of each vascular element. The graph structure allows determination of whether a vascular element is connected to an end-point or links two branching points, enabling calculation of the mean length of the free-ending and enclosed veins. Furthermore, LIMANI provides an output list that includes the lengths of all individual vascular elements. The areoles (areas in the lamina surrounded by vascular strands) are also extracted from the graph structure, and their number and mean areas are calculated (Figure 3f). All length and area measurements are calibrated from pixels to standard units based on a user-defined calibration value. Finally, vascular density (vein length per unit area) and complexity (sum of the number of end-points, branching points and vascular elements) are calculated. The number of branching points has been used previously to represent vascular complexity (Hamada *et al.*, 2000; Jun *et al.*, 2002). Kang *et al.* (2007) remarked correctly that the number of end-points provides additional information on the complexity of a venation network. Adding the term 'number of vascular elements' to the equation allows discrimination between networks that show an altered ratio between three-way and four-way junctions at vascular branching points, giving a complete representation of the factors affecting vascular complexity. Hence, LIMANI determines ten measures of the vascular network starting from a dark-field cleared leaf picture, providing quantitative values for the biologically most relevant vascular traits (Table S1).

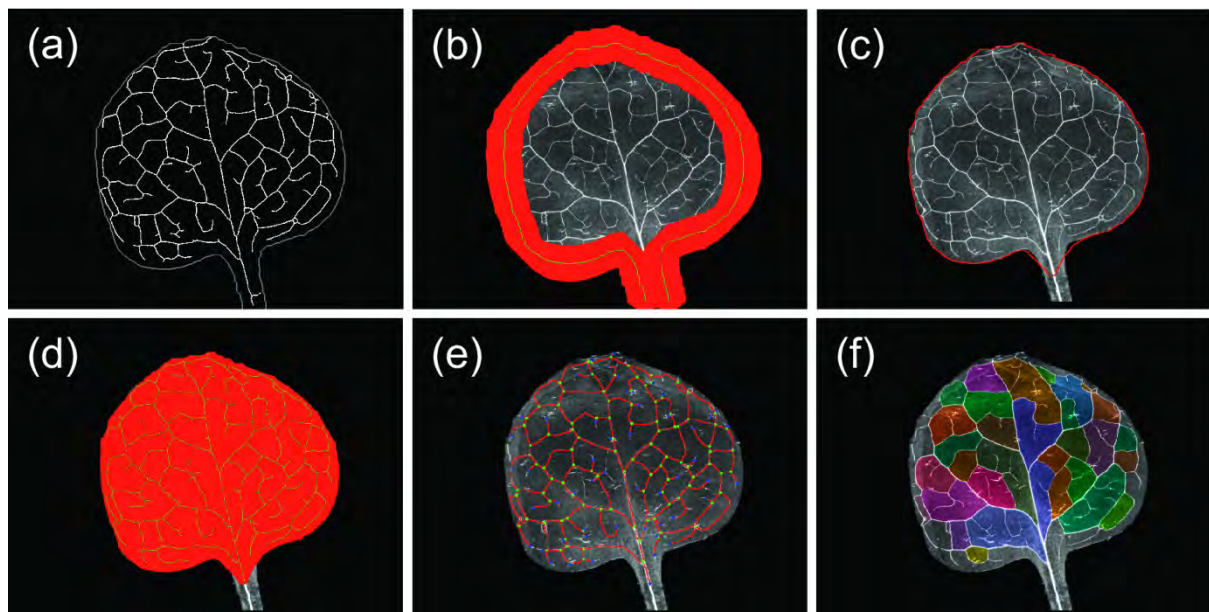


Figure 3. Quantification of the vascular network.

(a) Binary image comprising the leaf margin and the vascular network extracted by the first algorithm. (b) Dilation of the leaf margin, closing the petiole. For visualization, the original input image is used as the background image. (c) Determination of the leaf lamina. (d) Indication of the leaf area (red) and the vascular network covering the leaf lamina. (e) Visualization of the branching points (green), end-points (blue) and vascular segments (red). (f) Visualization of the areolas, which are randomly color-coded.

Vascular differentiation throughout leaf development

Using LIMANI, we analyzed development of the venation pattern in the third leaf of *Arabidopsis* (Col-0) to examine evolution of the vascular features during leaf growth. Leaves were analyzed at 11, 12, 13, 14, 15, 17, 19, and 21 days after stratification (DAS) ($n \geq 10$). The analysis started after differentiation of the midvein, which was only apparent in 20% of the samples at 10 DAS. This timing implies that the vascular differentiation process starts at the transition from primary to secondary leaf morphogenesis, which also occurs at approximately day 10 (Andriankaja M., Dhondt S., De Bodt S., Inzé D., unpublished data). Early during this period, the leaf lamina grows exponentially, with a progressive decrease in the relative expansion rate after day 14 (Figure 4a), while the vascular pattern length increases at a constant (exponential) rate from day 11 to 14, after which the rate of increase gradually declines (Figure 4b). Furthermore, the vascular density increased to 3.2 mm mm^{-2} at 14 DAS, and then rapidly decreased to 1.7 mm mm^{-2} (Figure 4c), indicating that the vascular pattern extends faster than growth of the leaf blade during the exponential growth phase, but undergoes a slower increase later during development. This developmental trend in vascular density is comparable to that previously identified in juvenile and more adult rosette leaves of *Arabidopsis* (Candela et al., 1999; Kang and Dengler, 2004; Rolland-Lagan et al., 2009). Interestingly, the vein density decreases and increases in leaves formed later during rosette development in Columbia (Col) and Landsberg erecta (Ler) backgrounds, respectively. Moreover, the corresponding density values in Col background are generally lower than those in Ler. Measurements of leaf 3 show that densities of branching points and end-points also peak at day 14, i.e. simultaneously with the vascular density (Figure S2), and this is also the time at which the mean length of the free-ending veins is minimal (Figure 4d). Three days later, at 17 DAS, the topology of the vascular pattern is complete, as reflected by the the vascular complexity (Figure 4h) and the plateau reached for the number of end-points, branching points and areoles (Figure 4e–g). In other words, the increase in total vein length at 17 DAS is primarily due to extension of the existing connections in the pattern. Interestingly, the numbers of end-points and branching points are strongly correlated (Figure 4i). A linear regression analysis with the intercept at the origin results in an R^2 value of 0.98 for $y = 3.6 x$, indicating that, for every vascular end-point, a mean of 3.6 branching points are present in the leaf, independently of the developmental stage. This observation suggests a balance between formation of free-ending veins and connection of veins to the existing pattern. Furthermore, during the period of rapid pattern extension, from days 12–15, the mean areola area is relatively constant (Figure 4j) but the number of end-points, branching points and areoles expands rapidly (Figure 4e–g). Thus, the mean number of pattern elements per unit area, i.e. the scaling of the pattern, remains approximately constant during rapid tissue expansion. Such a typical pattern scale is consistent with self-organization hypotheses for leaf venation patterning, in which motile chemical signals (Meinhardt, 1976), including auxin (Dimitrov and Zucker, 2006; Merks et al., 2007), or

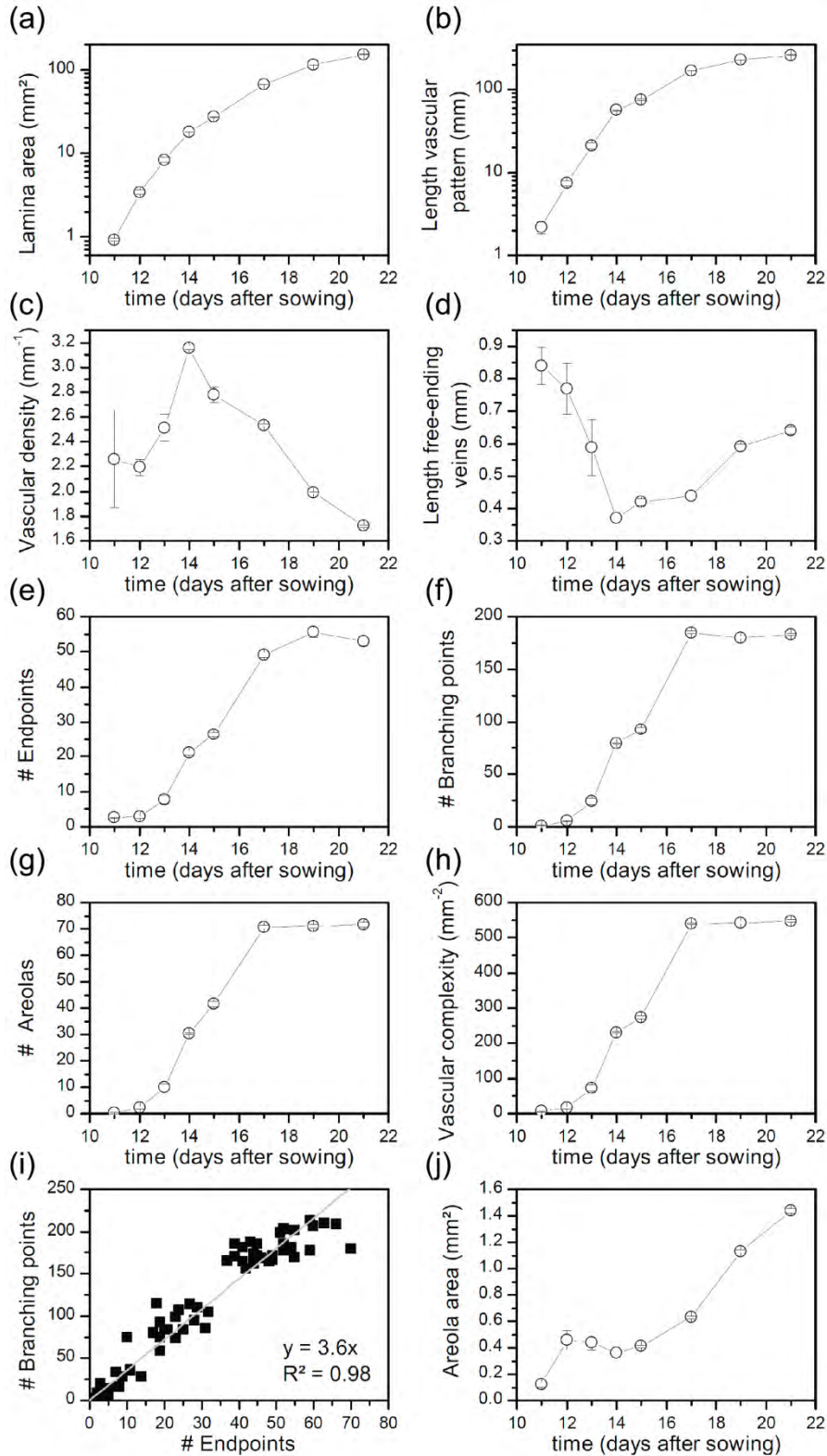


Figure 4. Time-lapse analysis of vascular differentiation during leaf development.

Venation patterns of third-node *Arabidopsis* Col-0 leaves were analyzed at 11, 12, 13, 14, 15, 17, 19 and 21 days after stratification (DAS). (a) Lamina area. (b) Vascular pattern length. (c) Vascular density. (d) Length of free-ending veins. (e) Number of end-points. (f) Number of branching points. (g) Number of areoles. (h) Vascular complexity. (i) Correlation between the numbers of end-points and branching points by linear regression with the intercept at the origin. (j) Areola area. Error bars represent SE ($n \geq 10$).

mechanical strain (Couder *et al.*, 2002; Laguna *et al.*, 2008) maintain a constant distance between newly formed pattern elements. Leaf growth creates more space between the permanently differentiated veins, driving further expansion of the network, but not necessarily meaning that areole areas are uniform across the leaf. A gradient in areole sizes from the centre of the leaf to the leaf margin has been reported (Rolland-Lagan *et al.*, 2009). Larger areole areas near the middle of the leaf may be indicative of a stronger sink strength of the midvein compared to the higher order veins or may represent local growth differences. Taken together, analysis of vascular differentiation during leaf development using the LIMANI framework provides a better insight into the patterning process. It showed that active expansion of the differentiated venation starts at the transition from primary to secondary leaf morphogenesis and ends before the shutdown of cell expansion. Furthermore, our analysis revealed a balance between the formation of new veins and the connection of veins to the existing pattern, and suggests a self-organizing mechanism for leaf venation patterning, followed by uniform expansion of a terminally differentiated pattern.

Cellular traits affect vascular patterning

In addition to analysis of vascular development in wild-type plants, we assessed whether cell density and leaf size affect vascularization. To this end, we studied the vascular topology in six transgenic lines with contrasting cellular and leaf growth traits that have been described previously. These lines included the *grandifolia* mutants *gra2-D* and *gra3-D*, which contain a large segmental duplication in the lower part of chromosome 4 (Horiguchi *et al.*, 2009), an over-expression line for the *CYCLIN D2;1* gene (35S:*CYCD2;1*) (Qi and John, 2007), the *SHORT-ROOT* and *SCARECROW* mutants *shr-6* and *scr-3* (Fukaki *et al.*, 1996; Gallagher *et al.*, 2004), and an over-expression line for the cell-cycle inhibitor KIP-RELATED PROTEIN 2 (35S:*KRP2*) (De Veylder *et al.*, 2001). Analysis of the vascular pattern of these lines was used for a correlation study between vascular parameters and leaf and cell growth traits. To obtain a better understanding of the effect of foliar cellular content on the vein patterning process, we determined the final leaf size, mesophyll cell area and mesophyll cell number per leaf in first-node leaves of the six transgenic lines, and compared them to the wild-type measurements at 24 DAS (Table 1). These cellular measurements were repeated on additional leaves at 8 DAS, early during vascular patterning of the first-node leaf pair (data not shown), allowing calculation of the number of cells produced per cell between 8 and 24 DAS (Table 1). The latter measurement was used as a proxy for the length of the cell proliferation phase in the leaf. The rationale behind the use of this numerical proxy is that 8 DAS is the time point at which the cell-cycle arrest front is usually established in leaves 1 and 2 of *Arabidopsis*, and that the leaves stop growing and reach a mature developmental stage at 24 DAS. The number of cells produced per cell between 8 and 24 DAS relates to the number of cell divisions between establishment of the cell-cycle arrest front and maturity on an individual cell basis, and thus serves as a reliable proxy for the length of the proliferation phase.

Table 1. Vascular analysis of wild-type plants and six transgenic lines, with contrasting cellular and leaf size phenotypes at 24 DAS.

Genotype	Leaf area (mm ²)	Cell area (μm ²) ^a	Cell number ^b	Cell divisions between days 8 and 24 DAS (Cell ⁻¹) ^c
<i>gra3-D</i>	44.66 ± 2.92	1215 ± 41	36741 ± 4117	15.27 ± 2.87
<i>gra2-D</i>	33.06 ± 2.40	1488 ± 97	22217 ± 2349	10.88 ± 1.64
Wild-type	18.75 ± 0.54	1313 ± 36	14276 ± 1365	3.68 ± 0.54
35S::CYCD2;1	15.76 ± 0.66	636 ± 73	24616 ± 3031	6.09 ± 0.96
<i>scr-3</i>	8.21 ± 0.45	1128 ± 84	7278 ± 582	3.64 ± 0.60
<i>shr-6</i>	4.40 ± 0.29	1065 ± 78	4130 ± 467	1.20 ± 0.19
35S::KRP2	2.78 ± 0.20	1845 ± 167	1506 ± 274	1.83 ± 0.46

^a The area of mesophyll cells in the subepidermal layer observed in a paradermal view.

^b Total number of mesophyll cells estimated by dividing leaf area by cell density.

^c Cell divisions per cell between 8 and 24 DAS calculated by dividing cell number at day 24 by that at day 8.

The genotypes are ranked according to their final leaf size. Data are means ± SE (n ≥ 5).

gra2-D and *gra3-D* produced large leaves primarily due to an increase in cell number as a consequence of an extended cell proliferation phase. This phenotype is more pronounced in *gra3-D* than in *gra2-D*, as reported previously (Horiguchi *et al.*, 2009). In the *CYCD2;1* over-expression line, the cell number increased twofold, accompanied by a similar decrease in cell size, without a drastic effect on the final leaf size (Qi and John, 2007). The leaves of *scr*, *shr* and 35S:*KRP2* lines were smaller than those of the wild-type. In the *scr* and *shr* mutants, the reduction was mainly due to a decrease in cell number, caused by a longer cell-cycle duration, together with an earlier exit from the cell proliferation phase in the case of *shr*, explaining its more drastic phenotype (Dhondt *et al.*, 2010). In the 35S:*KRP2* line, the extreme reduction in cell number was partially compensated for by a strongly increased cell size (De Veylder *et al.*, 2001). Leaves at 24 DAS were also utilized to analyze the vascular network by means of LIMANI. Vascular measures were obtained for all lines (Table S1), and correlations with leaf area, cell area, cell number and cell production per cell between days 8 and 24, corresponding to the duration of the cell-proliferation phase, were calculated for each of the vascular parameters (Figure 5a). The strongest correlation for most vascular parameters was found with the leaf area. Among these, the highest correlation was between leaf area and the total length of the vascular pattern ($R^2 = 0.98$) (Figure 5b). This suggests that formation of the vascular network and the space available within the leaf are tightly linked, in accordance with a self-organizing mechanism for pattern formation. The selected transgenic lines, together with the wild-type, covered a large range of leaf sizes, from 2 to 55 mm² (Figure 5b). The length of the proliferation phase was also strongly correlated with most vascular parameters. The fact that cell production is the only indirect measurement, derived from the difference between samples at 8 and 24 DAS, in this correlation analysis underlines the strength of this relationship even more. This finding confirms that

modifications of cell proliferation patterns are correlated with changes in vein complexity (Kang *et al.*, 2007), and is in line with the correlation found between termination of vein formation and mesophyll differentiation (Scarpella *et al.*, 2004). However, in our data set, the duration of cell proliferation and final leaf size were also very well correlated ($R^2 = 0.95$), making it difficult to separate the effect of the length of the cell proliferation phase and overall leaf growth on development of the vascular network. For the mean length of the free-ending veins, vascular density and the mean areole area, the highest correlation was found with total cell number in the leaf (Figure 5a). Furthermore, vascular density and mean areole area were the only parameters that significantly correlated with the mesophyll cell area (Figure 5a). This suggests that the cellular content of the leaf is affecting the process of vascular patterning. Analysis of vascular patterning during leaf growth revealed that the number of areoles stabilized while the leaf was still growing (Figure 4a,g), suggesting that expansion of the cells enclosed by the areole drove the increase in areole area during the later stages of leaf development. The more cells enclosed by the areole at that stage, the larger the net effect of expansion of the individual cells, explaining the observed correlations with the areole area. The same reasoning can explain the correlation with vascular density: the more cells in the leaf, the higher the net impact of expansion of the individual cells on enlargement of the network and the less dense the network will be at maturity. Moreover, the time window during which this process occurs has already started at shutdown of the vascular patterning, which is earlier during leaf development than observation of a stabilized differentiated pattern (17 DAS). Another interesting observation is the strong correlation between the numbers of end-points and branching points (Figure 5c). A linear regression analysis with the intercept at the origin resulted in an R^2 value of 0.98 for $y = 2.74 x$, indicating that the balance does not depend on the foliar cellular content. In comparison with leaf 3 from the developmental study, leaf 2 contains fewer branching points per end-point. A significant deviation from this constant is found for transgenic lines that are affected in the connection of vascular strands to pre-existing vascular bundles, such as *ron1/fry1/sal1*, *fkd2/sfc/van3* and *cvp2*, which have an open vascular pattern as a consequence (Steynen and Schultz, 2003; Carland and Nelson, 2004; Robles *et al.*, 2010).

These correlation studies reveal that many vascular phenotypes are linked to developmental changes. As vein patterning and growth occur concurrently, these processes are closely related. A shift in the developmental timing of cell proliferation or cell expansion, or a change in the cell division or cell expansion rate, will have a significant impact on a number of vascular parameters in the leaf. Hence, the observed vascular phenotype may be a primary as well as a secondary effect of the perturbation. In addition, a strong link between vascular patterning and leaf shape has been observed. Nevertheless, the question remains whether a change in leaf shape is the cause or consequence (or both) of the change in vascular patterning (Dengler and Kang, 2001; Runions *et al.*, 2005; Fujita and Mochizuki, 2006). As vascular differentiation occurs relatively late in development, we assume that the influence of

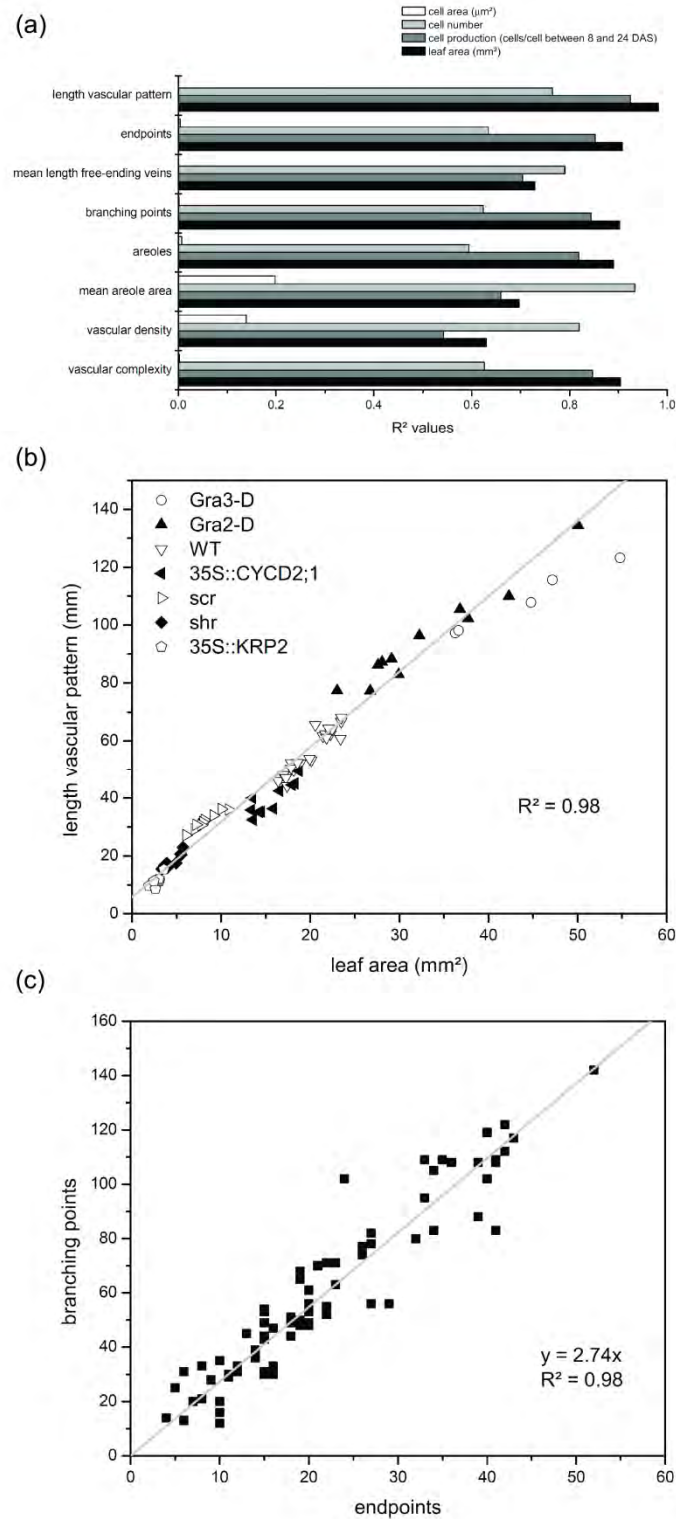


Figure 5. Correlation study between cellular traits and vascular parameters.

Correlations were determined by linear regression analysis using measurements from wild-type plants and six transgenic lines with contrasting cellular and leaf size traits (a) Correlations between cell area, cell number, cell production and leaf area, and differentiated vascular pattern traits in mature leaves. Cell production, expressed as the number of cells produced per cell between 8 and 24 DAS, is used as a proxy for the length of the cell proliferation phase. (b) Correlation between leaf area and total length of the vascular pattern. (c) Correlation between the numbers of end-points and branching points by linear regression with the intercept at the origin.

a fully functional and differentiated venation pattern on leaf shape and growth is rather limited, especially because differentiation of the midvein takes place near the end of the cell proliferation phase, the timing of which is strongly correlated with the final leaf size. This indicates that growth factors delivered locally by the differentiated vascular bundles probably do not contribute much to the final leaf size. However, at the time of vascular patterning, while the leaf is still proliferating, the developing vasculature also transports growth factors within the leaf, including auxin. The transport of these factors can affect local cell division and expansion, suggesting that removal of growth factors by the developing venation pattern may have more impact on leaf growth than their supply by the differentiated network. Nevertheless, the positive correlation of leaf vein density with the photosynthetic rate supports the hypothesis that vein positioning limits photosynthesis via its influence on foliar hydraulic efficiency (Brodribb *et al.*, 2007). Thus, a high vascular density in old leaves, acting as a source tissue, may increase the production of photoassimilates, which, after transportation, may drive growth in young leaves, acting as a sink tissue. A careful analysis of leaf growth in various mutants or ecotypes with an altered vascular density may resolve this question.

In conclusion, the online framework LIMANI was developed for analysis of vascular networks in leaves, allowing automatic segmentation and measurement of venation patterns and including an interactive interface for manual segmentation corrections. This tool enables more quantitative analysis of vascular mutants and is able to generate data that are necessary to test various theoretical and mathematical models describing the underlying mechanisms of vascular patterning (Couder *et al.*, 2002; Rolland-Lagan and Prusinkiewicz, 2005; Runions *et al.*, 2005; Dimitrov and Zucker, 2006; Feugier and Iwasa, 2006; Merks *et al.*, 2007; Laguna *et al.*, 2008). We used the LIMANI framework to study vascular differentiation during leaf development and to analyze the venation pattern in transgenic lines with contrasting cellular and leaf growth traits. The results show the evolution of vascular traits during leaf development, and suggest a self-organizing mechanism for leaf venation patterning. We examined the effect of cellular content and leaf growth on vein patterning, and revealed a tight balance between the number of end-points and branching points within the leaf vascular network, independent of the leaf developmental stage and cellular content, but dependent on the position of the leaf on the rosette. These findings indicate that use of LIMANI can lead to a better understanding of the interaction between two processes occurring concurrently in leaf development, i.e. vascular patterning and leaf growth.

EXPERIMENTAL PROCEDURES

Plant materials and growth conditions

Arabidopsis thaliana (L.) Heyhn. was used as the wild-type, and transgenic *gra2-D*, *gra3-D* (Horiguchi *et al.*, 2009), 35S:*CYCD2;1* (Qi and John, 2007), *shr-6* (Gallagher *et al.*, 2004), *scr-3* (Fukaki *et al.*, 1996), and 35S:*KRP2* (De Veylder *et al.*, 2001) plants were included in the analysis of how cellular traits affect vascular patterning. These lines were all in the Columbia (Col) background. Seeds were sterilized in a 3% NaClO solution (Carl Roth, <http://www.carlroth.com/>) for 15 min, and sown on medium containing half-strength Murashige and Skoog medium (Duchefa, <http://www.duchefa.com/>) solidified with 0.9 g l⁻¹ plant tissue culture agar (Lab M, <http://www.labm.com/>) on round plates (Becton-Dickinson, <http://www.bd.com/>). After a stratification period of 2 days, the plates were placed in a growth chamber under long-day conditions (16 h light/8 h darkness) at 22°C with a light intensity of 80–100 μmol m⁻² s⁻¹ supplied by cool-white fluorescent tubes (Spectralux Plus 36W/840; Radium, <http://www.radium.de/en/>).

Sample preparation and imaging

Leaves were harvested, cleared in 100% ethanol, and subsequently cleared and stored in lactic acid for microscopy. In cases of strong starch accumulation, the leaves were briefly cleared in a solution of 80 g chloral hydrate, 20 ml glycerol and 10 ml water. The cleared leaves were whole-mounted on slides in lactic acid and studied using a dark-field MZ16 stereomicroscope (Leica, <http://www.leica-microsystems.com/>). To overcome highlighting of scratches on the images, the glass object surface was replaced with the plastic lid of a square 9 × 9 cm Petri dish (Greiner Bio-One, <http://www.greinerbioone.com/>). Images were captured using a DS-5Mc camera (Nikon, <http://www.nikon.com/>) mounted on the stereomicroscope.

Image analysis and framework set-up

The Leaf Image Analysis Interface (LIMANI) is available online at <http://limani.psb.ugent.be/>, and is supported by the current versions of the Firefox, Google Chrome, and Safari web browsers. Demonstration videos that illustrate the functionality of the framework, FAQs, and user support are available online. The image analysis algorithms were written in Python, using the SDC Morphology Toolbox for Python (<http://www.mmorph.com/pymorphpro/>). The web interface was built using standards-compliant HTML5, with Java script to enable greater interaction with the user and making use of the Google Closure Library (<http://code.google.com/closure/library/>). All web pages are served by the Python Django web framework (<http://www.djangoproject.com/>) on top of Apache (<http://www.apache.org/>). Static data (e.g. images or scripts) are served by Apache as is.

Celery was chosen as the task queue server (<http://celeryproject.org/>). AMQP messaging was utilized to distribute tasks among multiple computers and multiple processes. The web server is incorporated into the data protection protocol of the Department of Plant Systems Biology, where the server is located.

ACKNOWLEDGEMENTS

We thank the members of the 'Systems Biology of Yield' research group at the department of Plant Systems Biology (VIB) and the members of the AGRON-OMICS consortium for testing and providing feedback on the LIMANI framework. This work was supported by grants from the Interuniversity Attraction Poles Program (Belgian Network BARN: 'Growth and Development of Higher Plants'; IUAP VI/33), initiated by the Science Policy Office of the Belgian State, the 'Bijzonder Onderzoeksfonds Methusalem project' (number BOF08/01M00408) of Ghent University, the European Community 6th Framework Programme ('AGRON-OMICS', LSHG-CT-2006-037704), and Marie Curie Intra-European Fellowship MEIF-CT-2005-025084 and Marie Curie European Reintegration Grant PERG03-GA-2008-230974 (to R.M.), and was co-financed by the Netherlands Consortium for Systems Biology, which is part of the Netherlands Genomics Initiative/Netherlands Organization for Scientific Research. S.D. is indebted to the Agency for Innovation by Science and Technology for a pre-doctoral fellowship.

SUPPORTING INFORMATION

The following materials are available in the online version of this article.
(<http://onlinelibrary.wiley.com/doi/10.1111/j.1365-313X.2011.04803.x/supinfo/>)

Figure S1. Detailed representation of venation segmentation steps.

- (a) Segmentation of the venation pattern after grayscale dilation and thresholding of the leaf picture with removed background.
 - (b) Removal of small structures disconnected from the vascular network (see arrowheads in a).
 - (c) Thinning of the resulting binary image and removal of small spurs (see arrowheads in b).
- Panels are zoom-ins of Figure 2g–i.

Figure S2. Branching point and endpoint density during leaf development.

Error bars represent SE ($n \geq 10$).

Table S1. Vascular analysis of wild-type plants and six transgenic lines, with contrasting cellular and leaf size phenotypes at 24 DAS.

CONTRIBUTIONS

Stijn Dhondt developed the imaging scripts for extraction of venation patterns from dark-field images. The image analysis script extracting vascular data from binary images was developed by Roeland Merks and Stijn Dhondt. Dirk Van Haerenborgh built the on-line framework, containing the interactive interface, and implemented the imaging algorithms. Stijn Dhondt examined the vascular differentiation throughout leaf development. Together with Caroline Van Cauwenbergh, he extracted the cellular content and conducted the vascular analysis of transgenic lines. The correlation studies were performed by Stijn Dhondt.

RELATED PUBLICATIONS NOT INCLUDED IN THE THESIS

An adjusted version of the image analysis script to extract vascular parameters from a binary representation of venation patterns has been applied to screen 114 lines, corresponding to the leaf shape mutant collection of José Luis Micol (Allicante), for vascular phenotypes starting from drawings of the vascular pattern (Perez-perez et al., 2011). I contributed to this published analyses of which the title page is included at the end of this chapter. Furthermore, this imaging script has been applied in a manuscript which describes a functional analysis of a gain-of-function of BRASSINOSTEROID INSENSITIVE1 (BRI1), a *bri1* loss-of-function mutant and a loss-of-function mutant of CONSTITUTIVE PHOTOMORPHOGENIC DWARF (*cpd*), involved in brassinosteroid biosynthesis (Zhiponova M. and Russinova, E. unpublished results).

REFERENCES

- Alonso-Peral, M.M., Candela, H., del Pozo, J.C., Martínez-Laborda, A., Ponce, M.R. and Micol, J.L.** (2006) The *HVE/CAND1* gene is required for the early patterning of leaf venation in *Arabidopsis*. *Development*, **133**, 3755-3766.
- Bohn, S., Andreotti, B., Douady, S., Munzinger, J. and Couder, Y.** (2002) Constitutive property of the local organization of leaf venation networks. *Phys. Rev. E*, **65**, 061914.
- Boyce, C.K., Brodribb, T.J., Feild, T.S. and Zwieniecki, M.A.** (2009) Angiosperm leaf vein evolution was physiologically and environmentally transformative. *Proc. R. Soc. B*, **276**, 1771-1776.
- Brodribb, T.J. and Feild, T.S.** (2010) Leaf hydraulic evolution led a surge in leaf photosynthetic capacity during early angiosperm diversification. *Ecol. Lett.* **13**, 175-183.

Brodribb, T.J., Feild, T.S. and Jordan, G.J. (2007) Leaf maximum photosynthetic rate and venation are linked by hydraulics. *Plant Physiol.* **144**, 1890-1898.

Busse, J.S. and Evert, R.F. (1999) Pattern of differentiation of the first vascular elements in the embryo and seedling of *Arabidopsis thaliana*. *Int. J. Plant Sci.* **160**, 1-13.

Candela, H., Martínez-Laborda, A. and Micol, J.L. (1999) Venation pattern formation in *Arabidopsis thaliana* vegetative leaves. *Dev. Biol.* **205**, 205-216.

Carland, F.M. and Nelson, T. (2004) *COTYLEDON VASCULAR PATTERN2*-mediated inositol (1,4,5) triphosphate signal transduction is essential for closed venation patterns of *Arabidopsis* foliar organs. *Plant Cell*, **16**, 1263-1275.

Carland, F.M., Berg, B.L., FitzGerald, J.N., Jinamornphongs, S., Nelson, T. and Keith, B. (1999) Genetic regulation of vascular tissue patterning in *Arabidopsis*. *Plant Cell*, **11**, 2123-2137.

Cnops, G., Neyt, P., Raes, J., Petrarulo, M., Nelissen, H., Malenica, N., Luschnig, C., Tietz, O., Ditengou, F., Palme, K., Azmi, A., Prinsen, E. and Van Lijsebettens, M. (2006) The *TORNADO1* and *TORNADO2* genes function in several patterning processes during early leaf development in *Arabidopsis thaliana*. *Plant Cell*, **18**, 852-866.

Couder, Y., Pauchard, L., Allain, C., Adda-Bedia, M. and Douady, S. (2002) The leaf venation as formed in a tensorial field. *Eur. Phys. J. B*, **28**, 135-138.

De Veylder, L., Beeckman, T., Beemster, G.T.S., Krols, L., Terras, F., Landrieu, I., Van Der Schueren, E., Maes, S., Naudts, M. and Inzé, D. (2001) Functional analysis of cyclin-dependent kinase inhibitors of *Arabidopsis*. *Plant Cell*, **13**, 1653-1667.

Dengler, N. and Kang, J. (2001) Vascular patterning and leaf shape. *Curr. Opin. Plant Biol.* **4**, 50-56.

Deyholos, M.K., Corder, G., Beebe, D. and Sieburth, L.E. (2000) The *SCARFACE* gene is required for cotyledon and leaf vein patterning. *Development*, **127**, 3205-3213.

Dhondt, S., Coppens, F., De Winter, F., Swarup, K., Merks, R.M.H., Inzé, D., Bennett, M.J. and Beemster, G.T.S. (2010) *SHORT-ROOT* and *SCARECROW* regulate leaf growth in *Arabidopsis* by stimulating S-phase progression of the cell cycle. *Plant Physiol.* **154**, 1183-1195.

- Dimitrov, P. and Zucker, S.W.** (2006) A constant production hypothesis guides leaf venation patterning. *Proc. Natl Acad. Sci. USA*, **103**, 9363-9368.
- Dougherty, E.R. and Lotufo, R.A.** (2003) *Hands-on Morphological Image Processing*. Bellingham, WA: SPIE-The International Society for Optical Engineering.
- Esau, K.** (1965) *Plant Anatomy*, 2nd edn. New York: John Wiley & Sons.
- Feugier, F.G. and Iwasa, Y.** (2006) How canalization can make loops: A new model of reticulated leaf vascular pattern formation. *J. Theor. Biol.* **243**, 235-244.
- Fujita, H. and Mochizuki, A.** (2006) The origin of the diversity of leaf venation pattern. *Dev. Dynam.* **235**, 2710-2721.
- Fukaki, H., Fujisawa, H. and Tasaka, M.** (1996) *SGR1*, *SGR2*, and *SGR3*: novel genetic loci involved in shoot gravitropism in *Arabidopsis thaliana*. *Plant Physiol.* **110**, 945-955.
- Gallagher, K.L., Paquette, A.J., Nakajima, K. and Benfey, P.N.** (2004) Mechanisms regulating SHORT-ROOT intercellular movement. *Curr. Biol.* **14**, 1847-1851.
- Hamada, S., Onouchi, H., Tanaka, H., Kudo, M., Liu, Y., Shibata, D., Machida, C., and Machida, Y.** (2000) Mutations in the *WUSCHEL* gene of *Arabidopsis thaliana* result in the development of shoots without juvenile leaves. *Plant J.* **24**, 91-101.
- Hickey, L.J.** (1988) A revised classification of the architecture of dicotyledonous leaves. In *Anatomy of the Dicotyledons, Volume 1*, 2nd edn. (Metcalfe, C.R. and Chalk, L., eds). Oxford: Clarendon Press, pp. 25-39.
- Hill, R.S.** (1980) A numerical taxonomic approach to the study of angiosperm leaves. *Bot. Gaz.* **141**, 213-229.
- Horiguchi, G., Gonzalez, N., Beemster, G.T.S., Inzé, D. and Tsukaya, H.** (2009) Impact of segmental chromosomal duplications on leaf size in the *grandifolia-D* mutants of *Arabidopsis thaliana*. *Plant J.* **60**, 122-133.
- Jun, J.H., Ha, C.M., and Nam, H.G.** (2002) Involvement of the *VEP1* Gene in vascular strand development in *Arabidopsis thaliana*. *Plant Cell Physiol.* **43**, 323 -330.
- Kang, J. and Dengler, N.** (2004) Vein pattern development in adult leaves of *Arabidopsis thaliana*. *Int. J. Plant Sci.* **165**, 231-242.

Kang, J., Mizukami, Y., Wang, H., Fowke, L. and Dengler, N.G. (2007) Modification of cell proliferation patterns alters leaf vein architecture in *Arabidopsis thaliana*. *Planta*, **226**, 1207-1218.

Laguna, M.F., Bohn, S. and Jagla, E.A. (2008) The role of elastic stresses on leaf venation morphogenesis. *PLoS Comput. Biol.* **4**, e1000055.

Meinhardt, H. (1976) Morphogenesis of lines and nets. *Differentiation*, **6**, 117-123.

Merks, R.M.H., Brodsky, S.V., Goligorsky, M.S., Newman, S.A. and Glazier, J.A. (2006) Cell elongation is key to in silico replication of in vitro vasculogenesis and subsequent remodeling. *Dev. Biol.* **289**, 44-54.

Merks, R.M.H., Van de Peer, Y., Inzé, D. and Beemster, G.T.S. (2007) Canalization without flux sensors: a traveling-wave hypothesis. *Trends Plant Sci.* **12**, 384-390.

Mezentzev, A., Merks, R.M.H., O'Riordan, E., Chen, J., Mendeleev, N., Goligorsky, M.S. and Brodsky, S.V. (2005) Endothelial microparticles affect angiogenesis in vitro: role of oxidative stress. *Am. J. Physiol. Heart Circ. Physiol.* **289**, H1106-H1114.

Pérez-pérez, J.M., Rubio-díaz, S., Dhondt, S., Hernández-romero, D., Sánchez-soriano, J., Beemster, G.T.S., Ponce, M.R., and Micol, J.L. (2011) Whole organ, venation and epidermal cell morphological variations are correlated in the leaves of *Arabidopsis* mutants. *Plant, Cell & Environment*, **34**, 2200-2211.

Price, C.A., Symonova, O., Mileyko, Y., Hilley, T. and Weitz, J.S. (2011) Leaf extraction and analysis framework graphical user interface: segmenting and analyzing the structure of leaf veins and areoles. *Plant Physiol.* **155**, 236-245.

Qi, R. and John, P.C.L. (2007) Expression of genomic *AtCYCD2;1* in *Arabidopsis* induces cell division at smaller cell sizes: implications for the control of plant growth. *Plant Physiol.* **144**, 1587-1597.

Robles, P., Fleury, D., Candela, H., Cnops, G., Alonso-Peral, M.M., Anami, S., Falcone, A., Caldana, C., Willmitzer, L., Ponce, M.R., Van Lijsebettens, M. and Micol, J.L. (2010) The *RON1/FRY1/SAL1* gene is required for leaf morphogenesis and venation patterning in *Arabidopsis*. *Plant Physiol.* **152**, 1357-1372.

Rolland-Lagan, A.-G., Amin, M. and Pakulska, M. (2009) Quantifying leaf venation patterns: two-dimensional maps. *Plant J.* **57**, 195-205.

Rolland-Lagan, A.-G. and Prusinkiewicz, P. (2005) Reviewing models of auxin canalization in the context of leaf vein pattern formation in *Arabidopsis*. *Plant J.* **44**, 854-865.

Runions, A., Fuhrer, M., Lane, B., Federl, P., Rolland-Lagan, A.-G. and Prusinkiewicz, P. (2005) Modeling and visualization of leaf venation patterns. *ACM Trans. Graph.* **24**, 702-711.

Scarpella, E. and Meijer, A.H. (2004) Pattern formation in the vascular system of monocot and dicot plant species. *New Phytol.* **164**, 209-242.

Scarpella, E., Francis, P. and Berleth, T. (2004) Stage-specific markers define early steps of procambium development in *Arabidopsis* leaves and correlate termination of vein formation with mesophyll differentiation. *Development*, **131**, 3445-3455.

Scarpella, E., Marcos, D., Friml, J. and Berleth, T. (2006) Control of leaf vascular patterning by polar auxin transport. *Genes Dev.* **20**, 1015-1027.

Sieburth, L.E. and Deyholos, M.K. (2006) Vascular development: the long and winding road. *Curr. Opin. Plant Biol.* **9**, 48-54.

Steynen, Q.J. and Schultz, E.A. (2003) The FORKED genes are essential for distal vein meeting in *Arabidopsis*. *Development*, **130**, 4695-4708.

Wenzel, C.L., Schuetz, M., Yu, Q. and Mattsson, J. (2007) Dynamics of *MONOPTEROS* and *PIN-FORMED1* expression during leaf vein pattern formation in *Arabidopsis thaliana*. *Plant J.* **49**, 387-398.

Whole organ, venation and epidermal cell morphological variations are correlated in the leaves of *Arabidopsis* mutants

JOSÉ MANUEL PÉREZ-PÉREZ¹, SILVIA RUBIO-DÍAZ¹, STIJN DHONDT^{3,4}, DIANA HERNÁNDEZ-ROMERO¹, JOAQUÍN SÁNCHEZ-SORIANO², GERRIT T. S. BEEMSTER^{3,4,5}, MARÍA ROSA PONCE¹ & JOSÉ LUIS MICOL¹

¹Instituto de Bioingeniería and ²Centro de Investigación Operativa, Universidad Miguel Hernández, Campus de Elche, 03202 Elche, Alicante, Spain, ³Department of Plant Systems Biology, Flanders Institute for Biotechnology (VIB), Technologiepark 927, 9052 Gent, Belgium, ⁴Department of Plant Biotechnology and Genetics, Ghent University, Technologiepark 927, 9052 Gent, Belgium and ⁵Department of Biology, University of Antwerp, Groenenborgerlaan 171, 2020 Antwerpen, Belgium

ABSTRACT

Despite the large number of genes known to affect leaf shape or size, we still have a relatively poor understanding of how leaf morphology is established. For example, little is known about how cell division and cell expansion are controlled and coordinated within a growing leaf to eventually develop into a laminar organ of a definite size. To obtain a global perspective of the cellular basis of variations in leaf morphology at the organ, tissue and cell levels, we studied a collection of 111 non-allelic mutants with abnormally shaped and/or sized leaves, which broadly represent the mutational variations in *Arabidopsis thaliana* leaf morphology not associated with lethality. We used image-processing techniques on these mutants to quantify morphological parameters running the gamut from the palisade mesophyll and epidermal cells to the venation, whole leaf and rosette levels. We found positive correlations between epidermal cell size and leaf area, which is consistent with long-standing Avery's hypothesis that the epidermis drives leaf growth. In addition, venation parameters were positively correlated with leaf area, suggesting that leaf growth and vein patterning share some genetic controls. Positional cloning of the genes affected by the studied mutations will eventually establish functional links between genotypes, molecular functions, cellular parameters and leaf phenotypes.

Key-words: leaf epidermis; palisade mesophyll; phenomics; principal component analysis; venation pattern.

INTRODUCTION

A major challenge in the post-genomic era is the functional characterization of all of the genes in the genomes of model species. To this end, large-scale approaches toward the targeted inactivation of every gene have been undertaken in animals such as *Caenorhabditis elegans* (Kamath *et al.* 2003), *Drosophila melanogaster* (Winkler *et al.* 2005),

mouse (Wu *et al.* 2007) and zebrafish (Wang *et al.* 2007), as well as in plants such as *Arabidopsis thaliana* (Alonso *et al.* 2003), maize (Fernandes *et al.* 2004) and rice (He *et al.* 2007). The emerging field of phenomics pursues the systematic study of phenotypes caused by individual mutations in every gene of a genome, an approach that is expected to provide a mechanistic link between genotypes and phenotypes (Lussier & Liu 2007). In these large-scale mutant screens, the phenotypes of mutants from gene-indexed collections must be recorded and quantified under standard conditions or in response to altered environments.


Forward genetic screens for mutations affecting the size and shape of *Arabidopsis* vegetative leaves have resulted in the isolation of hundreds of mutants (Berná, Robles & Micol 1999; Serrano-Cartagena *et al.* 1999; Horiguchi *et al.* 2006; Micol 2009). However, the causal genes for the phenotypes of most of these leaf mutants have yet to be identified. Thus far, we have positionally cloned 33 of the 76 genes initially identified in our laboratory based on the leaf phenotype of their mutant alleles (Robles & Micol 2001) and found that their wild-type products participate in processes as diverse as polar cell expansion, the transduction of hormonal signals, gene regulation, plastid biogenesis and chromatin remodelling (Pérez-Pérez *et al.*, 2009b). Strikingly, in several cases, mutations that we initially classified together based on macroscopic phenotype actually affect genes involved in a single pathway or molecular mechanism, implying that gene–morphology relationships are highly reproducible, such as in the *denticulata* (*den*) mutants with pointed leaves, where at least four of which carry alleles of genes encoding ribosomal proteins (Horiguchi *et al.* 2011). In addition, the *elongata* (*elo*) mutants, with narrow and elongated leaves, led to the identification of genes encoding subunits of the transcription Elongator complex (Nelissen *et al.* 2005). In this way, it is becoming possible to begin mapping the organizational levels that connect genes with the whole leaf phenotype, starting with the cellular and tissue levels.

Several methods have been developed for the automated quantification of shape and size variations in biological

Correspondence: J. L. Micol. E-mail: jlmicol@umh.es

6

Plant structure visualization by high-resolution X-ray computed tomography

Stijn Dhondt^{1, 2}, Hannes Vanhaeren^{1, 2}, Denis Van Loo³, Veerle Cnudde⁴, Dirk Inzé^{1, 2} 

¹ Department of Plant Systems Biology, VIB, Technologiepark 927, 9052 Ghent, Belgium

² Department of Plant Biotechnology and Genetics, Ghent University, Technologiepark 927, 9052 Ghent, Belgium

³ UGCT – Department of Physics and Astronomy, Ghent University, Proeftuinstraat 86, 9000 Ghent, Belgium

⁴ UGCT – Department of Geology and Soil Science, Ghent University, Krijgslaan 281/S8, 9000 Ghent, Belgium

This chapter is adapted from: Trends in Plant Science, 15, 419–422.

Received March 30, 2010; accepted May 13, 2010; published June 9, 2010.

Supplemental data is available online: <http://dx.doi.org/10.1016/j.tplants.2010.05.002/>

 Corresponding author; e-mail: dirk.inze@psb.vib-ugent.be.

ABSTRACT

New developments in high-resolution X-ray computed tomography (HRXCT) are promising for the broader application of this non-destructive imaging method in plant sciences. Here, we demonstrate how detailed three-dimensional morphological traits can be extracted rapidly from *in vivo Arabidopsis thaliana* seedlings without sample manipulation. Furthermore, *ex vivo* scanning at sub-micron resolution allows the quantification and visualization of the cellular organization of plant tissue samples, making HRXCT a desired tool in developmental plant biology.

X-ray computed tomography: past and present

X-ray computed tomography (CT) is a minimally-invasive structural imaging method that allows three-dimensional (3-D) reconstruction of scanned objects. This technique was first used as a medical diagnostic tool in 1971, but has since been applied to a broad range of sciences, including natural, material and earth sciences [1] and [2]. Today CT is commonly utilized in animal sciences, mainly in cancer research, bone architecture study, angiogenesis, and *in vivo* imaging of small animals. However, its first application in plants was not before the late 1990s in the form of high resolution CT, at that time called micro-CT, in the study of the architecture and morphological development of roots [3] and [4]. Since then, micro-CT has been applied in a number of studies focusing on root architecture [5] and [6], but apart from that this technology has hardly been adopted by plant scientists.

Micro-CT had primarily been used to visualize morphological features, but recent significant improvements in the technical set-up have boosted the scanning resolution to sub-micron level, filling the hiatus between visual observations and microscopic imaging. This evolution forced the field to change the term micro-CT into high-resolution X-ray computed tomography (HRXCT) [7] and [8]. Developments in image analysis allowed 3-D rendering and acquisition of volumetric data suitable for analysis, visualization, and quantification of scanning results [9]. Here, we introduce HRXCT as a method to visualize plant structures of *Arabidopsis thaliana* at cellular resolution.

Principles of HRXCT scanning

A general HRXCT scanner comprises an X-ray tube, an X-ray detector, a sample rotation stage and a computer. Most scanners use a micro-focus X-ray tube that irradiates a conical X-ray beam projecting the sample onto a flat two-dimensional (2-D) image detector. Rotation of the sample allows projections to be acquired under different viewing angles. By transforming these 2-D projections, the volumetric data can be reconstructed to represent the scanned object in a large 3-D matrix. Each element in this matrix is a voxel (3-D pixel), holding a grey value corresponding to the attenuation of the X-rays as they pass through the

sample that is correlated with the density and the atomic number of the imaged material [10]. Typically, this 3-D matrix is saved as 2-D images, called CT slices.

Depending on the resolution, the size of the object, and the desired signal-to-noise ratio, a scan might take from several minutes to hours. Furthermore, the spatial scanning resolution depends on the spot size of the X-ray source, the resolution of the X-ray detector, and the used magnification of the system, which relates to the diameter of the sample, indicating the trade-off between spatial resolution and measured volume in the HRXCT scanning [11]. Samples in this report were scanned with an in-house developed multi resolution CT system (www.ugct.ugent.be) that can accommodate samples with a maximum diameter of 37 cm (corresponding voxel size: 100 μm) and a maximum spatial resolution of 400 nm (corresponding sample diameter: 200 μm). All 3-D renderings were performed using VGStudio Max 2.0 (www.volumegraphics.com).

***In vivo* scanning**

The non-destructive and minimally invasive nature of HRXCT scanning should allow the application of this technology for *in vivo* imaging. Previously, HRXCT has been applied to analyze bone tissue-forming cell cultures in a time-lapse taking snapshots during 44 d, and to follow tuber growth of potato (*Solanum tuberosum*) for one week [12] and [13]. However, the ionizing effect of the X-rays has to be taken into account [14]. In our analysis we observed that daily *in vivo* scanning of *Arabidopsis* seedlings resulted in a temporal growth inhibition, indicating that caution should to be taken in analyzing small plant samples in a time lapse. To obtain a reliable representation of plant morphology during seedling development, we scanned different *Arabidopsis* plants until 13 d after sowing at a spatial resolution of 10.4 μm (Figure 1a and b). (see supplementary material for a movie and a stereo image of the 3-D rendering of an *Arabidopsis* shoot at 13 d) Moreover, to test the technology on very soft tissues, we also scanned an *Arabidopsis* flower with a voxel size of 5 μm^3 (Figure 1c). Individual scans took 10–20 min and no sample preparation was needed. The used spatial resolution reveals many detailed morphological features such as furrows in the hypocotyls, branching of trichomes, the pollen sacs on the anthers, and the stigma on the flower style (Figure 1). With these 3-D reconstructions, parameter values as volume, area, thickness and connectivity, can be extracted as well, resulting in a detailed quantification of the scanned objects (see accompanying article by Timotheüs van der Niet *et al.*).

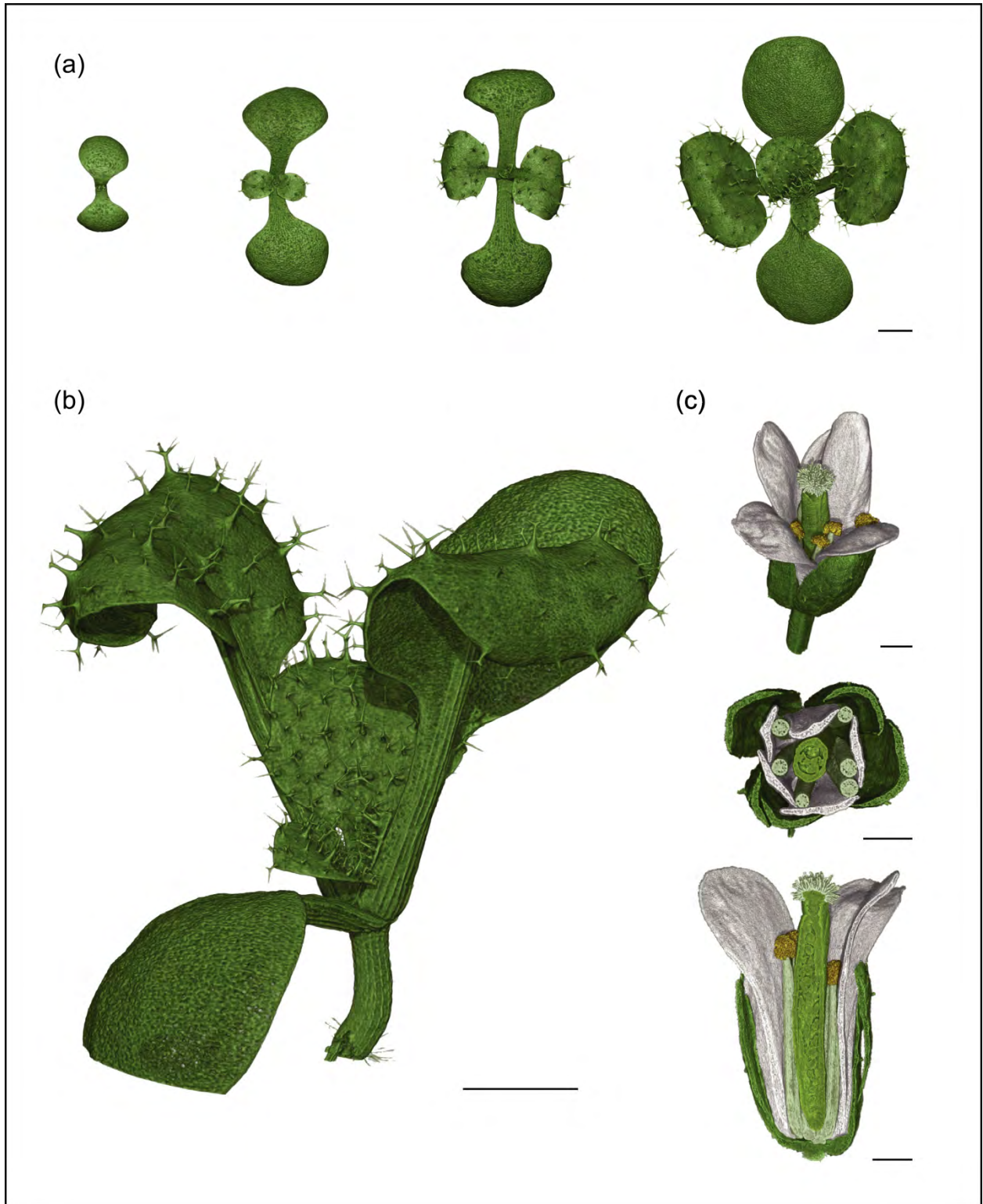


Figure 1. *In vivo* HRXCT scanning of an *Arabidopsis* Col-0 shoot and flower.

(a) Top view of different 3-D-reconstructed *Arabidopsis* seedlings at 7, 9, 11, and 13 d after sowing (DAS). Voxel size = 13.8 μm . Bar = 1 mm. **(b)** Side view of an *Arabidopsis* seedling at 13 DAS. Voxel size = 8.8 μm . Scale bar = 1 mm. **(c)** 3-D reconstruction of an *Arabidopsis* flower (side view, horizontal section, vertical section). Voxel size = 5 μm . Scale bar = 0.5 mm. Scanning periods < 20 min.

Scanning with cellular resolution

Discrimination of individual plant cells by micro-CT was first obtained in woody samples [15]. More recently, micro-CT had been used to quantify the spatial distribution of the very large trichomes on *Arabidopsis* leaves [11]. In the near past, visualization and quantification of sub-cellular features and intracellular spaces in plant tissue [16] and [17] were achieved with very large synchrotron facilities, which are however not accessible for daily research. With the introduction of sub-micron resolution systems, plant tissue samples can now be imaged with cellular resolution in a laboratory environment. Our scans are accomplished *ex vivo* after a fixation protocol (1 d) including dehydration with alcohol and staining with iodine as a contrasting agent, needed to exclude movement of the sample during the extended scanning period and to improve the contrast within relatively soft tissues. An *Arabidopsis* hypocotyl was recorded at a spatial resolution of 0.85 μm during a 1.6-h scan (Figure 2). Individual cells are very distinctive on the separate CT slices (Figure 2a and b). The 3-D representation gives volumetric insight in cellular organization of the tissue. Subsequently, a segmentation was performed with the in-house developed software MORPHO+. Intracellular space was thresholded and virtually separated using a watershed algorithm and subsequently color-coded according to its volume, allowing quantification of cellular features within the 3-D reconstructed sample (Figure 2c).

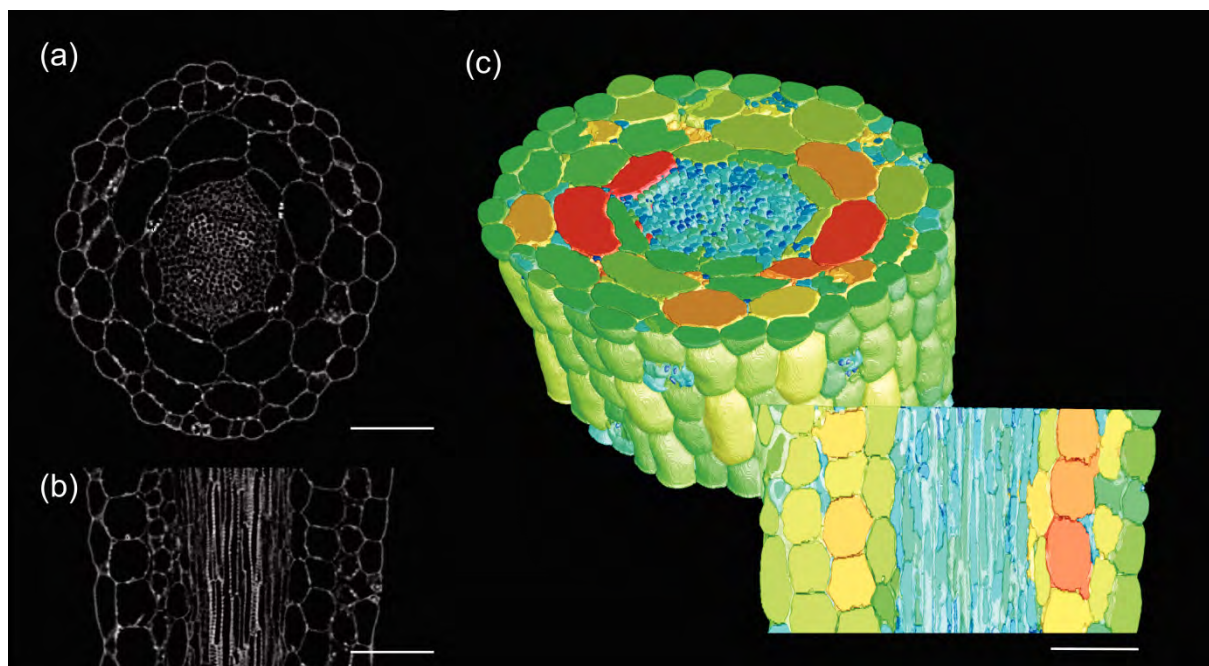


Figure 2. *Ex vivo* HRXCT scanning of an *Arabidopsis* hypocotyl at cellular resolution.

(a) HRXCT slice showing a cross-section of the hypocotyl. (b) HRXCT slice showing a longitudinal section of the hypocotyl (note the secondary cell wall thickening in the tracheids). (c) 3-D-reconstruction of a hypocotyl section with false coloring of the cells according to size. Voxel size = 0.8 μm . Scale bar = 50 μm .

Comparison with other 3-D imaging techniques

Currently, a number of imaging techniques are available for visualizing 3-D objects, each with its own strengths and disadvantages. Positron emission tomography (PET) and magnetic resonance imaging (MRI) are two non-destructive and non-invasive scanning technologies that have been applied in plant sciences to acquire 3-D structural information. PET scanning detects positron-emitting radio nuclides and can be used to measure the distribution of products labeled with unstable isotopes, such as ^{11}C -labeled photoassimilates [18]. The spatial imaging resolution ranges around 1 mm^3 . In plants, MRI is especially used to map and quantify water flows in xylem and phloem vessels by the nuclear magnetic resonance (NMR) of water protons, but can also be used to deliver structural information [19]. The imaging resolution of MRI is generally around $30\text{ }\mu\text{m}^3$. In MRI images, the contrast depends on differences in water content instead of density differences in HRXCT, making MRI a complementary imaging technique for *in vivo* analysis of soft tissues that usually give low-contrast data in HRXCT. In general, the fast scanning protocols and the ease of use are in favor of HRXCT. In 2006, optical projection tomography (OPT) was introduced as a method to capture 3-D data of primarily *ex vivo* plant specimens [20]. In transmission OPT the signal depends on the amount of light absorbed by a cleared specimen. This optical technique allows the visualization of gene expression patterns, which is not straightforward with HRXCT. For OPT, the maximum spatial resolution is $5\text{ }\mu\text{m}^3$. At comparable spatial resolution, the primary advantage of HRXCT over OPT is that no clearing and embedding of the specimens is needed, combined with much shorter scanning times. For this reason, HRXCT is also preferred above general sectional tomography, in which tissue cracks and cell wall damage often ruin the sample [15]. Furthermore, HRXCT allows the visualization in different directions and at accurate positions within the same sample (Figure 2a and b). The above comparison indicates that for relatively small samples HRXCT is a fast method to obtain morphological 3-D information at a resolution superior to that of other techniques. 3-D cellular tissue structure can be visualized by less related microscopic techniques, such as by rendering Z-stacks of confocal images [21]. However, many microscopic techniques suffer from low penetration capacities, restricting the depth at which structures can be imaged. Confocal microscopes typically operate at a depth of $40\text{ }\mu\text{m}$ [22]. This depth can be extended at the expense of spatial resolution using selective plane illumination microscopy (SPIM) and optical coherence microscopy (OCM), with a minimal voxel size of 6 and $1\text{ }\mu\text{m}$, respectively [23] and [24]. Unfortunately, none of these microscopic techniques have been applied to extract volumetric data of plant cells, prohibiting a comparison of their output qualities to HRXCT. Nevertheless, HRXCT turns out to be an imaging technique that succeeds in combining deep sample penetration with high resolution.

Concluding remarks and perspectives

The main limitation in HRXCT scanning is the trade-off between magnification and measured volume. The larger the sample, the farther away it has to be positioned from the X-ray tube to fit into the tip of the conical beam, reducing the distance between the sample and the detector and, thus, the possible magnification. Future improvements, especially the development of more sensitive detectors with higher temporal and spatial resolutions, better X-ray tubes, and highly adapted scanning protocols will allow imaging of larger objects at higher resolution. Larger samples could also be imaged by connecting scans, in which the detector moves in an extended field of view or by making high resolution zoom-in scans of a part of the object [25]. Reduction of the needed radiation dose might improve the applicability of *in vivo* scans, which could also be tackled by the use of contrasting agents to mark the structures of interest. Furthermore, future imaging challenges lie in coupling imaging techniques and combining the strength of specific methods. Through this approach, HRXCT could provide detailed structural information that might be overlaid with, for instance, functional activity and protein localization from PET or fluorescence imaging, without the need of a new combined scanner. Such data could be obtained by subsequent fusions of data sets recorded with separate scanners [10]. Moreover, detailed 3-D renderings of biological structures by HRXCT are very suited to building morphological models within dynamic modeling approaches [26]. In conclusion, HRXCT is an imaging technology providing 3-D data at a resolution suited for detailed analysis of morphological traits of *in vivo* plant samples and at a cellular resolution for *ex vivo* samples.

ACKNOWLEDGEMENTS

This work was supported by grants from the Belgian Network BARN (Growth and Development of Higher Plants IUAPVI/33), funded by the Interuniversity Attraction Poles Programme, initiated by the Belgian State Science Policy Office, the 'Bijzonder Onderzoeksfonds Methusalem Project' (BOF08/01M00408) of the Ghent University, the European Community Grant FP6 IP AGRON-OMICS (contract LSHG-CT-2006-037704), and the Fund for Scientific Research–Flanders (Project G.0100.08). S.D. is indebted to the Agency for Innovation through Science and Technology for a predoctoral fellowship. V.C. is a postdoctoral fellow of the Fund for Scientific Research–Flanders.

SUPPLEMENTARY DATA

Supplementary Material associated with this article can be found at:
<http://dx.doi.org/10.1016/j.tplants.2010.05.002/>

CONTRIBUTIONS

Hannes Vanhaeren and Stijn Dhondt optimized the growth conditions of scanned Arabidopsis plants. The CT scans and image reconstructions were conducted by Denis Van Loo. He also performed the hypocotyl sample preparation and the segmentation of its cellular content. Stijn Dhondt conducted the 3-D renderings, cleaned and colored the 3-D objects.

REFERENCES

1. W.H. Stuppy, *et al.* Three-dimensional analysis of plant structure using high-resolution X-ray computed tomography. *Trends Plant Sci.*, **8** (2003), pp. 2–6.
2. V. Cnudde, *et al.* Recent progress in X-ray CT as a geosciences tool. *Appl. Geochem.*, **21** (2006), pp. 826–832.
3. A. Pierret, *et al.* X-ray computed tomography to quantify tree rooting spatial distributions. *Geoderma*, **90** (1999), pp. 307–326.
4. D. Heeraman, *et al.* Three dimensional imaging of plant roots in situ with X-ray computed tomography. *Plant Soil*, **189** (1997), pp. 167–179.
5. A. Kaestner, *et al.* Visualizing three-dimensional root networks using computed tomography. *Geoderma*, **136** (2006), pp. 459–469.
6. S.R. Tracy, *et al.* The X-factor: visualizing undisturbed root architecture in soils using X-ray computed tomography. *J. Exp. Bot.*, **61** (2010), pp. 311–313.
7. V. Cnudde, *et al.* Virtual histology by means of high-resolution X-ray CT. *J. Microsc.*, **232** (2008), pp. 476–485.
8. J. Van den Bulcke, *et al.* Three-dimensional X-ray imaging and analysis of fungi on and in wood. *Microsc. Microanal.*, **15** (2009), pp. 395–402.
9. J.C. Russ, *The Image Processing Handbook*, (5th ed), CRC Press (2007).
10. S.J. Schambach, *et al.* Application of micro-CT in small animal imaging. *Methods*, **50** (2010), pp. 2–13.
11. E. Kaminuma, *et al.* Quantitative analysis of heterogeneous spatial distribution of Arabidopsis leaf trichomes using micro X-ray computed tomography. *Plant J.*, **56** (2008), pp. 470–482.
12. Ferreira, S.J. *et al.* Comparative transcriptome analysis coupled to X-ray CT reveals sucrose supply and growth velocity as major determinants of potato tuber starch biosynthesis. *BMC Genomics* **11**, (2010) 93.
13. H. Hagenmüller, *et al.* Non-invasive time-lapsed monitoring and quantification of engineered bone-like tissue. *Ann. Biomed. Eng.*, **35** (2007), pp. 1657–1667.
14. L. Zhou, *et al.* Linear energy transfer dependence of the effects of carbon ion beams on adventitious shoot regeneration from in vitro leaf explants of *Saintpaulia ionantha*. *Int. J. Radiat. Biol.*, **82** (2006), pp. 473–481.

15. K. Steppe, *et al.* Use of X-ray computed microtomography for non-invasive determination of wood anatomical characteristics. *J. Struct. Biol.*, **148** (2004), pp. 11–21.
16. P. Cloetens, *et al.* Quantitative phase tomography of Arabidopsis seeds reveals intercellular void network. *Proc. Natl. Acad. Sci. U. S. A.*, **103** (2006), pp. 14626–14630.
17. P. Verboven, *et al.* Three-dimensional gas exchange pathways in pome fruit characterized by synchrotron X-ray computed tomography. *Plant Physiol.*, **147** (2008), pp. 518–527.
18. S. Jahnke, *et al.* Combined MRI-PET dissects dynamic changes in plant structures and functions. *Plant J.*, **59** (2009), pp. 634–644.
19. C.W. Windt, *et al.* Most water in the tomato truss is imported through the xylem, not the phloem: a nuclear magnetic resonance flow imaging study. *Plant Physiol.*, **151** (2009), pp. 830–842.
20. K. Lee, *et al.* Visualizing plant development and gene expression in three dimensions using optical projection tomography. *Plant Cell*, **18** (2006), pp. 2145–2156.
21. E. Truernit, *et al.* High-resolution whole-mount imaging of three-dimensional tissue organization and gene expression enables the study of phloem development and structure in *Arabidopsis*. *Plant Cell*, **20** (2008), pp. 1494–1503.
22. S.N.S. Reihani and L.B. Oddershede, Confocal microscopy of thick specimens. *J. Biomed. Opt.*, **14** (2009), p. 030513.
23. J. Huisken, *et al.* Optical sectioning deep inside live embryos by selective plane illumination microscopy. *Science*, **305** (2004), pp. 1007–1009.
24. K. Grieve, *et al.* In vivo anterior segment imaging in the rat eye with high speed white light full-field optical coherence tomography. *Opt. Express*, **13** (2005), pp. 6286–6295.
25. J.A. Zeitler and L.F. Gladden, In-vitro tomography and non-destructive imaging at depth of pharmaceutical solid dosage forms. *Eur. J. Pharm. Biopharm.*, **71** (2009), pp. 2–22.
26. J.E. Cresswell, *et al.* Conifer ovulate cones accumulate pollen principally by simple impaction. *Proc. Natl. Acad. Sci. U. S. A.*, **104** (2007), pp. 18141–18144.

7

Towards an automated kinematic analysis of leaf growth

Introduction

Leaf growth is in essence the result of two, highly integrated, cellular processes, cell expansion and cell division. This means that to understand the nature of leaf growth phenomena, observations at the cellular level are key. During leaf development, a cell proliferation phase, characterized by actively dividing cells, is followed by a cell expansion phase, characterized by cell growth and differentiation. After expansion, cells mature and the final leaf size is reached (Beemster et al., 2005). At the transition from cell proliferation to cell expansion phase, cell division ceases along a longitudinal gradient from leaf tip to base (Donnelly et al., 1999). In the epidermis, the onset of differentiation is preceded with the formation of stomata (Andriankaja; Dhondt; De Bodt et al., 2011). A stomatal complex

consists of two guard cells that control the aperture of the stomatal pore. Starting from a precursor meristemoid cell, a series of subsequent asymmetric divisions produce a number of guard mother and daughter cells. Subsequently, the guard mother cells divide symmetrically into two guard cells, ending the stomatal lineage. The daughter cells undergo cell fate specifications identical to those of the majority of the cells produced during the proliferation phase, resulting in puzzle-shaped pavement cells (Larkin et al., 1997; Geisler et al., 2003). The final leaf size is determined by the total number of cells and the average cell size that result from cell division and cell expansion, respectively. A kinematic analysis of leaf growth examines the dynamics of cell division and expansion throughout leaf development in order to understand how these processes contribute to differences in growth rates at the whole organ level. In our laboratory, most often the first developing leaf pair (leaves 1 and 2) is harvested on a daily basis from 4 to 24 d after sowing (DAS). Leaves 1 and 2 usually are selected because they are nearly indistinguishable and probably the best synchronized among replicate plants. Microscopic drawings of the abaxial epidermis, containing approximately 100 cells, are made at two positions in the leaf, at 25% and 75% of the distance from the base to the tip of the leaf, with a drawing tube attached to the microscope equipped with differential interference contrast (DIC) optics. Five leaves are analyzed for each day in order to accommodate for biological variation between samples. This means that for a complete kinematic analysis of leaf growth, in which wild-type plants are compared to transgenic seedlings, 400 microscopic drawings have to be made (2 (genotypes) x 2 (positions) x 5 (replicates) x 20 (time-points)). Next, the microscopic drawings are scanned for digitization, after which they are analyzed manually with the aid of easy-to-use public-domain image analysis software like ImageJ (<http://rsbweb.nih.gov/ij/>) to define the average cell size in each of the drawings. For a detailed description of the experimental approaches and calculations we refer the reader to a methods book chapter to which I contributed (Rymen et al., 2010). Analyzing the drawings and performing the calculations in this manner can take up to two weeks. In order to speed up the analysis time and to make the kinematic leaf growth analysis less tedious, we set out to automate different parts of the analysis. We developed an image analysis script to automatically extract data from the scanned drawings; we set up a data analysis pipeline to calculate kinematic parameters from the measurements generated by the imaging software; and we performed a proof of concept of an image analysis approach to automatically extract the epidermal cell walls from DIC images of cleared Arabidopsis leaves.

Automated analysis of microscopic epidermal drawings

Manual analysis of 400 microscopic drawings, which build up a kinematic leaf growth analysis, can easily take a couple of weeks. In order to accelerate this tedious process, we developed an image analysis script, which can do the job in less than a day. The imaging algorithm takes the scans of the microscopic drawings as input images for the analysis (Figure 1A). In these

drawings the stomatal pores have been filled in black to prevent them from being recognized as a small cell. Furthermore, this will also allow for the automatic discrimination between pavement and guard cells. The analysis is usually performed in batch mode on all images in a certain folder by the use of a PERL script which loops through the images. The image analysis algorithm itself is written in C++ and makes use of the SDC Morphology Toolbox for C++ (www.mmorph.com/cppmorph/).

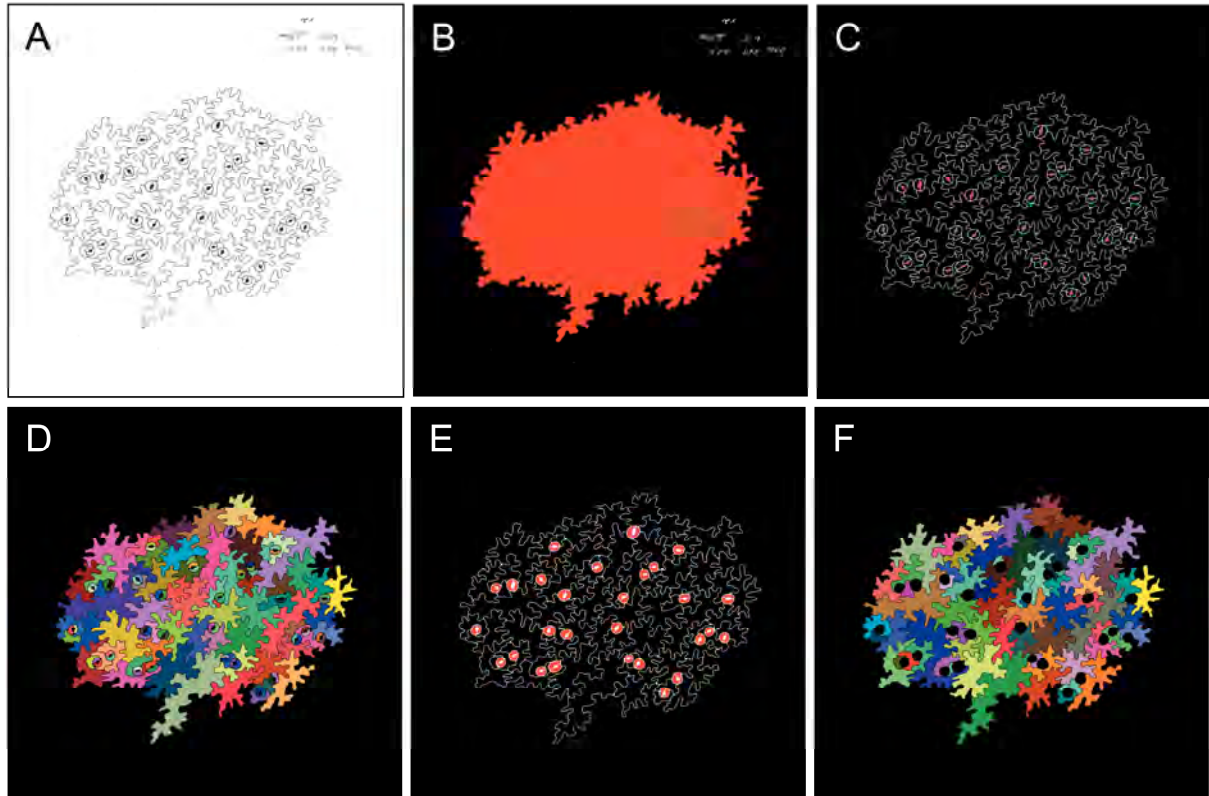


Figure 1: Image analysis of microscopic drawings.

(A) Original drawing. (B) The area of the drawing is determined automatically. (C) The number of stomata is identified by automatic recognition of the stomatal pores. (D) Total cell number is measured after automatic correction and optimization of the drawing. (E) Guard cells are identified as cells adjacent to the stomatal pores, allowing the measurement of individual guard cell sizes. (F) Non-guard cells are identified as pavement cells, allowing the measurement of individual pavement cell sizes.

In a first step, after applying a threshold to separate the drawing from all bright pixels (image background and noise from the scanner), the input image is cleaned by closing small gaps in order to prevent that small drawing errors will result in the fusion of cells. Secondly, the area of the drawn cells is measured and recognized as the largest object in the image (Figure 1B). Next, the stomatal pores are recognized as parts of the image that can fit a circle with a diameter, which can be set at the beginning of the script (Figure 1C). For this reason, the stomatal pores should be large enough in order to be able to distinguish between the cell walls and the pores. The amount of stomatal pores is counted and represents the number of stomata in the drawing. Then we perform a second closing before we start to measure the

cells. This is followed by extraction of the individual cells by taking the inverse of the closed drawing (Figure 1D). Since small extrusions in the drawing may have closed during the imaging procedures, cells with an area below a threshold, which can be set at the beginning of the script, will be excluded from the analysis. Furthermore, cells touching the edge of the image will also be excluded. Then the number of cells is recorded and the individual cell areas are written to a text file. Also the total area of the drawn cells and the number of stomates are saved. Based on this the average cell area will be calculated by dividing the total area of the drawn cells by the number of cells in the drawing. The next step is to discriminate guard cells from pavement cells. Therefore, we dilate the stomatal pores, extracted before, and define their intersection with the cells. Then we reconstruct all cells that contain a part of the intersection. Cells with an area above a threshold, which can be set at the beginning of the script, are removed to exclude the possibility that drawing errors will result in the classification of adjacent pavement cells as guard cells. The remaining cells are identified as guard cells and their areas are recorded and saved (Figure 1E). Cells that are not identified as guard cells are classified as pavement cells (Figure 1D). Also their areas are recorded and saved to a text file. Furthermore, the user-defined parameters settings are saved to allow repeating the analysis with the same settings. Images as presented in the different panels of Figure 1 are generated for each of the analyzed drawings to allow for a fast visual control of the analysis.

While total area, cell number and stomata used to be counted manually, it was not feasible to measure individual cell areas as this would be too time consuming. The automatic extraction of individual areas of guard cells and pavement cells separately by image analysis, allows for the calculation of cell area distributions, which can reveal a shift in cell area in a specific part of the distribution, while there is no significant difference in average cell area. This was the case for the *SHORT-ROOT (shr)* mutant. While the size distribution of larger cells was identical, the peak of cells with a size smaller than $300 \mu\text{m}^2$ was markedly shifted towards smaller sizes in the *shr* mutant compared to WT leaves (Figure 2). Data of such cell area distributions throughout leaf development together with general kinematic data was used as the experimental basis to build a mathematical model of Arabidopsis leaf epidermal cells, presented in Chapter 3 (Kheibarshekan Asl; Dhondt et al., 2011). The availability of these cell area distributions was key to uncover distinct division and expansion patterns for pavement and guard cells.

As an extension of the cellular image analysis script, we developed a number of ImageJ macros. These macros allows for the color-coding of pavement cells according to size or shape characteristics. Color-coding can be performed based on the extreme values in a single image or in a batch of images. Furthermore, it supports the extraction of cell area and circularity values linked to their x and y coordinates in the image. The tracking of positional information can also be applied to the stomatal pores in microscopic drawings. These features were applied in a study focusing on the transition from cell proliferation to cell expansion in the

Arabidopsis leaf (Chapter 4), where cell division ceases along a longitudinal gradient from the tip to the base of the leaf.

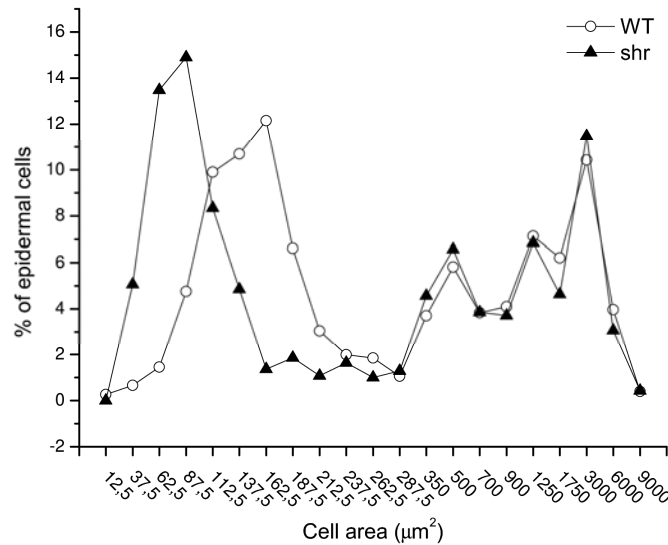


Figure 2: Cell area distributions of *shr* and WT epidermal cells at 24 DAS.

Note that the peak of the distribution is reduced from 162 µm² in wild-type to 87 µm² in *shr*.

This imaging approach has also been applied to speed up the kinematic analysis of *shr* and *SCARECROW* (*scr*) mutants presented in Chapter 2 (Dhondt et al., 2010). Furthermore, this software has been used in a kinematic analysis study of a quadruple-DELLA (*q-DELLA*) and *sly1-10* (Achard et al., 2009), and the *cyca2;2-3-4* triple mutant (Vanneste et al., 2011), and in a cellular analysis of leaf epidermal cells of five overexpression lines, which positively affect final leaf size (Gonzalez et al., 2010), and of 114 lines, corresponding to the leaf shape mutant collection of José Luis Micol (Allicante) (Pérez-pérez et al., 2011). By performing the kinematic analysis I contributed to these published analyses of which the title page is included at the end of this chapter. Moreover, the automated analysis of microscopic drawings has been applied in a number of manuscripts in preparation. A first manuscript is describing the growth parameters of a gain-of-function of *BRASSINOSTEROID INSENSITIVE1* (*BRI1*), a *bri1* loss-of-function mutant and a loss-of-function mutant of *CONSTITUTIVE PHOTOMORPHOGENIC DWARF* (*cpd*), involved in brassinosteroid biosynthesis (Zhiponova et al. unpublished results). A second manuscript identifies putative oncogenes through data integration and comparative genomics between plants and humans (Quimbaya et al., accepted for publication in Cellular and Molecular Life Sciences). A third manuscript describes the function of *CYCLIND5;1* as the most likely candidate gene in a quantitative trait loci (QTL) for endoreduplication (Sterken et al. unpublished results). And finally, the image analysis software has also been used to assist in the kinematic analysis of a loss-of-function mutation

of a new APC10 subunit, named SAMBA (Eloy et al, unpublished results). Together these publications and manuscripts underline the usefulness of automation of kinematic analysis that was developed in the context of this PhD.

Integration of a data analysis pipeline

Originally, the data analysis of a kinematic analysis was performed using a spreadsheet such as MS Excel (Microsoft, Washington, USA). Also this step in the analysis is relatively laborious, prone to errors, and did not include a proper statistical analysis using error propagation. Since the image analysis algorithm is producing standardized data in the form of tab-delimited text files, all data can be feed into an automated data analysis pipeline, which would again accelerate the processing. The data analysis pipeline was developed in our research group by Frederik Coppens and details are published in his doctoral thesis (Coppens, 2011). Therefore, I will only highlight the major principles.

The software runs on Mac OS X (Apple, CA, USA), and makes use of the application programming interface (API) Cocoa which defines a framework called CoreData that handles data storage and retrieval. A graphical user interface (GUI) was build with the help of Interface Builder.

Due to the large amount of data, the data import was set up in a hierarchical manner. The different levels are "Genotype", "Plant", "Leaf", "Drawing", and "Cell". For each leaf, average cell area and cell number are calculated based on the average cell area of the drawings of that leaf. Also the stomatal index (SI), which represents the fraction of guard cells in the epidermis, is calculated. Cell division rate (CDR) and relative leaf elongation rate (RLER) are calculated from the derivative of average cell number and leaf area over time, respectively. These derivatives are calculated by a local second degree polynomial fit to the log transformed data using the least squares method. Furthermore, a number of new kinematic parameters were introduced into the analysis, partly because the image analysis allowed to measure individual cell areas of pavement cells and guard cells separately. These new parameters include the calculation of pavement and guard cell area, relative cell, pavement cell and guard cell expansion rate, and rate of stomate production. Furthermore, error propagation was applied to all calculations and the result of the data analysis is visualized in the Graphical User Interface (GUI) by a set of automatically generated graphs. Figure 3 represents two screenshots of the data analysis program.

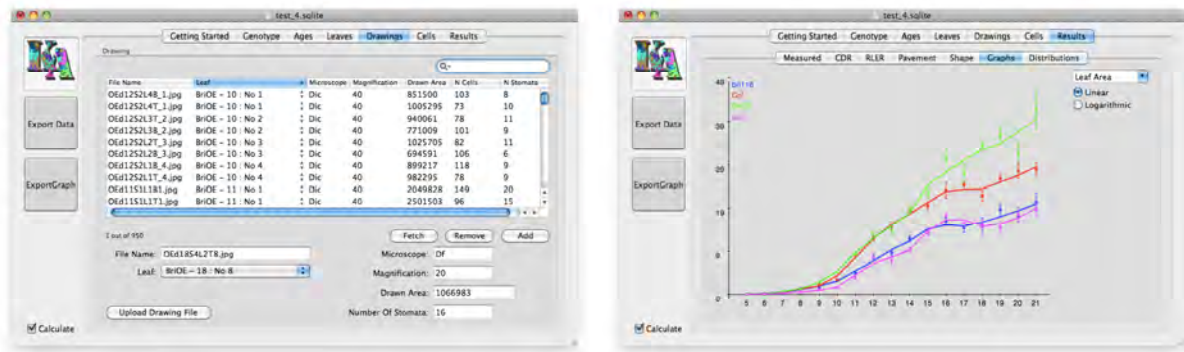


Figure 3: Screenshots of the kinematic data analysis program.

Data Input for the drawings containing genetic background, the leaf number, the age of the plant, and the microscope and magnification used for the drawing to calculate the calibration value (left). Example of the data output in the form of a graph of leaf area over time (right). The data can be represented with a linear or logarithmic scale. Reproduced from (Coppens, 2011) with permission.

Automated extraction of cell walls from DIC images

Currently, manual segmentation of epidermal cells of *Arabidopsis* leaves, is made by microscopic drawings of cleared leaves using DIC optics. Since making such a microscopic drawing takes on average 20 minutes, performing a cellular kinematic analysis is very laborious. Nevertheless, this approach is applied in multiple research groups within the Department of Plant Systems Biology and outside. This indicates that the manual segmentation of cellular content is currently one of the major bottlenecks in the department. Therefore we set out to develop an automatic segmentation of epidermal cell walls in DIC images. This work was performed in close collaboration with Daniel Ochoa and Jonas De Vylder from the research group Image Processing and Interpretation (IPI), headed by Wilfried Philips, in the Department of Telecommunication and Information Processing (TELIN) at the University of Ghent, who performed the image processing. The image processing was performed in Matlab (MathWorks, Massachusetts, USA) using the image processing toolbox. Details have been published in the doctoral thesis of Daniel Ochoa (Ochoa, 2011).

There are four main problems which make the automatic segmentation of epidermal cells of DIC images difficult. First of all, during the image capturing it is very likely that part of the image will be blurred because the bended nature of the leaf causes some regions in picture to be out-of-focus. Automated segmentation of cell walls that are out-of-focus is simply not possible. When using the drawing tube, biologists cope with this problem by continuously adjusting the microscope focus. Secondly, it is inherent to DIC optics that sample features in parallel to the shear direction suffer from low contrast because the optical path differences in this direction are minimized. This is obviously compromising the segmentation of cell walls. Thirdly, there is the non-linearity of the imaging process. Specimen features appear as highlighted and shadowed patterns, which change according to the relative orientation of features with respect to the shear direction. This creates a complex and varying appearance

of cell borders in the images. Finally, the shadow patterns create an inherent uncertainty about the true location of cell borders true location, compromising accurate cell measurements.

We set out to tackle each of these problems and to implement solutions into a single sample processing chain. The out-of-focus problem was assessed by using image fusion principles to combine DIC images captured at three focal depths into a single sharp DIC image. Multi-focus image fusion was performed on a pixel level. To deal with the lack of border information parallel to the shear direction, we used a revolving stage to capture images of epidermal tissue from different angles. Images were captured every 30 degrees over a complete rotation. This increases the possibility that a given cell border section will be imaged with maximum contrast, i.e. perpendicular to the shear direction. Regarding the complex appearance of cell borders, we chose an approach based on pattern matching. The idea is to model intensity profiles of cell walls with respect to the shear direction and to use this information to build 2-D oriented matching filters. Convolution of a DIC image with a range of oriented filters should report high responses for cell wall sections which match a filter orientation. Selecting the maximum response across filtered images, then allows for the extraction of a new image in which bright ridges are located on cell outlines. Finally, to come closer to the true location of cell wall segments, DIC images at opposing orientations (at θ and $\theta + 180$ degrees) were compared. As DIC imaging is equivalent to optical differentiation, two opposing images represent phase contrast images whose phase objects are displaced by the shear distance from their true location. Therefore, the average location of the cell wall segments will be closer to the actual location of the cell outline.

Taken together, the processing chain contains following steps (Figure 4). As input, our approach took a set of DIC images of the epidermis of Arabidopsis leaves taken at twelve orientations and captured at three focal depths for each orientation. First, for each orientation the corresponding z-stack of images, containing out-of-focus regions, was fused into a single in-focus image. Then, a series of matching filters, extracted from cell outlines, was convolved to each fused image. The resulting images displayed ridges at cell wall locations. To further enhance linear structures a line detector was applied. Next, the resulting response images were registered using the angle information of the revolving stage. However, imperfect manual alignment of the revolving stage caused the sample not to rotate perfectly around the focal point. For this reason, image rotation was followed by translation during the registration procedure. Moreover, translational parameters seemed to vary between samples. Then, the registered images were combined into one image by taking the average response value for each pixel location. This revealed that ridges away from the image center tend to be displaced, which could be explained by image distortion by the microscope lens. Therefore, a morphological closing was performed to avoid segmentation errors. Figure 5 shows a visual representation of the segmentation results for a combined response image. Quantitative

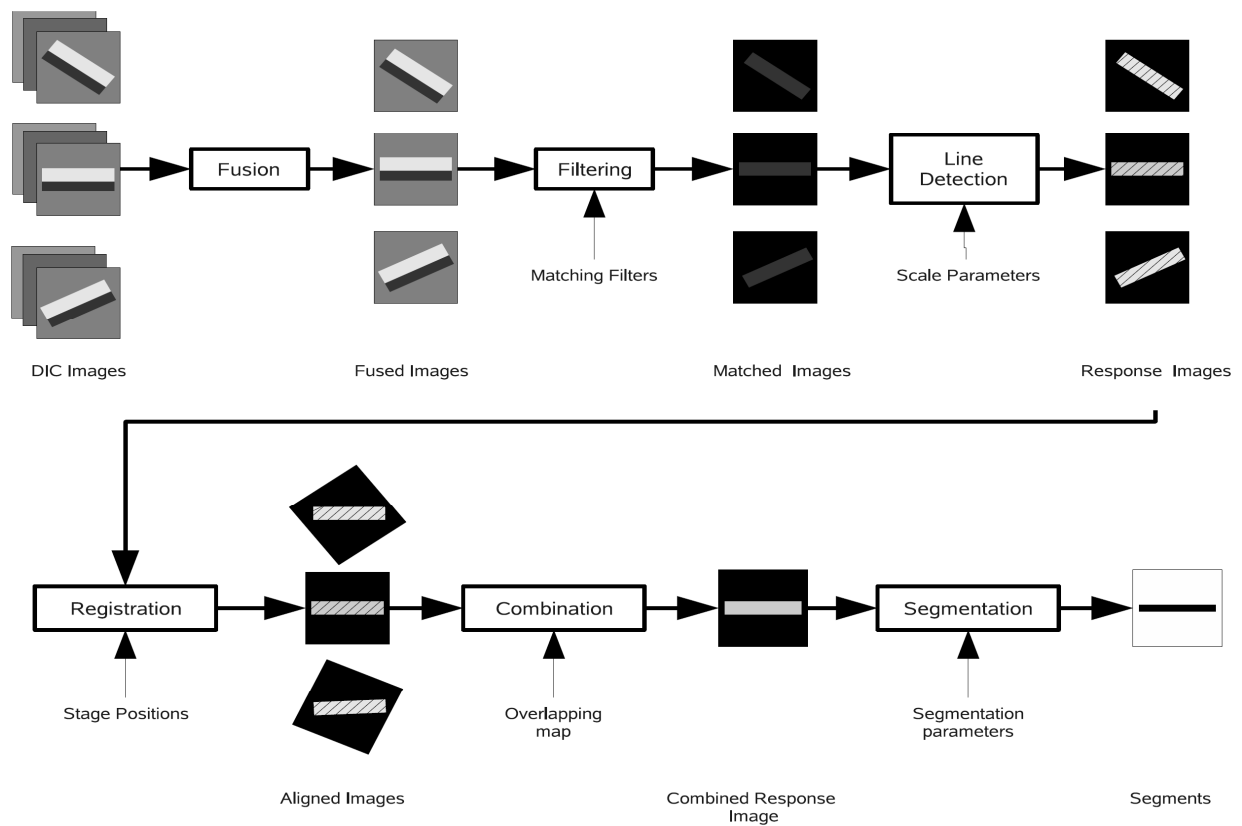


Figure 4: Schematic representation of the image processing chain to segment Arabidopsis leaf epidermal cells from DIC images.

DIC images of epidermal cells are captured at different focal depths and rotation angles. Images at different focal depths are fused to obtain an image with all cell walls in focus. Matching filters are applied to recognize cell wall sections. Next, a line detector further enhances linear structures. Resulting response images are registered using the angle information of the revolving stage. Then, the registered images were combined into one image by taking the average response value for each pixel location. Combined response images are segmented using a watershed algorithm to extract cellular content. Image reproduced from (Ochoa, 2011) with permission.

analysis of this resulting image was performed by comparison to a ground truth, which consisted of a manual tracing of the cell outlines. Analysis results showed that image fusion of the z-stack images yields a 40% increase in the detection of positive cell wall pixels. The utilization of the rotating stage further improved the results with 20%, bringing the final detection rate to 95%. Interestingly, reducing the number of rotation angles only decreased the pixel detection rates slightly, indicating that processing smaller datasets, with fewer orientations, would generate comparable results. The final step of the processing chain consists in segmentation of the combined response image using the morphological watershed approach. Quantitative analysis of the segmentation results of two test datasets show that 75% of the pavement cells are segmented perfectly (Figure 6A). 20% of the pavement cells would need one alteration, whereas only 2% would need multiple alterations and 3% of the

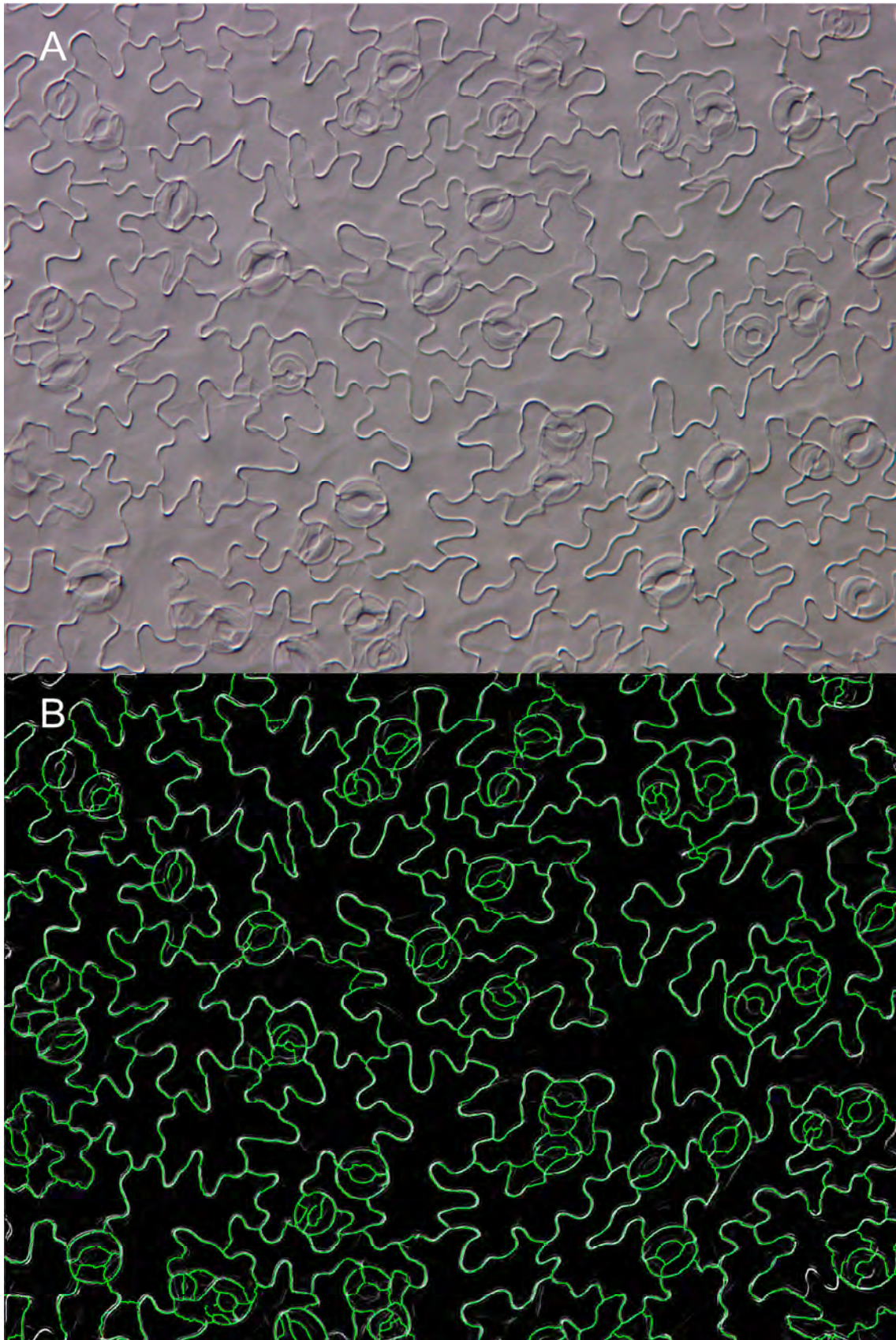


Figure 5: Watershed segmentation of epidermal DIC images

(A) Original DIC image of the mature abaxial leaf epidermis of Arabidopsis. (B) Watershed segmentation resulting from the combined response image of a testing set of 32 epidermal DIC images taken at different focal depths and orientation angles. Green lines represent the segmentation results.

cells were not detected. Most alterations would involve the removal of erroneous cell walls. For guard cells on the other hand, 53% was segmented perfectly, whereas 35% would need more than one alteration and 12% of the guard cells were not detected. Non-detected guard cells can be partially explained by the fact that not all of them had been captured in focus, as the guard cells arise somewhat above the plain of pavement cells. A visual representation of these segmentation results is shown in Figure 6B. Taken together, these results indicate that the extraction of pavement cells is going relatively well, but that the segmentation of guard cells suffers from over-segmentation, as visible in Figure 5. Hence, it is clear that, in its current state, the automated extraction of epidermal cells from the Arabidopsis leaf needs a manual correction step to ensure the quality of the segmentation.

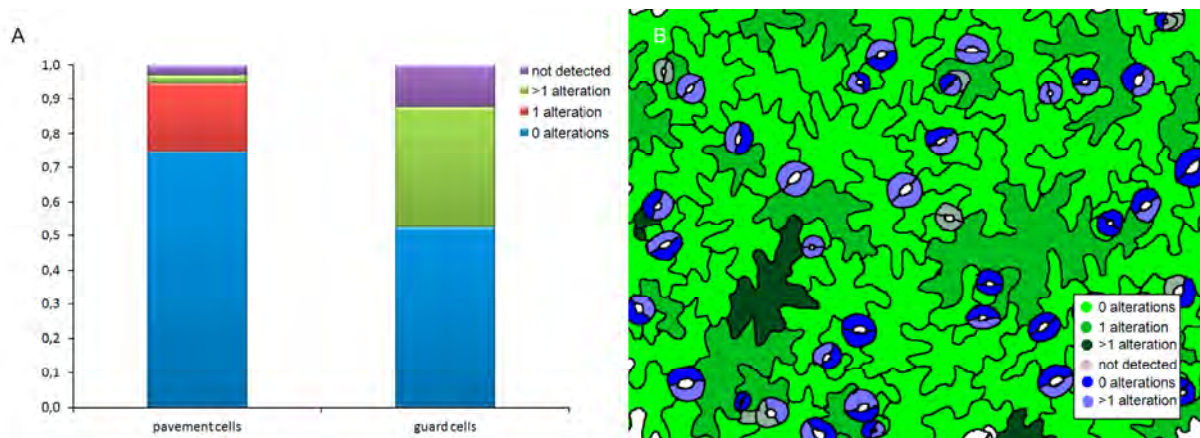


Figure 6: Quantitative analysis of the automated segmentation results of Arabidopsis leaf epidermal cells based on two test datasets. (A) Graphical representation of the segmentation quality. (B) Visual representation of the segmentation quality of dataset 1.

Future perspectives

In this chapter, we summarized the state of the art of our attempts to automate the kinematic analysis of leaf growth. The starting point of our approach was capturing cellular content in DIC microscopic images. Next to DIC optics, there are several possible solutions to enhance the contrast in the cell walls. Fluorescent labeling of the cell wall is a possibility, but this involves additional work in making transgenic marker lines that need to be crossed with mutant lines of interest before a kinematic analysis can be performed. Moreover, we observed that the available cell wall marker lines, 35S:GFP-PIP2a and EGFP-LTI6a (Cutler et al., 2000; Grebe et al., 2003), which encode for proteins that localize to the plasma membrane, are not cell wall specific in proliferating cells, making them useless for analyzing early stages in leaf development. Furthermore, staining of cell walls works well for early time points, but in our hands it is difficult to get a homogeneous staining in older leaves. However, improved protocols based on the pseudo-shiff reaction have recently been developed (Truernit et al.,

2008; Wuyts et al., 2010). Nevertheless, imaging such samples with confocal microscopes would result in a rapid overload the confocal microscopes and would not really speed up the analysis as performing z-stacks scans is time consuming. For these reasons, we believe that DIC imaging is currently still the most promising approach.

The final goal is to implement the image manipulations and segmentation algorithms proposed here into a microscopic setup, ensuring a user-friendly design. Moreover, the use of a designated microscopic setup will allow using fixed translational parameters for the image registration and coping with lens distortion properties. However, taking the segmentation results into account, we do realize that the extraction of cellular content will never be perfect, due to the complexity of the samples. Therefore, we are convinced that human supervision and manual correct will be needed to assure the quality of the cellular analysis. The idea is to integrate the system with an interactive graphical user interface such as presented in Chapter 5 to support the user with the rectification of the automatic segmentation. Next, the approved segmentations could be analyzed by the scripts comparable to those presented above to extract cell number and cell area. Next, the generated data could go through the data analysis pipeline to extract kinematic parameters. The realization of an integrated microscopic setup as presented here would strongly boost the throughput of the cellular analysis, while the quality of the data stays untouched, and would solve the major bottleneck encountered during the cellular analysis of plant growth.

REFERENCES

- Achard, P., Gusti, A., Cheminant, S., Alioua, M., Dhondt, S., Coppens, F., Beemster, G.T.S., and Genschik, P.** (2009) Gibberellin signaling controls cell proliferation rate in *Arabidopsis*. *Curr. Biol*, **19**, 1188-1193.
- Andriankaja, M., Dhondt, S., De Bodt, S., Vanhaeren, H., Coppens, F., De Milde, L., Mühlenbock, P., Skiryicz, A., Gonzalez, N., Beemster, G.T.S., and Inzé, D.** (2011) Exit from proliferation during leaf development in *Arabidopsis thaliana*: a not so gradual process. *Dev Cell*, **in press**.
- Beemster, G.T.S., Veylder, L.D., Vercruyssen, S., West, G., Rombaut, D., Hummelen, P.V., Galichet, A., Gruijsem, W., Inzé, D., and Vuylsteke, M.** (2005) Genome-wide analysis of gene expression profiles associated with cell cycle transitions in growing organs of *Arabidopsis*. *Plant Physiol.*, **138**, 734–743.
- Coppens, F.** (2011) Transcriptional and post-transcriptional regulation of leaf development in *Arabidopsis thaliana*. PhD Thesis. University of Ghent, Ghent.

Cutler, S.R., Ehrhardt, D.W., Griffiths, J.S., and Somerville, C.R. (2000) Random GFP::cDNA fusions enable visualization of subcellular structures in cells of Arabidopsis at a high frequency. *Proc Natl Acad Sci U S A*, **97**, 3718 -3723.

Dhondt, S., Coppens, F., De Winter, F., Swarup, K., Merks, R.M.H., Inzé, D., Bennett, M.J., and Beemster, G.T.S. (2010) SHORT-ROOT and SCARECROW regulate leaf growth in Arabidopsis by stimulating S-phase progression of the cell cycle. *Plant Physiol.*, **154**, 1183-1195.

Donnelly, P.M., Bonetta, D., Tsukaya, H., Dengler, R.E., and Dengler, N.G. (1999) Cell cycling and cell enlargement in developing leaves of Arabidopsis. *Dev Biol*, **215**, 407-419.

Geisler, M., Deppong, D., Nadeau, J., and Sack, F. (2003) Stomatal neighbor cell polarity and division in Arabidopsis. *Planta*, **216**, 571-579.

Gonzalez, N., De Bodt, S., Sulpice, R., Jikumaru, Y., Chae, E., Dhondt, S., Van Daele, T., De Milde, L., Weigel, D., Kamiya, Y., Stitt, M., Beemster, G.T.S., and Inzé, D. (2010) Increased leaf size: different means to an end. *Plant Physiol.*, **153**, 1261-1279.

Grebe, M., Xu, J., Möbius, W., Ueda, T., Nakano, A., Geuze, H.J., Rook, M.B., and Scheres, B. (2003) Arabidopsis sterol endocytosis involves actin-mediated trafficking via ARA6-positive early endosomes. *Current Biology*, **13**, 1378-1387.

Kheibarshekan Asl, L., Dhondt, S., Boudolf, V., Beemster, G.T.S., Beeckman, T., Inzé, D., Govaerts, W., and De Veylder, L. (2011) Model-based analysis of Arabidopsis leaf epidermal cells reveals distinct division and expansion patterns for pavement and guard cells. *Plant Physiology*, **156**, 2172 -2183.

Larkin, J.C., Marks, M.D., Nadeau, J., and Sack, F. (1997) Epidermal cell fate and patterning in leaves. *Plant Cell*, **9**, 1109-1120.

Ochoa, D. (2011) Biological image analysis of model organisms. PhD Thesis. University of Ghent, Ghent.

Pérez-pérez, J.M., Rubio-díaz, S., Dhondt, S., Hernández-romero, D., Sánchez-soriano, J., Beemster, G.T.S., Ponce, M.R., and Micol, J.L. (2011) Whole organ, venation and epidermal cell morphological variations are correlated in the leaves of Arabidopsis mutants. *Plant, Cell & Environment*, **34**, 2200-2211.

Rymen, B., Coppens, F., Dhondt, S., Fiorani, F., and Beemster, G.T.S. (2010) Kinematic analysis of cell division and expansion. In *Plant Developmental Biology*, L. Hennig and C. Köhler, eds (Humana Press: Totowa, NJ), pp. 203-227.

Truernit, E., Bauby, H., Dubreucq, B., Grandjean, O., Runions, J., Barthélémy, J., and Palauqui, J.-C. (2008) High-resolution whole-mount imaging of three-dimensional tissue organization and gene expression enables the study of phloem development and structure in *Arabidopsis*. *The Plant Cell*, **20**, 1494 -1503.

Vanneste, S., Coppens, F., Lee, E., Donner, T.J., Xie, Z., Van Isterdael, G., Dhondt, S., De Winter, F., De Rybel, B., Vuylsteke, M., De Veylder, L., Friml, J., Inzé, D., Grotewold, E., Scarpella, E., et al. (2011) Developmental regulation of CYCA2s contributes to tissue-specific proliferation in *Arabidopsis*. *EMBO J*, **30**, 3430-3441.

Wuyts, N., Palauqui, J.-C., Conejero, G., Verdeil, J.-L., Granier, C., and Massonnet, C. (2010) High-contrast three-dimensional imaging of the *Arabidopsis* leaf enables the analysis of cell dimensions in the epidermis and mesophyll. *Plant Methods*, **6**, 17-17.

Report

Gibberellin Signaling in the Endodermis Controls *Arabidopsis* Root Meristem Size

Susana Ubeda-Tomás,^{1,8,*} Fernán Federici,^{2,9} Ilda Casimiro,³ Gerrit T.S. Beemster,^{4,5,6} Rishikesh Bhalerao,⁷ Ranjan Swarup,¹ Peter Doerner,⁸ Jim Haseloff,² and Malcolm J. Bennett^{1,*}

¹Centre for Plant Integrative Biology, University of Nottingham, Nottingham LE12 5RD, UK

²Department of Plant Sciences, University of Cambridge, Cambridge CB2 3EA, UK

³Universidad de Extremadura, Facultad de Ciencias, Badajoz 06071, Spain

⁴Department of Plant Systems Biology, Flanders Institute for Biotechnology (VIB), 9052 Gent, Belgium

⁵Department of Biology, University of Antwerp, 2020 Antwerp, Belgium

⁶Department of Plant Biotechnology and Genetics, Gent University, 9052 Gent, Belgium

⁷Umeå Plant Science Centre, Department of Forest Genetics and Plant Physiology, SLU, SE-901 83 Umeå, Sweden

⁸Institute for Molecular Plant Sciences, School of Biological Sciences, University of Edinburgh, Edinburgh EH9 3JH, UK

Summary

Plant growth is driven by cell proliferation and elongation [1]. The hormone gibberellin (GA) regulates *Arabidopsis* root growth [2–5] by controlling cell elongation [6], but it is currently unknown whether GA also controls root cell proliferation. Here we show that GA biosynthetic mutants are unable to increase their cell production rate and meristem size after germination. GA signals the degradation of the DELLA growth repressor proteins [7–12] GAI and RGA, promoting root cell production. Targeting the expression of *gai* (a non-GA-degradable mutant form of GAI) in the root meristem disrupts cell proliferation. Moreover, expressing *gai* in dividing endodermal cells was sufficient to block root meristem enlargement. We report a novel function for GA regulating cell proliferation where this signal acts by removing DELLA in a subset of, rather than all, meristem cells. We suggest that the GA-regulated rate of expansion of dividing endodermal cells dictates the equivalent rate in other root tissues. Cells must double in size prior to dividing but cannot do so independently, because they are physically restrained by adjacent tissues with which they share cell walls. Our study highlights the importance of probing regulatory mechanisms linking molecular- and cellular-scale processes with tissue and organ growth responses.

Results and Discussion

A germinating seedling must obtain anchorage, water, and nutrients after emerging from its seed coat. Vigorous root growth is essential if the seedling is to rapidly secure these

resources. Root length is determined by the number of dividing cells and their final cell size [1]. Root cells first undergo repeated rounds of division in the root proximal meristem and then subsequently experience rapid cell expansion in the elongation-differentiation zone (EDZ; Figure 1A). In order to maximize root growth after germination, seedlings could increase either root cell production rate or final cell size or both.

In the model plant *Arabidopsis thaliana*, root growth rate rapidly increases after seed germination (Figure 1B; Figure S1A available online). We initially investigated the cellular basis for the increased root growth, measuring mature cell length, cell production in the meristem, and root meristem size. Mature cell size was essentially constant, whereas the rate of root cell production increased proportional to the root growth rate; wild-type roots exhibit a doubling in cell production rate over a 4 day period after germination (Figure 1C; Figures S1D and S1F). Increased cell production can be due to an increasing number of cells in the meristem because extensive variations in cell division rates are relatively rare [13]. Indeed, our measurements indicate that root meristem size doubles during the first days after germination (DAG), then plateaus by 4–6 DAG, depending on the *Arabidopsis* accession (Figures S1D–S1F). Similarly, cortical cell numbers in the root meristem reached a constant number of between 40 and 60 cells, depending on the *Arabidopsis* accession (Figures S1E and S1G). Hence, the acceleration in *Arabidopsis* root growth is correlated with increasing root meristem size and numbers of meristematic cells (Figure 1B; Figure S1).

The plant hormone gibberellin (GA) represents an important regulator of *Arabidopsis* root growth [2–5]. GA has recently been reported to regulate root cell elongation [6]. However, it is currently unclear whether GA also controls root cell production. To investigate this possibility, we used pharmacological and genetic approaches to test the role of GA in regulation of root meristem size. Reduction of endogenous GA levels by treating wild-type seedlings with Paclobutrazol (PAC, an inhibitor of GA biosynthesis [14]) results in a reduced root growth rate (Figure S1A). Detailed microscopy measurements revealed that PAC treatment caused a reduction in root meristem size (Figures S1D–S1G) and mature cell length (Figures S1B and S1C). Subsequently, roots of GA biosynthetic mutants *ga1-3* [15] and *ga3ox1/ga3ox2* [16] were analyzed. The *ga1-3* mutant failed to increase cell production rate, essentially remaining static (Figure 1C). Similarly, a reduction in cell production rate was also detected in *ga3ox1/ga3ox2* mutant (Figure S1K). Both mutants exhibited a smaller root meristem size compared to wild-type (Figures 1B–1D; Figure S1H). However, GA3 treatment was able to fully rescue root meristem size in the *ga1-3*, *ga3ox1/ga3ox2* mutants and PAC-treated seedlings (Figure 1B; Figures S1D–S1H). Conversely, removal of 7- to 8-day-old *ga1-3* seedlings from GA3-supplemented media resulted in a reduction in root meristem size (Figure S1L). Hence, GA levels appear to be required to promote and maintain the increase in root growth rate through control of root meristem size.

To investigate the relationship between gibberellins and root cell division, we monitored how changes in GA levels affect the expression of the mitotic cyclin *CycB1;1* (marks G2/M-phase

*Correspondence: susana.ubeda-tomas@nottingham.ac.uk (S.U.-T.), malcolm.bennett@nottingham.ac.uk (M.J.B.)

⁹These authors contributed equally to this work

Increased Leaf Size: Different Means to an End^{1[W][OA]}

Nathalie Gonzalez, Stefanie De Bodt, Ronan Sulpice, Yusuke Jikumaru, Eunyong Chae, Stijn Dhondt, Twiggy Van Daele, Liesbeth De Milde, Detlef Weigel, Yuji Kamiya, Mark Stitt, Gerrit T.S. Beemster, and Dirk Inzé*

Department of Plant Systems Biology, VIB, 9052 Ghent, Belgium (N.G., S.D.B., S.D., T.V.D., L.D.M., D.I.); Department of Plant Biotechnology and Genetics, Ghent University, 9052 Ghent, Belgium (N.G., S.D.B., S.D., T.V.D., L.D.M., D.I.); Max Planck Institute of Molecular Plant Physiology, 14476 Potsdam-Golm, Germany (R.S., M.S.); RIKEN Plant Science Center, Yokohama, Kanagawa 230-0045, Japan (Y.J., Y.K.); Department of Molecular Biology, Max Planck Institute for Developmental Biology, 72076 Tuebingen, Germany (E.C., D.W.); and Department of Biology, University of Antwerp, 2020 Antwerp, Belgium (G.T.S.B.)

The final size of plant organs, such as leaves, is tightly controlled by environmental and genetic factors that must spatially and temporally coordinate cell expansion and cell cycle activity. However, this regulation of organ growth is still poorly understood. The aim of this study is to gain more insight into the genetic control of leaf size in *Arabidopsis thaliana* by performing a comparative analysis of transgenic lines that produce enlarged leaves under standardized environmental conditions. To this end, we selected five genes belonging to different functional classes that all positively affect leaf size when overexpressed: *AVP1*, *GRF5*, *JAW*, *BRI1*, and *GA20OX1*. We show that the increase in leaf area in these lines depended on leaf position and growth conditions and that all five lines affected leaf size differently; however, in all cases, an increase in cell number was, entirely or predominantly, responsible for the leaf size enlargement. By analyzing hormone levels, transcriptome, and metabolome, we provide deeper insight into the molecular basis of the growth phenotype for the individual lines. A comparative analysis between these data sets indicates that enhanced organ growth is governed by different, seemingly independent pathways. The analysis of transgenic lines simultaneously overexpressing two growth-enhancing genes further supports the concept that multiple pathways independently converge on organ size control in *Arabidopsis*.

In a fixed environment, the final size of plant organs, such as leaves and flowers, is constant, implying that organ growth is tightly controlled by genetic factors. The two effector systems, cell division and cell expansion, contribute to the final organ size. It is important to note that cell division normally cooccurs with cell expansion to maintain cell size homeostasis (Green, 1976). To avoid ambiguity, we refer to cell proliferation to indicate this combined activity. In *Arabidopsis thaliana* leaves, proliferation, expansion,

and the mature state follow each other in a largely time-dependent fashion (Beemster et al., 2005; Skirycz et al., 2010). After emergence from the shoot apical meristem, the leaf primordium grows mainly through cell proliferation. This phase of growth is progressively replaced, in a distal-proximal manner (Donnelly et al., 1999), by a period of cell expansion associated, in *Arabidopsis*, with an alternative mode of cell cycle activity, namely, endoreduplication (Beemster et al., 2005). Endoreduplication enhances endopolyploidy linked, in many cases, to increased cell size (Melaragno et al., 1993; Inzé and De Veylder, 2006). The regulation of organ size is poorly understood but must include a complex spatial and temporal coordination of cell expansion and cell cycle activity (Beemster et al., 2003). Any perturbation of one of these processes by modification of the expression of distinct genes, therefore, might affect the final size of an organ. Smaller leaves are produced when the number and/or size of cells are decreased (Horiguchi et al., 2006). For example, down-regulation of the expression of the *GROWTH-REGULATING FACTOR5* (*GRF5*), encoding a putative transcription factor, leads to the production of small leaves containing fewer cells (Horiguchi et al., 2005). Similarly, a reduction in leaf size due to a decrease in cell number without change in cell size is observed in *avp1* mutants expressing a lower amount of *AVP1*, a tonoplast-located, pyrophosphate-dependent

¹ This work was supported by the Bijzonder Onderzoeksfonds Methusalem project of Ghent University (grant no. BOF08/01M00408), the Interuniversity Attraction Poles Program-Belgian Science Policy Office (grant no. IUAP VI/33), the European Union 6th Framework Program (AGRON-OMICS grant no. LSHG-CT-2006-037704), the Agency for Innovation by Science and Technology (predoctoral fellowship to S.D.), and the Research Foundation-Flanders (postdoctoral fellowship to S.D.B.).

* Corresponding author; e-mail dirk.inze@psb.vib-ugent.be.

The author responsible for distribution of materials integral to the findings presented in this article in accordance with the policy described in the Instructions for Authors (www.plantphysiol.org) is: Dirk Inzé (dirk.inze@psb.vib-ugent.be).

^[W] The online version of this article contains Web-only data.

^[OA] Open Access articles can be viewed online without a subscription.

www.plantphysiol.org/cgi/doi/10.1104/pp.110.156018

Whole organ, venation and epidermal cell morphological variations are correlated in the leaves of *Arabidopsis* mutants

JOSÉ MANUEL PÉREZ-PÉREZ¹, SILVIA RUBIO-DÍAZ¹, STIJN DHONDT^{3,4}, DIANA HERNÁNDEZ-ROMERO¹, JOAQUÍN SÁNCHEZ-SORIANO², GERRIT T. S. BEEMSTER^{3,4,5}, MARÍA ROSA PONCE¹ & JOSÉ LUIS MICOL¹

¹Instituto de Bioingeniería and ²Centro de Investigación Operativa, Universidad Miguel Hernández, Campus de Elche, 03202 Elche, Alicante, Spain, ³Department of Plant Systems Biology, Flanders Institute for Biotechnology (VIB), Technologiepark 927, 9052 Gent, Belgium, ⁴Department of Plant Biotechnology and Genetics, Ghent University, Technologiepark 927, 9052 Gent, Belgium and ⁵Department of Biology, University of Antwerp, Groenenborgerlaan 171, 2020 Antwerpen, Belgium

ABSTRACT

Despite the large number of genes known to affect leaf shape or size, we still have a relatively poor understanding of how leaf morphology is established. For example, little is known about how cell division and cell expansion are controlled and coordinated within a growing leaf to eventually develop into a laminar organ of a definite size. To obtain a global perspective of the cellular basis of variations in leaf morphology at the organ, tissue and cell levels, we studied a collection of 111 non-allelic mutants with abnormally shaped and/or sized leaves, which broadly represent the mutational variations in *Arabidopsis thaliana* leaf morphology not associated with lethality. We used image-processing techniques on these mutants to quantify morphological parameters running the gamut from the palisade mesophyll and epidermal cells to the venation, whole leaf and rosette levels. We found positive correlations between epidermal cell size and leaf area, which is consistent with long-standing Avery's hypothesis that the epidermis drives leaf growth. In addition, venation parameters were positively correlated with leaf area, suggesting that leaf growth and vein patterning share some genetic controls. Positional cloning of the genes affected by the studied mutations will eventually establish functional links between genotypes, molecular functions, cellular parameters and leaf phenotypes.

Key-words: leaf epidermis; palisade mesophyll; phenomics; principal component analysis; venation pattern.

INTRODUCTION

A major challenge in the post-genomic era is the functional characterization of all of the genes in the genomes of model species. To this end, large-scale approaches toward the targeted inactivation of every gene have been undertaken in animals such as *Caenorhabditis elegans* (Kamath *et al.* 2003), *Drosophila melanogaster* (Winkler *et al.* 2005),

Correspondence: J. L. Micol. E-mail: jlmicol@umh.es

2200

mouse (Wu *et al.* 2007) and zebrafish (Wang *et al.* 2007), as well as in plants such as *Arabidopsis thaliana* (Alonso *et al.* 2003), maize (Fernandes *et al.* 2004) and rice (He *et al.* 2007). The emerging field of phenomics pursues the systematic study of phenotypes caused by individual mutations in every gene of a genome, an approach that is expected to provide a mechanistic link between genotypes and phenotypes (Lussier & Liu 2007). In these large-scale mutant screens, the phenotypes of mutants from gene-indexed collections must be recorded and quantified under standard conditions or in response to altered environments.

Forward genetic screens for mutations affecting the size and shape of *Arabidopsis* vegetative leaves have resulted in the isolation of hundreds of mutants (Berná, Robles & Micol 1999; Serrano-Cartagena *et al.* 1999; Horiguchi *et al.* 2006; Micol 2009). However, the causal genes for the phenotypes of most of these leaf mutants have yet to be identified. Thus far, we have positionally cloned 33 of the 76 genes initially identified in our laboratory based on the leaf phenotype of their mutant alleles (Robles & Micol 2001) and found that their wild-type products participate in processes as diverse as polar cell expansion, the transduction of hormonal signals, gene regulation, plastid biogenesis and chromatin remodelling (Pérez-Pérez *et al.*, 2009b). Strikingly, in several cases, mutations that we initially classified together based on macroscopic phenotype actually affect genes involved in a single pathway or molecular mechanism, implying that gene–morphology relationships are highly reproducible, such as in the *denticulata* (*den*) mutants with pointed leaves, where at least four of which carry alleles of genes encoding ribosomal proteins (Horiguchi *et al.* 2011). In addition, the *elongata* (*elo*) mutants, with narrow and elongated leaves, led to the identification of genes encoding subunits of the transcription Elongator complex (Nelissen *et al.* 2005). In this way, it is becoming possible to begin mapping the organizational levels that connect genes with the whole leaf phenotype, starting with the cellular and tissue levels.

Several methods have been developed for the automated quantification of shape and size variations in biological

© 2011 Blackwell Publishing Ltd

Developmental regulation of CYCA2s contributes to tissue-specific proliferation in *Arabidopsis*

Steffen Vanneste^{1,2,7}, Frederik Coppens^{1,2,7}, EunKyoung Lee³, Tyler J Donner⁴, Zidian Xie⁵, Gert Van Isterdael^{1,2}, Stijn Dhondt^{1,2}, Freya De Winter^{1,2}, Bert De Rybel^{1,2,8}, Marnik Vuylsteke^{1,2}, Lieven De Veylder^{1,2}, Jiří Friml^{1,2}, Dirk Inzé^{1,2}, Erich Grotewold⁵, Enrico Scarpella⁴, Fred Sack³, Gerrit TS Beemster^{1,2,6} and Tom Beekman^{1,2,*}

¹Department of Plant Systems Biology, VIB, Ghent, Belgium, ²Department of Plant Biotechnology and Bioinformatics, Ghent University, Ghent, Belgium, ³Department of Botany, University of British Columbia, Vancouver, British Columbia, Canada, ⁴Department of Biological Sciences, University of Alberta, Edmonton, Alberta, Canada, ⁵Department of Plant Cellular and Molecular Biology and Plant Biotechnology Center, The Ohio State University, Columbus, OH, USA and ⁶Department of Biology, University of Antwerp, Antwerp, Belgium

In multicellular organisms, morphogenesis relies on a strict coordination in time and space of cell proliferation and differentiation. In contrast to animals, plant development displays continuous organ formation and adaptive growth responses during their lifespan relying on a tight coordination of cell proliferation. How developmental signals interact with the plant cell-cycle machinery is largely unknown. Here, we characterize plant A2-type cyclins, a small gene family of mitotic cyclins, and show how they contribute to the fine-tuning of local proliferation during plant development. Moreover, the timely repression of CYCA2;3 expression in newly formed guard cells is shown to require the stomatal transcription factors FOUR LIPS/MYB124 and MYB88, providing a direct link between developmental programming and cell-cycle exit in plants. Thus, transcriptional downregulation of CYCA2s represents a critical mechanism to coordinate proliferation during plant development.

The EMBO Journal (2011) 30, 3430–3441. doi:10.1038/emboj.2011.240; Published online 19 July 2011

Subject Categories: plant biology

Keywords: A2-type cyclins; differentiation; G2-to-M; proliferation; transcriptional repression

*Corresponding author. Department of Plant Systems Biology, VIB, Technologiepark 927, Ghent 9052, Belgium. Tel.: +32 9 331 3930; Fax: +32 9 331 3809; E-mail: tom.beekman@psb.vib-ugent.be

⁷These authors contributed equally to this work

⁸Present address: Laboratory of Biochemistry, Wageningen University, Wageningen, The Netherlands

Received: 1 February 2011; accepted: 24 June 2011; published online: 19 July 2011

Introduction

After germination, the minimal body plan of the seedling is elaborated by iterative organ development that will shape the adult plant. Each new organ is formed according to a predictable pattern, which reflects a complex interplay between plant hormones and developmental programs (De Veylder *et al.*, 2007). One of the targets of morphogenetic cues is the modulation of local cell proliferation and differentiation. Because plant cells cannot move within the plant body due to their rigid cell walls, cell proliferation must be highly controlled in time and space. While recent studies provide insights into the coordination of plant development and cell-cycle regulation, only a few connections between these processes have been identified at the molecular level (Brownfield *et al.*, 2009; Sozzani *et al.*, 2010; Xie *et al.*, 2010).

Cell proliferation is characterized by consecutive cycles of DNA replication (Synthesis; S-phase) and cell division (Mitosis; M-phase). S-phase is preceded by G1-phase, when cells prepare for DNA synthesis, and M-phase by G2-phase, when cells prepare to divide. The orderly transition between phases depends largely on oscillations of Cyclin-Dependent Kinase (CDK) activity. Recently, it was shown that thresholds of CDK activity delineate independent cell-cycle phases (Coudreuse and Nurse, 2010), providing support for a quantitative model of cell-cycle progression. Importantly, CDK activity is modulated at multiple levels. As monomers, CDKs are usually inactive due to a steric blockage of their catalytic cleft. Binding to a cyclin partner removes this block, and thus represents a major regulatory switch of CDK activity (Jeffrey *et al.*, 1995). Further fine-tuning of CDK activity is achieved by phosphorylation, dephosphorylation and binding to several cofactors and/or inhibitors (Morgan, 1995, 1997; Inzé and De Veylder, 2006).

Compared with the relatively simple cell-cycle regulatory module in yeast, which includes just one major CDK and a few cyclins (CYC), higher eukaryotes harbour an elaborate repertoire of CDKs and cyclins. Here, the specialized phase- and tissue-specific expression of multiple CDKs and cyclins provides a wide combinatorial range that enables to deal with the increased complexity associated with multicellularity (De Veylder *et al.*, 2007; Satyanarayana and Kaldis, 2009).

Animals utilize well-characterized D- and E-type cyclins which are expressed at the onset of cell division (G1-to-S) and which connect extracellular signals with the cell cycle (Matsushima *et al.*, 1991; Koff *et al.*, 1992; Motokura and Arnold, 1993; Payton and Coats, 2002). Moreover, A- and B-type cyclins are primarily restricted to G2-to-M phase, with A-type cyclins being more broadly expressed, starting as early as S-phase (Pines and Hunter, 1990; Fung and Poon, 2005). Such expression patterns suggest that they function specifically in respective phases of the cell cycle. However, in some cases the loss of one cyclin type can be compensated for by the expression of another cyclin type (Fisher and Nurse, 1996).

8

Automated analysis of rosette growth parameters by time resolved imaging

Introduction

The use of non-invasive image analysis for plant growth phenotyping was first described in the late nineties (Leister et al., 1999). Projected leaf area measurements of individual *Arabidopsis* seedlings were utilized to determine plant growth rates and were correlated with biomass. Although very promising, only few studies employed this methodology to identify QTLs and genes involved in plant growth (El-Lithy et al., 2004). Nevertheless, imaging of projected rosette area in visible light was incorporated in several growth analysis platforms (Granier et al., 2006; Walter et al., 2007; Skiryicz et al., 2011; Arvidsson et al., 2011). Two approaches were utilized for distinction between plant and background. The first approach

applies a red, green and blue (RGB) channel weighting to create an 8-bit grayscale image which is especially bright for green-colored areas, followed by the application of a global threshold (Skiryecz et al., 2011; Arvidsson et al., 2011). The second approach converted the RGB-value into the so-called hue, saturation, and value (HSV) parameters which allow for a direct selection of a green color region in the HSV color space (Walter et al., 2007). Traits determined from extracted plants include projected rosette area, leaf number, surface coverage (ratio of leaf-covered area and the convex hull of the plant), and stockiness (ratio of leaf area to the square of rosette perimeter). Here, surface coverage relates to the compactness of the rosette and stockiness is a good parameter to identify plants with serrated leaves (Jansen et al., 2009; Pérez-pérez et al., 2011).

On the down side, extracting morphometric measurements of Arabidopsis plants based on a top view picture also introduces a number of pitfalls. Extracting leaf number by counting the local maxima of a distance map usually yields an underestimation of the actual number of leaves as small leaves in the centre of the rosette are overlapping existing leaves, preventing the formation of an extra local maximum. Furthermore, one should keep in mind that leaf overlap in the rosette can account for a 20% reduction in measured plant area (Leister et al., 1999).

Nevertheless, several image acquisition setups have been developed to reveal temporal growth patterns by time resolved image capturing. Taking multiple images over time allows for the calculation of plant growth rates. Imaging platforms published today, which extract morphometric plant measurements from color images, include PHENOPSIS, GROWSCREEN, WIWAM and a growth phenotyping system, based on the commercially available LemnaTec ScanalyzerHTS system (Granier et al., 2006; Walter et al., 2007; Skiryecz et al., 2011; Arvidsson et al., 2011). These setups combine image segmentation procedures with automated data extraction protocols.

In this chapter we present the phenotyping platforms, developed in the context of this PhD, applying time resolved image capturing, together with the image analysis procedures that allow for high-throughput data extraction. I subdivided this section in the automated measurements of plants grown *in vitro* (in Petri dishes), and plant grown *in vivo* (on soil).

Setting up a system for *in vitro* growth analysis

In order to examine the growth patterns of *in vitro* grown Arabidopsis plants, we set out to develop an imaging system, called IGIS, which is an acronym for *In vitro* Growth Imaging System. The setup was based on the idea of a carousel. Rotating Petri dishes on a disk brings each of them underneath a single-lens reflex (slr) camera, which captures a top view picture of the germinating seedlings growing inside the Petri dishes. Coordinating the movement of the carousel with the timer of the camera allowed following the growth of the plants throughout their development. However, building the prototype of the imaging setup revealed

a number of pitfalls which led to the extension of the phenotyping system and the integration of a number of controls. Placing the carousel on a shelf in one of the tissue culture rooms allowed growing the monitored plants in controlled environmental conditions, with respect to light and temperature.

Here, we present the major concepts of the carousel and the adjustments that were put in to improve the system (Figure 1). The center of the imaging setup is a metal disk, which can contain up to ten Petri dishes. This disk is put into motion by a step motor driving a central axle. The motor is connected to a programmable logic controller (PLC), allowing for the integration of timers and sensors that control the motor. To ensure an accurate and fixed positioning of the Petri dishes underneath the slr camera, screws were inserted in the rotating disk in between the positions of the Petri dishes. These screws stop the motor and the movement of the carousel as they pass and are detected by a metal sensor. Next, to prevent condensation at the top of the Petri dishes, the disk had to be cooled. Therefore, the carousel was connected to the cooling system of the tissue culture room, blowing cooled air, which was contained by a metal ring, underneath the disk. The temperature of the disk can be controlled by elevating the disk above the metal ring. Furthermore, the EOS Utility software (Canon, Tokyo, Japan), running from an onsite computer, was used to control the camera settings and to acquire the time-lapse observations. To enable secure data storage of the high amount of pictures, the computer was connected to the network to allow copying the data to one of the servers, which contain an up-to-date backup system. Finally, to preserve the setup from short electricity failures, we hooked it up to an uninterruptible power supply (UPS).

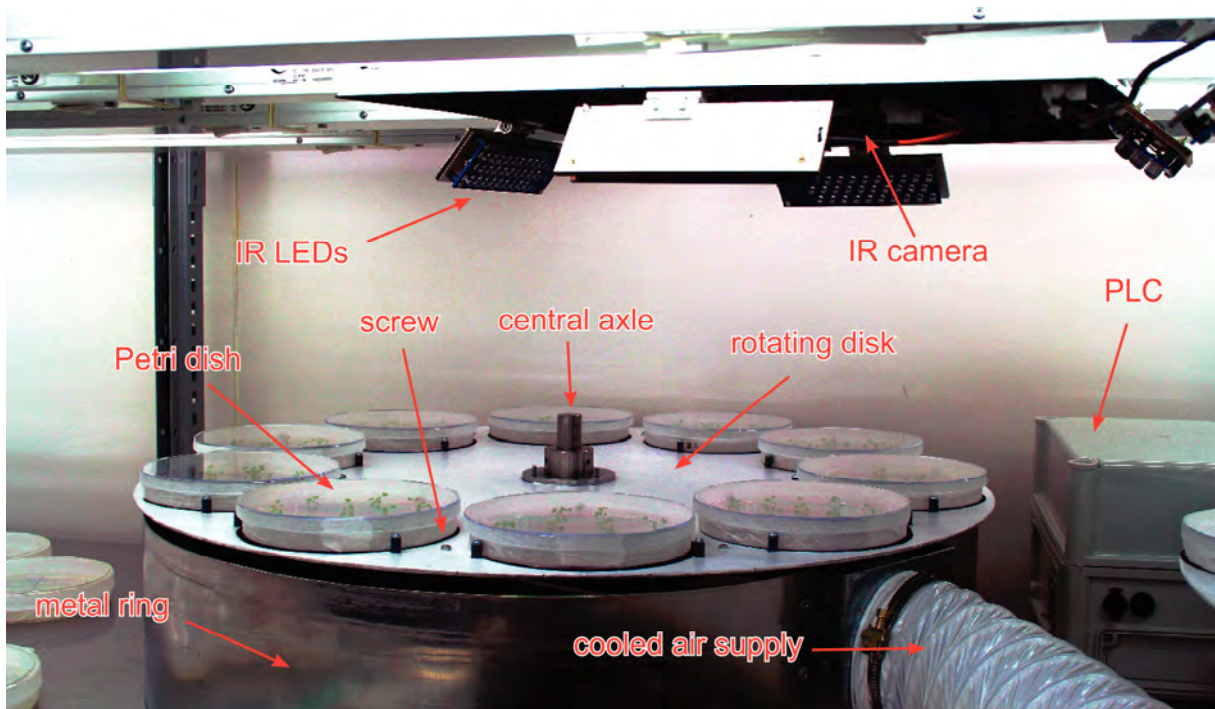


Figure 1: Picture of the IGIS setup to monitor *in vitro* Arabidopsis rosette growth in day-night conditions using an IR camera. The major parts of imaging platform are indicated.

The setup, as described above, allows monitoring plant growth under continuous light conditions. However, if plants were grown in day-night conditions, no data could be extracted during the night. To enable the possibility to view the plants during the dark period, the platform was equipped with infrared (IR) light emitting diodes (LEDs). LEDs with a wavelength peak around 940 nm, which is well outside the visible spectrum for plants, were positioned at the level of the camera's objective, at a radius which ensures that no IR light reflects in the objective through the surface of the Petri dishes. Furthermore, to allow the reflex camera to capture the IR light some adjustments had to be employed. In general, image sensors of digital cameras can detect light up to 1100 nm. However, normally an IR filter is blocking the IR light before it reaches the sensor. In order to be able to capture the IR light reflected by the plants, we used a commercially available slr camera (Canon EOS 60D) in which the IR filter had been removed (<http://www.maxmax.com/>). Finally, to ensure that the pictures taken during the light period are comparable to those taken during the dark period, a day light filter was screwed onto the objective. This amendment to the imaging platform now provides us with a system which can also monitor plant growth in a light regime closer to the one plants perceive in their natural environment, being a day-night cycle. Representative pictures of a Petri dish captured with a camera adjusted for IR imaging and an RGB camera are presented in Figure 2A and 2B, respectively.

How images can tell the story of plant growth

To monitor rosette growth of *Arabidopsis* plants, the imaging carousel was set up to move one position each six minutes, bringing each of the ten Petri dishes underneath the camera position within the time frame of one hour. Pictures of each plate were captured in between the movement of the carousel. Plant growth was followed from the moment the plates go into the tissue culture room (day 1) until day 21, ending the time lapse before bolting of the plants, generating a total of 4800 images per analysis. For each Petri dish twelve seeds were evenly spread over the plate, to prevent overlapping plants at the final stages, meaning that individual rosette growth of 120 plants was followed over 480 hours in a typical time-lapse sequence.

Combining all images of a specific Petri dish allowed composing a movie of that particular plate, which visualized the development and growth of the plants on it. However, to extract growth features from these rosette plants, there was a need for an image processing pipeline as the number of pictures is too high for a manual analysis. Before starting the image analysis procedure, some steps had to be performed in order to generate the input data. First, a mask image was created for each of the Petri dishes, based on their last image in the time lapse (Figure 2C). These images contain black disks at the positions of the plants that should be analyzed. This provides a method to exclude plants which did not germinate or which did not grow well. Next, the selected plants on each plate were numbered automatically based on the position of the corresponding disks in the mask images (Figure 2D). Now, every plant in the

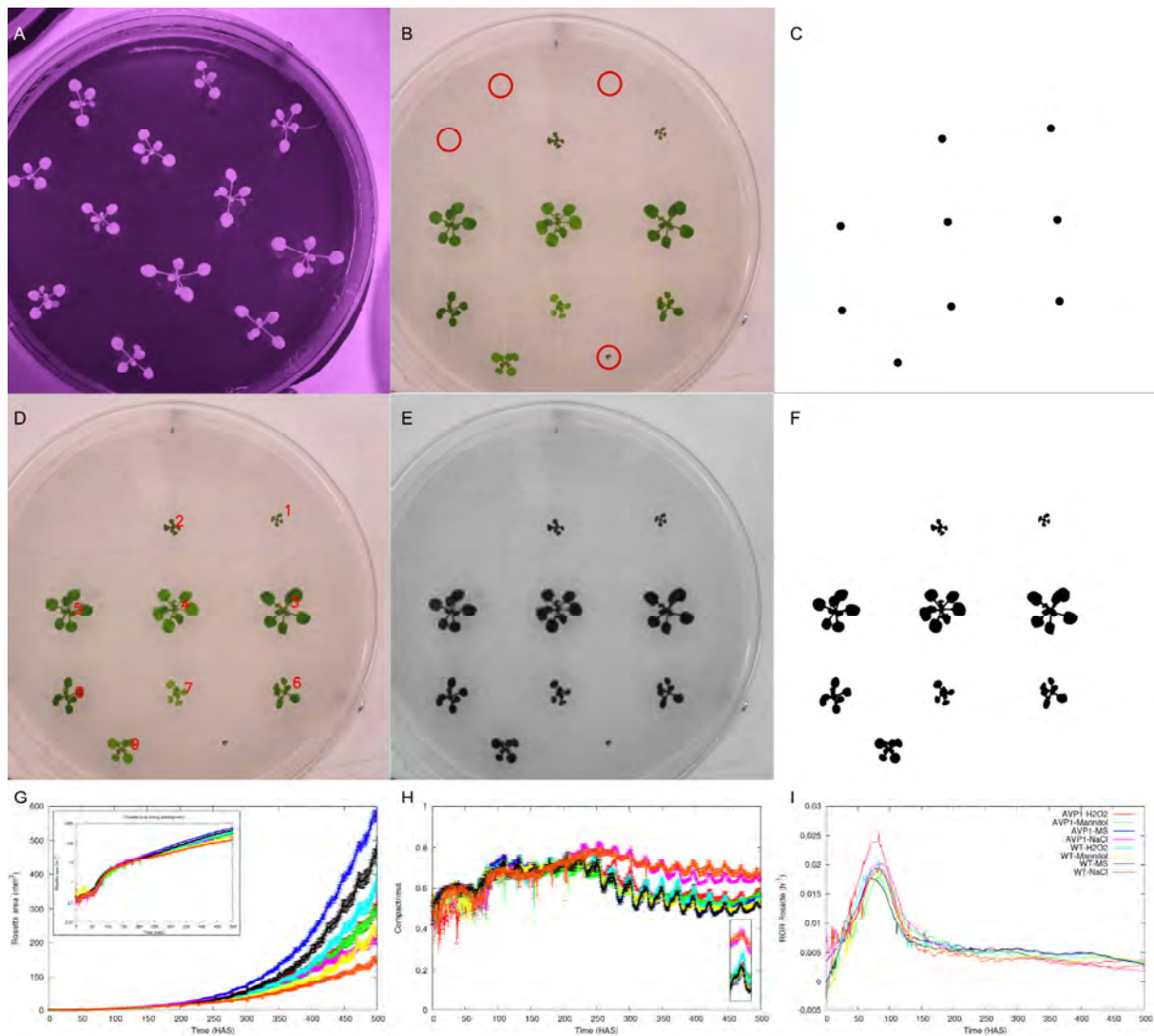


Figure 2: Image and data analysis of pictures captured with IGIS.

(A) Representative picture of a Petri dish captured with a camera adjusted for IR imaging. (B) Representative picture of a Petri dish captured with a normal slr camera. Red circles indicate non-germinated seeds and badly grown plants which should be excluded from the analysis. (C) A mask image containing black disks on the position of selected plants. (D) Automated numbering of the plants based on the position of the disks in the mask image. (E) Selection of the blue channel after an RGB split of the original color figure in B to increase the contrast between the plants and their background. (F) Extraction of the rosettes after the application of a threshold and a reconstructive opening based on the disks in the mask image. (G-I) Automatically generated graphs after image and data analysis of the complete time lapse, showing data of wild type and AVP1 over-expression plants grown on different growth media under day-night light conditions. (G) Rosette area during development. Inset shows the same data with log scale. Error bars show SE. (H) Rosette compactness during development. Inset shows rosette compactness between day 14 and 15. Error bars show SE. (I) Relative rosette growth rate per hour during development.

analysis could be identified by its number on the plate and the number of the plate it was on. This allowed preparing an input file, in the form of a tab delimited text file, which contains data on the genotype of each plant, identified by these numbers. Later on, this would allow

for the automatic calculation of mean values for the rosette growth features for each genotype included in the analysis at each time point. At this point all necessary background information, being the selection and identification of the plants of interest and linking them to their genotype, was gathered and the image procedure could start.

Here, we describe the different steps to extract the rosette growth features from *Arabidopsis* plants grown on a Petri dish. In the case of an analysis under continuous light conditions, the contrast between the plants and their background was increased by selection of the blue channel after an RGB-split (Figure 2E). An upper threshold was applied to the resulting image to extract the plants from their background. IR images, on the other hand, already showed a high contrast between the plants and the black paper underneath the Petri dish and the application of a lower threshold was sufficient to extract the plants. From this point on, RGB and IR image processing are parallel. Because the application of the thresholds also extracted small noise particles, a reconstructive opening is applied to only recover the plants based on the position of the disks in the corresponding mask image (Figure 2F). A reconstructive watershed segmentation starting from the same disks ensures that contingent overlapping plants are separated. Next, all plants on the image are saved into separate images. The rosette area is calculated and a convex hull is build starting from the outline of the rosette. The rosette compactness is calculated by the ratio between the rosette area and the area covered by the covex hull. Both data points are stored in a text file. This automated image analysis chain is applied to all 4800 images in the time lapse sequence.

After the image processing, all the generated data was fed into a data analysis script, written in the perl scripting language (<http://www.perl.org/>). This script is developed to combine the individual time point measurements, which allows for the visualization of the evolution of the rosette features over time, and to summarize the rosette measurements of the different plants per genotype. Because the plate number was integrated in the file name of each picture and because the position of the disks in the mask images was the basis for the assignment of the plant numbers, the rosette area and compactness measurements could be linked to the individual plant, whose genotype was supplied in the input file. Also the time point was integrated in the file name of each picture, which allowed for the positioning of the measurements in time. Mean rosette area and compactness values were calculated for each genotype over time, together with their standard errors. Furthermore, relative rosette growth rates and the relative change in rosette compactness are calculated from the derivatives of the mean rosette area and compactness over time, respectively.

These derivatives are calculated by a local second degree polynomial fit to the log transformed data using the least squares method. Graphs of the data are generated automatically using GNUplot (<http://www.gnuplot.info/>). Figure 2G-I show examples of such plots for wild type and *AVP1* over-expression plants grown on different growth media under day-night light conditions. Differences in exponential growth yield a range of final rosette areas between the treatments. Leaf movements in the rosette generate a cyclic pattern in the

compactness measurements over time. Calculation of the relative rosette growth rates allows for a close comparison of the growth patterns between treatments and genotypes.

In summary, a rosette growth time lapse analysis contains following steps. Plants are grown in Petri dishes and are standing on a rotating disk. Pictures from each plate are taken on an hourly basis. Automated image analysis segments the plants from the background and rosette area and compactness measurements are extracted. Next, a data analysis script combines the individual time point measurements to reveal the temporal growth patterns and calculates the mean rosette measurements per genotype over time, after which the data is automatically plotted in a number of graphs. These data indicate that we were able to develop an imaging setup and analysis pipeline, which allows following rosette growth of *in vitro* grown Arabidopsis plants over time.

From *in vitro* to *in vivo*

The imaging setup for *in vitro* growth analysis, IGIS, has been adjusted to allow for plants to grow under day-night conditions by NIR imaging, in order to study rosette development in environmental conditions closer to nature. We do, however, realize that growing plants in Petri dishes on sugar containing media is far away from their natural environment. Therefore, we set out to assess rosette growth of plants grown on soil by adjusting the image analysis scripts. Figure 3A shows an individual Arabidopsis plant grown on a jiffy (<http://www.jiffygroup.com/jiffy/>) in a small pot. The contrast between the green leaves and the soil is lower compared to a color picture of plants grown on Petri dishes (Figure 2B). Performing an RGB split did not reveal a high contrast in any of the channels (Figure 3B-D), as was the case for the blue channel in *in vitro* grown plants (Figure 2E). However, combination of the channels according to the formula $G-(B+(R-G))$ did result in a higher contrast between the plant and its background by removing most of the background (Figure 3E-G). Application of a lower threshold can now extract the rosette. Cleaning the extraction and removing small noise allows us to get a clean extraction of the rosette by selecting for the largest object in the image, shown as a binary image in Figure 3H. This binary image can be used to extract the plant from the original color picture (Figure 3I), but it is also the basis to measure the rosette area, to calculate the rosette perimeter and to examine the rosette compactness based on the convex hull (Figure 3J).

These adjustments to the image analysis procedures, set up for *in vitro* analysis, support the extraction of plants grown on soil. However, compared to plants grown on Petri dishes, soil grown plants show much more variation in their growth, mainly due to the more heterogeneous soil environment and the differences in soil water content. To minimize the biological variation our research group developed an imaging platform, called WIWAM, which is an acronym for Weighing, Imaging and Watering Machine (Figure 4A). This platform contains a table, which can hold 228 plants, and a robotic arm, which takes the individual

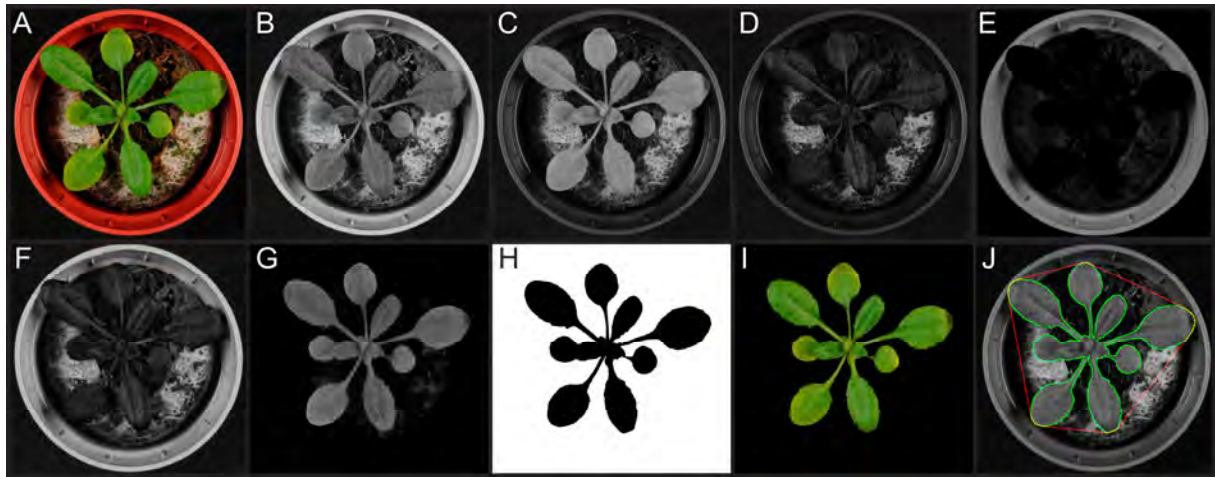


Figure 3: Image analysis of Arabidopsis rosettes grown on soil.

The image analysis algorithm extracts a rosette from its background and measures projected rosette area, perimeter and convex hull. The final image is saved for quick visual control. (A) Original picture. (B-D) RGB split of the original image. (B) Red channel. (C) Green channel. (D) Blue channel. (E) Green channel subtracted from the red channel. (F) Blue channel added to E. (G) G subtracted from the green channel. (H) Cleaned threshold image of G. (I) Rosette extracted from the original image based on H. (J) Visualization of the extracted rosette perimeter and the computed convex hull on top of the original image.

pots to an imaging, weighing and watering station on a daily basis. This means that for each pot one picture is captured every day and that the soil water content is controlled on the individual pot level. Implementation of the image analysis script described above, allows the setup to automatically extract rosette growth features from the set of images. Hence, WIWAM can be used to perform rosette growth analysis of plants grown on soil under controlled watering conditions. This imaging platform was used to analyze a set of published drought stress survival lines under mild drought conditions and the results of this study recently have been published in Nature Biotechnology (Skirycz et al., 2011). The title page of the article is included at the end of this section. In the scope of the European Agron-Omics project (<http://www.agron-omics.eu/>), this image analysis pipeline has also been applied to extract rosette growth features of about 120,000 images from the group of Detlef Weigel (Germany) in a study to map growth QTLs (unpublished results Salome et al.).

Next, to the WIWAM, we developed a simpler setup to image soil grown plants, which we called MIRGIS (Figure 4B). MIRGIS stands for Multi Camera *in vivo* Rosette Growth Imaging System. This setup consists of three cameras mounted above six trays. The whole has been united in a custom designed rack which contains fluorescent lamps and is put in a temperature and humidity controlled growth chamber. The three cameras are connected to one laptop and a computer script was developed so that each camera would take a picture of the two trays underneath on a daily basis. Figure 5A shows a representative picture of one of the cameras. This setup can image a total of 144 plants, but cannot automatically control the watering of the plants.

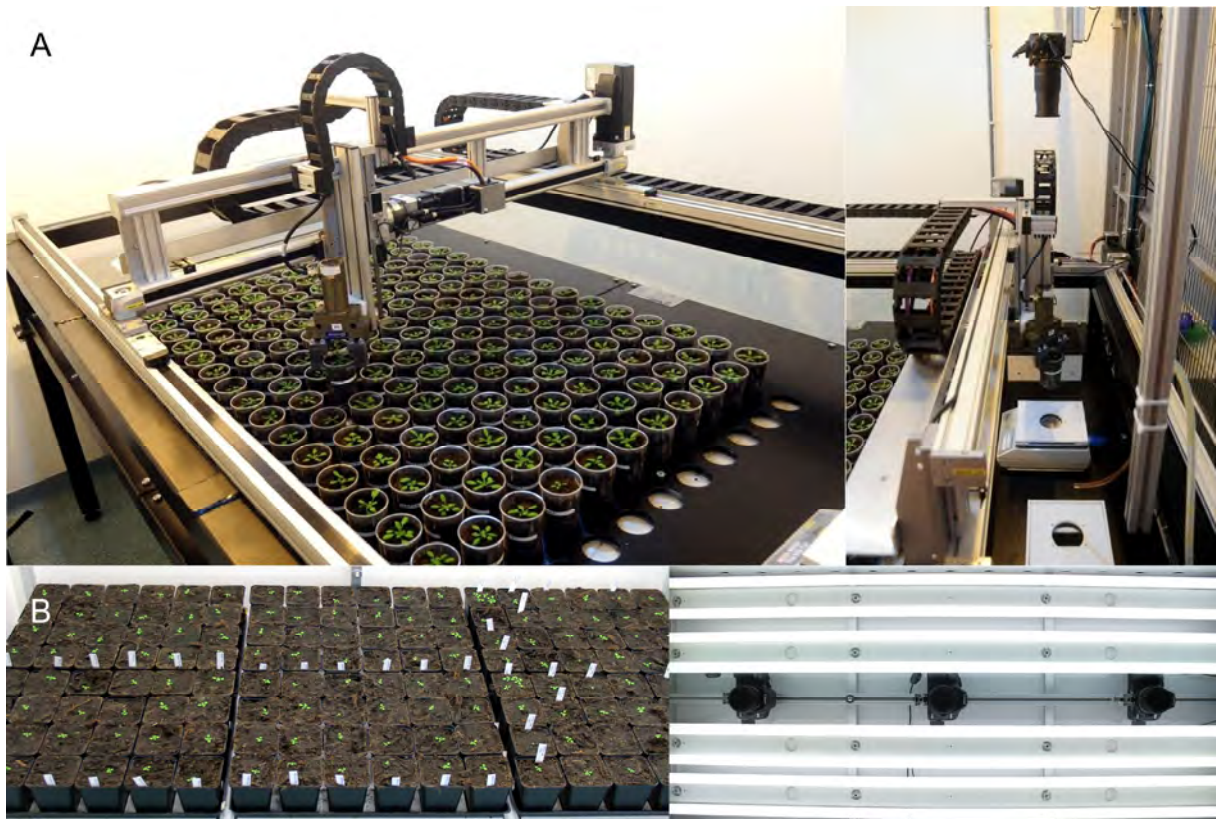


Figure 4: Setups for *in vivo* rosette growth measurements of *Arabidopsis* plants grown on soil.

(A) WIWAM. (left) Robotic arm and table contain 228 pots. (right) Imaging, weighing, and watering station from top to bottom. (B) MIRGIS. (left) Six trays with 144 pots standing on a custom designed rack in the growth room. (right) Three identical slr cameras (Canon EOS 450D) fixed at the top of the rack between the fluorescent lamps.

In order to cope with the increased biological variation within soil grown plants, plants are compared based on their relative growth rates, which are more robust, compared to absolute rosette area measurements (Paul-Victor et al., 2010). Next to the more heterogeneous soil environment and the differences in soil water content, a lot of the biological variation in rosette size is introduced by differences in the timing of seed germination. To tackle this problem, four seeds are sown per pot and early in development all but one seedling are removed to keep the plant which most represents the average of the population. Initially this selection process was done by eye, but currently the seedlings are selected automatically by image analysis. To this end we created three mask images (one for each camera), which contain squares on the positions of the individual pots (Figure 5B). Changing the color of the squares allows us to differentiate between genotypes. Ten contrasting colors were selected so that the individual colors can easily be extracted by applying an upper and lower threshold after conversion to a grayscale image (Figure 5C). This allows for the automatic generation of mask images for each genotype separately. These mask images are used to extract the seedlings from the pots by the methods described above, but in this case all seedlings within the pot are extracted instead of selecting for the biggest object in the image. Next, the

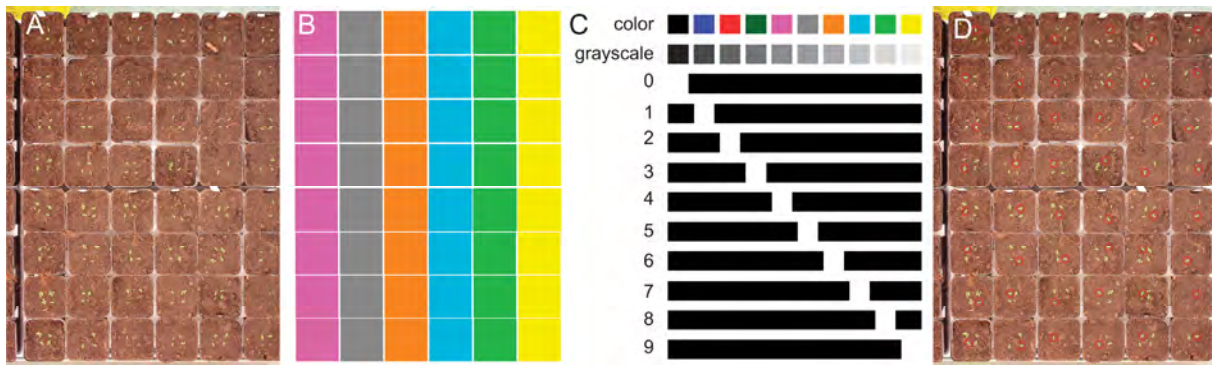


Figure 5: Seedling selection in the MIRGIS platform to reduce biological variation

(A) Representative picture captured by the MIRGIS platform containing 48 pots on two trays. (B) Mask image of the pots shown in A. Squares correspond to the position of the pots and the different colors represent different genotypes. (C) The upper row shows ten contrasting colors which can be used for selecting different genotypes. The second row corresponds to row 1 converted to a grayscale image. The rows underneath correspond to the grayscale segmentation of row 2 by application of an upper and lower threshold according to the following formulas where a corresponds to the numbers on the left. Upper threshold = $12 + a * 25$; lower threshold = higher threshold - 25. This extraction method is applied to automatically generate mask images for each genotype in the analysis. (D) The seedling closest to the median projected area of that genotype is selected for each pot. A red circle indicates the selected seedlings on the original image A.

projected areas of all seedlings of a specific genotype (which are usually spread over the six trays) are measured and the median seedling area of that genotype is calculated. Then, the seedling with an area closest to the median value is selected within each pot of that genotype. A selection image is generated in which the selected plant is indicated by a red circle (Figure 5D). This image is used to manually remove the remaining plants in the pots. This methodology ensures that the seedling, selected per pot, is the one closest to the average plant in the population of its genotype. Because the selection of the seedling can return its precise position, new mask images can be created which allow tracking the seedling growth at the days prior to the selection when still multiple seedlings were growing per pot. For WIWAM, the seedling selection is currently done in 96-well plates prior to the transformation to the bigger pots.

Taken together, we developed the IGIS to monitor rosette growth of *Arabidopsis* plants grown on Petri dishes. Pictures are captured on an hourly basis and 10 plates are concurrently imaged. Recently, we installed a second IGIS to increase the throughput. WIWAM and MIRGIS are the setups for *in vivo* analysis and they take 228 and 144 plants, respectively. WIWAM takes pictures of individual pots and controls the soil water content, making it the ideal system for plant growth analyses under controlled watering conditions. MIRGIS captures 2 trays, each containing 24 plants, in one image. In general, both platforms extract daily measurements. In the coming year a second WIWAM will be installed and also the MIRGIS could easily be extended. In conclusion, the development of the different time resolved

imaging platforms has boosted the throughput of the plant growth analyses in our research group and this with a throughput and temporal resolution that was not feasible before.

References

- Arvidsson, S., Pérez-Rodríguez, P., and Mueller-Roeber, B.** (2011) A growth phenotyping pipeline for *Arabidopsis thaliana* integrating image analysis and rosette area modeling for robust quantification of genotype effects. *New Phytologist*, 191, 895-907.
- El-Lithy, M.E., Clerkx, E.J.M., Ruys, G.J., Koornneef, M., and Vreugdenhil, D.** (2004) Quantitative trait locus analysis of growth-related traits in a new *Arabidopsis* recombinant inbred population. *Plant Physiol*, 135, 444-458.
- Granier, C., Aguirrezabal, L., Chenu, K., Cookson, S.J., Dauzat, M., Hamard, P., Thioux, J., Rolland, G., Bouchier-Combaud, S., Lebaudy, A., Muller, B., Simonneau, T., and Tardieu, F.** (2006) PHENOPSIS, an automated platform for reproducible phenotyping of plant responses to soil water deficit in *Arabidopsis thaliana* permitted the identification of an accession with low sensitivity to soil water deficit. *New Phytologist*, 169, 623-635.
- Jansen, M., Gilmer, F., Biskup, B., Nagel, K.A., Rascher, U., Fischbach, A., Briem, S., Dreissen, G., Tittmann, S., Braun, S., De Jaeger, I., Metzlauff, M., Schurr, U., Scharr, H., and Walter, A.** (2009) Simultaneous phenotyping of leaf growth and chlorophyll fluorescence via GROWSCREEN FLUORO allows detection of stress tolerance in *Arabidopsis thaliana* and other rosette plants. *Funct. Plant Biol.*, 36, 902-914.
- Leister, D., Varotto, C., Pesaresi, P., Niwergall, A., and Salamini, F.** (1999) Large-scale evaluation of plant growth in *Arabidopsis thaliana* by non-invasive image analysis. *Plant Physiology and Biochemistry*, 37, 671-678.
- Paul-Victor, C., Züst, T., Rees, M., Kliebenstein, D.J., and Turnbull, L.A.** (2010) A new method for measuring relative growth rate can uncover the costs of defensive compounds in *Arabidopsis thaliana*. *New Phytologist*, 187, 1102-1111.
- Pérez-pérez, J.M., Rubio-díaz, S., Dhondt, S., Hernández-romero, D., Sánchez-soriano, J., Beemster, G.T.S., Ponce, M.R., and Micol, J.L.** (2011) Whole organ, venation and epidermal cell morphological variations are correlated in the leaves of *Arabidopsis* mutants. *Plant, Cell & Environment*, 34, 2200-2211.
- Skirycz, A., Vandenbroucke, K., Clauw, P., Maleux, K., De Meyer, B., Dhondt, S., Pucci, A., Gonzalez, N., Hoerberichts, F., Tognetti, V.B., Galbiati, M., Tonelli, C., Van Breusegem, F., Vuylsteke, M., and Inzé, D.** (2011) Survival and growth of *Arabidopsis* plants given limited water are not equal. *Nat Biotech*, 29, 212-214.

Walter, A., Scharr, H., Gilmer, F., Zierer, R., Nagel, K.A., Ernst, M., Wiese, A., Virnich, O., Christ, M.M., Uhlig, B., Jünger, S., and Schurr, U. (2007) Dynamics of seedling growth acclimation towards altered light conditions can be quantified via GROWSCREEN: a setup and procedure designed for rapid optical phenotyping of different plant species. *New Phytologist*, 174, 447-455.

CORRESPONDENCE

Survival and growth of *Arabidopsis* plants given limited water are not equal

To the Editor:

Although drought tolerance is a central concern of plant research, the translatability for crop improvement is relatively low. Here we report on a major contributing factor to this lack of success. Drought tolerance is predominately scored based on an improved survival rate under lethal conditions that, as demonstrated by our study, does not predict superior growth performance and, thus, biomass yield gain, under moderate drought often encountered in the field.

Drought tolerance is a major subject of trait research for agbiotech companies and thousands of academic papers have been published on the topic. Consequently, there is a plethora of reports on improved drought tolerance, mainly in the model plant *Arabidopsis thaliana*¹. Classic genetic engineering approaches involve target genes that function in mechanisms used by plants to avoid and/or tolerate drought, such as stomatal conductance or osmolyte production². Such genes, frequently identified through expression profiling, include signaling components and downstream effector genes. However, despite the apparent success of stress research on model plants, rarely are the findings applied to improve crops. Only a few genes have been characterized that enhance stress tolerance in model plants or crops leading to increased yields^{3–6} and the molecular mechanisms through which they work remain only partly understood. One of the key reasons relates to the genetic and physiological differences between model and crop species.

In *Arabidopsis* research, drought tolerance is assessed predominantly under quite severe conditions in which plant survival is scored after a prolonged period of soil drying. However, in temperate climates, limited water availability rarely causes plant death, but restricts biomass and seed yield. To study the relation between survival and biomass gain under drought, we analyzed the growth of transgenic *Arabidopsis* plants with increased tolerance to lethal stress in a mild stress assay. An extensive literature screen was conducted to identify *Arabidopsis* genes that, in gain- or loss-of-function situations, confer stress tolerance in *Arabidopsis*, without growth penalty under control conditions. Although drought and osmotic stresses were prioritized,

other related ones, including salt, heat and oxidative stresses, were considered as well. The final selection consisted of 25 genes, which we designate 'stress tolerance genes' (STGs), involved in diverse aspects of stress tolerance and in a wild-type Columbia-0 (Col-0) background (Table 1, Supplementary Table 1).

We added two additional lines (MYB90 and tAPX) that had previously not been analyzed to 15 of the 25 STG lines that had already been demonstrated to survive better upon severe drought (Table 1, Fig. 1a and Supplementary Fig. 1). To quantify growth of the STG lines, we developed an assay mimicking relatively mild drought stress conditions in which the rosette size of plants grown in soil was followed over time (Supplementary Methods). To ensure test reproducibility, we also used a large number of plants in an automated platform, designated the 'weighing imaging and watering machine' (WIWAM; Fig. 1b and

Supplementary Fig. 2). WIWAM enabled the daily imaging and controlled watering of 216 plants. Plants were germinated and grown under control conditions until stage 1.04 (ref. 7), after which watering continued for the control plants, but was stopped for the stressed plants until the set stress level was reached and subsequently kept constant (Supplementary Figs. 3 and 4). In wild-type plants, progressive soil drying resulted in a gradual decrease of growth rates, with a final reduction of the rosette area of 30–40% as a consequence (Fig. 1c, Table 1 and Supplementary Fig. 4).

To assess the performance of the STG lines in terms of genotype differences and genotype-specific responses to the drought stress, we analyzed genotype, environment, time effects and their interactions with a linear mixed model (Table 1, Supplementary Figs. 5 and 6, Supplementary Methods). Significant ($P < 0.01$) genotype differences were

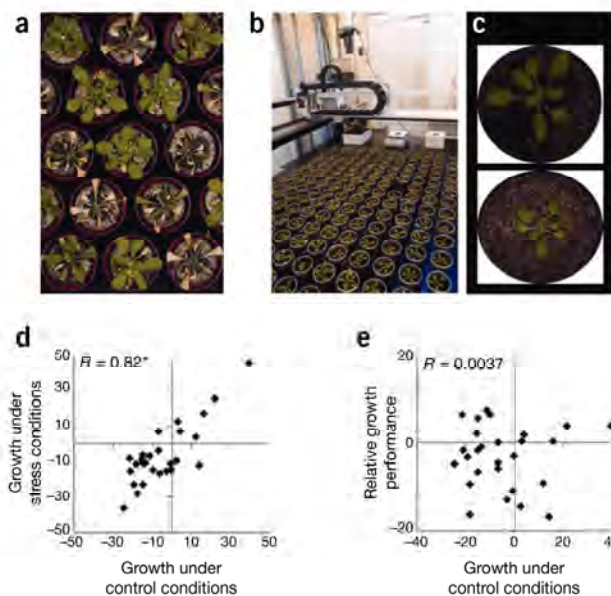


Figure 1 Growth reduction caused by stress is independent of rosette size under control conditions. (a, b) Tolerance to severe stress was scored in the survival assay (a), whereas growth under mild drought was assessed with WIWAM in a drought stress regime (b) that reduced final rosette area by 30–40%. (c) The top panel shows a wild-type plant grown under control conditions. The bottom panel shows a plant grown under drought conditions. (d, e) End-time-point area measurements were used to calculate differences between STG and wild-type (WT) plants under control (area C) ($1 - (\text{area C STG}/\text{area C WT}) \times 100$) and drought (area D) conditions ($1 - (\text{area D STG}/\text{area D WT}) \times 100$), as well as the difference in drought-related growth inhibition (relative growth performance) ($(1 - (\text{area D WT}/\text{area C WT})) - (1 - (\text{area D STG}/\text{area C STG})) \times 100$). Asterisk marks significance ($P < 0.01$).

9

General conclusion and future perspectives

Analyzing cellular dynamics during leaf development as a basis to understand growth

Global agriculture is currently facing major challenges. The world population is increasing steadily at an exponential rate (<http://www.prb.org/>), drastically increasing the demand for food, feed and fuel. Furthermore, annual yields of many crops have hit plateaus. Already now, worldwide yield increases can no longer meet the projected demand for the major cereal crops. Shortage of food is raising the prices dramatically and many countries are struggling with a food crisis. These statements indicate that food security is more than ever a global issue. Moreover, global warming is likely to lead to reduction in yields due to abiotic stress (Tester and Langridge, 2010). On top of that, the rapid increasing standard of living in developing countries is driving the rising energy needs, while the natural resources are running out. This indicates that growing feedstock crops for biofuel production will become more important in the future. However, these cannot go in competition with food crops for

arable land. Taken together to tackle these challenges, in the next decades agricultural crops must have a higher intrinsic yield, while they ensure yield stability under abiotic stresses.

Since conventional breeding programs are likely not to fulfill these needs in a short timeframe, new approaches coming from the field of plant biotechnology are required. Increasing crop productivity is the major goal, and in a number of crops this comes down to increasing plant biomass. One way to do this is to try increasing final leaf size. This is however not trivial, since final leaf size is in essence the result of two processes, being cell expansion and cell division (Green, 1976), indicating that to understand the nature of growth differences, observations at the cellular level are key. Furthermore, one should put this in a developmental context. We currently identified up to six mechanisms which have the potential to increase leaf size. Final cell number can be increased by 1. recruiting more cells from the SAM at bulging of the leaf primordium, 2. by increasing cell division rate and 3. by postponing the exit of cell proliferation. 4. Boosting cell cycle activity of meristemoid cells, which give rise to the cells in the stomatal lineage, is another emerging mechanism to increase cell number. Final cell size, on the other hand, can be enhanced by 5. increasing cell expansion rate or by 6. extending the cell expansion phase. Transcriptome, proteome, and metabolome profiling techniques are more and more applied to unravel the basis of growth phenotypes caused by genetic differences or changing environmental conditions. However, these approaches often only focus on the molecular level and lack details on the growth process at cellular resolution. In order to fully understand growth regulatory mechanisms, profiling experiments should be combined with cellular growth analyses in order to link regulatory processes at the molecular level to organ and subsequently whole plant level growth. Many molecular pathways converge on growth related processes and every genetic perturbation affecting leaf size must act through one of the mechanisms described above. This indicates that knowledge on the dynamics of cell division and cell expansion processes are pivotal to obtain a mechanistic view on how molecular changes can lead to observed growth phenomena.

The goal of this thesis was to investigate and develop new imaging methods and to use these to increase our knowledge of leaf growth mechanisms by examining the cellular dynamics during leaf development. In our studies we used the model plant, *Arabidopsis thaliana*, because of its fast life cycle and the availability of a large variety of genetic resources. First, in Chapter 1 we reviewed the current methods in plant growth imaging. Next, in Chapter 2 we showed that the transcription factors, SHORT-ROOT (SHR) and SCARECROW (SCR), originally discovered as regulators of (stem) cell identity in the root tip also regulate leaf growth, where the stem-cell niche is absent (Dhondt et al., 2010). A kinematic analysis revealed a reduced cell division rate and an early exit of the proliferation phase. The increased cell cycle duration is due to a prolonged S-phase duration, which is mediated by up-regulation of cell cycle inhibitors known to restrain the activity of the transcription factor, E2Fa. Binding of SHR and SCR to the promoters of *CYCD6;1* and *RBR*, respectively (Sozzani et al., 2010; Unpublished results Ben Scheres), confirm the direct link between these transcription factors and cell cycle

regulation. We conclude that, in contrast to their specific roles in cortex/endodermis differentiation and stem cell maintenance in the root, *SHR* and *SCR* primarily function as general regulators of cell proliferation in leaves.

In this work, a kinematic analysis of leaf growth allowed us to focus on a specific developmental time point and helped to unravel the molecular processes involved, explaining the observed leaf growth phenotypes. Nevertheless, from the moment that multiple aspects of cell division and cell expansion are affected, it is difficult to distinguish their individual contributions to the final leaf size. This is mainly because of the experimental difficulties to disentangle them in a developing organ, due to their tight interconnection, shown by the fact that a reduced cell proliferation is often compensated by an increase in cell size and vice versa. To circumvent this problem, we set out to build a mathematic model that describes the possible division patterns and expansion rates for individual epidermal cells (Kheibarshekan Asl; Dhondt et al., 2011). This model, described in Chapter 3, was used to fit experimental data on cell numbers and sizes obtained over one day time intervals throughout the development of the first leaf pair of *Arabidopsis*. The model allowed us to calculate probabilities for a cell to divide into guard or pavement cells, the maximum size at which it can divide, and its average cell division and expansion rates at each point during the leaf developmental process. Surprisingly, average cell cycle duration remained constant throughout leaf development, whereas no evidence for a maximum cell size threshold for cell division of pavement cells was found. Furthermore, the model predicted that neighboring cells of different sizes within the epidermis expand at distinctly different relative rates, which could be verified by direct observations. We conclude that cell division seems to occur independently from the status of cell expansion, whereas the cell cycle might act as a timer rather than as a size-regulated machinery. By fitting a mathematical model to experimental data, we could therefore estimate the division and expansion parameters of pavement and guard cell populations within the growing leaf separately, allowing us to gain a better and more detailed insight into the processes that define leaf growth.

Although we were now able to separate the proliferating and expanding populations of epidermal cells within a developing leaf, there was still an important event during leaf development that was not yet characterized in detail, being the transition from cell proliferation to expansion. Due to the exponential nature of the division process the timing of this transition can have a drastic effect on overall leaf size. A number of genes have been found to alter leaf size by affecting the transition from primary to secondary morphogenesis, including *SHR*, *DA1*, *ANT*, *KLUH/CYP78A5* and *GRF5* have been proposed to play a role in the arrest front progression (Mizukami and Fischer, 2000a; Li, Zheng, Corke, Smith, and Bevan, 2008a; Horiguchi et al., 2009; Kazama et al., 2010; Gonzalez et al., 2010; Dhondt et al., 2010). Over time, the transition was shown to proceed in a gradient down the leaf, with cell proliferation first ceasing in the leaf tip and then progressively down the longitudinal axis of the leaf (Donnelly et al., 1999; Kazama et al., 2010). In Chapter 4, we characterized the

progression of the Arabidopsis leaf through the transition from primary to secondary morphogenesis using transcriptome analysis and imaging algorithms to visualize and quantify the size and shape of pavement cells along the complete proximal-distal axis of the leaf during transition. Both analyses showed that the transition from cell proliferation to expansion was established and abolished abruptly (Andriankaja; Dhondt; De Bodt et al., 2011). Furthermore, the relative amount of cells maintained within the proliferation and expansion zones was almost completely constant during the transition. Previously, the progression of the cell cycle arrest front was hypothesized to be driven by diffusion of a mobile growth factor, inducing cell proliferation and entering the leaf via the petiole (Kazama et al., 2010). However, taking our results into account, this view seems less obvious. More likely, the progression of the cell cycle arrest front results from a balance between multiple antagonistic processes that act within the expansion and proliferation zones of the transitioning leaf. Interestingly, stomatal patterning followed a similar basipetal pattern, but proliferative pavement cell and formative meristemoid divisions were independent with respect to their onset and persistence. Furthermore, the establishment of the cell cycle arrest front occurs simultaneously with the onset of photomorphogenesis. We provide evidence that retrograde signaling from chloroplasts can affect the onset of transition revealing a previously unknown level of regulatory complexity during the transition from primary to secondary morphogenesis.

Taken together, concerning studying leaf development, a functional analysis of the SHR and SCR transcription factors, revealing their function in leaf growth control, building a mathematical model which helped to disentangle cell division and cell expansion parameters for individual cell types, and a detailed characterization of the transition from cell proliferation to cell expansion are the major experimental results in this thesis, providing important new insights into the mechanisms controlling leaf growth.

Several genes that affect the transition from cell proliferation to cell expansion, such as *ANT*, *GRF5*, *DA1*, and *KLUH* (Mizukami and Fischer, 2000b; Li, Zheng, Corke, Smith, and Bevan, 2008b; Horiguchi et al., 2009; Gonzalez et al., 2010), turn out to produce bigger leaves upon misexpression, indicating the promising potential of this developmental time point in organ growth control. In this respect, the transcriptome analysis can yield a number of candidate genes for follow-up studies. Also the intriguing finding that differentiation of the photosynthetic machinery is important for regulating the exit from cell proliferation is a lead that should be examined in more detail. It also suggests that sugar signaling could be an important regulatory process for the establishment of the cell cycle arrest front. Furthermore, the hypothesis that the progression of the cell cycle arrest front results from a balance between multiple antagonistic processes that act within the expansion and proliferation zones of the transitioning leaf, based on the constant relative amount of cells maintained within the proliferation and expansion zones, suggests a complex regulatory mechanism that requires further investigation. The validity of the proposed mechanism should be tested by a dynamic

modeling approach and should be compared to the hypothesis of a diffusible mobile growth factor (Kazama et al., 2010).

The mathematical model developed in chapter 3, on the other hand, could be the starting point for a bottom-up modeling approach, investigating the cellular mechanisms controlling leaf size. The mathematical model optimized a high number of parameters to fit the biological data. Such numerical values could be used as input parameter settings in a dynamic growth model, simulating *in silico* leaf growth. Such a model could be used to investigate the cellular growth mechanics of transgenic lines, whereas the mathematical model only yielded data on wild-type leaves. Furthermore, a lot of data from kinematic growth analyses of such transgenic lines is available and could be used to test model hypotheses and compare to *in silico* growth curves. Live imaging of cell divisions and cell growth could be employed to generate additional parameter values. Also the quantification of meristemoid cells during leaf development would be very informative to elucidate the contributions of divisions in the stomatal lineage to final leaf size, because for every stoma formed, one to three pavement cells arise from its meristemoid precursor.

In the long run, increasing crop productivity in order to safeguard food security has the largest chance to succeed if it is based on scientific research, because annual yields of many crops based on classical breeding approaches have hit plateaus. Selecting candidate genes which affect specific developmental stages and expanding our knowledge of cellular growth mechanisms by live imaging and integrative modeling approaches will be crucial in this process. This thesis contains elements that could be employed in future studies in order to achieve this goal.

Imaging plant growth to speed up phenotyping

Genetic resources and sequence data is piling up quickly while linking this information to gene function is progressing at a slow pace, indicating that plant phenotyping is the major bottleneck in the process of understanding the genomic blue print of plant life. Phenotyping is widely recognized as a laborious and technically challenging process, making it costly and time consuming. The goal of plant phenomics is to accelerate the progress in understanding gene function and environmental plant responses, closing the gap between genomics and functional biology (Furbank, 2009; Finkel, 2009). Researchers try to address this problem by combining novel image capturing technologies, robotics, image analysis, and data integration. Over the last decade, many software tools have been developed to extract phenotypic plant data. Such tools can ensure a fast and precise phenotypic description of plant structures, limiting laborious, costly, and often repetitive manual intervention. Furthermore, in comparison to manual screening experiments, often more phenotypic measurements are recorded.

In this thesis, we employ rapidly advancing digital imaging technology and develop image analysis algorithms to speed up the functional analysis of genes and to increase the phenotyping throughput. Imaging experiments included in this thesis range from the cellular level to the leaf and rosette level. At the cellular level we developed an imaging algorithm to analyze microscopic drawings of the *Arabidopsis* epidermis (Chapter 7), which drastically increased the speed and resolution of kinematic analysis of leaf growth in the *shr* and *scr* mutants (Dhondt et al., 2010) (Chapter 2). The ability to distinguish guard cells from other epidermal cells and the ability to measure individual cell areas implemented in the newly developed imaging algorithm subsequently formed the basis of a mathematical model of leaf growth (Kheibarshekan Asi; Dhondt et al., 2011) (Chapter 3). Extension of the algorithm to extract shape features and positional information yielded interesting data on the progression of the cell cycle arrest front along the longitudinal axis of the leaf (Andriankaja; Dhondt; De Bodt et al., 2011) (Chapter 4). Moreover, a data analysis pipeline to process the imaging data was established and we showed proof of concept of an imaging strategy to extract cellular content from DIC images, setting a basis for an automated kinematic analysis of leaf growth (Chapter 7). In the future we would like to integrate the cellular imaging and data analysis into a microscopic setup with graphical user interface to support the user with the rectification of the automatic segmentation. The realization of such an integrated setup would strongly boost the throughput of the cellular analysis, speeding up the functional analysis of growth regulating genes. Furthermore, on the cellular level, we also applied live imaging technology to reveal differential cell expansion within the leaf epidermis. Live imaging of cell division and cell expansion is likely to reveal more insight in the underlying mechanisms controlling these processes and unraveling the links between them.

At the leaf level, we developed an online framework, designated Leaf Image Analysis Interface (LIMANI), in which venation patterns are automatically segmented and measured on dark-field images (Dhondt et al., 2011) (Chapter 5). Image segmentation may be manually corrected through use of an interactive interface, allowing supervision and rectification steps in the automated image analysis pipeline and ensuring high-fidelity analysis. The framework was used to study vascular differentiation during leaf development and to analyze the venation pattern in transgenic lines with contrasting cellular and leaf size traits. The results show the evolution of vascular traits during leaf development, suggest a self-organizing mechanism for leaf venation patterning, and reveal a tight balance between the number of end-points and branching points within the leaf vascular network that does not depend on the leaf developmental stage and cellular content, but on the leaf position on the rosette. The extraction of up to ten vascular features allows for a thorough quantitative analysis of venation patterns, required to identify subtle perturbations in the pattern and to test dynamic modeling hypotheses using biological measurements. Furthermore, I believe that future imaging efforts must further focus on the development of imaging applications useful for the scientific community at large. This requires the programming of a graphical user interface and usually asks for some flexibility in the input images. In order to anticipate to this challenge,

we developed LIMANI in a modular fashion so it would be relatively straightforward to implement different imaging tools in this interface.

In the field of 3-D imaging, we investigated the use of high-resolution X-ray computed tomography (HRXCT) in plant biology (Chapter 6). We demonstrated how detailed three-dimensional morphological traits can be extracted rapidly from *in vivo* Arabidopsis seedlings without sample manipulation. Furthermore, *ex vivo* scanning at sub-micron resolution allows the quantification and visualization of the cellular organization of plant tissue samples, making HRXCT a powerful tool for developmental plant biology. Nevertheless, we realized that future developments in 3-D imaging should focus on extraction of morphological information. Recording volume and surface area of 3-D objects is relatively straightforward, but defining shoot and root branching patterns and leaf blade area or the characterization of shape variables is a challenge, requiring high-level image processing. A current solution is the recording of 3-D coordinates by the manual placement of landmarks on the 3-D object, which can be used to extract shape information (van der Niet et al., 2010).

At the rosette level, we developed imaging scripts to extract complete shoots grown on soil and on Petri dishes (Chapter 8). The measured features include rosette area, perimeter, and compactness. The image analysis scripts are optimized to analyze pictures coming from three in-house developed phenotyping setups. The IGIS is used to monitor rosette growth of Arabidopsis plants grown on Petri dishes. Pictures are captured on an hourly basis and 10 plates are concurrently imaged. WIWAM and MIRGIS are the setups for *in vivo* analysis of plant growth. WIWAM takes pictures of individual pots and controls the soil water content, making it an ideal system for plant growth analyses under controlled watering conditions (Skirycz et al., 2011). MIRGIS captures two trays, each containing 24 plants, in one image. In general, both platforms extract daily measurements. The development of different time resolved imaging platforms has boosted the throughput of the plant growth analyses in our research group and this with a time resolution which was not feasible before. These phenotyping setups should speed up our quest to important growth regulators and the identification of growth regulatory networks. The era of plant phenomics has started. Worldwide plant phenotyping setups are being developed and large phenotyping facilities are founded. In the coming years a richness of screens will aim at the identification of high-yielding and stress tolerant germplasm, bringing high-throughput plant imaging to the crop level. Plant phenomics, with automated and high-throughput plant growth imaging as its major pillar, has the potential to make a large contribution to the demanding increase in crop productivity, by acceleration of the high-precision phenotyping process. Nevertheless, imaging should be considered as a tool, and a general effort is needed to correlate gene function, plant performance, and environmental response, in order to ensure food security in a world that is facing several major challenges.

In conclusion, this thesis contains imaging solutions at different plant scales, ranging from the cellular level to the rosette. They were particularly employed to examine growth mechanisms

during leaf development and to speed up and increase the throughput of plant phenotyping studies. Finally, I would like to end with two remarks. First, a good quality picture taken with a standardized setup is drastically facilitating the image analysis. Half of the imaging solution is to standardize and to optimize the process of image capturing. Secondly, I believe that imaging tools for the scientific community should not be designed as a data generating black box, but should allow checking and improving the quality of the generated data. Furthermore, one should realize that imaging algorithms often do not implement enough knowledge to cover all possible variability, indicating that researchers should indeed check the data quality. Advances in plant imaging are very promising and imaging tools can definitely help scientists to accelerate phenotypic studies, but they should not be trusted blindly to do the functional biology for you.

REFERENCES

- Andriankaja, M., Dhondt, S., De Bodt, S., Vanhaeren, H., Coppens, F., De Milde, L., Mühlenbock, P., Skirycz, A., Gonzalez, N., Beemster, G.T.S., and Inzé, D.** (2011) Exit from proliferation during leaf development in *Arabidopsis thaliana*: a not so gradual process. *Dev Cell*, **in press**.
- Dhondt, S., Coppens, F., De Winter, F., Swarup, K., Merks, R.M.H., Inzé, D., Bennett, M.J., and Beemster, G.T.S.** (2010) SHORT-ROOT and SCARECROW regulate leaf growth in *Arabidopsis* by stimulating S-phase progression of the cell cycle. *Plant Physiol.*, **154**, 1183-1195.
- Dhondt, S., Van Haerenborgh, D., Van Cauwenbergh, C., Merks, R.M.H., Philips, W., Beemster, G.T.S., and Inzé, D.** (2011) Quantitative analysis of venation patterns of *Arabidopsis* leaves by supervised image analysis. *The Plant Journal*, **in press**.
- Donnelly, P.M., Bonetta, D., Tsukaya, H., Dengler, R.E., and Dengler, N.G.** (1999) Cell cycling and cell enlargement in developing leaves of *Arabidopsis*. *Dev Biol*, **215**, 407–419.
- Finkel, E.** (2009) With “phenomics,” plant scientists hope to shift breeding into overdrive. *Science*, **325**, 380 -381.
- Furbank, R.T.** (2009) Foreword: Plant phenomics: from gene to form and function. *Functional Plant Biol.*, **36**, v-vi.
- Gonzalez, N., De Bodt, S., Sulpice, R., Jikumaru, Y., Chae, E., Dhondt, S., Van Daele, T., De Milde, L., Weigel, D., Kamiya, Y., Stitt, M., Beemster, G.T.S., and Inzé, D.** (2010) Increased leaf size: different means to an end. *Plant Physiol.*, **153**, 1261-1279.

Green, P.B. (1976) Growth and cell pattern formation on an axis: critique of concepts, terminology, and modes of study. *Botanical Gazette*, **137**, 187-202.

Horiguchi, G., Gonzalez, N., Beemster, G.T.S., Inzé, D., and Tsukaya, H. (2009) Impact of segmental chromosomal duplications on leaf size in the grandifolia-D mutants of *Arabidopsis thaliana*. *The Plant Journal*, **60**, 122-133.

Kazama, T., Ichihashi, Y., Murata, S., and Tsukaya, H. (2010) The mechanism of cell cycle arrest front progression explained by a KLUH/CYP78A5-dependent mobile growth factor in developing leaves of *Arabidopsis thaliana*. *Plant and Cell Physiology*, **51**, 1046 -1054.

Kheibarshekan Asl, L., Dhondt, S., Boudolf, V., Beemster, G.T.S., Beeckman, T., Inzé, D., Govaerts, W., and De Veylder, L. (2011) Model-based analysis of Arabidopsis leaf epidermal cells reveals distinct division and expansion patterns for pavement and guard cells. *Plant Physiology*, **156**, 2172 -2183.

Li, Y., Zheng, L., Corke, F., Smith, C., and Bevan, M.W. (2008a) Control of final seed and organ size by the DA1 gene family in *Arabidopsis thaliana*. *Genes & Development*, **22**, 1331 - 1336.

Li, Y., Zheng, L., Corke, F., Smith, C., and Bevan, M.W. (2008b) Control of final seed and organ size by the DA1 gene family in *Arabidopsis thaliana*. *Genes Dev*, **22**, 1331-1336.

Mizukami, Y. and Fischer, R.L. (2000a) Plant organ size control: AINTEGUMENTA regulates growth and cell numbers during organogenesis. *Proc Natl Acad Sci U S A.*, **97**, 942-947.

Mizukami, Y. and Fischer, R.L. (2000b) Plant organ size control: AINTEGUMENTA regulates growth and cell numbers during organogenesis. *Proc Natl Acad Sci U S A*, **97**, 942-947.

Skirycz, A., Vandenbroucke, K., Clauw, P., Maleux, K., De Meyer, B., Dhondt, S., Pucci, A., Gonzalez, N., Hoerberichts, F., Tognetti, V.B., Galbiati, M., Tonelli, C., Van Breusegem, F., Vuylsteke, M., and Inzé, D. (2011) Survival and growth of Arabidopsis plants given limited water are not equal. *Nat Biotech*, **29**, 212-214.

Sozzani, R., Cui, H., Moreno-Risueno, M.A., Busch, W., Van Norman, J.M., Vernoux, T., Brady, S.M., Dewitte, W., Murray, J.A.H., and Benfey, P.N. (2010) Spatiotemporal regulation of cell-cycle genes by SHORTROOT links patterning and growth. *Nature*, **466**, 128-132.

Tester, M. and Langridge, P. (2010) Breeding technologies to increase crop production in a changing world. *Science*, **327**, 818 -822.

van der Niet, T., Zollikofer, C.P.E., León, M.S.P. de, Johnson, S.D., and Linder, H.P. (2010) Three-dimensional geometric morphometrics for studying floral shape variation. *Trends in Plant Science*, **15**, 423-426.

Acknowledgements

Dit doctoraat en meer bepaald de inhoud van de vorige hoofdstukken zou niet tot stand gekomen zijn zonder de hulp en ondersteuning van vele mensen. Mijn wetenschappelijk verhaal aan het departement 'Plant Systems Biology' begon in 2005 bij het aanvangen van mijn master thesis. Het was de professionele uitstraling van het departement en gemoedelijke maar toch overtuigende babbel met Gerrit die me over de streep haalde. Frederik gaf me de perfecte begeleiding. Na een tof thesisjaar besloot ik om me te wagen aan een doctoraat bijgestaan door twee 'Nederlandse' groepsleiders: Gerrit en Roeland. Gerrit introduceerde mij tot de wondere wereld van de kinematische analyse van bladgroei. Zijn wetenschappelijk enthousiasme wist hij al snel op mij over te zetten. Ik wil hem vooral bedanken voor de blijvende ondersteuning, zijn kritische bemerkingen en de joviale omgang. Roeland wil ik bedanken voor het tot leven brengen van mijn interesse voor modeling en beeldanalyse. Ongepland werd dit laatste dan ook de rode draad door mijn doctoraat. Hij leerde me de kneepjes van het wetenschappelijk schrijven en stimuleerde mijn zelfstandig werken en denken. Freya gaf me praktische ondersteuning bij de experimenten en bracht extra leven in onze hoek. "Da was nen schonen tijd hé ...". Frederik bleef een collega waar ik steeds met mijn vragen terecht kon, we vormden een team in het automatiseren van het lableven en hadden plezier in een andere hoek. Inderdaad, de desintegratie van de buitenmuur en aanlokkelijke posities voor de Nederlandse begeleiders dreef ons naar andere oorden.

Gelukkig werden we met open armen ontvangen in de onderzoeksgroep van Dirk, een bewonderingswaardig man die al snel de helft van mijn projecten schrapte. 'Focus' was zijn toverwoord en toegegeven werd dit het succes van mijn doctoraat. Hij steunde me volop bij het ontplooiën van mijn talenten en vertrouwde me verantwoordelijkheden toe waarvan ik voorheen niet durfde dromen. Bedankt! Many thanks go to many 'yields': Aleksandra, Elena, Els, Hannes C, Hannes V, Hilde, Jasper, Jérôme, Joke, Jolien, Jonas, Judith, Katrien, Kirin, Korneel, Liesbeth DM, Liesbeth V, Lieven, Marieke, Mattias, Megan, Nubia, Nathalie, Pieter, Rosella, Sergei, Stefanie, Twiggy, Wim, Wannes, Xiaohuan, Youn-Jeong. I have very much enjoyed working with you. Nathalie, unfortunately we got somewhat separated in the lab, but I feel we are still close. The water is not that deep. Thanks for the nice discussions and fun we had over the years. Megan, I believe we were able to set up a very nice collaboration, the perfect mix of science and joy, with a lovely result. We will miss you.

José Manuel and José Luis, you were and will always be my first real international collaborators. Thanks for the nice experience and the good food in Spain. Malcolm, although you are focusing on the hidden half, our roads on the trip to Jerusalem seem to cross quite often. I hope we can keep in touch. Leila and Willy, you showed me the key to the world of applied mathematics in biology. We had fun trying to speak the same language. In dit project apprecieerde ik ook heel erg de input van Lieven en zijn volharding in het re-resubmitten.

Verder beantwoordde hij ook al mijn celcyclus vraagjes met plezier. De steeds goed geluimde Veerle en de deskundige Denis zorgden voor mijn aanbevolen dosis X-stralen. Verrassend genoeg resulteerde het gebruik van huis-, tuin- en keukenhulpjes al snel in een harde schijf vol mooie beelden. Ook onze vrienden bij TELIN mag ik niet vergeten. Daniel, Jonas, en Wilfried bedankt voor jullie imaging bijdrage tot de pavement cell analyse. Filip, Hiep en Wilfried stonden me bij in de begeleiding van Dirk. Dirk je deed een prima job in het implementeren van de interface. Ik had het niet beter gekund. Samen met o.a. de resultaten van het harde werk van mijn master studente, Caroline, werd dit project tot een mooi einde gebracht. Bedankt voor jullie inzet!

Near the end of my PhD Enrico Coen welcomed me for a short stay in his research group at the John Innes Centre in Norwich. It was a wonderful experience. I learned a lot and had a great time. Enrico, you are doing great science and you own a fantastic group. Des, Erika, Hugo, Jerome, Jordy, Karen, Katie, Katharina, Lucy, Matthew, Navid, Paul, Samantha, Susana, Tilly, Veronica, Wiebke, Yara, and Xana: thanks a lot for the discussions, chats, hospitality, and football games.

Verder zijn er nog een heleboel mensen die er achter de schermen voor zorgen dat alles op wieljes loopt. Annick, Bernard, Christine, David, Diane, Delphine, Hilde, Martine, Nathalie en Sophie: bedankt voor de administratieve ondersteuning. Dany, Frederik, Hendrik, Luc en Raf: merci voor de nodige opslagruimte en IT support. An, Agnieszka, Blancheke, Dirk, Jackie, Karel, Kristof, Miguel, Nancy en Nico: bedankt voor de logistiek. De derde Dirk in dit dankwoord krijgt hierbij een speciale vermelding voor de hulp bij het in elkaar timmeren van onze camera setups. Ook mijn lunch maatjes: Bert, Frederik, Gert, Giel, Leen, Marlies en Wim, wil ik bedanken voor de gezellige pauzes.

Dit doctoraat was ook niet tot stand gekomen zonder de nodige ondersteuning en afleiding op het thuisfront waardoor alles plots weer helderder leek. In de eerste plaats wil ik mijn ouders bedanken voor de geboden kansen en onvoorwaardelijke steun. Merci! Ruben, Lieske en Dieter: bedankt voor alles! Ook mijn schoonfamilie: mama, Bert, Liesbeth, Tom, Katelijn en de kindjes, jullie hebben veel voor mij betekend. Vrienden en aanhangsels van Chiro Bottelare: merci voor de vele feestjes, weekends en gezellige momenten! De meeste steun vond ik echter bij mijn lief vrouwke. Bolleke, ik zie je nog steeds super graag. De laatste maanden was ik er misschien wat minder voor jou, ook al had je me soms extra hard nodig. Vanaf nu krijg je opnieuw de welverdiende aandacht, maar al gauw zal je die met iemand moeten delen: ... ons klein wondertje, nog veilig in mama's buik. Dankzij jouw komst had ik een streefdatum en was een prachtige belonging achteraf verzekerd. Ik zal je liefhebben, verzorgen en koesteren.

Best regards,

Balegem, 12 februari 2012

Stijn Dhondt

Curriculum Vitae

PERSONALIA

Name: Stijn Dhondt

Address: Poststraat 5, 9860 Oosterzele, Belgium

Email: st.dhondt@gmail.com

Mobile: +32 (0) 497/84.66.30

Date of birth: April 17, 1983

Place of birth: Gent, Belgium

Nationality: Belgian

Marital status: married to An Van de Wiele

Languages: Dutch: native, English: fluent, French: good, German: basic

CURRENT POSITION

Position: Pre-doctoral fellow

Research group: Systems Biology of Yield

Institute: Department of Plant Systems Biology, VIB - UGENT, Gent, Belgium

Address: Technologiepark 927, 9052 Gent, Belgium

Email: stdho@psb.vib-ugent.be

Tel: +32 (0)9/331 39 53

EDUCATION

- **2006 – 2011 Ph.D. fellowship**

Department Plant Biotechnology and Bioinformatics, Ghent University, Gent, Belgium;

Department of Plant Systems Biology, VIB, Gent, Belgium;

Promoters: Prof. Dr. Dirk Inzé and Prof. Dr. Ir. Gerrit Beemster

2007 - 2008: in the research group of "Organ Growth Regulation" headed by Prof. Dr. ir. Gerrit Beemster

2008 – 2011: in the research group of "Systems Biology of Yield" headed by Prof. Dr. Dirk Inzé

2007 – 2008: indebted to the European Community Grant FP6 IP AGRON-OMICS
(Contract LSHG-CT-2006-037704)

2008 – 2011: indebted to the Agency for Innovation through Science and Technology for a predoctoral fellowship

- **2001 – 2006: Master in Bioscience Engineering**, option Cell and Gene biotechnology; Obtained at the Faculty of Bioscience Engineering, Ghent University, Gent, Belgium, June 2006
- **2005-2006: Undergraduate dissertation**
“Functional analysis of proliferation genes from the HMGB and ENODL family in *Arabidopsis thaliana*” performed in the research group of “Organ Growth Regulation” headed by Prof. Dr. ir. Gerrit Beemster at the Department of Plant Systems Biology, Flanders Institute of Biotechnology (VIB), Gent, Belgium. Promoters: Prof. Dr. Dirk Inzé, Prof. Dr. Godelieve Gheysen

EXPERIENCE

- **2006 – 2011: PhD fellow** Ghent University
- **2008 – 2009: Supervising** Caroline Van Cauwenbergh (Master in Industrial sciences: Biochemistry) with her master thesis entitled “Correlation between cell size, vasculature, and leaf growth in *Arabidopsis thaliana*.”
- **2009 – 2011: Assistance** practical courses Plant Physiology by Prof. Dr. Dirk Inzé (2nd Bachelor Biology, UGent)

AWARDED GRANTS

- **PhD fellowship of the Agency for Innovation through Science and Technology (IWT)** (73295) January 2008 – December 2011; Project title: De rol van auxine en celcyclusregulatie in de morfogenese van *Arabidopsis* bladeren. Promoter: Prof. Dr. Dirk Inzé (PSB, VIB-UGENT); Co-promoter: Prof. Dr. ir. Gerrit Beemster (PSB, VIB-UGENT).
- **EMBO short-term fellowship** (ASTF 346.00-2011; 30 days) from 3 October 2011 in the lab of Prof. Enrico Coen, John Innes Center, Colney Lane, Norwich NR4 7UH, United Kingdom. Project title: How do changes in cell division patterns imply differences in leaf shape?

PUBLICATIONS

Peer-reviewed publications

- **Achard, P., Gusti, A., Cheminant, S., Alioua, M., Dhondt, S., Coppens, F., Beemster, G.T.S., and Genschik, P.** (2009). Gibberellin signaling controls cell proliferation rate in Arabidopsis. *Curr. Biol.* **19**: 1188-1193. (IF = 10.99)
- **Gonzalez, N., De Bodt, S., Sulpice, R., Jikumaru, Y., Chae, E., Dhondt, S., Van Daele, T., De Milde, L., Weigel, D., Kamiya, Y., Stitt, M., Beemster, G.T., and Inze, D.** (2010). Increased Leaf Size: Different Means to an End. *Plant Physiol.* **153**: 1261-1279. (IF = 6.45)
- **Dhondt, S., Vanhaeren, H., Van Loo, D., Cnudde, V., and Inzé, D.** (2010). Plant structure visualization by high-resolution X-ray computed tomography. *Trends Plant Sci.* **15**: 419-422. (IF = 10.10)
- **Dhondt, S., Coppens, F., De Winter, F., Swarup, K., Merks, R.M., Inzé, D., Bennett, M.J., and Beemster, G.T.** (2010). SHORT-ROOT and SCARECROW Regulate Leaf Growth in Arabidopsis by Stimulating S-Phase Progression of the Cell Cycle. *Plant Physiol.* **154**: 1183-1195. (IF = 6.45)
- **Skirycz, A., Vandenbroucke, K., Clauw, P., Maleux, K., De Meyer, B., Dhondt, S., Pucci, A., Gonzalez, N., Hoerberichts, F., Tognetti, V., van Breusegem, F., Vuylsteke, M., and Inzé, D.** (2011) Survival and growth under limited water are not equal. *Nature Biotechnol.* **3**: 212-214. (IF = 31.09)
- **Kheibarshekan, L*., Dhondt, S.*, Boudolf, V., Beemster, G.T., Beeckman, T., Inzé, D., Govaerts, W., De Veylder, L.** (2011) Model-Based Analysis of Arabidopsis Leaf Epidermal Cells Reveals Distinct Division and Expansion Patterns for Pavement and Guard Cells. *Plant Physiol.* **156**: 2172-2183. (IF = 6.45)
(*: shared first author)
- **Vanneste S, Coppens F, Lee E, Donner TJ, Xie Z, Van Isterdael G, Dhondt S, De Winter F, De Rybel B, Vuylsteke M, De Veylder L, Friml J, Inzé D, Grotewold E, Scarpella E, Sack F, Beemster GT, Beeckman T.** (2011) Developmental regulation of CYCA2s contributes to tissue-specific proliferation in Arabidopsis. *EMBO J.* **30**:3430-3441 (IF = 10.12)

- **Pérez-Pérez JM, Rubio-Díaz S, Dhondt S, Hernández-Romero D, Sánchez-Soriano J, Beemster GT, Ponce MR, Micol JL.** (2011) Whole organ, venation and epidermal cell morphological variations are correlated in the leaves of Arabidopsis mutants. *Plant Cell Environ.* **34**:2200-2211 (IF = 5.15)
- **Andriankaja, M. *, Dhondt, S.*, De Bodt, S.*, Vanhaeren, H., Coppens, F., De Milde, L., Mühlenbock, P., Skirycz, A., Gonzalez, N., Beemster, G.T.S., and Inzé, D.** Exit from proliferation during leaf development in Arabidopsis thaliana: a not so gradual process. *Dev Cell.* **22**:64-78 (IF = 13.95)
(*: shared first author)
- **Dhondt S, Van Haerenborgh D, Van Cauwenbergh C, Merks RM, Philips W, Beemster GT, Inzé D.** (2011) Quantitative analysis of venation patterns of Arabidopsis leaves by supervised image analysis. *Plant J.* doi: 10.1111/j.1365-313X.2011.04803.x. (in press) (IF = 6.95)
- **Quimbaya, M., Vandepoele, K., Raspé, E., Matthijs, M., Dhondt, S., Beemster, G.T.S., Berx, G., and De Veylder, L.** Identification of putative oncogenes through data integration and comparative genomics between plants and humans. *Cellular and Molecular Life Sciences* (in press) (IF = 7.05)
- **Sterken, R., Kiekens, R., Boruc, J., Zhang, F., Vercauteren, A., Vercauteren, I., de Smet, L., Dhondt, S., Inzé, D., Russinova, E., Vuylsteke, M.** Combined linkage and association mapping reveals CYCD5;1 as a quantitative trait gene for endoreduplication in Arabidopsis. *P Natl Acad Sci USA* (in press) (IF = 9.77)

Manuscripts in preparation

- **Zhiponova, M., Vanhoutte, I., Boudolf, V., Dhondt, S., Coppens, F., Gonzalez-Garcia, M.P., Betti, C., Mylle, E., Inzé, D., Cano-Delgado, A., Beemster, G.T.S., De Veylder, L., and Russinova, E.** Brassinosteroids control the G2-to-M transition of the plant cell cycle to promote leaf growth in Arabidopsis. (submitted to *Plant Physiology*).
- **Eloy, N.B., Van Leene, J., Maleux, K., De Milde, L., Vanhaeren, H., Dhondt, S., Gonzalez, N., Mercier, R., Beemster, G.T.S, Remaut, H., Van Montagu, M., De Jaeger, G., Ferreira, P.C.G., and Inzé D.** SAMBA, a novel Arabidopsis Anaphase Promoting Complex APC/C subunit with a role in growth and pollen development. (submitted to *P Natl Acad Sci USA*).

Book chapters

- **Rymen, B., Coppens, F., Dhondt, S., Fiorani, F. and Beemster, G. T. S.** (2010). Kinematic analysis of cell division and expansion, *Methods Mol Biol*, 655, 203–227.

ATTENDED MEETINGS

Presenting speaker

- UIAPVI/33 meeting, Louvain-la-Neuve - Belgium, 28 September 2007: Dhondt, S., and Beemster G.T.S. "SHR: more than just root patterning."
- Annual AGRON-OIMCS meeting, Berlin - Germany, 21-22 February: Dhondt, S., Beemster, G.T.S., and Inzé, D. "Imaging vascular patterns."
- Plant Growth Biology and Modeling Workshop, Elche - Spain, 13-17 October 2009: Dhondt, S., Skiryecz, A., Maleux, K., De Meyer, B., Coppens, F., Merks, R.M., Beemster, G.T.S., Hilson, P., and Inzé, D. "Image analysis tracks plant growth and supports in the phenotypic analysis of leaves."
- Annual AGRON-OMICS meeting, Bern – Switzerland, 4-5 February 2010: Dhondt, S., Beemster, G.T.S., and Inzé, D. "Limani: a leaf image analysis interface."
- VRTC- Lectures on Emerging Technologies, Leuven – Belgium, 11 May 2010: Dhondt, S., Vanhaeren, H., Van Loo, D., Cnudde, V., and Inzé, D. "High resolution X-ray computed tomography as a powerful tool for plant imaging."
- UGCT seminar: X-ray tomography as a multidisciplinary research tool: exploring new frontiers, Ghent – Belgium, 8 December 2010, Dhondt, S., Vanhaeren, H., Van Loo, D., Cnudde, V., and Inzé, D. "Plant structure visualization by HRXCT."
- Annual AGRON-OMICS meeting, Tuebingen - Germany, 22-24 February 2011. Dhondt, S., Van Haerenborgh, D., Van cauwenbergh, C., Merks, R.M., Beemster, G.T.S, Philips, W., and Inzé, D. "Analyzing vascular networks of leaves by supervised imaging."
- 2nd International Plant Phenotyping Symposium, Jülich – Germany, 5-7 September 2011. Dhondt, S., Van Haerenborgh, D., Van cauwenbergh, C., Merks, R.M., Beemster, G.T.S, Philips, W., and Inzé, D. "Quantitative analysis of venation patterns of Arabidopsis leaves by supervised image analysis."

Poster presentation

- Workshop on Growth phenotyping and imaging in plants, Montpellier - France, 17-19 July 2009. Dhondt, S., Merks, R.M., and Beemster, G.T.S. "Unraveling the interplay between vascularization and leaf growth."
- Summer school: Computational and Mathematical Modeling for Plant Systems Biology, Ghent - Belgium, 1-5 September 2008. Dhondt, S., Merks, R.M., and Beemster, G.T.S. "Understanding the link between vascularization and leaf growth."
- Plant Growth Biology and Modeling Workshop, Elche, Spain, 13-17 October 2009: Dhondt, S., Skiryycz, A., Maleux, K., De Meyer, B., Coppens, F., Merks, R.M., Beemster, G.T.S., Hilson, P., and Inzé, D. "Image analysis tracks plant growth and supports in the phenotypic analysis of leaves."

Attendee

- EMBO Conference Series – From basic genomics to systems biology, Ghent - Belgium, 2-4 May 2007.
- Ontologies, Standards and Best Practice, Ghent - Belgium, 21 May 2007.
- Advanced Workshop - The understanding and modelling of auxin transport in plants, Nottingham – United Kingdom, 14-16 May 2008.
- UIAPVI/33 meeting, Antwerpen - Belgium, 22 January 2009.
- Annual AGRON-OMICS meeting, Warwick – United Kingdom, 9-10 February 2009.
- Modelling in Plant Biology: Models at the cellular and tissular scales, Montpellier - France, 6 Mar 2009.
- CPIB Summer School 2009: Introduction to biological modeling. Nottingham – United Kingdom, 14-17 September 2009.
- EPSO Workshop on Plant Phenotyping, Julich – Germany, 2-3 November 2009
- International Symposium: Growth and Development of Roots, Louvain-la-Neuve - Belgium 27 January 2011

- Plant Growth Biology and Modeling Workshop, Elche - Spain, 19-21 September 2011
- Annual Science meeting – Excellence with impact, JIC – TSL, Norwich – UK, 12-14 October 2011
- Solvay Workshop on Design principles and Hardware of Biological Circuits, ULB, Brussels - Belgium, 15-17 February 2012

